LOW-PRESSURE VAPOUR-LIQUID EQUILIBRIUM AND MOLECULAR SIMULATION OF CARBOXYLIC ACIDS

by

Scott Llewellyn Clifford

[BSc.(Eng.)]

University of Natal, Durban

Submitted in fulfillment of the academic requirements for the degree of Master of Science in Engineering at the School of Chemical Engineering, University of KwaZulu-Natal

Durban

2004

SUMMARY

Most industrially important separation processes depend upon good-quality, reliable vapour-liquid equilibrium (VLE) data for design and optimization purposes. Although a great deal of VLE (and, in particular, binary VLE) data have been measured and compiled in databases such as the Dortmund Data Bank, little work has been done on hydrogen-bonding, polar compounds such as carboxylic acids. Furthermore, there is currently a great deal of interest in techniques such as molecular simulation that allow prediction of pure component and binary VLE data using computer clusters. Thus, the main focus of this project was the low-pressure VLE and molecular simulation of carboxylic acids.

The VLE measurements were carried out using a dynamic, glass VLE still designed by Raal (Raal and Mühlbauer [1998]). The still was controlled using a graphical user interface run on the computer accompanying the equipment. The still could operate in both isobaric and isothermal modes, with the temperature and pressure being regulated via a pulse-width modulation control strategy (Joseph et al. [2001]). This setup allowed the pressure to be controlled to within 0.01 kPa of the set-point pressure, whilst the temperature control varied between 0.01 and 0.05 °C (depending upon the species volatility).

The carboxylic acid vapour pressure measurements were undertaken at the outset of the project for a homologous series of seven acids from propionic acid through to heptanoic acid. The data compared extremely well to the available literature data and were regressed to obtain parameters for the familiar Antoine equation, as well as the more complex Reid et al. [1988] equation. In addition, acentric factors and parameters for the alpha function of Twu et al. [1991] were evaluated from the experimental vapour pressures.

The next phase of the project involved the measurement of the binary VLE systems. To ensure that the equipment and experimental procedures were operating as desired, the cyclohexane (1) – ethanol (2) test system at 40 kPa was measured. The data were then compared with reliable literature sources and this revealed an excellent agreement between the experimental and published data. Hence, a high degree of confidence was placed in the

experimental setup and procedures, as well as the new carboxylic acid VLE data. This data consisted of two carboxylic acid systems: propionic acid (1) – valeric acid (2) and isobutyric acid (1) – valeric acid (2). For both systems, an isobar at 20 kPa and three isotherms at 120, 130 and 140 °C respectively were measured, none of which are currently available in the literature.

The VLE data were then subjected to a rigorous thermodynamic analysis. Two different reduction techniques were employed – the combined (gamma-phi) method and the direct (phi-phi) method. For the combined method, three liquid-phase activity coefficient models were used to successfully correlate the VLE data, namely the Wilson, NRTL and UNIQUAC models. The vapour phase imperfections were accounted for using the Pitzer-Curl correlation (Pitzer and Curl [1957]), the Hayden and O'Connell [1975] correlation and the chemical theory approach. The Peng-Robinson equation of state (Peng and Robinson [1976]) was utilized in the direct method, with both liquid and vapour phase non-idealities represented by fugacity coefficients. The Wong-Sandler and Twu-Coon mixing rules were employed in conjunction with the Peng-Robinson equation of state. The values returned by both methods were good; with the direct method results comparing favourably to those obtained using the combined method.

The experimental liquid-phase activity coefficients were evaluated by applying the chemical theory to the liquid phase, after traditional methods for determining these quantities failed to produce acceptable results. The activity coefficient values calculated using the models differed significantly from the experimental values in the dilute regions. This was attributed to the effects of hydrogen bonding; with these association end effects also being visible in the experimental phase diagrams.

To determine the consistency of the experimental data, two thermodynamic consistency tests were applied. All the data sets passed the highly rigorous direct test; however, the indices were fairly high. This is a direct result of the models proving incapable of adequately fitting the experimental activity coefficients. Thus, the point test was regarded as providing a far better indication of the thermodynamic consistency of the carboxylic acid

systems. All of the data sets successfully passed the point test and, hence, the experimental data is considered to be thermodynamically consistent.

The method of Ellis and Jonah [1962] (as modified by Maher and Smith [1979]) was used in an attempt to determine the infinite dilution activity coefficients for the acids from the experimental VLE data. Unfortunately, the method could not be satisfactorily employed due to the association effects discussed above.

The Gibbs-Hermholtz equation was utilized in determining the excess thermodynamic properties for both carboxylic acid systems. The molar excess enthalpy, excess Gibbs energy and excess entropy were evaluated from the isothermal VLE data. The heat-of-mixing data (i.e. excess enthalpy) constitutes new data.

The molecular simulation portion of the project involved the prediction of pure component and binary VLE data of polar compounds using the Stockmayer potential. A straight-chain alkane (n-pentane) was initially simulated to allow the researcher to become familiar with the simulation procedures and the Linux-based software. The vapour pressure and density results matched the literature data exceedingly well. Two polar compounds were predicted, viz. methanol and acetic acid. In both cases, the vapour pressures were too high and the phase-coexistence figures too large when compared to the published experimental data. However, the values determined for methanol were in close agreement with the results reported by van Leeuwen [1994b].

In addition to the pure component data that was predicted, a binary VLE system comprised of methanol and acetic acid was also simulated. As expected, the simulation data did not correspond well with the literature data. The overall shape of the phase diagram followed that exhibited by the experimental data. However, the temperature range was too low, whilst the phase envelope was broader than it ought to be.

Considerable scope exists for further investigation into carboxylic acids and other associating species, particularly in the area of molecular simulation.

PREFACE

The work presented in this thesis was performed at the University of Natal, Durban, from January 2002 to December 2003. The project was supervised by Professor D. Ramjugernath and Professor J. D. Raal.

This thesis is submitted as the full requirement for the degree M.Sc. in Chemical Engineering. All of the work presented in this thesis is original, unless otherwise stated. It has not (in whole or in part) been previously submitted to any tertiary institute as part of a degree.

S. L. Clifford

As supervisor of this candidate, I approve this thesis for submission:

Professor D. Ramjugernath

Professor J. D. Raal

ACKNOWLEDGEMENTS

The following people have made a significant contribution to this work, and I would, therefore, like to take this opportunity to acknowledge and thank them:

- My supervisors, Professor D. Ramjugernath and Professor J. D. Raal for their support and guidance over the past two years of research. Without their knowledge, ideas and experience this project would not have been possible.

- My colleagues in the Chemical Engineering Department and, in particular, Roger, John-Roy, Nick, Tyrone, Sebastien, Minal, Prathika, Yash, Warren, Ranjeetha, Alex, Kasuren and Natasha for their valuable advice and generous friendship.

- SASOL Ltd., Thrip, SIDA and the NRF Thuthuka Programme for their financial assistance during my degree.

- On a more personal note, I would like to thank my parents, Darryl and Margaret, and my brother Zane, for their many years of love, support, encouragement and motivation.

TABLE OF CONTENTS

LIST OF FIGURES

Chapter 2

Chapter 3

Chapter 4

Chapter 5

Chapter 6

Chapter 8

Chapter 9

Appendix B

Appendix C

LIST OF TABLES

Chapter 2

Chapter 3

Chapter 6

Chapter 8

Chapter 9

Appendix A

NOMENCLATURE

English Letters

A'	Constant in the Antoine or Reid et al. vapour pressure equations
a	Intermolecular attraction force parameter in Peng-Robinson [1976] equation of state
a'	Parameter in the Tsonopoulos [1974] correlation
a_1^*	Parameter in Twu et al. [1993] equation of state (section 3.4.2.2)
B'	Constant in the Antoine or Reid et al. vapour pressure equations
B^0	Parameter in the Pitzer-Curl [1957] correlation
B^1	Parameter in the Pitzer-Curl [1957] correlation
B_{ii}	Second virial coefficient of pure component i [cm^3/mol]
B_{ij}	Second virial coefficient for species i - species j interaction [cm^3/mol]
b	Molecular size parameter in Peng-Robinson [1976] equation of state
b'	Parameter in the Tsonopoulos [1974] correlation
b_1^*	Parameter in Twu et al. [1993] equation of state (section 3.4.2.2)
C'	Constant in the Antoine or Reid et al. vapour pressure equations
c	Numerical constant defined in equation (3-129)
D'	Constant in the Reid et al. vapour pressure equation
D	Summation term in the Wong-Sandler [1992] mixing rule (equation (3-123))
E_i	Energy of a particular configuration i in a simulation [J/mol]
f	Fugacity [kPa]
$\hat{f}$	Fugacity in solution [kPa]
G	Molar or specific Gibbs energy [J/mol]
G_{12}	Parameter in the NRTL [1968] model
G_{21}	Parameter in the NRTL [1968] model
$\overline{G}$	Partial molar Gibbs energy [J/mol]

g_{ij}-g_{ii}	Parameter representing energy interactions between species in the NRTL [1968] model
H	Enthalpy [J/mol]
ΔH_{vap}	Enthalpy of vapourization [J/mol]
K	Equilibrium constant
k	Mixing rule parameter
k_B	The Boltzmann constant [1.381 x 10^{-23} J/mol.K]
k_{ij}	Binary interaction parameter
L	Length of a simulation box [Å]
L'	Parameter in the Twu et al. [1991] alpha correlation (equation (3-112))
l_i	Parameter in the UNIQUAC [1975] model (equation (3-96))
l_{ij}	Binary interaction parameter (Twu-Coon [1996] mixing rule)
M	Represents a general thermodynamic property
M'	Parameter in the Twu et al. [1991] alpha correlation (equation (3-112))
M_W	Molecular weight [g/mol]
N	Indicates a constant number of moles in a simulation
N'	Parameter in the Twu et al. [1991] alpha correlation (equation (3-112))
N_A	Avogadro's number (6.022137 x 10^{23} mol^{-1})
n	Number of moles
n_{ex}	Number of experimentally measured points (section 9.2)
n_i	Number of moles of dimer or monomer in Twu et al. [1993] equation of state
n_T	Total number of moles of monomer and dimer in Twu et al. [1993] equation of state
n_0	Number of moles that would exist if no association was occurring (section 3.4.2.2)
P	System pressure [kPa]
P'	Parachor
P_D	The deviation pressure used in the Maher and Smith method [1979]; defined by equation (3-152) [kPa]
p_i	Point charge in the Ewald sum (section 4.3)

Q	Quadratic sum of second virial coefficients
q_i	Pure component area parameter in the UNIQUAC [1975] model (section 3.4.1.4)
R	Universal gas constant [J/mol.K]
R_d	Mean radius of gyration [Å]
r	Position relative to the centre of the Gaussian distribution (equation (4-25))
r_i	Pure component volume parameter in the UNIQUAC [1975] model (section 3.4.1.4)
r_{ij}	Distance between particles i and j in the Ewald Sum (section 4.3)
S	Molar or specific entropy [cm^3/mol]
s	Molecular separation in the Ewald sum (section 4.3)
T	System temperature [°C or K]
u	Constant integer value in Twu et al. [1993] equation of state
V	Molar or specific volume [cm^3/mol]
w	Constant integer value in Twu et al. [1993] equation of state
x	Liquid phase mole fraction (or composition)
x_R	Parameter in the Reid et al. equation; defined by equation (8-3)
y	Vapour phase mole fraction (or composition)
Z	Compressibility factor
z	Coordination number in the UNIQUAC equation (section 3.4.1.4)
z_I	Overall mole fraction (Table 8-21)
z_i	True mole fraction of species i

Greek Letters

α	Scaling factor in Peng-Robinson [1976] equation of state
α_{12}	Parameter in NRTL [1968] model representing solution non-randomness
α_E	Gaussian distribution parameter (equation (4-25))
β_j	Term in equation (3-148); defined by equation (3-150)
δ	Denotes a residual (e.g. δP)

δ_{ij}	Term relating the second virial coefficients (equations (3-41) and (3-62)); defined by equation (3-151)
ε_A	Tolerance in the flow diagrams for the bubblepoint iterations
ε_B	Tolerance in the flow diagrams for the bubblepoint iterations
ε_C	Tolerance in the flow diagrams for the bubblepoint iterations
ε_i^{∞}	Term in equation (3-148); defined by equation (3-149)
ε_P	Constant temperature term in the direct test (Van Ness [1995]); defined by equation (3-159)
ε_{PR}	Constant in the Peng-Robinson [1976] equation of state
ε_T	Constant pressure term in the direct test (Van Ness [1995]); defined by equation (3-160)
Φ	Ratio of fugacity coefficients, with the Poynting correction factor (equation 3-38))
Φ_1	Segment fraction in the UNIQUAC [1975] model (section 3.4.1.4))
Φ_2	Segment fraction in the UNIQUAC [1975] model (section 3.4.1.4))
ϕ	Fugacity coefficient
$\hat{\phi}$	Fugacity coefficient in solution
ϕ^*	True species fugacity coefficient
Γ_i	Temperature dependent constant of integration
γ	Activity coefficient
γ_i^{∞}	Infinite dilution activity coefficient
η	Solvation (unlike species) and association (pure species) parameters
κ	Characteristic constant in Peng-Robinson[1976] equation of state
Λ_{12}	Parameter in the Wilson [1964] model
Λ_{21}	Parameter in the Wilson [1964] model
λ_{ij}-λ_{ii}	Parameter representing molar interactions between species in the Wilson [1964] model
μ	Dipole moment [debye]
μ_i	Chemical potential of component *i*

μ_i^m	Molecular dipole
θ_1	Area fraction in the UNIQUAC [1975] model (section 3.4.1.4))
θ_2	Area fraction in the UNIQUAC [1975] model (section 3.4.1.4))
P_i	Probability of a state occurring in a simulation
P_{acc}	Probability that a certain move will be accepted in a simulation
ρ	Density [kg/m^3 or mol/cm^3]
ρ_{Gauss}	The Gaussian charge distribution (equation (4-25))
σ_{PR}	Constant in the Peng-Robinson [1976] equation of state
τ_{12}	Parameter in the NRTL [1968] model
τ_{21}	Parameter in the NRTL [1968] model
ω	Acentric factor

Subscript

1	Denotes component 1
2	Denotes component 2
A	Denotes phase A of a two-phase simulation
Ant	Denotes the Antoine equation
ad	Denotes absolute deviation (section 3.7.1)
avg	Denotes an average value
B	Denotes phase B of a two-phase simulation
b	Denotes the boiling point
c	Denotes a critical property
calc	Denotes a calculated value
ex	Denotes an experimental value
i	Denotes component *i*
lit	Denotes a literature value
m	Denotes a mixture property
Reid	Denotes the Reid et al. [1988] equation
r	Denotes a residual property

vdw	Denotes a "van der Waals" property

Superscript

D	Denotes the "dimerized" contribution to the second virial coefficient in the Hayden and O'Connell method [1975]
E	Denotes an excess property
ex	Denotes an experimental value in the direct test of thermodynamic consistency (Van Ness [1995])
F	Denotes the "free" contribution to the second virial coefficient in the Hayden and O'Connell method [1975]
id	Denotes an ideal solution
ig	Denotes an ideal gas
l	Denotes the liquid phase
sat	Denotes a saturated value
v	Denotes the vapour phase
*	Denotes a reduced property in the Stockmayer potential model equations
∞	Denotes the infinite pressure state

CHAPTER
1

INTRODUCTION

The science of thermodynamics was born in the nineteenth century of the need to describe the operation of steam engines and to set forth the limits of what they were capable of achieving (Smith et al. [1996]). This origin of the discipline in heat engines is evident in the name, which basically means "movement from heat". However, the thermodynamic laws developed to express the functioning of engines soon found application in many other scientific fields. Indeed, today thermodynamics is an inseparable part of modern engineering and is relevant in all facets of technology.

However, in order to allow practical information to be extracted from the thermodynamic equations developed during the nineteenth and twentieth centuries, experimental data are required. This is especially true in the area of separations technology. Industrially important separation operations include processes such as distillation, absorption and extraction. It is critical for the effective design of such pieces of equipment that accurate and reliable experimental equilibrium data are available. With this data it becomes possible to optimize the running and design of separation processes and, this frequently results in considerable savings in both the capital and running costs of the operation.

A group of organic compounds that have received relatively little attention, despite a variety of economically important uses, are carboxylic acids. These acids are often formed as byproducts of industrial processes and frequently appear in aqueous waste streams. An

example from industry is SASOL, who produce a waste carboxylic acid stream at a substantial rate. To prevent contamination of the environment (particularly the ground water system as the acids are harmful to aquatic organisms), the carboxylic acids must be removed. Once removed, they may be purified and sold at a profit. However, pertinent VLE data are necessary before either the separation or the purification operations may take place. A literature survey revealed that very little data pertaining to carboxylic acids are readily available. When data were found, the measurements had almost invariably been undertaken at atmospheric pressure. This is probably due to the complicated VLE systems formed by the acids, since they associate to a large degree. This gave rise to the main focus of this project, namely, the study of binary carboxylic acid VLE.

The measurements were undertaken on a glass, recirculating VLE still designed by Raal (Raal and Mühlbauer [1998]). The still could be controlled (within fine tolerances) in both isobaric and isothermal modes of operation, via a computer. The experimental setup and method were tested through the measurement (and comparison with consistent literature data - Morachevsky and Zharov [1963] and Joseph et al. [2001]) of the highly non-ideal cyclohexane (1) – ethanol (2) system. Before moving onto the carboxylic acid VLE experiments, the vapour pressures of the following acids were measured: propionic acid, butyric acid, isobutyric acid, valeric acid, isovaleric acid, hexanoic acid and heptanoic acid. Once this initial phase of the project was completed, the binary carboxylic acid systems were measured. Two systems were selected for study (based on the fact that these acids are prevalent in the acid waste stream produced by SASOL): propionic acid (1) – valeric acid (2) and isobutyric acid (1) – valeric acid (2). For both systems, a single isobar was measured at 20 kPa and three isotherms at 120, 130 and 140 °C respectively.

The VLE data then became the focus of a thorough thermodynamic analysis. First, the binary data were regressed using various thermodynamic models and equations of state, and the model parameters acquired. Concurrently, the VLE data were checked for thermodynamic consistency, which provides an indication of the data's quality and reliability. The thermodynamic excess properties were evaluated and the infinite dilution

activity coefficients investigated using the modified Ellis and Jonah [1962] method (Maher and Smith [1979]).

The final portion of this project involved molecular simulations using a Linux-operated Beowulf cluster. Computer simulations are utilized to predict thermodynamic data, as opposed to experimentally measuring the data. The field of molecular simulation is still relatively new and there is a great deal of industrial and academic interest in this area. Certainly, the scope available for research is enormous. In this work, molecular simulation is not the main focus and the purpose of the data presented is to demonstrate that the author was able to effectively manage and run molecular simulations. To this end, a thorough literature review of the subjects pertinent to the simulation of associating systems is presented and a detailed operating procedure discussed. In addition, vapour pressure curves were predicted for pentane and acetic acid and were compared with literature data. A binary VLE system incorporating these two species was also simulated.

CHAPTER
2

CARBOXYLIC ACIDS

The active group in carboxylic acids (which gives rise to their name) is the carboxyl functional group, usually written as: -COOH. The oxidation state of the carbon in this group is +3, which is the highest oxidation state attained by carbon in organic molecules. The carbon atom is able to reach an oxidation state of +4 (CO_2), but this is only brought about by combustion. The carboxyl group contains two strongly polar elements; both the C=O (carbonyl group) and the O-H (alcohol group) are highly polar. This fact allows carboxylic acids to form double hydrogen bonds, resulting in the creation of dimers (refer to Section 2.5 for a more detailed description).

2.1 Nomenclature of Carboxylic Acids

The generally accepted IUPAC nomenclature system names carboxylic acids by removing the "-e" from the end of the alkane with the same number of carbon atoms as the acid and replacing that with "-oic acid". For example, a three-carbon alkane is called propane and the carboxylic acid with three carbons is propanoic acid. According to Bruice [1998], carboxylic acids composed of fewer than seven carbon atoms are regularly referred to by their common (i.e. non-IUPAC) names. Early chemists did not have an established, accepted method for naming compounds and, hence, the names were usually chosen based on a noticeable or distinguishing feature of the chemical. Frequently, this chosen feature described the origin of the species. Consider the following examples:

- formic acid is found in many stinging insects such as ants and bees and its name comes from "formica", the Latin word for "ant"
- acetic acid (vinegar) found its name from the Latin word for "vinegar", viz. "acetum"
- butyric acid is encountered in rancid butter and "butyrum" is Latin for "butter"

Isomers of carboxylic acids also exist and were part of this study. Their names are found in the Table 2-1 in which the names and structures of the acids used in this project are given. The carbonyl carbon is always C^1 for a carboxylic acid. The positions of groups attached to the main alkyl chain of the acid (the so-called substituents) are designated by number, with the numbers increasing from the carbonyl atom.

Table 2-1: Names (common and IUPAC) and structures of the carboxylic acids used in this project.

Common Name	IUPAC Name	Structure
propionic acid	propanoic acid	CH_3-CH_2-COOH
isobutyric acid	2-methyl-propionic acid	$(CH_3)_2$-CH-COOH
butyric acid	butanoic acid	CH_3-$(CH_2)_2$-COOH
isovaleric acid	3-methyl-butanoic acid	$(CH_3)_2$-CH_2-CH-COOH
valeric acid	pentanoic acid	CH_3-$(CH_2)_3$-COOH
caproic acid	hexanoic acid	CH_3-$(CH_2)_4$-COOH
enanthic acid	heptanoic acid	CH_3-$(CH_2)_5$-COOH

2.2 Uses of Carboxylic Acids

As was mentioned briefly in the Introduction (Chapter 1), carboxylic acids have a number of industrial applications. The primary use of carboxylic acids is probably in the production of soaps. Soaps are Na^+ or K^+ salts of long-chain (12 – 20 carbon) carboxylic acids (commonly known as fatty acids) that are formed via the process of saponification. The properties of these soaps are as follows:

- they are amphipathic i.e. they have both hydrophilic (water-loving, polar) and hydrophobic (water-repellant, nonpolar) portions, which is critical for soaps
- they emulsify (suspend) nonpolar materials in water through the formation of micelles
- they form insoluble salts with Ca^{2+} and Mg^{2+} which precipitate out of solution

Various detergents are also manufactured from carboxylic acids. These are synthetic compounds that preserve the vital amphipathic property of the soaps which is crucial for efficient cleaning of grease and other oily or fatty stains while maintaining their water solubility. Examples of such detergents are sodium lauryl sulfate and potassium dodecylbenzenesulfonate (also carboxylic acid salts). In addition to their use as soaps and detergents, the salts are also used as dyes.

Carboxylic acids are also utilized as a raw material in the manufacture of nylon and biodegradable plastics and are particularly beneficial in the pharmaceutical sector where the acids are utilized as chemical intermediates. The food industry benefits greatly from the application of carboxylic acids, since they act as natural buffers and acidulents (food preservatives), for example: sodium propionate and sodium benzoate. Furthermore, the acids are highly attractive biomass products (e.g. from corn starch fermentation). Lastly, a number of exceedingly useful compounds are derived from carboxylic acids, including acyl halides, acid anhydrides, esters and amides.

2.3 Carboxylic Acid Synthesis

A number of chemical reactions may be employed to manufacture carboxylic acids, depending upon the raw material available:

1. The reaction preferentially used in the industrial production of the acids is the oxidation of *primary alcohols* and/or *aldehydes* to form carboxylic acids. An example (Bruice [1998]) is the oxidation of butanol to butanaldehyde (by Na_2CrO_7 and H_2SO_4), which undergoes further oxidation to produce butanoic acid.
2. Acid-catalyzed hydrolysis of *amides*.

3. *Nitriles* may be hydrolyzed to form carboxylic acids by both acids (H^+) and hydroxide ions (OH^-). They are even harder to hydrolyze than amides and the reaction occurs very slowly, even when heated.
4. Several reactions with an *acid anhydride* may be used to produce a carboxylic acid. Reacting an acid anhydride with:
   - an alcohol forms an ester and a carboxylic acid
   - an amine forms an amide and a carboxylic acid
   - water forms two equivalents of a carboxylic acid (e.g. benzoic anhydride with water produces two benzoic acid molecules).
5. *Acyl halides* react with water (hydrolysis) to produce carboxylic acids.
6. Hydrolysis of an *ester* will form a carboxylic acid. These reactions occur slowly and so are usually catalyzed using an acid (H^+). The hydrolysis rate may also be improved through the addition of hydroxide ions (OH^-).
7. Carbonation of *Grignard reagents* (i.e. R-MgX where X represents a halide ion such as Cl^- or Br^-).
8. *Malonic ester synthesis* is an extremely important reaction, since it may be used to produce a carboxylic acid of any desired chain length. The procedure takes its name from the starting material used in the reaction, viz. the diethyl ether of malonic acid. The first two carbons of the acid (including the carboxyl functional group) are provided by the malonic ester, whilst the rest of the carbons forming the carboxylic acid are supplied by the alkyl halide (R-Br) that is introduced in the second step of the reaction.

2.4 Carboxylic Acid Reactions

The first type of reaction that carboxylic acids will undergo is acid/base type reactions. Naturally, if a carboxylic acid is brought into the presence of a base, whether it is a weak base (e.g. sodium carbonate) or a strong base (e.g. sodium hydroxide), a reaction will take place. Carboxylic acids will also react with pure metals (such as sodium or magnesium). All three of these reactions would result in a metal-carboxylate salt (e.g. sodium ethanoate) and water.

Carboxylic acids may also undergo reduction reactions. In Section 2.3, the first method of synthesizing the acids involved oxidation of a primary alcohol and/or aldehyde. It follows that a carboxylic acid may be reduced back to an aldehyde, and finally back to a primary alcohol. However, an extremely powerful reducing agent (such as $LiAlH_4$) is necessary in order to reduce the acid to an aldehyde.

Possibly the most important reaction involving a carboxylic acid is the esterification reaction. In this reaction, a carboxylic acid and an alcohol undergo a condensation reaction (i.e. a water molecule is removed) to produce an ester and water. This is an exceedingly slow reaction and, hence, requires catalysis (and usually heating) to increase the reaction rate. The catalysts that are commonly used are dry hydrogen chloride or concentrated sulfuric acid, although resins (e.g. amberlyst) are popular. Excess alcohol must be used to force the reaction toward the right (i.e. toward the products) since an intermediate is formed during the reaction that has two groups of approximately the same basicity (Bruice [1998]). This reaction is known as the Fischer esterification reaction and is named after Emil Fischer who first discovered it. Other methods are available for forcing the equilibrium to the right, such as removing the products as they are formed (e.g. via distillation).

2.5 Physical Properties of Carboxylic Acids

2.5.1 Acidity

The most significant property of carboxylic acids is, naturally, their acidity. Interestingly, carboxylic acids are both Lewis acids (i.e. donate e^- pairs) and Bronsted-Lowry acids (i.e. donate H^+ ions). They are usually referred to as weak acids, but this is relative to the extraordinarily strong mineral acids such as hydrochloric acid and sulfuric acid. When they are compared to other organic acids, carboxylic acids are in fact rather strong. They are certainly stronger acids than alcohols and phenols. Acid strength is measured by the degree to which the acid dissociates in water. This dissociation may be represented by the following equilibrium equation:

$$RCOOH_{aq} + H_2O_l \leftrightarrow RCOO^-_{aq} + H_3O^+_{aq} \qquad (2\text{-}1)$$

The acid dissociation constant, K_a, is presented below, with most carboxylic acids having dissociation constants of approximately 10^{-5} (compared to 1.2×10^{-2} for sulfuric acid).

$$K_a = \frac{[RCOO^-][H_3O^+]}{[RCOOH]} \approx 10^{-5} \qquad (2\text{-}2)$$

Such a small value for K_a indicates that very little of the acid is ionized in water (i.e. that they are weak acids). However, this is still significantly higher than the acid dissociation constants of phenols (approximately 10^{-10}). The reason that carboxylic acids are stronger than alcohols and phenols is as a result of the two oxygen atoms making up the carboxyl functional group. This structure allows the charge of the dissociated carboxyl anion to be distributed over both C-O bonds in the form of a *resonance structure* (Figure 2-1). This resonance structure has a far greater stability than the single C-O^- bond that occurs in alcohols and phenols. Consequently, the degree of dissociation is higher resulting in increased acidity.

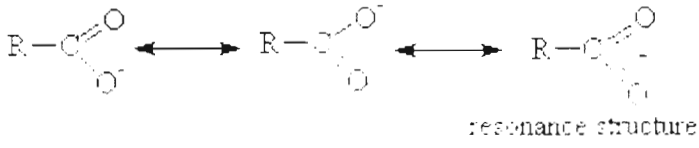

Figure 2-1: The resonance structure of the dissociated carboxyl anion.

2.5.2 Association

The second distinguishing feature of carboxylic acids is the fact that they associate through the formation of hydrogen bonds (see below). This bonding results in the formation of dimers (and sometimes even trimers), which in effect doubles the molecular weight of the acid. This is one of the reasons for the elevated boiling points characteristic of carboxylic acids. The other is that the dimers or trimers may be broken during boiling, which requires extra energy (i.e. heat) in order to sever the strong hydrogen bonds. They consequently boil at far higher temperatures than the alkanes and alcohols with the corresponding number of carbon atoms and/or molecular weights. This is clearly demonstrated in Table 2-2:

Table 2-2: Boiling point comparison between carboxylic acids, alcohols and alkanes.

Compound	Molecular Weight	Boiling Point / °C	Intermolecular Force
butane	58	-1	dispersion
methyl ethyl ether	60	6	weak dipole
propionaldehyde	58	49	strong dipole
1-propanol	60	97	hydrogen bonds
acetic acid	60	118	dimers

The carboxyl group portion of a carboxylic acid is highly polar. The positive charge (δ^+) is located on the hydrogen atom of the O-H group, whilst the negative charge (δ^-) is centered on the double bonded oxygen atom (C=O). Now, the O-H group contains both a hydrogen bond donor ($H^{\delta+}$) and a hydrogen bond acceptor ($O^{\delta-}$), and the C=O group contains a hydrogen bond acceptor. This allows carboxylic acid molecules to hydrogen bond with each other through the formation of double-hydrogen bonds, resulting in the creation of dimers (Figure 2-2). Naturally, the acids are also able to hydrogen bond with other polar species such as water and alcohols. However, in those cases only a single hydrogen bond is formed.

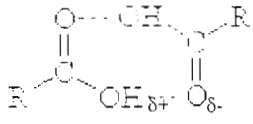

Figure 2-2: Carboxylic acid dimer formed through double-hydrogen bonding.

2.5.3 Solubility

Carboxylic acids are soluble in water up to a carbon-chain length of four carbons. Thereafter, the long, nonpolar, hydrophobic alkyl chain attached to the carboxyl group has an ever increasing effect on the water-solubility of the carboxylic acids, and they become progressively less soluble. The structure of the alkyl group also has an effect on the water-solubility since a branched alkyl group results in greater solubility than a straight-chain

alkyl group. This is as a result of the branching minimizing the contact surface of the non-polar portion of the acid. Hence, isobutyric acid is more soluble than butyric acid. In general, carboxylic acids are slightly more soluble in water than alcohols with an equivalent number of carbon atoms.

As was mentioned in Section 2.2, salts formed by reacting carboxylic acids with bases such as NaOH, NH_4OH and KOH are water-soluble. Hence, practically any length carboxylic acid may be dissolved simply by reacting it with one of the afore-mentioned bases. However, the salts formed from reaction with $Ca(OH)_2$ and $Mg(OH)_2$ are insoluble in water and precipitate out of solution. This provides an efficient means of removing unwanted acids from aqueous solutions.

2.5.4 Miscellaneous

As was noted previously in the section dealing with the uses of carboxylic acids, they are amphipathic molecules. This is as a result of the acids being comprised of a nonpolar, hydrophobic portion (the alkyl chain) and a polar, hydrophilic section (the carboxyl group). This property allows the acids to form extremely effective soaps (Section 2.2). Carboxylic acids are also tremendously resilient to air oxidation. This was also found to be the case in Section 2.3 where extremely powerful oxidizing agents were necessary to synthesize the acids and did not result in further oxidation of the carboxylic acids once they were formed. In fact, extraordinarily harsh conditions, such as burning, are required to oxidize the acids. The products are usually carbon dioxide and water. Since carboxylic acids form such stable oxidation products, they are often found in aqueous waste streams and as byproducts of other processes.

In terms of colour, the short-chain carboxylic acids are clear (i.e. colourless). The acids all have extremely strong and unpleasant odours. Examples are pungent cheese (propionic acid), rancid butter (butyric acid), bile (isobutyric acid) and sweaty, used socks (valeric acid). Fortunately, the carboxylic acids are not exceptionally volatile, with the longer-chain acids have little odour due to their exceedingly low volatilities.

CHAPTER
3

LOW-PRESSURE VAPOUR-LIQUID EQUILIBRIUM

A large number of industrially important separation processes bring two phases into contact. The most widely encountered processes are distillation, absorption and extraction. In general, the two phases involved in the separation process are vapour and liquid, although liquid-liquid, liquid-solid and vapour-solid systems do occur. Until equilibrium between the two phases is achieved, mass transfer will occur between the two phases with the transfer rate dependent on the system's departure from equilibrium.

Equilibrium is a static condition, in which the macroscopic properties of the system remain constant with respect to time i.e. the chemical potentials of all species in each phase are equal (this is the criterion for phase equilibrium; refer to Section 3.1). Smith et al. [1996] state that in engineering practice, the assumption of equilibrium is justified when it leads to results of satisfactory accuracy. Vapour-liquid equilibrium (VLE) depends on the nature of the chemical species involved, their respective compositions in the two phases, system temperature and overall system pressure. According to Van Ness and Abbott [1997] VLE relationships are needed in the solution of many engineering problems. Often, these problems involve multi-component systems, the VLE of which are difficult and, for the most part, impractical to measure. However, by measuring binary VLE data for the species involved in the multi-component process, the multi-component phase equilibrium properties can be predicted (Raal and Mühlbauer [1998]). Theoretical treatment of this binary data allows calculation of the excess Gibbs energy, system temperature and pressure

over the entire composition range. Thermodynamics provides the tools and techniques that allow such calculations.

This chapter presents a review of the theoretical aspects and techniques of low-pressure VLE computation, including the methods proposed for determining fugacity and activity coefficients. In addition, the analysis and regression of the experimental data are appraised. This includes the gamma-phi formulation of VLE and the associated activity coefficient models, and also the direct (phi-phi) method of modeling VLE data using equations of state. Thermodynamic consistency (and the associated tests pertinent to the project), infinite dilution activity coefficients and excess thermodynamic properties are also discussed. The following excellent texts are suggested to the reader if a more detailed review of low-pressure thermodynamics is desired: Walas [1985], Smith et al. [1996] and Raal and Mühlbauer [1998].

3.1 The Criterion for Phase Equilibrium

Consider any closed system: the temperature and pressure of the system are related to the Gibbs energy by the following expression:

$$d(nG) = (nV)dP - (nS)dT \tag{3-1}$$

If we then apply Equation (3-1) to a fluid consisting of a single, nonreactive phase (i.e. the composition of the closed system does not fluctuate), we can deduce by inspection that

$$\left[\frac{\partial(nG)}{\partial P}\right]_{T,n} = nV \tag{3-2}$$

and

$$\left[\frac{\partial(nG)}{\partial T}\right]_{P,n} = -nS \tag{3-3}$$

where n indicates that a constant number of moles of all chemical species exist within the closed system.

If the more general case of a single-phase, open system is now considered the Gibbs energy remains a function of pressure and temperature. However, material from the surroundings may now enter the system, and similarly, material existing within the system may escape into the surroundings. Thus, the matter within the open system is in a constant state of flux. Consequently, the Gibbs energy is now also a function of n_i, the number of moles of a particular species i that are present in the system. This may be written as follows:

$$nG = g(P, T, n_i) \tag{3-4}$$

Taking the total differential of nG and substituting Equations (3-2) and (3-3) into the resulting expression produces:

$$d(nG) = (nV)dP - (nS)dT + \sum_i \left[\frac{\partial(nG)}{\partial n_i}\right]_{P,T,n_i} dn_i \tag{3-5}$$

The term $\left[\frac{\partial(nG)}{\partial n_i}\right]_{P,T,n_i}$ in the above equation is of particular significance and is referred to as the chemical potential of species i. Chemical potential is given the symbol μ. Hence, Equation (3-5) may be re-written as:

$$d(nG) = (nV)dP - (nS)dT + \sum_i \mu_i dn_i \tag{3-6}$$

Equation (3-6) is commonly known as the fundamental property relation.

The criterion for phase equilibrium is obtained by writing the fundamental property relation for a closed system consisting of two phases, α and β, that are in equilibrium. Each phase may be considered as an open system (within the overall closed system) with respect to the second phase, and therefore there is a constant transfer of matter between the phases. Assuming the temperature and pressure to be constant throughout the closed system at equilibrium, the following equations may be written for each phase:

$$d(nG)^{\alpha} = (nV)^{\alpha} dP - (nS)^{\alpha} dT + \sum_i \mu_i^{\alpha} dn_i^{\alpha} \tag{3-7}$$

$$d(nG)^{\beta} = (nV)^{\beta} dP - (nS)^{\beta} dT + \sum_{i} \mu_i^{\beta} dn_i^{\beta} \tag{3-8}$$

Summing Equations (3-7) and (3-8), the total change in the Gibbs energy of the system is obtained:

$$d(nG) = (nV)dP - (nS)dT + \sum_{i} \mu_i^{\alpha} dn_i^{\alpha} + \sum_{i} \mu_i^{\beta} dn_i^{\beta} \tag{3-9}$$

Each total system property (e.g. nG) is found using the following relation:

$$nM = (nM)^{\alpha} + (nM)^{\beta} \tag{3-10}$$

Acknowledging that the overall system is closed, Equation (3-1) must be valid. Combining this equation with Equation (3-9) leads (at equilibrium) to the following summation:

$$\sum_{i} \mu_i^{\alpha} dn_i^{\alpha} + \sum_{i} \mu_i^{\beta} dn_i^{\beta} = 0 \tag{3-11}$$

Since no chemical reaction is occurring (the system is non-reactive), the changes dn_i^{α} and dn_i^{β} are purely as a result of mass transfer between the phases. Conservation of mass demands that $dn_i^{\alpha} = -dn_i^{\beta}$. Hence, Equation (3-11) becomes:

$$\sum_{i} (\mu_i^{\alpha} - \mu_i^{\beta}) dn_i^{\alpha} = 0 \tag{3-12}$$

The quantities dn_i^{α} are arbitrary and independent. Therefore, to satisfy the right-hand side of Equation (3-12), each term in parentheses must separately be zero. Hence

$$\mu_i^{\alpha} = \mu_i^{\beta} \tag{3-13}$$

It is a simple matter to extend (and generalize) this result to include more than two phases by successively considering phase pairs. For π phases consisting of N chemical species, the general result is:

$$\mu_i^{\alpha} = \mu_i^{\beta} = \ldots = \mu_i^{\pi} \tag{3-14}$$

where $i = 1, 2, \ldots, N$.

Thus, the criterion for phase equilibrium of a system consisting of multiple phases at the same temperature and pressure is that the chemical potential of each species must be the same in all phases. This proof is laid out in greater detail in Appendix 1B of Raal and Mühlbauer [1998].

3.2 Fugacity and Fugacity Coefficient

As was shown in Section 3.1, the chemical potential serves as a vital means of determining criteria for phase equilibria. Unfortunately, however, the chemical potential is an unwieldy quantity with which to work, since it relies by definition upon the quantities internal energy and entropy (for which absolute values are not known). As a result, no absolute values for chemical potential are available. This does not prevent the use of the chemical potential quantity, however, a more physically meaningful quantity, called the *fugacity*, f_i, (units of pressure), was introduced by G. N. Lewis (Smith et al. [1996]). Fugacity can be related to chemical potential (at constant temperature) by manipulation of the following equation (at constant temperature):

$$\overline{G}_i = \Gamma_i(T) + RT \ln f_i \tag{3-15}$$

where the partial molar Gibbs energy is given by

$$\overline{G}_i = \left[\frac{\partial(nG)}{\partial n_i}\right]_{T,P,n_j} \tag{3-16}$$

Therefore, by definition (refer to Section 3.1):

$$\mu_i = \overline{G}_i \tag{3-17}$$

Comparing Equations (3-17) and (3-15) results in the following relation between chemical potential and fugacity:

$$\mu_i = \Gamma_i(T) + RT \ln f_i \tag{3-18}$$

This equation leads to another (equally general criterion for phase equilibrium – refer to Section 3.1). $\Gamma_i(T)$ is dependent on temperature only, and since all phases are at a common temperature (because the closed system is at equilibrium), substitution of Equation (3-18) into Equation (3-14) yields directly:

$$f_i^{\alpha} = f_i^{\beta} = \ldots = f_i^{\pi} \tag{3-19}$$

for $i = 1, 2, \ldots, N$.

For an ideal gas, we have the relation:

$$G_i^{ig} = \Gamma_i(T) + RT \ln P \tag{3-20}$$

where $\Gamma_i(T)$ is the same integration constant as was introduced in Equation (3-15) and remains a function of temperature only. Incorporating the concept of fugacity for a real fluid:

$$G_i = \Gamma_i(T) + RT \ln f_i \tag{3-21}$$

Writing Equations (3-20) and (3-21) for the same temperature and pressure and subtracting yields:

$$G_i - G_i^{ig} = RT \ln \frac{f_i}{P} \tag{3-22}$$

The left-hand side of Equation (3-22) is referred to as the residual Gibbs energy, G^R, and the ratio f_i/P is termed the *fugacity coefficient* of component i, ϕ_i. Equations (3-20) through (3-22) apply to a pure species. For a species in solution we may write an expression analogous to Equation (3-18):

$$\mu_i = \Gamma_i(T) + RT \ln \hat{f}_i \tag{3-23}$$

where the *fugacity of a species in solution*, $\hat{f}_i$, replaces the pure species fugacity in the expression for chemical potential. From Equation (3-19) we obtain:

$$\hat{f}_i^{\alpha} = \hat{f}_i^{\beta} = \ldots = \hat{f}_i^{\pi} \tag{3-24}$$

Considering this equation in the light of vapour-liquid equilibria leads to:

$$\hat{f}_i^{v} = \hat{f}_i^{l} \tag{3-25}$$

with $i = 1, 2, \ldots, N$ in both equations. Equation (3-25) is of no great benefit until the vapour and liquid phase fugacities are related to experimental quantities such as pressure, temperature and composition. The fugacity coefficient has already been introduced, and this definition is now extended to include the *fugacity coefficient of a species i in solution*, $\hat{\phi}_i$. Another concept that must be introduced at this stage is the *activity coefficient of a species i in solution*, γ_i (the activity coefficient is covered in more detail in Section 3.3). The vapour phase fugacity may be expressed in terms of the fugacity coefficient:

$$\hat{f}_i^{v} = y_i \hat{\phi}_i P \tag{3-26}$$

and the activity coefficient is related to the liquid phase fugacity:

$$\hat{f}_i^{l} = x_i \gamma_i f_i \tag{3-27}$$

Considering a phase change from a saturated liquid to a saturated vapour at saturated pressure and constant temperature, the following expression results from Equation (3-19):

$$f_i^{v} = f_i^{l} = f_i^{sat} \tag{3-28}$$

The corresponding fugacity coefficient at saturated pressure is:

$$\phi_i^{sat} = \frac{f_i^{sat}}{P_i^{sat}} \tag{3-29}$$

This leads to the following relation:

$$\phi_i^{v} = \phi_i^{l} = \phi_i^{sat} \tag{3-30}$$

Now, differentiating Equation (3-21) results in:

$$dG_i = RTd \ln f_i \tag{3-31}$$

Also, the fundamental property relation for Gibbs energy is $dG = VdP - SdT$. Writing this equation for a particular species i in a solution at constant temperature and composition yields:

$$dG_i = V_i dP \tag{3-32}$$

Combining Equations (3-31) and (3-32) to eliminate dG_i gives:

$$d \ln f_i = \frac{V_i}{RT} dP \tag{3-33}$$

Integrating (isothermally) from the initial state of a saturated liquid to the final state of a compressed liquid at pressure P produces the following expression:

$$\ln \frac{f_i}{f_i^{sat}} = \frac{1}{RT} \int_{P_i^{sat}}^{P} V_i dP \tag{3-34}$$

V_i represents the liquid molar volume. At temperatures well below the critical temperature, T_c, the liquid molar volume is a weak function of pressure and hence can be considered approximately constant when evaluating the integral in Equation (3-34). V_i is assumed to be constant at the saturated liquid molar volume, V_i^l. Hence, Equation (3-34) becomes:

$$\ln \frac{f_i}{f_i^{sat}} = \frac{V_i^l (P - P_i^{sat})}{RT} \tag{3-35}$$

Re-arranging to solve for f_i and substituting for f_i^{sat} from Equation (3-29) finally yields:

$$f_i = \phi_i^{sat} P_i^{sat} \exp\left[\frac{V_i^l (P - P_i^{sat})}{RT}\right] \tag{3-36}$$

The exponential term in Equation (3-36) is commonly referred to as the *Poynting correction factor*. Combining Equations (3-26), (3-27) and (3-36) gives the expression:

$$y_i \Phi_i P = x_i \gamma_i P_i^{sat} \tag{3-37}$$

where

$$\Phi_i = \frac{\hat{\phi}_i}{\phi_i^{sat}} \exp\left[\frac{-V_i^l (P - P_i^{sat})}{RT}\right] \tag{3-38}$$

Equation (3-37) is a tremendously useful general equation relating the liquid and vapour phases and is the basis for a great deal of the low-pressure VLE theory. It is significant to observe that by setting Φ_i and γ_i equal to one (i.e. assuming the system is completely ideal – the vapour phase represented by an ideal gas and the liquid phase by an ideal solution), Equation (3-37) reverts to an equation that expresses Raoult's Law. Raoult's Law is the simplest possible VLE relation and, therefore, fails to provide an accurate interpretation of observed behaviour for the majority of systems. Smith et al. [1996] report that at low to moderate pressures, the Poynting correction factor differs from unity by only a few parts per thousand and, thus, its omission introduces negligible error. However, this assumption is not satisfactory for systems that contain polar molecules (such as carboxylic acids).

3.2.1 Calculating the Fugacity Coefficients from the Virial Equation of State

A number of methods exist for determining the fugacity coefficients of species in gas mixtures. At low to moderate pressures, most assume that the coefficients may be evaluated by presuming that the vapour phase is adequately described by the truncated (at the second term), generalized, pressure explicit form of the virial equation of state:

$$Z = 1 + \frac{BP}{RT} \tag{3-39}$$

The quantity Z is known as the *compressibility factor* and is equal to one for an ideal gas. The *second virial coefficient*, B, is a function of temperature and composition (for mixtures) and this is reflected in the following rigorous mixing rule based on statistical mechanics:

$$B_{mixture} = \sum_i \sum_j y_i y_j B_{ij} \tag{3-40}$$

where B_{ij} represents the pure component and mixture second virial coefficients and is a function of temperature only. Note that $B_{ij} = B_{ji}$ since the coefficient typifies a specific molecular interaction between species i and j. Tsonopoulos [1974] states that the effect of vapour-phase imperfection can be reliably calculated using only the second virial coefficient B of the pure components and cross coefficients for each binary. The assumption that the truncated virial equation of state characterizes the vapour phase of a VLE system results in a generalized modification of Equation (3-38):

$$\Phi_i = \exp\left[\frac{(B_{ii} - V_i^l)(P - P_i^{sat}) + P y_j^2 \delta_{ij}}{RT}\right] \tag{3-41}$$

Here $\delta_{ij} = 2B_{ij} - B_{ii} - B_{jj}$.

Second virial coefficients (for pure components, B_{ii}, and mixtures, B_{ij}) may be determined experimentally and are available in various compilations. Examples of such compilations are those of Cholinski et al. [1986] and Dymond and Smith [1980]. However, it is often impossible to obtain experimental values for the species of interest (B_{ij} generally presents the greatest difficulty), or at the necessary temperature. Hence, it becomes essential that a satisfactory correlation be found and used to determine the second virial coefficients. This is particularly useful when a computer programme is utilized in order to regress VLE data. Several correlations that have found widespread popularity are discussed below.

3.2.1.1 The Pitzer-Curl Correlation

Pitzer and Curl [1957] proposed a correlation of the form:

$$\frac{BP_c}{RT_c} = B^0 + \omega B^1 \tag{3-42}$$

The symbol, ω, represents the *acentric factor* of a species, a parameter introduced by Pitzer and co-workers. The acentric factor is fully described by Pitzer et al. [1955] and is treated in more detail later in this work in Section 9.2.2. The parameters B^0 and B^1 found in Equation (3-42) are functions of reduced temperature only, $T_r = T/T_c$, and may be calculated from the following equations:

$$B^0 = 0.083 - \frac{0.422}{T_r^{1.6}} \tag{3-43}$$

and

$$B^1 = 0.139 - \frac{0.172}{T_r^{4.2}} \tag{3-44}$$

Pure component second virial coefficients may be easily determined using Equation (3-42), however, to generalize the expression to include cross coefficients the following equation is suggested by Prausnitz et al. [1986]:

$$B_{ij} = \frac{RT_{cij}}{P_{cij}}(B^0 + \omega_{ij} B^1) \tag{3-45}$$

To allow calculation of the cross coefficient parameters T_{cij}, P_{cij} and ω_{ij}, the following empirical combining rules were proposed by Prausnitz and co-workers [1986]:

$$\omega_{ij} = \frac{\omega_i + \omega_j}{2} \tag{3-46}$$

$$T_{cij} = \sqrt{(T_{ci} T_{cj})}(1 - k_{ij}) \tag{3-47}$$

and

$$P_{cij} = \frac{Z_{cij} RT_{cij}}{V_{cij}} \tag{3-48}$$

where

$$Z_{cij} = \frac{Z_{ci} + Z_{cj}}{2} \tag{3-49}$$

and

$$V_{cij} = \left(\frac{V_{ci}^{1/3} + V_{cj}^{1/3}}{2} \right)^3 \tag{3-50}$$

The parameter k_{ij}, introduced in Equation (3-47) is an empirical interaction parameter that is particular to a specific molecular pairing, *i-j*. When species *i* and *j* are chemically similar (as was the case in this project) and when $i = j$, k_{ij} is set equal to zero.

3.2.1.2 The Tsonopoulos Correlation

The Tsonopoulos correlation [1974] uses a modified form of the Pitzer-Curl correlation (Section 3.2.1.1). The correlation is capable of calculating second virial coefficients for both non-polar and polar compounds, although for species that exhibit hydrogen bonding, two parameters are required instead of one. For non-polar gases, Tsonopoulos suggests:

$$\frac{BP_c}{RT_c} = f^{(0)}(T_r) + \omega f^{(1)}(T_r) \tag{3-51}$$

where

$$f^{(0)}(T_r) = 0.1445 - \frac{0.330}{T_r} - \frac{0.1385}{T_r^2} - \frac{0.0121}{T_r^3} - \frac{0.000607}{T_r^8} \tag{3-52}$$

and

$$f^{(1)}(T_r) = 0.0637 + \frac{0.331}{T_r^2} - \frac{0.423}{T_r^3} - \frac{0.008}{T_r^8} \tag{3-53}$$

Polar compounds are typified by the effect of electrostatic forces between the molecules of the compound. This results in these compounds having a non-zero dipole moment. An additional parameter is included in the modified Pitzer-Curl equation, Equation (3-51):

$$\frac{BP_c}{RT_c} = f^{(0)}(T_r) + \omega f^{(1)}(T_r) + f^{(2)}(T_r) \tag{3-54}$$

where the last term incorporates the polar effects and is given by

$$f^{(2)}(T_r) = \frac{a'}{T_r^6} \tag{3-55}$$

For hydrogen bonding compounds, dimerization in the vapour phase results in an increased complexity in the polar contribution to the second virial coefficient:

$$f^{(2)}(T_r) = \frac{a'}{T_r^6} - \frac{b'}{T_r^8} \tag{3-56}$$

The parameters a' and b' are functions of the dipole moment and differ for different compounds. They are found by fitting Equations (3-55) and (3-56) to experimental B data.

The mixing rules for T_{cij} and ω_{ij} are identical to those given for the Pitzer-Curl correlation in Section 3.2.1.1. However, the mixing rule for P_{cij} differs significantly:

$$P_{cij} = \frac{4T_{cij}(P_{ci}V_{ci}/T_{ci} + P_{cj}V_{cj}/T_{cj})}{(V_{ci}^{1/3} + V_{cj}^{1/3})^3} \tag{3-57}$$

For polar/non-polar binaries, a_{ij} and b_{ij} are set equal to zero (i.e. it is assumed that B_{ij} has no polar term). In the case of polar/polar binaries, B_{ij} is determined by assuming that the polar term of B_{ij} can be found using $a_{ij} = 0.5(a_i + a_j)$ and $b_{ij} = 0.5(b_i + b_j)$.

3.2.1.3 The Hayden and O'Connell Correlation

The Hayden and O'Connell method for determining second virial coefficients has found widespread use due to its applicability to a large range of compounds, including both polar and non-polar chemicals. According to Hayden and O'Connell [1975], the virial coefficient can be considered the sum of two interactions:

$$B_{ij} = B_{ij}^{F} + B_{ij}^{D} \tag{3-58}$$

where B_{ij}^{F} is the interaction due to so-called "free" molecules (i.e. molecules in which the physical forces are weak), for both non-polar and polar compounds, and B_{ij}^{D} represents the interactions of those molecules in which substantial chemical forces occur. B_{ij}^{D} consists of the contribution to B of "metastable", "bound" and "dimerized" molecules – i.e. those compounds in which chemical forces predominate. The calculation procedure is complex and will thus not be set out in full here. The procedure is given in detail in Appendix A of Prausnitz et al. [1980]. Several parameters are required for each species before the Hayden and O'Connell method may be implemented. These include pure component properties such as critical pressure P_c, critical temperature T_c, mean radius of gyration, R_d, dipole moment, μ, as well as the solvation and association parameters, η. The values for these parameters that were used in this work are presented in Appendix A. For the most part, they were obtained from literature sources such as Prausnitz et al. [1980], Reid et al. [1988] and the Dortmund Data Bank (DDB). The dipole moments were acquired from the extensive compilation of McClellan [1974]. An alternative method for determining dipole moments not listed by McClellan [1974] is suggested by Hayden and O'Connell [1975]: the bond addition method of Smyth [1955]. Values for the mean radius of gyration could not be found in the literature and, hence, the group contribution method suggested by Reid et al. [1977] was used to determine these parameters. The mean radius of gyration is calculated using a property known as the *parachor*, P', which is determined using the group contribution method mentioned above. Harlacher and Braun [1970] described the relationship between the parachor and the mean radius of gyration by the equation:

$$P' = 50 + 7.6R_d + 13.75R_d^2 \tag{3-59}$$

Thus, once the value for the parachor has been determined for a particular species, it is a simple matter of solving the quadratic Equation (3-59) for R_d. The positive root of the equation is clearly the real value of R_d. The association and solvation parameters were found from the tables given by Prausnitz et al. [1980]. Prausnitz et al. [1980] suggested that if the exact system in question cannot be found in the tables, then the values for a

chemically similar system should be taken. Therefore, the values given for the propionic acid and acetic acid system were used. To determine the liquid molar volume, the equation proposed by Rackett [1970] was employed:

$$V_i = V_{ci} Z_{ci}^{(1-T_r)^{0.2857}} \tag{3-60}$$

The critical molar volume, V_{ci}, and critical compressibility factor, Z_{ci}, were also obtained from the DDB.

Other analytical correlations also exist for determining second virial coefficients, but were not considered in this project as those described above were sufficiently accurate. These include those of Black [1958], O'Connell and Prausnitz [1967] and Kreglewski [1969].

3.2.2 Calculating the Fugacity Coefficients from Chemical Theory

Vapour phase divergence from the behaviour of an ideal gas is represented by fugacity coefficients (Prausnitz [1969]). Nothnagel et al. [1973], introduced a correlation for determining fugacity coefficients by applying the chemical theory of vapour imperfections. The Nothnagel correlation was designed to deal with dimerization in the vapour phase due to hydrogen bonding by incorporating chemical theory. The chemical theory has been used previously to calculate fugacity coefficients for systems involving carboxylic acids (Tsonopoulos and Prausnitz [1970]). In compounds for which strong intermolecular hydrogen bonding exists, dimerization will occur. This process may be viewed in a similar manner to a chemical reaction:

$$i + j \leftrightarrow ij \tag{3-61}$$

Here, the dimer is represented by the complex ij, and i and j are the individual molecules. To complete the calculation two assumptions are made (Prausnitz et al. [1980]): firstly, to determine the true species fugacity coefficients, the Lewis fugacity rule is employed, and secondly, B_{ii}^{V} is taken to be the second virial coefficient for the monomer and dimer of

species i whilst B_{ii}^{V} is used for the second virial coefficient of dimer ij. The equation of chemical equilibrium is written as follows (according to Prausnitz et al. [1980]):

$$K_{ij} = \frac{1}{P}\frac{z_{ij}}{z_i z_j}\frac{\phi_{ij}^{*}}{\phi_i^{*}\phi_j^{*}} = \frac{-B_{ij}^{D}(2-\delta_{ij})}{RT} \tag{3-62}$$

where K_{ij} is the equilibrium constant, z is the true mole fraction of the species in equilibrium, P is the system pressure and ϕ^{*} is the true species fugacity coefficient. Note that δ_{ij} is set equal to zero for $i \neq j$ and to one for $i = j$. Nothnagel et al. [1973] show that ϕ_i may be calculated from:

$$\phi_i = \frac{z_i \phi_i^{*}}{y_i} \tag{3-63}$$

Here, y_i represents the apparent vapour phase mole fraction of species i. As was mentioned above, the Lewis fugacity rule is assumed to be applicable and, hence:

$$\ln \phi_i^{*} = \frac{PB_i^{V}}{RT} \tag{3-64}$$

The Hayden and O'Connell method (refer to Section 3.2.1.3) is utilized in order to calculate the "free" and "dimerized" contributions to the second virial coefficient, B_i^{V} and B_{ij}^{D} respectively. Once B_{ij}^{D} has been determined, the equilibrium constant may be obtained from Equation (3-62). The desired fugacity coefficients, ϕ_i and ϕ_j, are then calculated by solving iteratively over Equations (3-62) to (3-64) with the constraint that the overall sum of z_i, z_j and z_{ij} must be equal to one.

3.3 Activity Coefficient

The liquid phase activity coefficient was introduced in Section 3.2 as a means of representing the departure of a solution from ideality. According to Prausnitz et al. [1980],

the activity coefficient is completely defined only if the standard-state fugacity is clearly specified. The definition of the standard-state fugacity is, however, arbitrary and may vary, but should be chosen such that the activity coefficients have a numerical value of approximately one. The temperature used to define the standard-state fugacity must be the equilibrium solution temperature, and composition and pressure must also be selected. The composition and pressure may be chosen at will and are specified for calculation expediency.

The liquid phase activity coefficient is integrally related to the excess Gibbs energy (see Equation (3-70) below). Walas [1985] states that activity coefficients are closely related to various excess properties. In addition, Gess et al. [1991] note that to obtain some physical sense of the activity coefficient, the concept of excess properties must be introduced. Excess properties refer to a solution mixture and are the difference between the true value of a certain property of the solution and the value attributed to an ideal solution under the same conditions. Excess thermodynamic properties are discussed in more detail later in the chapter (Section 3.6).

Equation (3-27) may be re-written to provide a convenient definition for the activity coefficient of species *i*:

$$\gamma_i = \frac{\hat{f}_i}{x_i f_i} \tag{3-65}$$

Also, Equation (3-23) may equivalently be written in terms of Gibbs energy:

$$\overline{G}_i = \Gamma_i(T) + RT \ln \hat{f}_i \tag{3-66}$$

The Lewis/Randall rule states that $\hat{f}_i^{id} = x_i f_i$ and therefore, for an ideal solution Equation (3-66) becomes:

$$\overline{G}_i^{id} = \Gamma_i(T) + RT \ln x_i f_i \tag{3-67}$$

Subtracting Equation (3-67) from Equation (3-66) leads to an expression for the partial molar excess Gibbs energy:

$$\overline{G}_i^E = RT \ln \gamma_i \tag{3-68}$$

Now, the fundamental excess-property relation (see below) is an equation that expresses the relationship between the various excess thermodynamic properties:

$$d\left(\frac{nG^E}{RT}\right) = \frac{nV^E}{RT}dP - \frac{nH^E}{RT^2}dT + \sum_i \frac{\overline{G}_i^E}{RT}dn_i \tag{3-69}$$

Combining this equation with Equation (3-68) leads to an alternative form of the fundamental excess-property relation in which the excess properties are shown to be related to the activity coefficient (as was stated above):

$$d\left(\frac{nG^E}{RT}\right) = \frac{nV^E}{RT}dP - \frac{nH^E}{RT^2}dT + \sum_i \ln \gamma_i dn_i \tag{3-70}$$

Since the natural logarithm of the activity coefficient is a partial molar property with respect to G^E:

$$\ln \gamma_i = \left[\frac{\partial(nG^E/RT)}{\partial n_i}\right]_{P,T,n_j} \tag{3-71}$$

This equation is significant as it allows γ_i to be calculated from an expression for the excess Gibbs energy as a function of composition. In addition, from the properties of a partial molar quantity, the following holds for a binary mixture:

$$\ln \gamma_1 = \frac{G^E}{RT} + \frac{x_2 d(G^E/RT)}{dx_1} \tag{3-72}$$

$$\ln \gamma_2 = \frac{G^E}{RT} - \frac{x_1 d(G^E/RT)}{dx_1} \tag{3-73}$$

Furthermore, the relationship between the excess Gibbs energy and the activity coefficient may also be expressed (again, due to the fact that $\ln\gamma_i$ is a partial property with respect to G^E) as follows:

$$\frac{G^E}{RT} = \sum_i x_i \ln \gamma_i \tag{3-74}$$

It is important to note that G^E is zero for $x_1 = 1$ and $x_1 = 0$.

The excess-property equations discussed above are significant because V^E, H^E and γ_i may all be determined experimentally. Also, the molar excess Gibbs energy is a function of measurable system properties such as temperature, pressure and composition, which are experimentally accessible. Another important equation relating excess-properties to the activity coefficient should be discussed at this point, and this is the *Gibbs-Duhem equation*:

$$\sum_i x_i d\ln\gamma_i = \frac{\overline{V}_i^E}{RT}dP - \frac{\overline{H}_i^E}{RT^2}dT \tag{3-75}$$

Interestingly, at constant temperature and pressure this relation reduces to the following useful form:

$$\sum_i x_i d\ln\gamma_i = 0 \tag{3-76}$$

The Gibbs-Duhem equation plays an integral role in determining the thermodynamic consistency of VLE data. Thermodynamic consistency testing is discussed in greater detail later in this chapter (Section 3.7).

3.4 Low Pressure VLE Data Interpretation

Two different methods for regressing low pressure VLE data exist and were used to analyze the VLE data measured in this project. The first method is known as the *combined method* (i.e. the gamma-phi formulation of VLE) and is commonly used in the reduction of

low pressure data. The second method that was utilized was the *direct (phi-phi) method*. In the combined method the vapour phase non-idealities are determined by using an equation of state to calculate the fugacity coefficients, while the liquid phase deviations from ideality are calculated using an activity coefficient model. The direct method differs in that fugacity coefficients (from an equation of state) are used to describe non-idealities in both the vapour and liquid phases. Both methods are discussed below and the procedure followed in each case is outlined. The difficulties in correlating and predicting with either method are also explored.

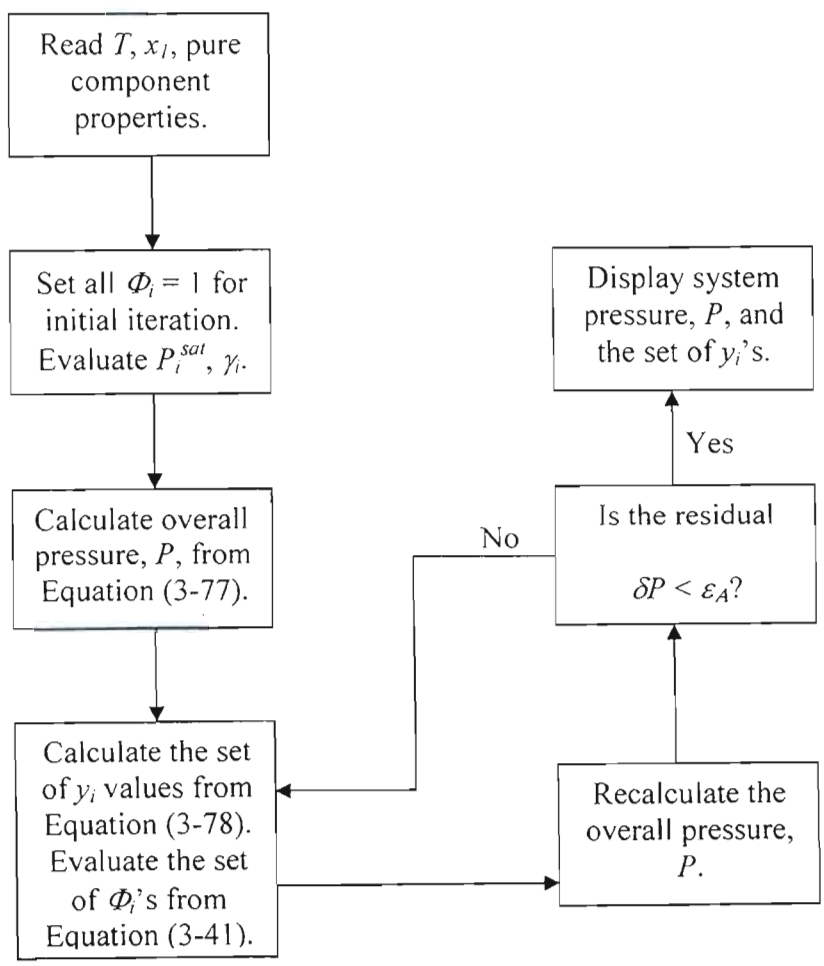

Figure 3-1: Flow diagram for bubblepoint pressure iteration (combined method).

Different calculation procedures are necessary depending on whether the VLE data are isobaric or isothermal. If the data are isothermal, values for the pressure and vapour composition are calculated (bubblepoint pressure iteration, see Figures 3-1 and 3-3) whereas isobaric data necessitates calculation of the temperature and vapour composition (bubblepoint temperature iteration, see Figures 3-2 and 3-4) for each experimental point.

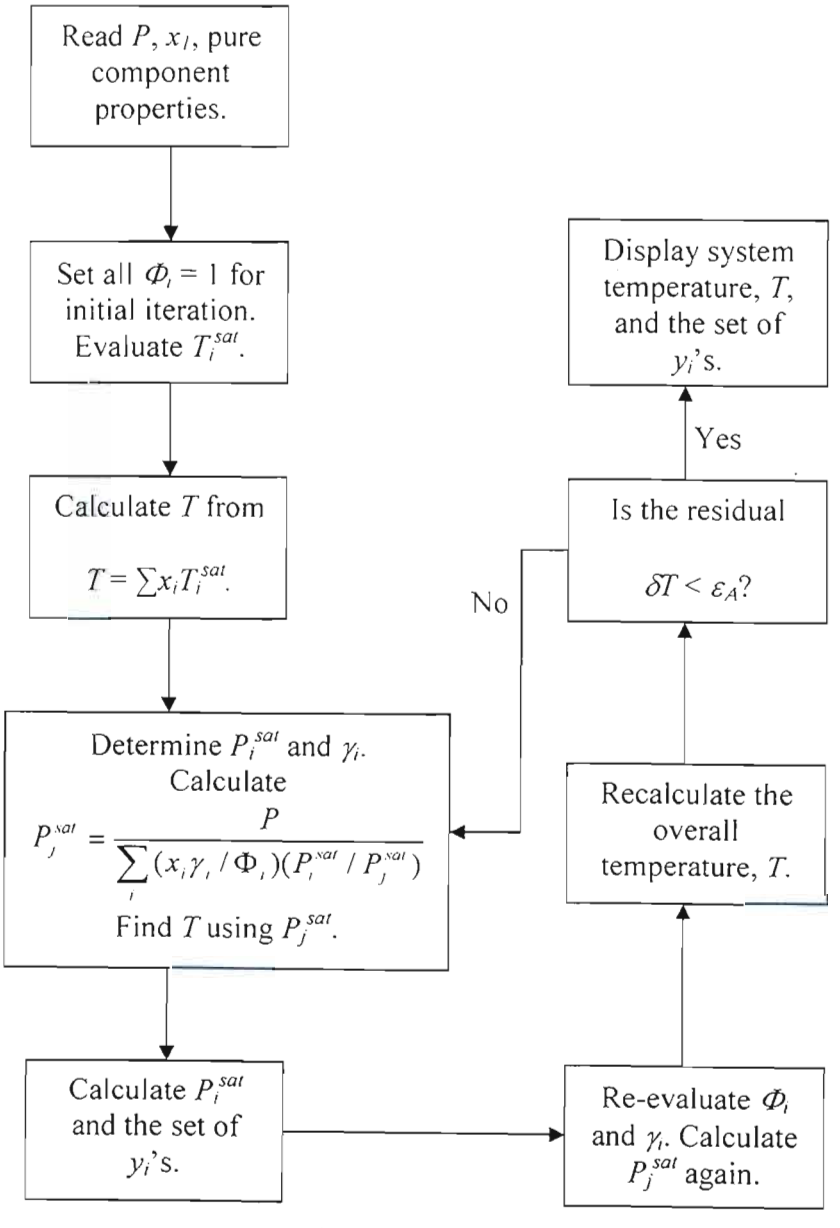

Figure 3-2: Flow diagram for bubblepoint temperature iteration (combined method).

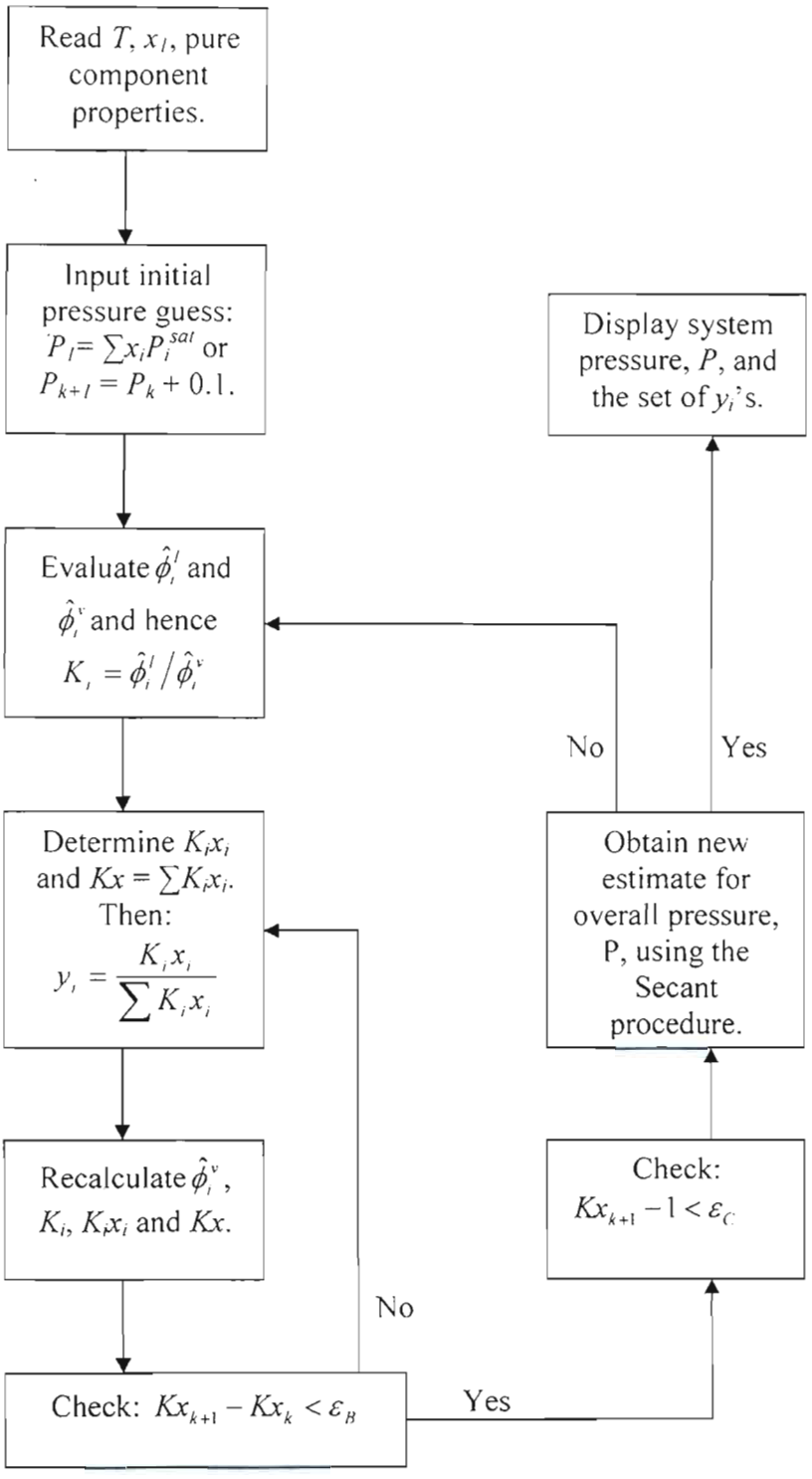

Figure 3-3: Flow diagram for bubblepoint pressure iteration (direct method).

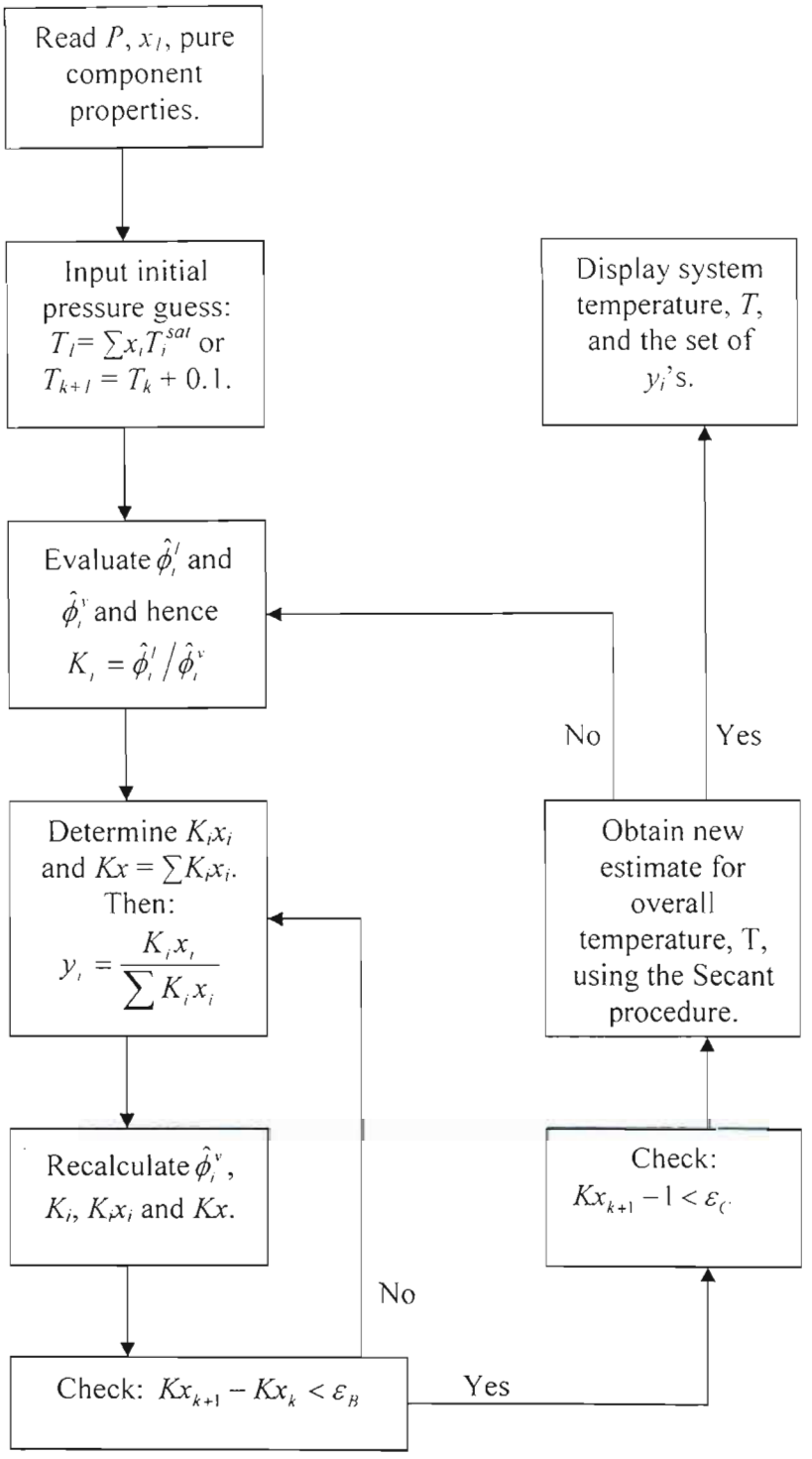

Figure 3-4: Flow diagram for bubblepoint temperature iteration (direct method).

Hence, a set of data incorporating only *P-x* or *T-x* values (at a set temperature or pressure respectively) is sufficient to enable determination of the activity coefficient model parameters. However, it is preferable that the vapour phase mole fractions are also measured to permit thermodynamic consistency testing (Section 3.7). An additional complication exists for isobaric data in that the system temperature is not constant and, thus, the temperature dependence of the model parameters and system properties must be taken into account.

3.4.1 The Combined (Gamma-Phi) Method

This method relies chiefly upon liquid phase activity coefficient models such as the Wilson, NRTL and UNIQUAC equations (discussed below) in order to represent the experimental VLE data. In his discussion of activity coefficient models, Walas [1985] notes that many equations have been proposed for the purpose of correlating activity coefficients with composition (and to a lesser extent, temperature). Usually the composition is expressed as a mole fraction (x_i), but when the system components differ significantly in size or chemical nature then volume fractions or molecular surface fractions may be used instead. Since a specific model is sometimes better suited to a particular system, it is common practice to analyze a system with more than one model to determine which provides the best fit of the data. At present, up to nine correlations for the liquid phase activity coefficient find frequent use in the modeling of VLE data. However, in this work only the three most widely utilized models will be used: the Wilson, NRTL (Non-Random Two Liquid) and UNIQUAC (Universal Quasi-Chemical Theory) equations. For a comprehensive comparison of at least five of these correlations, Walas [1985] suggests consulting the DECHEMA Vapour-Liquid Data Collection (Gmehling and Onken [1977-1982]). For a detailed review of these methods the following excellent texts should be consulted: Walas [1985] and Raal and Mühlbauer [1998].

No matter which model is selected, the liquid phase activity coefficients are determined from the relationship between the molar excess Gibbs energy and the liquid composition. Therefore, an appropriate model for the excess Gibbs energy must be chosen (Walas

[1985], Gess et al. [1991] and Raal and Mühlbauer [1998] provide lists of the well known models). In addition, a dependable correlation for evaluating the liquid molar volume must be selected. Generally, the Rackett [1970] equation is employed for this purpose. Lastly, but perhaps most importantly, a suitable procedure or algorithm for obtaining the model parameters via regression must be chosen. A common method is the method of least squares (Marquardt [1963] and Gess et al. [1991]). However, programmes such as MATLAB have inbuilt functions that allow such calculations to be performed with relative ease.

The first model-dependent method was proposed by Barker [1953]. The following steps (for an isothermal data set) are involved in the method (Raal and Mühlbauer [1998]):

1. A suitable Gibbs excess energy expression (as a function of composition) is selected. Barker [1953] used the Scatchard [1949] polynomial, but any acceptable expression for G^E could be used.
2. The overall system pressure may then be calculated from:

$$P = \frac{x_1 \gamma_i P_1^{sat}}{\Phi_1} + \frac{x_2 \gamma_2 P_2^{sat}}{\Phi_2} \tag{3-77}$$

and the activity coefficients corresponding to the G^E expression selected in step 1 are determined from Equations (3-72) and (3-73).

3. The vapour mole fractions are only involved in the expression for Φ_i and these are thus set equal to one in the initial iteration loop. Thereafter, the vapour compositions are found from Equation (3-78) in step 4. Therefore, the only remaining unknowns are the model parameters. These are obtained via an optimal regression technique that is designed to produce the best fit to the experimental P-x data over the entire composition range.
4. Once the model parameters have been determined, the vapour compositions are calculated using:

$$y_i = \frac{x_i \gamma_i P_i^{sat}}{\Phi_i P} \tag{3-78}$$

The vapour phase correction factor, Φ_i, is then found from Equation (3-41). The various procedures available for acquiring values for quantities such as second virial coefficients have already been discussed (Section 3.2). The regression procedure is normally conducted by minimizing the error between the experimental and model values for a particular quantity. The difference between the two values (model and experimental) is commonly termed a *residual* and is given the symbol δ. Usually, the quantity selected for minimization is one of the following: pressure, vapour composition or excess Gibbs energy i.e. δP, δy or δg, where $g = G^E/RT$. The regression is then run until the chosen *objective function* (Van Ness and Abbot [1982]) has reached a specified, minimum value. This objective function is usually of the form $S = \sum (\delta P)^2$, although certain regression programmes require that the standard deviation be used as the objective function: $S = \frac{1}{n}\sum \sqrt{(\delta P)^2}$. Unless the VLE data being analyzed are thermodynamically perfect, different objective functions will produce different parameters for a specific model (as was found in this work). Thus, the issue of which residual results in the best fit exists and must be decided. In this project, it was found that for the majority of systems, the δP residual produced the best results. The same trend was found by Van Ness et al. [1978] who compared all of the objective functions. Van Ness [1995] states that the objective function, $\sum (\delta P)^2$, (i.e. Barker's method) is at least as good as any other, and is certainly the simplest and most direct. Furthermore, Van Ness et al. [1978] state that Barker's method is at least as successful in reducing VLE data (and in some cases is even superior) to any other maximum likelihood method.

3.4.1.1 The Wilson Equation

After Barker [1953] first pioneered the model-dependent method of data reduction, the next major breakthrough was accomplished by Wilson [1964]. He derived his equations for $G^E(T,P,x_i)$ by considering local compositions (as opposed to overall liquid compositions), which (according to Van Ness and Abbott [1997]) are presumed to account for the short-range order and non-random molecular orientations that result from differences in molecular size and intermolecular forces. Previously, the models that were employed were

based on rational functions (i.e. ratios of polynomials were used to express G^E). Examples of such models are the Margules equation (first proposed in 1895) and that of van Laar [1910]. Van Ness and Abbott [1997] state that although these models provide great flexibility in the fitting of VLE data for binary systems, they are without theoretical foundation and have no rational basis for their extension to multicomponent systems. Furthermore, the model parameters do not incorporate an explicit temperature dependence. According to Raal and Mühlbauer [1998], the Wilson equation is considered to be generally at least as good as the van Laar and Margules three-suffix equations and frequently appreciably superior, particularly for polar/non-polar mixtures. A major advantage of the Wilson equation is that it may be readily extended to multicomponent mixtures without the necessity of introducing parameters, other than for the constituent binaries. Raal and Mühlbauer [1998] note that the equation also has two disadvantages: firstly, it is not possible to find parameters for the model that are capable of predicting liquid immiscibility, and secondly, the equation is not suitable for systems that exhibit a maximum or minimum in the $\ln\gamma_i$ versus x_1 curves. A number of modifications of the original Wilson equation exist in an attempt to improve the model. That of Tsuboka and Katayama [1975] allows systems that exhibit partial miscibility to be modeled satisfactorily. For a binary system, the excess Gibbs energy expression for the Wilson equation is:

$$\frac{G^E}{RT} = -x_1 \ln(x_1 + x_2\Lambda_{12}) - x_2 \ln(x_2 + x_1\Lambda_{21}) \tag{3-79}$$

and the corresponding equations that allow calculation of the activity coefficients are:

$$\ln\gamma_1 = -\ln(x_1 + x_2\Lambda_{12}) + x_2\left(\frac{\Lambda_{12}}{x_1 + x_2\Lambda_{12}} - \frac{\Lambda_{21}}{x_2 + x_1\Lambda_{21}}\right) \tag{3-80}$$

$$\ln\gamma_2 = -\ln(x_2 + x_1\Lambda_{21}) - x_1\left(\frac{\Lambda_{12}}{x_1 + x_2\Lambda_{12}} - \frac{\Lambda_{21}}{x_2 + x_1\Lambda_{21}}\right) \tag{3-81}$$

where the Wilson parameters, Λ_{12} and Λ_{21}, are related to pure component liquid volumes (calculated using the Rackett [1970] equation) by the general equation:

$$\Lambda_{ij} = \frac{V_i}{V_j} \exp\left[-\frac{\lambda_{ij} - \lambda_{ii}}{RT} \right] \tag{3-82}$$

The temperature dependence of the adjustable model parameters can be clearly seen in Equation (3-82) (however, it should be noted that this temperature dependence is only an approximation). The parameters (λ_{ij}-λ_{ii}) represent the molecular interactions between the species that comprise the system.

3.4.1.2 The NRTL (Non-Random Two Liquid) Equation

In 1968, Renon and Prausnitz published an improved local composition model known as the Non-Random Two Liquid (NRTL) model. This equation represents an improvement over that of Wilson as it is able to adequately model systems that are partially (or even completely) miscible. Raal and Mühlbauer [1998] assert that the NRTL equation is particularly suitable for highly non-ideal systems and is readily (and implicitly) generalized to multicomponent systems. The model has three parameters: g_{12}-g_{22}, g_{21}-g_{22} and α_{12}, and like the Wilson equation, these contain a limited explicit temperature dependence. According to Van Ness and Abbott [1997], these parameters are specific to a particular binary pair and are independent of composition and temperature. Walas [1985] states that the g_{ij}-g_{ii} parameters represent the interaction between species i and j, whereas the α_{12} parameter represents the non-randomness of the solution. In general, suitable values for α_{12} fall in the range -1 to 0.5, with an arbitrary value often assigned within this range since activity coefficients are relatively insensitive to values of α_{12} between -1 and 0.5. According to Walas [1985] for non-aqueous mixtures α_{12} should be approximately 0.3, whereas for aqueous organic systems a value around about 0.4 is better. However, Raal and Mühlbauer [1998] found these results to be rather inconclusive and they suggest that it is better to find a value through experimental data reduction. The NRTL equation is:

$$\frac{G^E}{x_1 x_2 RT} = \frac{G_{21}\tau_{21}}{x_1 + x_2 G_{21}} + \frac{G_{12}\tau_{12}}{x_2 + x_1 G_{12}} \tag{3-83}$$

where

$$G_{ij} = \exp(-\alpha_{12}\tau_{ij}) \tag{3-84}$$

$$\tau_{ij} = \frac{g_{ij} - g_{jj}}{RT} \tag{3-85}$$

The equations for the activity coefficients are:

$$\ln \gamma_1 = x_2^2 \left[\tau_{21} \left(\frac{G_{21}}{x_1 + x_2 G_{21}} \right)^2 + \frac{G_{12}\tau_{12}}{(x_2 + x_1 G_{12})^2} \right] \tag{3-86}$$

$$\ln \gamma_2 = x_1^2 \left[\tau_{12} \left(\frac{G_{12}}{x_2 + x_1 G_{12}} \right)^2 + \frac{G_{21}\tau_{21}}{(x_1 + x_2 G_{21})^2} \right] \tag{3-87}$$

3.4.1.3 The UNIQUAC (Universal Quasi-Chemical Theory) Equation

The UNIQUAC equation was developed by Abrams and Prausnitz [1975] in an effort to represent systems without the restriction to completely miscible mixtures, yet maintaining the two-parameter benefits of the Wilson equation. This equation is also based on local composition theory, but is more complex than the previous two models in that the expression for the excess Gibbs energy consists of two parts, a combinatorial part (accounting for molecular size and shape differences) and a residual part (accounting for molecular interactions). Anderson and Prausnitz [1978] introduced a slightly modified form of the UNIQUAC equation. The equation is as follows:

$$G^E = G^E(combinatorial) + G^E(residual) \tag{3-88}$$

For a binary mixture, the two parts of G^E are:

$$\frac{G^E(combinatorial)}{RT} = x_1 \ln \frac{\Phi_1}{x_1} + x_2 \ln \frac{\Phi_2}{x_2} + \frac{z}{2}\left(q_1 x_1 \ln \frac{\theta_1}{\Phi_1} + q_2 x_2 \ln \frac{\theta_2}{\Phi_2} \right) \tag{3-89}$$

and

$$\frac{G^E(residual)}{RT} = -q_1 x_1 \ln[\theta_1 + \theta_2 \tau_{21}] - q_2 x_2 \ln[\theta_2 + \theta_1 \tau_{12}] \tag{3-90}$$

where the two adjustable model parameters are given by:

$$\tau_{ij} = \exp\left(-\left[\frac{u_{ij} - u_{jj}}{RT}\right]\right) \tag{3-91}$$

Again, the temperature dependence of the model parameters is apparent in Equation (3-91). However, the u_{ij}-u_{jj} parameters (also known as the characteristic energies, Prausnitz et al. [1980]) are usually considered to be temperature-independent (Raal and Mühlbauer [1998]). The symbol, z, represents the coordination number which is accepted as having a value of 10 for most liquids under normal conditions. However, according to Walas [1985], introducing a temperature dependent coordination number can result in a better correlation of the experimental VLE data being obtained (also, Raal and Naidoo [1990] considered a coordination number having an Arrhenius-type temperature dependence). The area fraction, θ_i, and segment fraction, Φ_i, found in Equations (3-89) and (3-91) are described by:

$$\theta_i = \frac{x_i q_i}{x_i q_i + x_j q_j} \tag{3-92}$$

$$\Phi_i = \frac{x_i r_i}{x_i r_i + x_j r_j} \tag{3-93}$$

The parameters r_i and q_i are the pure component volume and area structural parameters respectively. A group-contribution method (summarized in Raal and Mühlbauer [1998]) is followed in order to determine the values that should be used for these parameters.

Since the G^E expression consists of two terms, the analogous activity coefficient equation must also contain a combinatorial and residual part:

$$\ln \gamma_i = \ln \gamma_i(combinatorial) + \ln \gamma_i(residual) \tag{3-94}$$

and

$$\ln \gamma_i = \ln \frac{\Phi_i}{x_i} + \frac{z}{2} q_i \ln \frac{\theta_i}{\Phi_i} + \Phi_j \left(l_i - \frac{r_i}{r_j} l_j \right) - q_i \ln(\theta_i + \theta_j \tau_{ji}) + \theta_j q_i \left(\frac{\tau_{ji}}{\theta_i + \theta_j \tau_{ji}} - \frac{\tau_{ij}}{\theta_j + \theta_i \tau_{ij}} \right) \tag{3-95}$$

where

$$l_i = \frac{z}{2}(r_i - q_i) - (r_i - 1) \tag{3-96}$$

The UNIQUAC equation has a wide range of applicability and may be used for both polar and non-polar liquid mixtures. The equation may also be extended to represent multicomponent mixtures in terms of the binary parameters alone. Perhaps the greatest advantage of the UNIQUAC equation is its extension to predicting system parameters from pure component data via the group-contribution UNIFAC method (the reader is referred to Smith et al. [1996] and Fredunslund et al. [1977] for a fuller description of this technique). The main drawbacks to the model according to Walas [1985] are its greater algebraic complexity as compared to the NRTL and Wilson equations and the fact that often the representation of the VLE data is poorer than for some simpler equations.

3.4.2 The Direct (Phi-Phi) Method

According to Van Ness and Abbott [1997], the direct method represents a generally applicable alternative to the gamma-phi approach. The key characteristic of the direct method is the use of an equation of state (EOS) to express both the vapour and liquid non-idealities via fugacity coefficients. This leads, along with Equation (3-25), to the following:

$$\hat{f}_i^l = x_i \hat{\phi}_i^l = \hat{f}_i^v = y_i \hat{\phi}_i^v \tag{3-97}$$

The fugacity coefficients are determined from:

$$\ln \hat{\phi}_i = -\int_{\infty}^{V} \left(\left[\frac{\partial (nZ)}{\partial n_i} \right]_{T,V,n,n_j} - 1 \right) \frac{dV}{V} - \ln Z \tag{3-98}$$

where both ln$Z$ and the derivative lying within the integral are evaluated using a suitable equation of state. The phase equilibrium ratio, K_i, is defined simply as the ratio of the vapour compositions to the liquid compositions. Hence, Equation (3-97) leads directly to:

$$K_i = \frac{y_i}{x_i} = \frac{\hat{\phi}_i^l}{\hat{\phi}_i^v} \tag{3-99}$$

A major advantage of the direct method is that it is equally applicable to both low pressure and high pressure systems. Generally, however, the direct method has been used mainly in the modeling of high pressure VLE data, whilst the combined method has traditionally been used when low pressure data have been analyzed. In this project, the direct method was used in addition to the combined method since cubic equations of state were available that incorporated association (i.e. applied to polar mixtures). Indeed, certain cubic equations of state have been published that are designed specifically for carboxylic acids (e.g. Twu et al. [1993]). According to Orbey and Sandler [1996], the range of such equations of state has been extended to the accurate description of the VLE of highly non-ideal mixtures through the recent development of new mixing and combining rules. The iteration procedure is rather involved (refer to Figures 3-3 and 3-4) and will not be discussed in detail here. For an in-depth discussion of the direct method the excellent texts of Raal and Mühlbauer [1998], Sandler et al. [1994] and Walas [1985] should be consulted.

One of the major hurdles to overcome when tackling the direct method of data regression is selection of the appropriate combination of EOS and mixing rule. The challenges associated with the method are outlined by Raal and Mühlbauer [1998] as follows:

1. Selection of the most appropriate EOS to describe both the liquid and vapour phase non-idealities. Literally hundreds of equations of state are described in the literature. The main criterion in the selection of an EOS is that it must be flexible enough to

fully describe a pure substance's P, V, T behaviour for both phases in the temperature and pressure range under study.

2. Selection of appropriate mixing rules, which are required to extend the pure-component form of the EOS to mixtures. Most mixing rules, although derived using theoretical assumptions, are somewhat empirical and tend to be system specific.
3. Location of the appropriate roots for liquid and vapour molar densities when higher than cubic equations of state are used.

3.4.2.1 The Peng-Robinson Equation of State

The Peng-Robinson equation of state (Peng and Robinson [1976]) was selected as one of the equations of state to be used in this project as it had been found to be successful in representing systems that are liable to show large deviations from ideality (Orbey and Sandler [1996]). Prior to the development of the Peng-Robinson EOS, several other cubic equations of state were employed. The first attempt was made in 1873 by van der Waals. Many modifications to that original semi-empirical equation have since been proposed, but the most successful are the Redlich-Kwong [1949] equation and the Soave-Redlich-Kwong (Soave [1972]) equation. However, Peng and Robinson [1976] note that these equations still have some shortcomings. The most important inadequacy is that they fail to produce acceptable liquid density values. The Peng-Robinson equation (according to Peng and Robinson [1976]) yields improved liquid densities and, in addition, accurate vapour pressures and equilibrium ratios.

The Peng-Robinson equation (like most cubic equations of state) represents pressure as a sum of two terms, a repulsive term and an attractive term:

$$P = P_R + P_A = \frac{RT}{V-b} - \frac{a(T)}{(V+\varepsilon_{PR}b)(V+\sigma_{PR}b)} \tag{3-100}$$

Here, the constant b (related to molecular size) is considered to be temperature independent, whereas the parameter a (related to the intermolecular attraction force) is dependent on temperature. For the Peng-Robinson equation, $\varepsilon_{PR} = 1-\sqrt{2}$ and $\sigma_{PR} = 1+\sqrt{2}$.

Equation (3-100) may be rewritten as a polynomial in order to ease the computational complexity. The equation is written in terms of the compressibility factor and the reason for these equations of state being termed "cubic" becomes clear:

$$Z^3 - (1-B)Z^2 + (A - 3B^2 - 2B)Z - (AB - B^2 - B^3) = 0 \tag{3-101}$$

where $A = \dfrac{aP}{R^2T^2}$ and $B = \dfrac{bP}{RT}$. Since Equation (3-101) is a third order polynomial, solving the equation will yield three roots. For a binary system, the largest root corresponds to the vapour-phase compressibility factor, whilst the smallest (positive) root gives the liquid-phase compressibility factor. To determine a and b the following equations are used:

$$a(T) = a(T_{ci})\alpha(T_{ri}, \omega_i) \tag{3-102}$$

$$b(T) = b(T_{ci}) \tag{3-103}$$

where

$$a(T_{ci}) = 0.45724\frac{R^2T_{ci}^2}{P_{ci}} \tag{3-104}$$

$$b(T_{ci}) = 0.07780\frac{RT_{ci}}{P_{ci}} \tag{3-105}$$

$$\alpha(T_{ri}, \omega_i) = \left[1 + \kappa(1 - T_{ri}^{1/2})\right]^2 \tag{3-106}$$

The parameter κ represents a constant that is characteristic for each species. For the Peng-Robinson equation, $\kappa = 0.37464 + 1.54226\omega - 0.26992\omega^2$. To calculate the fugacity coefficient of species i, the following equation is employed:

$$\ln\hat{\phi}_i = \frac{\bar{b}_i}{b}(Z-1) - \ln\frac{(V-b)Z}{V} + \frac{a/bRT}{\varepsilon_{PR} - \sigma_{PR}}\left(1 + \frac{\bar{a}_i}{a} - \frac{\bar{b}_i}{b}\right)\ln\frac{V + \sigma_{PR}b}{V + \varepsilon_{PR}b} \tag{3-107}$$

where $\bar{a}_i$ and $\bar{b}_i$ are partial properties of the parameters a and b respectively. The original mixing rules used by Peng and Robinson are:

$$a = \sum_i \sum_j x_i x_j a_{ij} \tag{3-108}$$

$$b = \sum_i x_i b_i \tag{3-109}$$

where

$$a_{ij} = (1 - \delta_{ij}) a_i^{1/2} a_j^{1/2} \tag{3-110}$$

The *binary interaction coefficient*, δ_{ij}, is unique to each binary system and is found using the same regression techniques discussed in Section 3.4.1. In almost all cases, more precise (theoretically based as opposed to purely empirical) mixing rules are used than those given in the original paper by Peng and Robinson [1976]. The mixing rules utilized in this work are the Wong-Sandler and the Twu-Coon mixing rules, which are discussed below. Both mixing rules introduce a Hermholtz-free-energy model (usually the NRTL model, refer to Section 3.4.1.2) and hence the number of parameters for which the regression must be carried out increases. However, the benefit gained in terms of both flexibility and accuracy is substantial.

An improved Peng-Robinson EOS was suggested by Stryjek and Vera [1986], who modified the temperature and acentric factor (ω) dependence of the attractive term, $a(T)$. This was accomplished by altering the equation for κ. The new expression is:

$$\kappa = \kappa_0 + \kappa_1 (1 + T_r^{0.5})(0.7 - T_r) \tag{3-111}$$

where $\kappa_0 = 0.378893 + 1.4897153\omega - 0.171131848\omega^2 + 0.0196554\omega^3$ and κ_1 is an adjustable parameter that is unique to each species. Stryjek and Vera [1986] assert that this modification improves the results obtained with the Peng-Robinson EOS. The modified EOS, termed the Peng-Robinson-Stryjek-Vera (PRSV) EOS, will not be used in this work; instead, the more precise alpha correlation of Twu et al. [1996] will be employed. The expression they proposed (as was the case for the Peng and Robinson [1976] and Stryjek and Vera [1986] correlations) relies merely on the reduced temperature, $T_r = T/T_c$.

However, the form of the Twu et al. [1996] correlation differs considerably from those that preceded it:

$$\alpha(T) = T_r^{N'(M'-1)} e^{L'(1-T_r^{N'M'})} \tag{3-112}$$

The three parameters L', M' and N' are unique to each pure species and are obtained through regression of the pure-compound vapour pressure data. According to Twu et al. [1996], Equation (3-112) usually results in an alpha value that provides a very accurate prediction of the vapour pressures for all the chemicals involved in the VLE system.

3.4.2.2 An Equation of State for Carboxylic Acids

Twu et al. [1993] developed an EOS designed specifically for the modeling of carboxylic acid systems. As such, the EOS was perfectly suited for this project. The equation of state is based on a cubic EOS (CEOS) that is extended to systems of carboxylic acids through the incorporation of association via chemical theory (also discussed earlier in the chapter, Section 3.2.2). According to Twu et al. [1993], this incorporation is based on the simple and elegant approach for pure components put forward by Heidemann and Prausnitz [1976]. Twu et al. [1993] propose that obtaining the chemical equilibrium constant and momomer parameters through regression without applying the EOS critical constraints is dis-advantageous. Instead, they provide an internally consistent method to determine the pure monomer parameters for the associated component.

Twu and co-workers use a generic two-parameter CEOS in their derivation:

$$P = \frac{n_T RT}{(V - n_T b)} - \frac{n_T^2 a(T)}{V^2 + u n_T b V + w n_T^2 b^2} \tag{3-113}$$

where n_T is the total number of moles of monomer and dimer, u and w are constant integer values specific to each particular EOS. Twu et al. [1993] explain that the parameters a and b at T_c (i.e. a_c and b_c) are found by setting the first and second derivatives of pressure with respect to volume to zero at the critical point. n_T varies with temperature and density for an

associating fluid and, therefore, cannot be considered constant. Interestingly, by setting $n_T = 1$, $u = \varepsilon_{PR} + \sigma_{PR}$ and $w = \varepsilon_{PR}.\sigma_{PR}$, Equation (3-113) reverts to Equation (3-100) for the Peng-Robinson EOS.

Chemical theory states that the carboxylic acid mixture is comprised of monomers and dimers that are in chemical equilibrium. Defining z_i to be the mole fraction of species i, including monomers and dimers, the following mixing rules are proposed by Twu and co-workers:

$$a = \sum_i \sum_j z_i z_j (a_i a_j)^{1/2} \tag{3-114}$$

$$b = \sum_i z_i b_i \tag{3-115}$$

Along with these mixing rules, Heidemann and Prausnitz [1976] assumed that $a_i = i^2 a_1$ and $b_i = i b_1$ where i refers to the "i-mer" and 1 to the monomer. They also derived, for a pure fluid $a = (n_o / n_T)^2 a_1$ and $b = (n_o / n_T) b_1$. Here, n_o represents the number of moles that would exist if no association was taking place i.e. if no dimers were present in solution. This leads to $(n_o / n_T) = \sum i z_i$ and consequently:

$$z_i = n_i / n_T \tag{3-116}$$

where n_1 and n_2 are defined as the number of moles of monomer and dimer respectively. Substituting these equations into Equation (3-113) and defining the *extent of association*, $n_r = n_T / n_o$ yields:

$$P = n_r \frac{RT}{(v - b_1)} - \frac{a_1(T)}{v^2 + u b_1 v + w b_1^2} \tag{3-117}$$

where $v = V / n_o$. When $n_r = 1$, then no association is occurring and when $n_r = 0.5$, complete dimerization has taken place.

In their paper, Twu et al. [1993] use the Redlich-Kwong EOS i.e. they set $u = 1$ and $w = 0$. Hence, the expression obtained for the fugacity coefficient is:

$$\ln\phi = \ln(z_1 n_r) + (Z - n_r) - \ln(Z - b_1^*) - \frac{a_1^*}{b_1^*}\ln\left(1 + \frac{b_1^*}{Z}\right) \tag{3-118}$$

where $Z = \frac{PV}{n_o RT}$, $a_1^* = \frac{Pa_1}{R^2T^2}$, $b_1^* = \frac{Pb_1}{RT}$ and z_1 is the true monomer mole fraction. To find Z, the following equation is solved:

$$Z^3 - n_r Z^2 + (a_1^* - n_r b_1^* - b_1^{*2})Z - a_1^* b_1^* = 0 \tag{3-119}$$

According to Twu et al. [1993], the parameters that appear in the associating CEOS may be treated in the same manner as those for a common CEOS. As was discussed above, the monomer parameters a and b are found from the critical point by setting the first and second derivatives of pressure with respect to volume to zero. As is the case for the common CEOS, the critical constraints yield three equations with three unknowns: a_c, b_c and Z_c. Actually, this results in an over-specification of the problem, since the critical compressibility factor, Z_c, is available for the carboxylic acids in the literature. Twu and co-workers suggest treating V_c as the third unknown, which, combined with the known P_c and T_c values, enables calculation of Z_c.

3.4.2.3 The Wong-Sandler Mixing Rule

In a solution, two types of interactions occur: there are those between like molecules (i.e. *ii* interactions), and, in addition, interactions occur between unlike molecules (i.e. *ij* interactions between species *i* and species *j*). Application of an equation of state to a mixture demands that these interactions be characterized. For this purpose, *mixing rules* have been introduced that incorporate system-specific parameters describing the interactions between the molecules of the two species comprising the binary system. In this work, two different combining rules have been used: viz. the Wong-Sandler and Twu-Coon mixing rules. An excellent and extremely detailed review of the mixing rules currently available is presented by Raal and Mühlbauer [1998].

In 1992, Wong and Sandler developed a theoretically correct mixing rule for cubic equations of state that correctly produced the low and high-density limits without being density dependent. According to Wong and Sandler [1992], the mixing rule combined with a CEOS may be used to accurately correlate VLE data. Also, the Wong-Sandler rule is just as applicable to simple systems as it is to complex mixtures comprised of polar and associating species (Wong and Sandler [1992]). Since the rule incorporates an activity coefficient model (to calculate the Hermholtz free energy), the Wong-Sandler mixing rule provides a link between the direct and combined methods. Consequently, equations of state may now be used to accurately model mixtures that previously could only be described using activity coefficient models. Wong and Sandler [1992] state that their rule represents an improvement over previous combining rules (such as that of Huron and Vidal [1977]), since it is consistent with statistical mechanics.

The Wong-Sandler mixing rule [1992] expresses the mixture parameters a_m and b_m as:

$$b_m = \frac{Q}{(1-D)} \tag{3-120}$$

$$\frac{a_m}{RT} = \frac{QD}{(1-D)} \tag{3-121}$$

where Q and D are defined as follows:

$$Q = \sum_i \sum_j x_i x_j \left(b - \frac{a}{RT} \right)_{ij} \tag{3-122}$$

$$D = \sum_i x_i \frac{a_i}{b_i RT} + \frac{A_\infty^E}{cRT} \tag{3-123}$$

In order to evaluate the expression for the fugacity coefficient generated from the equation of state, the partial derivatives of a_m and b_m with respect to the number of moles are required:

$$\frac{\partial n b_m}{\partial n_i} = \frac{1}{(1-D)} \left(\frac{1}{n} \frac{\partial n^2 Q}{\partial n_i} \right) - \frac{Q}{(1-D)^2} \left(1 - \frac{\partial n D}{\partial n_i} \right) \tag{3-124}$$

$$\frac{1}{RT}\left(\frac{1}{n}\frac{\partial n^2 a_m}{\partial n_i}\right) = D\frac{\partial n b_m}{\partial n_i} + b_m\frac{\partial nD}{\partial n_i} \tag{3-125}$$

with the corresponding partial derivatives of Q and D given by:

$$\left(\frac{1}{n}\frac{\partial n^2 Q}{\partial n_i}\right) = 2\sum_j x_j\left(b - \frac{a}{RT}\right)_{ij} \tag{3-126}$$

$$\frac{\partial nD}{\partial n_i} = \frac{a_i}{b_i RT} + \frac{\ln\gamma_i^\infty}{c} \tag{3-127}$$

with

$$\ln\gamma_i^\infty = \frac{1}{RT}\frac{\partial nA_\infty^E}{\partial n_i} \tag{3-128}$$

$$c = \frac{1}{\sqrt{2}}\ln(\sqrt{2}-1) \tag{3-129}$$

In this project the NRTL activity coefficient model (discussed in Section 3.4.1.2) was used to describe the Hermholtz free energy, A_∞^E, and the infinite dilution activity coefficients, $\ln\gamma_i^\infty$:

$$\frac{A_\infty^E}{RT} = \sum_i x_i\left(\frac{\sum_j x_j\tau_{ji}g_{ji}}{\sum_k x_k g_{ki}}\right) \tag{3-130}$$

$$\ln\gamma_i^\infty = \frac{\sum_j x_j\tau_{ji}g_{ji}}{\sum_k x_k g_{ki}} + \sum_j\frac{x_j g_{ij}}{\sum_k x_k g_{kj}}\left(\tau_{ij} - \frac{\sum_l x_l\tau_{lj}g_{lj}}{\sum_k x_k g_{kj}}\right) \tag{3-131}$$

The advantage to using the excess Hermholtz free energy (A_∞^E) as opposed to the excess Gibbs free energy is that A_∞^E is far less pressure-dependent and, therefore, the correct

behaviour is obtained at both low and infinite pressure (Wong and Sandler [1992]). The following equation is also required in order to apply the Wong-Sandler rule:

$$\left(b-\frac{a}{RT}\right)_{ij}=\frac{\left(b_i-\frac{a_i}{RT}\right)+\left(b_j-\frac{a_j}{RT}\right)}{2}(1-k_{ij}) \tag{3-132}$$

The binary interaction parameter, k_{ij}, is the parameter that is regressed for during the VLE data reduction. It is unique to each binary system and describes the second virial coefficient behaviour. Hence, k_{ij} should be small for systems that are practically ideal, and large for systems that deviate significantly from ideality. Usually, k_{ij} lies within the range -1 to 1.

3.4.2.4 The Twu-Coon Mixing Rule

Twu and Coon [1996] developed a new class of mixing rules for cubic equations of state to deal with highly non-ideal chemical systems. According to Twu and Coon [1996], the new rule retains the excellent features of the Wong-Sandler mixing rule while avoiding the problems associated with it. In addition, they state that the Twu-Coon mixing rule is more flexible than either the Huron-Vidal or Wong-Sandler mixing rules. A major advantage of the Twu-Coon mixing rule is that it reduces to the classical van der Waals combining rules when the parameters in the non-random excess Hermholtz free energy are set to zero. This is significant since the older, classic mixing rules worked extremely well for most non-polar systems.

The Twu-Coon mixing rule [1996] is as follows:

$$b_m=\frac{b_{vdw}-a_{vdw}}{1-\left(\frac{a_{vdw}}{b_{vdw}}+\frac{1}{c}\frac{A_\infty^E}{RT}\right)} \tag{3-133}$$

$$a_m=b_m\left(\frac{a_{vdw}}{b_{vdw}}+\frac{1}{c}\frac{A_\infty^E}{RT}\right) \tag{3-134}$$

where a_{vdw} and b_{vdw} are EOS a and b parameters evaluated using the classic van der Waals mixing rules:

$$a_{vdw} = \sum_i \sum_j x_i x_j \sqrt{a_i a_j}(1 - k_{ij}) \tag{3-135}$$

$$b_{vdw} = \sum_i \sum_j x_i x_j \left[\frac{1}{2}(b_i + b_j)\right](1 - l_{ij}) \tag{3-136}$$

To solve for the fugacity coefficient, Equation (3-107) again applies. However, Q and D are defined in a slightly different manner and, hence, so are the partial derivatives for a, b, Q and D. The partial derivatives of a and b are:

$$\frac{1}{na}\left(\frac{\partial n^2 a}{\partial n_i}\right) = \frac{1}{b}\left(\frac{\partial nb}{\partial n_i}\right) + \frac{1}{D}\left(\frac{\partial nD}{\partial n_i}\right) \tag{3-137}$$

$$\frac{1}{b}\left(\frac{\partial nb}{\partial n_i}\right) = \frac{1}{Q}\left[\frac{1}{n}\left(\frac{\partial n^2 Q}{\partial n_i}\right)\right] - \frac{1}{1-D}\left[1 - \left(\frac{\partial nD}{\partial n_i}\right)\right] \tag{3-138}$$

with Q and D defined as:

$$D = \frac{a_{vdw}}{b_{vdw}} + \frac{1}{c}\frac{A_\infty^E}{RT} \tag{3-139}$$

$$Q = b_{vdw} - \frac{a_{vdw}}{RT} \tag{3-140}$$

and, therefore, the partial derivatives of Q and D are:

$$\left(\frac{\partial nD}{\partial n_i}\right) = \frac{a_{vdw}}{b_{vdw}}\left(\left[\frac{1}{na_{vdw}}\left(\frac{\partial n^2 a_{vdw}}{\partial n_i}\right)\right] - \left[\frac{1}{b_{vdw}}\left(\frac{\partial nb_{vdw}}{\partial n_i}\right)\right]\right) + \frac{1}{c}\ln\gamma_{\infty i} \tag{3-141}$$

$$\frac{1}{Q}\left[\frac{1}{n}\left(\frac{\partial n^2 Q}{\partial n_i}\right)\right]=\frac{2\sum_j x_j(b_{ij}-a_{ij})}{\sum_i\sum_j x_i x_j(b_{ij}-a_{ij})} \tag{3-142}$$

with the partial derivatives of a_{vdw} and b_{vdw} expressed by:

$$\frac{1}{na_{vdw}}\left(\frac{\partial n^2 a_{vdw}}{\partial n_i}\right)=\frac{2}{a_{vdw}}\sum_j x_j a_{ij} \tag{3-143}$$

$$\frac{1}{b_{vdw}}\left(\frac{\partial n b_{vdw}}{\partial n_i}\right)=\frac{2}{b_{vdw}}\sum_j x_j b_{ij}-1 \tag{3-144}$$

To calculate the cross parameters a_{ij} and b_{ij}, the following equations are used:

$$a_{ij}=\sqrt{a_i a_j}(1-k_{ij}) \tag{3-145}$$

$$b_{ij}=\frac{1}{2}(b_i+b_j)(1-l_{ij}) \tag{3-146}$$

The Hermholtz free energy, A_∞^E, infinite dilution activity coefficients, $\ln\gamma_i^\infty$ and constant c are given by Equations (3-130), (3-131) and (3-129) respectively.

3.5 Infinite Dilution Activity Coefficients

In Section 3.3, the concept of the activity coefficient was discussed. As the mole fraction of a certain species in solution approaches zero, the activity coefficient approaches a definite value. This value is an important thermodynamic mixture property, the *infinite dilution activity coefficient*, γ_i^∞, and is the focus of this section. This property is exceedingly important in industrial operations since the most complicated and difficult part of a separation process frequently occurs in the extremely dilute regions. Any process that produces high purity (and therefore expensive) chemicals must inevitably operate in this

region. Hence, there is a great deal of industrial interest in this area. According to Raal and Mühlbauer [1998], the greatest departure from ideality is usually found in the very dilute regions and infinite dilution activity coefficients provide the most accurate characterization of system behaviour in these regions. Experimentally, γ_i^{∞} can be determined in a number of ways. However, the chief methods used are differential ebulliometry, differential static methods, gas chromatographic techniques and inert gas stripping. These procedures will not be discussed here; instead the reader is referred to the texts of Raal and Mühlbauer [1998] and Raal [2000], which provide a thorough review.

3.5.1 Determination of Infinite Dilution Activity Coefficients

Raal and Mühlbauer [1998] pointed out that extrapolation of activity coefficients measured at finite concentration is not an acceptable procedure, whether the extrapolation is carried out graphically or through the use of a correlating equation for $\ln\gamma_i$. Furthermore, Hartwick and Howat [1995] state that extrapolation of activity coefficients into the infinite dilution region using solution models introduces a systematic error in the estimation of phase equilibria.

To determine the infinite dilution activity coefficients, the Smith and Maher method [1979] (as modified from the Ellis and Jonah [1962] method) is employed. This allows γ_i^{∞} values to be calculated from isothermal data using the equations originally postulated by Gautreaux and Coates [1955]:

$$\gamma_i^{\infty} = \frac{P_j^{sat}\hat{\phi}_{i,P_j^{sat}}}{P_1^{sat}\hat{\phi}_{i,P_i^{sat}}}\left[1+\left(\frac{dP}{dx_i}\right)_{x_i=0}^{\infty}\left(\frac{V_j^v - V_j^l}{RT}\right)\right]\exp\left(-\int_{P_1^{sat}}^{P_2^{sat}}\frac{V_i^l}{RT}dP\right) \qquad (3\text{-}147)$$

Pividal et al. [1992] propose that at low pressures and moderate temperatures, the virial equation of state may be truncated at the second virial coefficient. Hence, Equation (3-147) becomes:

$$\gamma_i^{\infty} = \varepsilon_i^{\infty} \frac{P_j^{sat}}{P_i^{sat}} \left(1 + \beta_j \frac{1}{P_j^{sat}} \left(\frac{\partial P}{\partial x_i} \right)_T^{x_i \to 0} \right) \tag{3-148}$$

where

$$\varepsilon_i^{\infty} = \exp\left[\frac{(B_{ii} - V_i^l)(P_j^{sat} - P_i^{sat}) + \delta_{ij} P_j^{sat}}{RT} \right] \tag{3-149}$$

$$\beta_j = 1 + P_j^{sat} \left(\frac{B_{ij} - V_j^l}{RT} \right) \tag{3-150}$$

$$\delta_{ij} = 2B_{ij} - B_{ii} - B_{jj} \tag{3-151}$$

Here, the parameters B_{ii} and B_{jj} are the second virial coefficients of the pure components, whereas B_{ij} is the analogous virial coefficient for the *i-j* interaction. P_i^{sat} is the saturated vapour pressure of species *i* and V_i^l the corresponding liquid molar volume. Calculation procedures for these variables have been discussed in previous sections.

To determine the gradient (i.e. partial derivative) in Equation (3-148), Maher and Smith [1979] adapted the method formerly proposed by Ellis and Jonah [1962]. This is accomplished by converting P versus x_1 data to P_D versus x_1 data where P_D is found from:

$$P_D = P - [P_j^{sat} + (P_i^{sat} - P_j^{sat}) x_i] \tag{3-152}$$

P_D is the *deviation pressure* and is basically an expression of the extent to which the system in question differs from Raoult's law i.e. it reveals the degree to which the system deviates from ideality. Differentiation of Equation (3-152) yields:

$$\frac{dP}{dx_i} = \frac{dP_D}{dx_i} + (P_i^{sat} - P_j^{sat}) \tag{3-153}$$

In order to evaluate the gradients found in Equations (3-148) and (3-153), plots of P_D/x_ix_j and x_ix_j/P_D versus x_i are constructed. As x_i approaches values of 0 or 1, these ratios become indeterminate and l'Hospital's rule is applied, resulting in:

$$\left(\frac{P_D}{x_i x_j}\right)_{x_i=0} = \left(\frac{\partial P}{\partial x_i}\right)_{x_i=0} - P_i^{sat} + P_j^{sat} \tag{3-154}$$

The left-hand term of Equation (3-154) may be evaluated via extrapolation to $x_i = 0$ in the P_D/x_ix_j and x_ix_j/P_D versus x_i plots. According to Maher and Smith [1979], both curves are usually necessary since one normally provides a reliable extrapolation at one end whilst the second works better at the other end. For certain systems, such as ethanol (1) – aniline (2), reliable extrapolations may be obtained at both ends and only one of the graphs discussed above is required. Clearly, once the left-hand term in Equation (3-154) is known, it is a simple matter to calculate the partial derivative of pressure with respect to x_i at $x_i = 0$. Substitution into Equation (3-147) yields γ_i^{∞}.

3.6 Calculation of Excess Thermodynamic Properties

Excess properties are quantities that express the difference between the actual value of a certain solution property and the value that would be exhibited by an ideal solution under the same conditions. For a general property, M, this relationship is written as follows:

$$M^E = M - M_{id} \tag{3-155}$$

Wisniak and Tamir [1978] provide a list summarizing the importance of excess thermodynamic properties:

- Excess properties provide key values for calculation of multicomponent mixture properties from pure component data;
- Excess properties are often used to define the various kinds of solutions;
- Excess properties are used in testing solution theories;

- Excess properties can provide data for evaluation of parameters characterizing interactions between unlike species in a mixture;
- The excess Gibbs energy is one of the most useful thermodynamic concepts for expressing non-ideality of a liquid mixture;
- The excess Gibbs energy is the most useful quantity for determining phase stability and phase separation;
- The excess enthalpy (also termed the heat of mixing) is a very useful quantity in predicting isothermal VLE and testing the thermodynamic consistency of isobaric VLE data.

When considering an expression to represent these excess properties, proper selection of the correct equation for a given application depends on the following considerations (according to Wisniak and Tamir [1978]):

1. the need for simplicity of equations
2. the availability of data with which to evaluate parameters
3. the need to make predictions without excessive data (e.g. multicomponent systems from binary systems)
4. the desire for accurate correlations
5. the desire to assign physical meaning to the parameters
6. unusual non-idealities like partial miscibility
7. the nature of the system (aqueous, non-aqueous, metallic)

An equation relating the excess enthalpy and entropy to the excess Gibbs energy and that also satisfies all seven criteria given by Wisniak and Tamir [1978] is the fundamental excess-property relation:

$$d\left(\frac{nG^E}{RT}\right) = \frac{nV^E}{RT}dP - \frac{nH^E}{RT^2}dT + \sum_i \frac{\overline{G}_i^E}{RT}dn_i \qquad (3\text{-}69)$$

By inspection, the following equations may be obtained:

$$V^E = RT\left[\frac{\partial(G^E/RT)}{\partial P}\right]_{T,x} \tag{3-156}$$

$$H^E = -RT^2\left[\frac{\partial(G^E/RT)}{\partial T}\right]_{P,x} \tag{3-157}$$

Therefore, provided that VLE data have been measured for a particular system at two or more temperatures, Equation (3-157) allows calculation of the excess enthalpy. This is accomplished by regressing the VLE data using one of the methods discussed in Section 3.4.1. The model that provided the best fit of the data is then used (along with the parameters obtained) to calculate G^E/RT over the entire composition range. A plot of G^E/RT versus temperature yields the gradient $\left[\frac{\partial G^E/RT}{\partial T}\right]_{P,x}$ found in Equation (3-157). Hence, the excess enthalpy, H^E, may be easily calculated from Equation (3-157) for the whole composition range. Clearly, G^E is obtained directly from the G^E/RT values by multiplying by RT. This allows the excess entropy, S^E, to be found from the fundamental relation:

$$G^E = H^E - TS^E \tag{3-158}$$

This simple procedure was used in this project to determine the excess thermodynamic properties of both carboxylic acid systems studied. However, the gradients used in this technique are often difficult to evaluate accurately. An alternative method that may be considered when calculating H^E is that of Münsch [1979].

3.7 Thermodynamic Consistency Tests

It is perfectly acceptable when measuring binary VLE data, to only measure three out of the four variables P, T, x and y, since the fourth property may be easily obtained from the other three. Measuring the fourth variable inevitably over-specifies the system. However, there is a distinct advantage to measuring all four variables because the fourth variable may then be used to test for thermodynamic consistency. This highlights the importance of

measuring both the liquid and vapour phase compositions, particularly since the vapour compositions usually display the greatest error. Hence, the tests usually focus on the y-data in order to determine consistency of the VLE data set.

The ultimate basis for all thermodynamic consistency tests is the Gibbs-Duhem equation:

$$\sum_i x_i d\ln\gamma_i = \frac{\overline{V}_i^E}{RT}dP - \frac{\overline{H}_i^E}{RT^2}dT \tag{3-75}$$

If the VLE data conforms to the Gibbs-Duhem equation, then the data set is said to be thermodynamically consistent. Various modifications and adaptions of the equation have been used in order to test for thermodynamic consistency. Initially, the *slope test* was employed that compared slopes of curves drawn to fit $\ln\gamma_1$ and $\ln\gamma_2$ vs x_1 graphs. According to Van Ness [1995], this test proved to be tedious and uncertain, and as such, never found serious application. An improvement over the slope test was provided by the *area test* (Redlich and Kister [1948] and Herington [1947]). However, the area test is a necessary, not a sufficient condition for consistency and is far from a stringent requirement for consistency (Van Ness [1995]). In the area test, the pressure is cancelled off and, therefore, one of the most accurately measured system properties is lost. Thus, this test would sometimes pass data sets that were inconsistent while failing data sets that actually were consistent. Furthermore, the area test requires an approximation that is fully justified for isothermal data, but is unlikely to be realistic for isobaric data since the excess enthalpy term that is set to zero cannot be regarded as negligible at constant pressure (Van Ness [1995]). These problems are avoided in the two tests utilized in this work to check the consistency of the VLE data:

- The point test of Van Ness at al. [1973]
- The direct test of Van Ness [1995].

3.7.1 The Point Test

The point test was put forward by Van Ness and co-workers [1973] as a more stringent assessment of data consistency. As was mentioned above, a complete VLE data set (i.e. all four variables are measured) results in an over-specification of the system. This means that any three of the experimentally determined variables may be used to calculate the fourth using an accepted correlation. In general, the vapour phase compositions introduce the most error. Thus, they are the most logical variable to be used when testing for thermodynamic consistency since if the y-values are consistent, T, P and x should also be consistent. In the point test, the data are regressed using either the combined or the direct method (Sections 3.4.1 and 3.4.2 respectively) and the calculated y_i's are compared to those measured experimentally. The extent to which the correlated values deviate from the measured values provides an indication of the consistency of the VLE data (Van Ness et al. [1973]). Danner and Gess [1990] suggest that the average absolute deviation, $\Delta y_{ad} = \frac{1}{n}\left(\left|y_{ex} - y_{calc}\right|\right)$ should be less than 0.01 for the data to be consistent. This benchmark was used in this work.

3.7.2 The Direct Test

The *direct test* was developed by Van Ness [1995]. According to Van Ness [1995], the test is a long sought goal – a simple and direct test of thermodynamic consistency for each point of a VLE data set with respect to the Gibbs-Duhem equation itself. To begin formulation of the test, the following definitions are necessary:

$$\varepsilon_P = \frac{V^E}{RT}\frac{dP}{dx_1} \tag{3-159}$$

$$\varepsilon_T = \frac{-H^E}{RT^2}\frac{dT}{dx_1} \tag{3-160}$$

Binary VLE data are always measured either isobarically or isothermally. When the pressure is constant, ε_P will be zero and when the temperature is held constant, ε_T will naturally be zero. Hence, only one ε term is required in the equations derived for the direct

test. Defining $g = G^E/RT$ and dividing through by dx_1 (i.e. the equations are written for one mole of the liquid phase), we obtain the following expressions from Equation (3-70) and the Gibbs-Duhem equation, respectively:

$$\frac{dg}{dx_1} = \ln\frac{\gamma_1}{\gamma_2} + \varepsilon \tag{3-161}$$

$$x_1\frac{d\ln\gamma_1}{dx_1} + x_2\frac{d\ln\gamma_2}{dx_1} - \varepsilon = 0 \tag{3-162}$$

where the appropriate equation for ε is selected depending on whether the VLE data have been measured isobarically or isothermally. Re-writing Equation (3-74), which expresses the summability relation of partial properties, yields:

$$g = x_1\ln\gamma_1 + x_2\ln\gamma_2 \tag{3-163}$$

Letting g^{ex} represent the experimental value of g, and differentiating Equation (3-163) with respect to x_1:

$$\frac{dg^{ex}}{dx_1} = x_1\frac{d\ln\gamma_1^{ex}}{dx_1} + \ln\gamma_1^{ex} + x_2\frac{d\ln\gamma_2^{ex}}{dx_1} - \ln\gamma_2^{ex} \tag{3-164}$$

This may be written as:

$$\frac{dg^{ex}}{dx_1} = \ln\frac{\gamma_1^{ex}}{\gamma_2^{ex}} + \varepsilon + x_1\frac{d\ln\gamma_1^{ex}}{dx_1} + x_2\frac{d\ln\gamma_2^{ex}}{dx_1} - \varepsilon \tag{3-165}$$

Subtracting Equation (3-165) from Equation (3-161) and re-writing in terms of residuals ($\delta g = g - g^*$) leads to:

$$\frac{d(\delta g)}{dx_1} = \delta\ln\frac{\gamma_1}{\gamma_2} - \left(x_1\frac{d\ln\gamma_1^{ex}}{dx_1} + x_2\frac{d\ln\gamma_2^{ex}}{dx_1} - \varepsilon\right) \tag{3-166}$$

Reduction of a VLE data set (whether isobaric or isothermal) using $\sum(\delta g)^2$ as the objective function (so as to force the δg residuals to scatter about zero) results in the left-hand side term of Equation (3-166) being, to all intents and purposes, zero. Hence:

$$\delta \ln \frac{\gamma_1}{\gamma_2} = x_1 \frac{d \ln \gamma_1^{ex}}{dx_1} + x_2 \frac{d \ln \gamma_2^{ex}}{dx_1} - \varepsilon \qquad (3\text{-}167)$$

From the Gibbs-Duhem equation (Equation (3-162)), the right-hand side of the above equation is required to be zero, provided that the experimental VLE data are consistent. Thus, the residual on the left is a direct measure of deviations from the Gibbs-Duhem equation (Van Ness [1995]). Van Ness [1995] also notes that the extent to which the values of this residual fail to scatter about zero provides a measure of the departure of the data from thermodynamic consistency.

In order to quantify the degree to which the data departs from consistency, Van Ness [1995] developed the following table, Table 3-1. The table provides an indication of thermodynamic consistency using indices, with an index of one signifying excellent data and an index of ten extremely poor data.

Table 3-1: Consistency index table for the direct test (Van Ness [1995]).

Index	RMS $\delta\ln(\gamma_1/\gamma_2)$	
1	> 0	≤ 0.025
2	> 0.025	≤ 0.050
3	> 0.050	≤ 0.075
4	> 0.075	≤ 0.100
5	> 0.100	≤ 0.125
6	> 0.125	≤ 0.150
7	> 0.150	≤ 0.175
8	> 0.175	≤ 0.200
9	> 0.200	≤ 0.225
10	> 0.225	

CHAPTER
4

MOLECULAR SIMULATION

In recent years there has been a remarkable and rapid increase in the processing power of computers, without the associated costs becoming exorbitant. This, combined with simultaneous advancements in molecular simulation algorithms (to take advantage of this increased computing power), has led to molecular simulation becoming a viable alternative to traditional methods for obtaining experimental VLE data. Computer simulations differ from the familiar forms of modeling VLE data (such as equations of state, Section 3.4.2, and activity coefficient models, Section 3.4.1) in that the simulations are predictive in nature. They do not attempt to fit a particular model to a data set by regressing for particular parameters. Instead, they are a numerical calculation based on pure component data and statistical probabilities. Thus, the resulting data have inherent statistical errors, as would be expected in any experiment.

A number of advantages are offered to researchers by molecular simulation. The most obvious benefit is in terms of safety. Operating conditions that would be extremely dangerous (i.e. high temperature and/or pressures) or even impossible in a laboratory may be run on a computer as safely and easily as a system at room temperature and atmospheric pressure. Similarly, hazardous substances that would otherwise put the wellbeing of the researcher at risk may be measured in absolute safety. There is also an associated monetary saving because once the computer cluster is in place (this involves an initial capital outlay) the cost (in terms of maintenance and upkeep) is comparatively low. This is especially true of those systems involving hazardous species or unusual operating conditions as the costs

involved are often excessive due to the difficulty of undertaking the measurements. Two of the disadvantages associated with the simulations are accuracy and reliability. The results are often not as accurate as they ideally should be since large deviations from accepted experimental data often occur. Statistically, the data often leaves much to be desired as the standard deviations are, on occasion, unacceptably high. Furthermore, at this time reliable, transferable potential models are not available and this limits the number of systems to which molecular simulation may be applied. Clearly these drawbacks are highly significant when dealing with processes involving separation of high-purity chemicals where accurate data are essential. However, these areas are continually being improved upon as more powerful computers and more advanced potential models become available. Moreover, this need for improvement provides the impetus for ongoing research into the subject of molecular simulation.

Currently, two broad fields exist in molecular simulation: Molecular Dynamics and Monte Carlo. Molecular Dynamics is based on the solution of equations of motion (Newton's Second Law, usually with relativistic effects not taken into consideration). Here, an initial (non-equilibrium) state is encouraged towards a steady-state condition. Generally, Molecular Dynamics finds application in systems where time-dependent properties are the focus of the study. Monte Carlo simulations are employed when only the equilibrium properties are of interest. The method is based on statistical probabilities, with states possessing a higher probability occurring more frequently and, hence, providing a greater contribution to the system averages (discussed below). Several variations of the Monte Carlo simulation exist, with the Gibbs ensemble modification being the focus of this work.

4.1 The Gibbs Ensemble

4.1.1 Introduction

The Gibbs ensemble was developed by Panagiotopoulos [1987] and was extended to the study of binary phase equilibria by Panagiotopoulos et al. [1988]. The method takes its name from the fact that J. W. Gibbs originally derived the equations describing the

conditions necessary for the ensemble. According to Panagiotopoulos [1987], the new ensemble allows the direct calculation of the phase co-existence properties of pure components and mixtures from a single simulation, without the need to determine the chemical potential.

As was mentioned above, the Gibbs ensemble is a variant of a Monte Carlo simulation. Thus, the basis for the ensemble rests upon the supposition that the true thermodynamic properties of a system may be obtained by calculating the average of each of the properties for all possible molecular configurations of that system. In essence, each property is a weighted average:

$$M_{avg} = \sum_i M_i \mathrm{P}_i \tag{4-1}$$

where M_i represents the thermodynamic property in a specific molecular configuration, and P_i the probability of occurrence of that state. Clearly, certain configurations have a far greater likelihood of occurring than others i.e. the probability that particular states will exist is higher than for certain other states. For an *NVT* system (i.e. a system that has a constant number of moles, *N*, constant volume, *V* and constant temperature, *T*), these probabilities may be written in the following form:

$$\mathrm{P}_i = \frac{\exp\left[\dfrac{-E_i}{k_B T}\right]}{\sum_i \left[\dfrac{-E_i}{k_B T}\right]} \tag{4-2}$$

where k_B represents the Boltzmann constant, T is the system temperature and E_i the energy of the configuration of interest.

The technique followed in the Gibbs ensemble is similar to the methodology adopted by Metropolis et al. [1953]. Metropolis and co-workers realized the impossibility of summing the term in the denominator of Equation (4-2) over all states. They chose instead to set up a representative sample of the system by analyzing a so-called *box* of molecules. The box must contain enough molecules (typically of the order 10^2 or 10^3) to be characteristic of the system as a whole and this box is then considered to be repeated throughout the system.

Another innovation implemented by Metropolis et al. [1953] was importance sampling, in which only states that appreciably influence the average are sampled. This implies the need for some form of acceptance criterion by which the significance of a particular state may be ascertained. A convenient choice based on probability and the concept of *microscopic reversibility* (Allen and Tildesley [1987]) is given by:

$$P_{acc} = \min\left(1, \exp\left[\frac{-\Delta E}{k_B T}\right]\right) \tag{4-3}$$

Thus, when the energy change resulting from a particular move is negative, that state will always be accepted since in that case the exponential term has to be greater than one. When a positive energy change occurs, the move is accepted provided that the probability represented by the exponential term in Equation (4-3) is greater than a random number generated between zero and one.

4.1.2 Theory

The Gibbs ensemble attempts to simulate a two-phase system by constructing two boxes, one representing the liquid phase and the other the vapour phase. The two boxes are initially set up with a certain volume and number of molecules. The two regions are then allowed to interact (as is described below) until equilibrium is achieved. The box with fewer molecules in it (or, alternatively, the larger volume) has a lower density and represents the vapour phase, whilst the second box naturally forms the liquid phase. According to Panagiotopoulos [1987], the two regions will generally have different compositions and densities, yet they are in thermodynamic equilibrium, both internally and with each other by the time the simulation is ended.

The system is brought to thermodynamic equilibrium through specific modifications to the boxes. These changes are conducted repeatedly while the simulation is being run until a steady-state is achieved. As was discussed in Section 4.1.1, the change to the system is accepted or discarded based on the probability of that change being viable in reality. Thus, highly improbably modifications to the boxes are possible, but have an extremely small

likelihood of actually occurring. In the Gibbs ensemble, three different changes are possible (refer to Figure 4-1) in achieving total thermodynamic equilibrium:

1. random molecule movements within one or both simulation boxes (to achieve thermal equilibrium)
2. volume changes to the simulation boxes (to achieve mechanical equilibrium)
3. movement of molecules between the two boxes (to achieve chemical equilibrium)

Furthermore, for systems containing non-spherical molecules a move that randomizes the molecular orientation (or conformation) is also performed.

Theoretically, in the statistical limit of an infinitely long simulation, all ensembles will be equivalent, i.e. they will produce the same results irrespective of the starting conditions. However, in practice simulations can fail due to a number of reasons e.g. instability near the critical point. The simulation stability depends upon several factors, such as the initial compositions and volumes. Thus, it is advisable to begin the simulations with a reasonable guess as to the final values so as to give the system a viable opportunity to reach equilibrium. However, the question of how to accomplish this remains.

One solution to this problem is to set the starting values close to those that have been determined experimentally. This presents an immediate difficulty though: experimental data are then required before the simulations may be undertaken. Since one of the goals of molecular simulation is to alleviate the need for experimentally measured VLE data, this is clearly not the most attractive method for obtaining initial conditions. An alternative method (in the case of binary VLE) is to use Raoult's Law as an approximation of the system. This would then give a satisfactory starting point for the simulation without the necessity of obtaining experimental data. If the system under investigation was too complicated for Raoult's Law to provide an acceptable guess (e.g. systems that exhibit azeotropes), modified Raoult's Law could be used instead. However, both laws still require certain pure component data (e.g. vapour pressures). If these data were not available in literature, a pure component NVT Gibbs ensemble could be run (under the correct system conditions) to obtain the necessary values.

Initial system state before any moves are attempted:

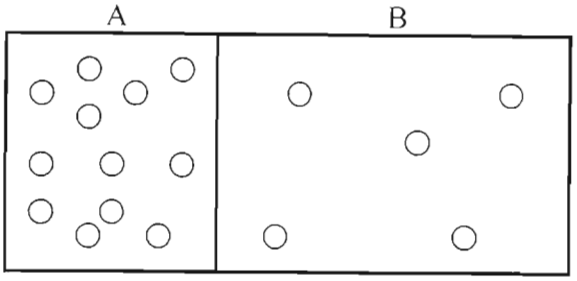

1. Random molecule translations within each box

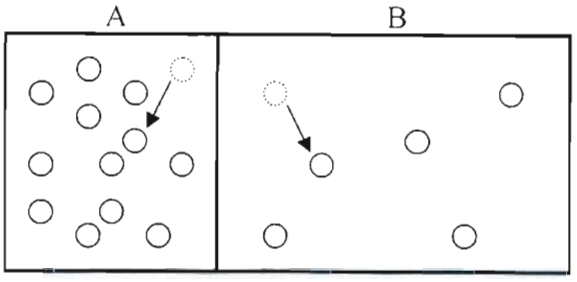

2. Volume changes to the simulation boxes

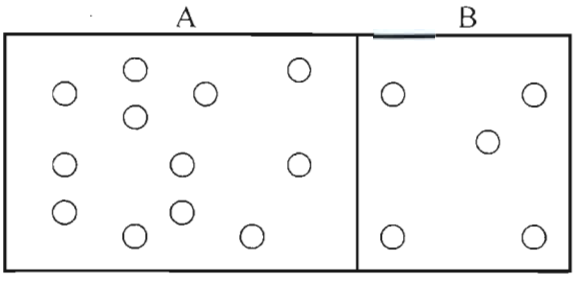

3. Molecular translations between simulation boxes

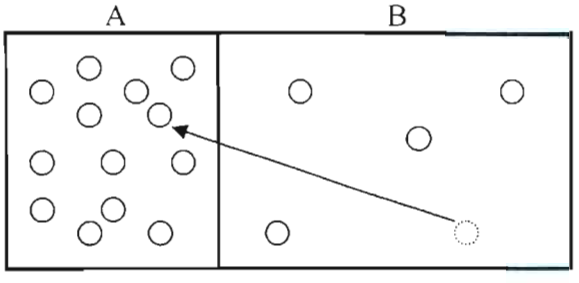

Figure 4-1: Schematic diagram showing the moves allowed in the NVT Gibbs ensemble simulation.

Panagiotopoulos [1987] derived the equations by which the change to the system energy may be calculated for each step presented in Figure 4-1:

1. The first move shown in Figure 4-1 results in an overall energy change given by:

$$\Delta E = \Delta E_A + \Delta E_B \tag{4-4}$$

2. The second move involves a volume perturbation of random magnitude:

$$\Delta E = \Delta E_A + \Delta E_B - N_A k_B T \ln \frac{V_A + \Delta V}{V_A} - N_B k_B T \ln \frac{V_B + \Delta V}{V_B} \tag{4-5}$$

3. In the third move illustrated in Figure 4-1, a molecular "swap" occurs:

$$\begin{aligned} \Delta E = \Delta E_A + \Delta E_B + N_A k_B T \ln \frac{N_A + 1}{N_A} + N_B k_B T \ln \frac{N_B - 1}{N_B} \\ + k_B T \ln \frac{V_B}{N_B - 1} - k_B T \ln \frac{V_A}{N_A + 1} \end{aligned} \tag{4-6}$$

4.1.3 Advantages and Disadvantages

Panagiotopoulos et al. [1988] state that the most attractive features of the technique are its generality (it may be applied to any physical situation between two phases provided that appropriate equilibrium conditions are stipulated) and simplicity. The method also offers a distinct reduction in the time required to complete a simulation when compared to previous approaches. This increase in speed is particularly pronounced for phase co-existence curves of binary mixtures. Furthermore, a single simulation results in a phase co-existence point. According to Panagiotopoulos [1988], the method is sensitive to small free energy differences and does not require an accurate evaluation of the free energy or chemical potential.

The key limitation of the Gibbs ensemble technique in its current form is that it is dependent upon a reasonable number of successful insertions, usually of the order 10^3 (Panagiotopoulos [1988]). The method fails if these insertions are not performed. In

addition, the present method is unable to simulate equilibria that involve solids. Another drawback is that the particle insertion step has a very low probability of success for molecules that are flexible or that display other structural complexities (such as non-sphericity or branching). Furthermore, close to the critical temperature (T_c), the free energy difference between the liquid and vapour phases decreases, resulting in these phases becoming unstable. On the other hand, far from T_c the liquid phase becomes particularly dense and the probability of inserting a molecule becomes very low. As was mentioned above, this will result in the simulation failing.

One solution to this difficulty in the insertion of complex molecules is *configurational bias*. This technique was proposed by Siepmann [1990] and Siepmann and Frenkel [1991]. Instead of trying to insert the entire molecule at once, the molecule is grown group by group from an initial starting point. The chain may be twisted and different growth directions attempted until a successful configuration is found. If this is not possible, then the insertion fails. In this way, the success rate for the insertion of these complex molecules is dramatically increased and, hence, fewer simulations fail.

4.2 The Stockmayer Potential Model

There are essentially two approaches when attempting to simulate VLE. One can choose a highly complicated model to describe the intermolecular interactions, but this type of approach lacks transferability to a wide range of chemicals. In addition, it leads to long calculation times that rapidly increase with increasing molecular complexity. Alternatively, one can choose a simpler potential model to represent a wider range of compounds. Generally, this option is preferable since it allows the researcher to investigate a large number of systems without intensive theoretical manipulation.

Thermodynamic behaviour is influenced extensively by electrostatic interactions between the molecules comprising a chemical system. Vapour pressures and liquid densities are two examples of properties that are characteristically affected by these polar forces. In general, fluids that exhibit a high polarity (i.e. they possess a large dipole moment in relation to their

size) deviate significantly from corresponding-states behaviour. According to van Leeuwen [1994a], the principle of corresponding states claims that: 'all substances obey the same equation of state in terms of reduced variables', with the thermodynamic variables being reduced by the analogous critical property. Therefore, the entire reduced co-existence curve for a particular species will overlap with that of another substance using a different reduction factor. The potential model chosen to simulate a particular chemical system must be capable of describing a comparable deviation from corresponding-states behaviour as that exhibited by the real system.

Many potential models (or forcefields) have been proposed over the years. Possibly the most widely used and accepted potentials are the TraPPE model (Martin and Siepmann [1998], Wick et al. [2000]), the NERD model (Nath et al. [1998], Nath et al. [2001]) and the Buckingham exp-6 model (Errington and Panagiotopoulos [1999]). However, these potential functions have not as yet been extended to highly polar compounds such as carboxylic acids. Thus, they proved to be of no use for the work conducted in this project. Therefore, the Stockmayer potential model (using the van Leeuwen [1994b] method of obtaining model parameters) was selected for the simulations. The Stockmayer model successfully incorporates dipoles and has been used previously in the prediction of pure component data of polar compounds (van Leeuwen [1994b]) and binary VLE of non-polar fluorocarbons (Gao et al. [1997]). In this work, the method will be extended to prediction of binary VLE of polar compounds.

4.2.1 Theory

According to Gao et al. [1997], the Stockmayer potential is a convenient model for polar fluids. A distinct property of a Stockmayer fluid is its deviation from corresponding-states behaviour. The Stockmayer potential is based upon the Lennard-Jones (LJ) model, which represents the dispersion interactions. The polarization effects are incorporated through the addition of an embedded point dipole. The Stockmayer potential function is given by (van Leeuwen [1994b]):

$$U(\mathbf{r}_{ij}) = 4\varepsilon\left[\left(\frac{\sigma}{\mathbf{r}_{ij}}\right)^{12} - \left(\frac{\sigma}{\mathbf{r}_{ij}}\right)^{6}\right] - \frac{\mu^2}{4\pi\varepsilon_0 \mathbf{r}_{ij}^3} g(\theta_1^S, \theta_2^S, \phi^S) \tag{4-7}$$

where σ and ε are the LJ size and energy parameters respectively, ε_0 is the permittivity of free space (i.e. a vacuum), $\boldsymbol{r}_{ij}$ is the vector of the distances r_{ij} between particles i and j and μ is the dipole moment. The orientation-dependent function $g(\theta_1^S, \theta_2^S, \phi^S)$ represents the electrostatic energy interaction between two point dipoles and is given by:

$$g(\theta_1^S, \theta_2^S, \phi) = 2\cos\theta_1^S \cos\theta_2^S - \sin\theta_1^S \sin\theta_2^S \cos\phi^S \tag{4-8}$$

Here, the angles θ_1^S and θ_2^S are the inclinations of the respective dipole axes to the intermolecular axis and ϕ^S is the azimuth angle between the two dipole axes.

The two LJ parameters have the following definitions (van Leeuwen [1994b]: ε is the characteristic depth of the energy well (this is the curve that the potential model describes) due to non-polar forces alone, whilst σ is the intermolecular distance at which the potential due to non-polar forces alone would be zero.

In molecular simulation it is common practice to work with *reduced variables*. For a polar fluid, the polar parameter of interest is the reduced dipole moment, μ^*, which gives the ratio between polar and non-polar interactions:

$$\mu^* = \sqrt{\mu^2 / 4\pi\varepsilon_0\varepsilon\sigma^3} \tag{4-9}$$

The other necessary reduced parameters are:

$$T^* = k_B T / \varepsilon \tag{4-10}$$

$$\rho^* = N_A \rho \sigma^3 / M_W \tag{4-11}$$

$$P^* = P\sigma^3 / \varepsilon \tag{4-12}$$

$$Z^* = P^* / \rho^* T^* \tag{4-13}$$

$$\Delta H_{vap}^* = \Delta H_{vap} / N_A \varepsilon \tag{4-14}$$

where T is temperature, P is pressure, Z is the compressibility factor, ρ is density, k_B is Boltzmann's constant and ΔH_{vap} is the enthalpy of vapourization.

The critical properties of the components defined in Equations (4-10) through (4-14) have been parameterized in terms of the reduced dipole moment by van Leeuwen [1994a]:

$$T_c^* = 1.313 + 0.2999\mu^{*2} - 0.2837\ln(\mu^{*2}+1) \tag{4-15}$$

$$\rho_c^* = 0.3009 - 0.00785\mu^{*2} - 0.00198\mu^{*4} \tag{4-16}$$

$$P_c^* = 0.127 + 0.0023\mu^{*2} \tag{4-17}$$

$$Z_c^* = 0.3282 - 0.0383\mu^{*2} + 0.00281\mu^{*4} \tag{4-18}$$

$$\frac{\Delta H_{vap}^*}{T_c^* \Delta Z^*} = 5.154 + 0.329\mu^{*2} \tag{4-19}$$

These correlations hold for a reduced dipole range of $0 \le \mu^* \le 2.45$. If the reduced dipole falls outside of this range (which is unlikely, even for extremely polar substances) then extrapolations should be carried out with care.

An additional parameterized equation was also proposed by van Leeuwen [1994b]:

$$\rho_l^*|_{T_r^*=0.75} = 0.7197 - 0.00362\mu^{*2} + 0.00666\mu^{*4} - 0.00142\mu^{*6} + 0.0000863\mu^{*8} \tag{4-20}$$

According to van Leeuwen [1994b], this equation results from simulation data using a pragmatic approach. She states that this approach was preferred to a theoretical description since the fore-most available theory only suffices for μ^* less than 1.7.

4.2.2 Determining the Stockmayer Parameters

In the Stockmayer potential model only two adjustable parameters exist, namely: ε and σ. The reduced dipole moment is obtained from its defining equation (Equation (4-9)) using the experimental dipole moment and the optimized values calculated for ε and σ. Prior to

the method proposed by van Leeuwen [1994b], two methods for determining these parameters existed:

1. The first (and most widely employed) method uses experimentally measured second virial coefficient data to derive the parameters. Exact expressions may be obtained for the second virial coefficients for Stockmayer fluids from statistical mechanics (van Leeuwen [1994b]).
2. The second method derives the Stockmayer potential parameters from low-pressure gas-viscosity data.

Many parameters for the Stockmayer potential model have been reported in literature for both methods. For the first method, the compilation of Polak and Lu [1972] represents the largest (and relatively recent) source. For the latter method, a significant collection of parameters was published by Mourits and Rummens [1977].

However, these two methods have several drawbacks that are discussed in detail by van Leeuwen [1994b]. The main disadvantage of the second-virial coefficient method is that for strongly polar molecules (such as carboxylic acids) the non-polar forces become masked. As a direct result of this fact, the value of ε determined from the second-virial coefficient data is inadequate. Since VLE from Stockmayer parameters relies largely on a precise value for ε, this presents a significant problem for researchers. The gas-viscosity method yields different parameters to the second-virial coefficient method. For polar fluids, σ is larger than the value determined from the second-virial coefficients. However, for non-polar fluids σ is systematically smaller. Thus, the Stockmayer parameters are method dependent rather than system dependent.

In general, a parameter set determined from a certain experimental property will lead to an excellent description of that quantity, but will not necessarily successfully predict any other thermodynamic properties of the system. Further, the simple intermolecular potential energy models are incapable of predicting system properties over a significant temperature range (van Leeuwen [1994b]). To alleviate this problem, van Leeuwen [1994b] developed an alternative method for evaluating the Stockmayer potential model parameters. The procedure yields an appropriate value of μ^* and the analogous ε and σ values from which

an experimental phase co-existence envelope may be successfully reproduced. The method of van Leeuwen was employed in this project.

4.2.2.1 Evaluation of Stockmayer Parameters Using the Method of van Leeuwen [1994b]

The first requirement for the correct prediction of a phase co-existence curve is an accurate value for the reduced dipole moment. This results from the fact that the reduced dipole moment has a significant effect on the location of the co-existence curve of Stockmayer fluids (plotted in reduced variables). This is one of the key advantages to van Leeuwen's procedure, since the method generates an accurate value for the reduced dipole moment through an iterative calculation. Another benefit provided by this method is that three-body interactions are included since liquid-like densities are involved (van Leeuwen [1994b]). Both methods discussed in Section 4.2.2 incorporate only two-body effects and low fluid densities (and, hence, are unsuitable for the description of VLE properties).

Several assumptions are necessary in order to evaluate the Stockmayer parameters (van Leeuwen [1994b]):

- the deviation from corresponding-states behaviour in liquid density is the same for real polar fluids as for Stockmayer fluids
- the polarity of a real fluid is sufficiently typified by determining its experimental dipole moment
- the Stockmayer potential in all its simplicity can describe the phase behaviour of non-spherical, off-central dipolar, multipolar or even hydrogen-bonding types of fluids.

The procedure rests in essence on two factors:

1. the reduced dipole moment is the free-varying parameter in the Gibbs ensemble (Monte Carlo) simulations
2. the parameters ε and σ are derived by demanding that the critical temperature, T_c, and one liquid density point of the real fluid (the liquid density at T_r = 0.75 is used: $\rho_l\,|_{T_r=0.75}$) coincide with the equivalent properties of the model fluid.

The two properties selected (in addition to the experimental dipole moment) to allow evaluation of the Stockmayer parameters are not randomly chosen. It is necessary that one property should be energy-related and the other size-related (refer to Section 4.2.1). The obvious choice for an energy-related quantity is the critical temperature, and (similarly) the liquid density may be easily applied to determine the size parameter (σ). Other properties such as pressure are less suitable as they rely on a combination of the LJ parameters (for pressure: σ^3/ε). Considering the liquid density, it is inadvisable to use the critical density because at this point the density is not particularly sensitive to μ^*. Instead, a liquid density at a lower temperature (T_r = 0.75) is employed since polar effects are most evident at low temperatures. Conversely, T_c^* is extremely sensitive to changes in the reduced dipole moment and is, therefore, ideally suited to derivation of the Stockmayer parameters.

The actual iterative procedure proposed by van Leeuwen [1994b] is based on the two equations expressing the relationship between the reduced properties of a Stockmayer fluid and the experimental values of a real fluid:

$$\varepsilon = k_B \frac{T_c}{T_c^*} \tag{4-21}$$

$$\sigma^3 = \frac{\rho_l^* |_{T_r^*=0.75}}{\rho_l |_{T_r=0.75}} \frac{M_W}{N_A} \tag{4-22}$$

where T_c^* and $\rho_l^* |_{T_r^*=0.75}$ are defined by Equations (4-15) and (4-20) respectively. Multiplying Equations (4-21) and (4-22) together to provide the term $\varepsilon\sigma^3$, and substituting into the definition of μ^* (Equation (4-9)) yields the following expression:

$$\mu^{*2} = \frac{T_c^*}{\rho_l^* |_{T_r^*=0.75}} \frac{\rho_l |_{T_r=0.75}\, \mu^2}{T_c M_w} \frac{N_A}{4\pi\varepsilon_0 k_B} \tag{4-23}$$

Substituting Equations (4-15) and (4-20) for T_c^* and $\rho_l^* |_{T_r^*=0.75}$ in Equation (4-23) results in an equation that is implicit in μ^*. An iterative calculation procedure may therefore be followed to solve for μ^*. Once the reduced dipole moment has been evaluated, ε is found using

Equations (4-15) and (4-21) and σ results from Equations (4-20) and (4-22). Using this method, van Leeuwen [1994b] calculated the Stockmayer parameters for 63 polar compounds and showed that the method yielded better results than the two methods discussed in Section 4.2.2 (Gao et al. [1997]).

4.3 Ewald Summation

4.3.1 Introduction

The technique commonly referred to as *Ewald summation* was introduced as a means of efficiently summing the long-range Coulombic interactions that exist between simulation particles and all their infinite periodic images. Put another way, the Ewald sum is used to calculate long-range contributions to the potential energy of a system with periodic boundary conditions (Frenkel and Smit [1996]).

According to Allen and Tildesley [1987], a long-range force may be defined as one for which the spatial interaction falls off no faster than s^{-d}, where d is the dimensionality of the system and s is the molecular separation. These forces frequently present researchers with considerable difficulties because for a typical simulation ($N < 500$) their range is greater than half the box length. One possible solution to this dilemma is to simply increase the box size until the effect has become essentially negligible. However, even with the considerable advances in computing technology, this is not feasible as the time required per simulation becomes unacceptably high (simulation time $\propto N^2$ i.e. L^6). The Ewald sum offers a viable means of overcoming this problem.

4.3.2 Theory

The potential energy of a system of point charges may be written as:

$$U = \frac{1}{2}\sum_{\mathbf{n}}{}' \left(\sum_{i=1}^{N}\sum_{j=1}^{N} p_i p_j \left| \mathbf{r}_{ij} + \mathbf{n} \right|^{-1} \right) \qquad (4\text{-}24)$$

where the point charges are represented by p_i and p_j. The sum over $\boldsymbol{n}$ is the sum over all cubic lattice points possessing a length of $L = 1$ and integer coordinates $\boldsymbol{n} = (n_x, n_y, n_z)$. The prime over the sum indicates that all terms having $\boldsymbol{n} = 0$ are omitted whenever $i = j$. $\boldsymbol{r}_{ij}$ represents the vector of distances between the particles i and j ($r_{ij} = r_j - r_i$).

The sum presented in Equation (4-24) is only conditionally convergent for long-range Coulombic potentials. Thus, the result is dependent on the order in which the summation is performed. A sensible approach is to sum the boxes based on their proximity to the central box (i.e. the first term added will have $|\mathbf{n}| = 0 (\boldsymbol{n} = (0, 0, 0))$, the second term $|\mathbf{n}| = L$ etc.). In essence, this summation procedure builds the infinite system in roughly spherical layers. According to Allen and Tildesley [1987], it is essential that the properties of the medium surrounding the sphere be specified. The relative permittivity, ε_s, is of particular importance when applying this method. For instance, different results are obtained for spheres surrounded by a metal ($\varepsilon_s = \infty$) and a vacuum ($\varepsilon_s = 1$) respectively.

As was mentioned in the previous paragraph, the summation given in Equation (4-24) is conditionally convergent. In the Ewald method this difficulty is removed by surrounding each point charge with a charge distribution of opposite sign to the point charge, but possessing equal magnitude. Hence, the overall effect is to neutralize the charge of the particle in question. The functional form of the screening charge must be selected. For calculation convenience, it is common practice to apply a Gaussian distribution (in order to acquire a smoothly varying screening distribution):

$$\rho_{Gauss}(r) = p_i \left(\alpha_E / \pi \right)^{\frac{3}{2}} \exp(-\alpha_E r^2) \tag{4-25}$$

where the parameter α_E essentially determines the distribution width (it is commonly referred to as the Gaussian distribution parameter) and r is the position relative to the centre of the distribution. Since the screening distribution has been added to the point charge, a canceling distribution must also be added to return the overall potential to its original value. This correcting effect is illustrated in Figure 4-2.

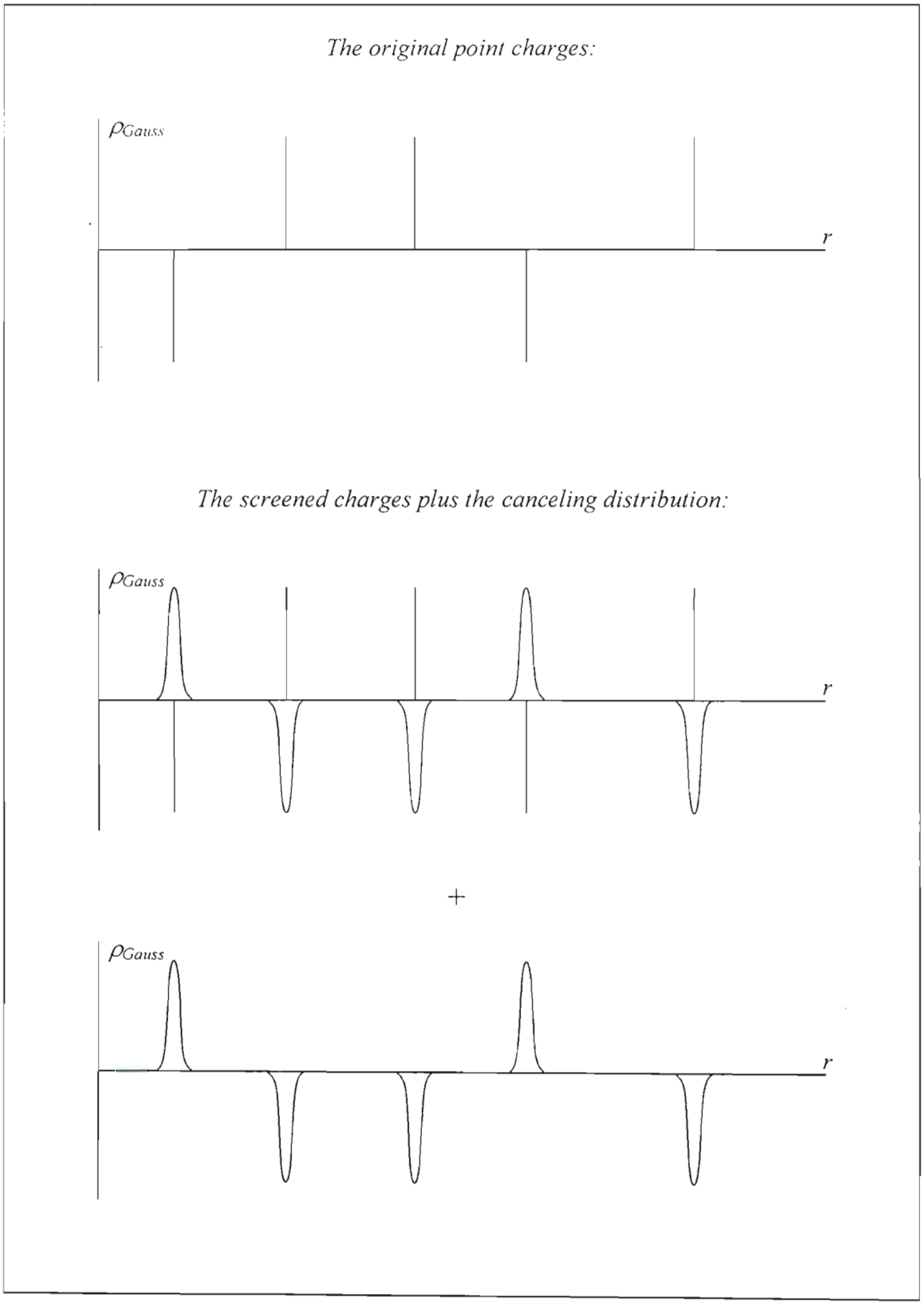

Figure 4-2: The charge distribution in the Ewald sum.

where the parameter α_E essentially determines the distribution width (it is commonly referred to as the Gaussian distribution parameter) and r is the position relative to the centre of the distribution. Since the screening distribution has been added to the point charge, a canceling distribution must also be added to return the overall potential to its original value. This correcting effect is illustrated in Figure 4-2.

Allen and Tildesley [1987] state that the canceling distribution is summed in *reciprocal space* (i.e. the Fourier transforms of the canceling distributions for each point charge are added and the total is transformed back into real space). A correction is also necessary for the self-interaction between each charge and the compensating charge cloud that has been introduced to neutralize the point charge. This so-called *self term* is subtracted from the total. The end result of all this mathematical manipulation (details may be found in de Leeuw et al. [1980]) is Equation (4-26), which is unconditionally convergent.

$$U = \frac{1}{2}\sum_{i=1}^{N}\sum_{j=1}^{N}\left(\sum_{|\mathbf{n}|=0}^{\infty}{}' p_i p_j \frac{erfc\left(\sqrt{\alpha_E}\,|\mathbf{r}_{ij}+\mathbf{n}|\right)}{|\mathbf{r}_{ij}+\mathbf{n}|}\right) + \frac{1}{2}\sum_{i=1}^{N}\sum_{j=1}^{N}\left(\frac{1}{\pi L^3}\sum_{k\neq 0} p_i p_j \frac{4\pi^2}{k^2}\exp\left(-k^2/\alpha_E\right)\cos(\mathbf{k}.\mathbf{r}_{ij})\right) - \sqrt{\frac{\alpha_E}{\pi}}\sum_{i=1}^{N} p_i^2 + \frac{2\pi}{3L^3}\left|\sum_{i=1}^{N} p_i \mathbf{r}_i\right|^2 \tag{4-26}$$

The parameter, $\boldsymbol{k}$, that appears in the second term corresponds to a reciprocal vector given by $\boldsymbol{k} = 2\pi\boldsymbol{n}/L$. According to Allen and Tildesley [1987], when α_E is chosen to have a large value, a sharp charge distribution will result. Hence, a considerable number of k-vectors will be needed in order to model it. The greater the number of k-vectors, the longer the simulation will take to run and, therefore, it is desirable to minimize this quantity. Allen and Tildesley [1987] note that the sum over the k-vectors is generally computed using a separate subroutine, whereas the modified point charge interactions are evaluated within the main program loop. When selecting a value for α_E, it is important to note that this parameter determines the relative rate of convergence of the real (first term) and reciprocal (second term) sums. A large value of α_E results in the real-space sum converging faster (as α_E tends to ∞, $erfc\left(\sqrt{\alpha_E}\,|r_{ij}+n|\right)$ tends to zero (where *erfc* is the complimentary error

function)). Conversely, a small value of α_E will encourage the reciprocal-space sum to converge faster since the exponential term tends to zero as α_E tends to zero. Hence, an optimal figure for α_E must exist. Usually, the parameter is chosen so as to minimize the required computational time, without sacrificing accuracy when solving the real and reciprocal sums.

A means of extending the original Ewald method to dipolar systems (like those simulated in this work) was proposed by Allen and Tildesley [1987]. They suggested that Equation (4-26) be modified by substituting $\mu_i'''\nabla_{r_i}$ for the point charge p_i, where μ_i''' represents the molecular dipole. Furthermore, Allen and Tildesley [1987] proposed that a conceptually simple method for modeling dipoles was to represent them as partial charges within the molecule core. This allows the Ewald method to be applied to each particular partial charge directly. However, certain complications do arise in the formulation and evaluation of the self term. More detail on the extension of the Ewald method to dipoles may be obtained from Smith [1982].

CHAPTER
5

EQUIPMENT

This chapter deals with the equipment that was used during this project. The vapour-liquid equilibrium (VLE) experimental data were measured using a glass, recirculating VLE still designed by Raal (Raal and Mühlbauer [1998]). In order to operate the still effectively, a number of peripheral pieces of equipment are necessary and these are also presented below. The molecular simulation portion of this work was carried out using a twenty node (nineteen slave nodes and one master node) Beowulf cluster. The Linux operating system was utilized in the efficient running of this computer system.

5.1 Vapour-Liquid Equilibrium Equipment

The experimental VLE apparatus utilized in this project has been used previously by Joseph et al. [2001] and Sewnarain et al. [2002]. The equipment was discussed in detail by Joseph et al. [2001] and Joseph et al. [2002] and an excellent review on the history of circulating VLE stills, as well as the still used in this work, is available in Raal and Mühlbauer [1998]. Photographs of the still and related equipment are given in Appendix C.

Figure 5-1 shows a schematic block diagram of the experimental setup. The experimental apparatus includes the following pieces of equipment: a VLE still (discussed in Section 5.1.1), three Pyrex 5 L ballast flasks (two of which are joined to provide a 10 L ballast flask), a Julabo FT 200 cold finger, a Hewlett-Packard model34401A multimeter, a

Sensotec Super TJE pressure transducer, a vacuum pump, two solenoid valves, a differential mercury manometer, a LABOTECH water bath complete with pump and cooling water, three DC power supplies (one providing power for the motors used to turn the magnetic stirrers, and one each for the two solenoid valves), two AC voltage regulators allowing adjustment of the internal and external heaters, and a computer.

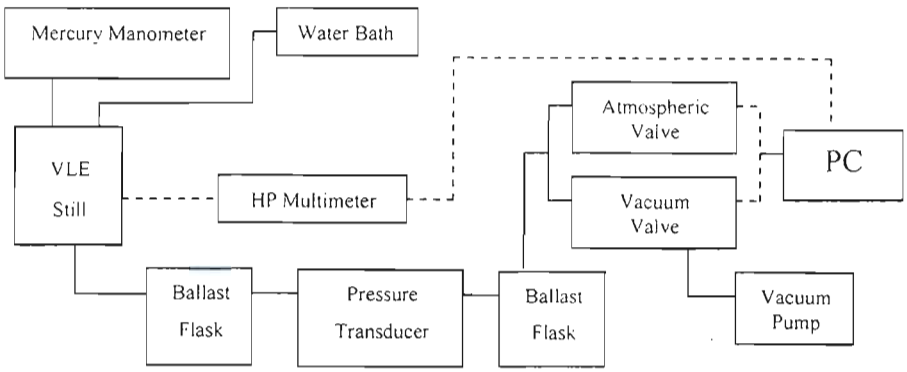

Figure 5-1: Schematic block diagram of the experimental VLE equipment showing electronic connections (-----)

5.1.1 Vapour-Liquid Equilibrium Still

The glass VLE still used to measure the carboxylic acid binary VLE systems was expertly constructed by P. Siegling. Figure 5-2 provides a detailed view of this apparatus. The highly refined still was designed by Raal (Raal and Mühlbauer [1998]) and incorporates all the positive features of the Yerazunis et al. [1964] design; whilst several improvements result in a piece of equipment capable of far more precise VLE measurement.

One of the central features of this still was the concentrically designed equilibrium chamber, surrounded by a vacuum jacket in order to ensure adiabatic operation of the chamber. The liquid sample was charged into the boiling chamber where the external and internal heaters brought the sample to a boil. The external heater consisted of nichrome wire wrapped around the boiling chamber, compensating for heat losses to the environment, while the internal heater consisted of a heater cartridge that provided the actual impetus for boiling. Further, the internal heater provided nucleation sites for smooth

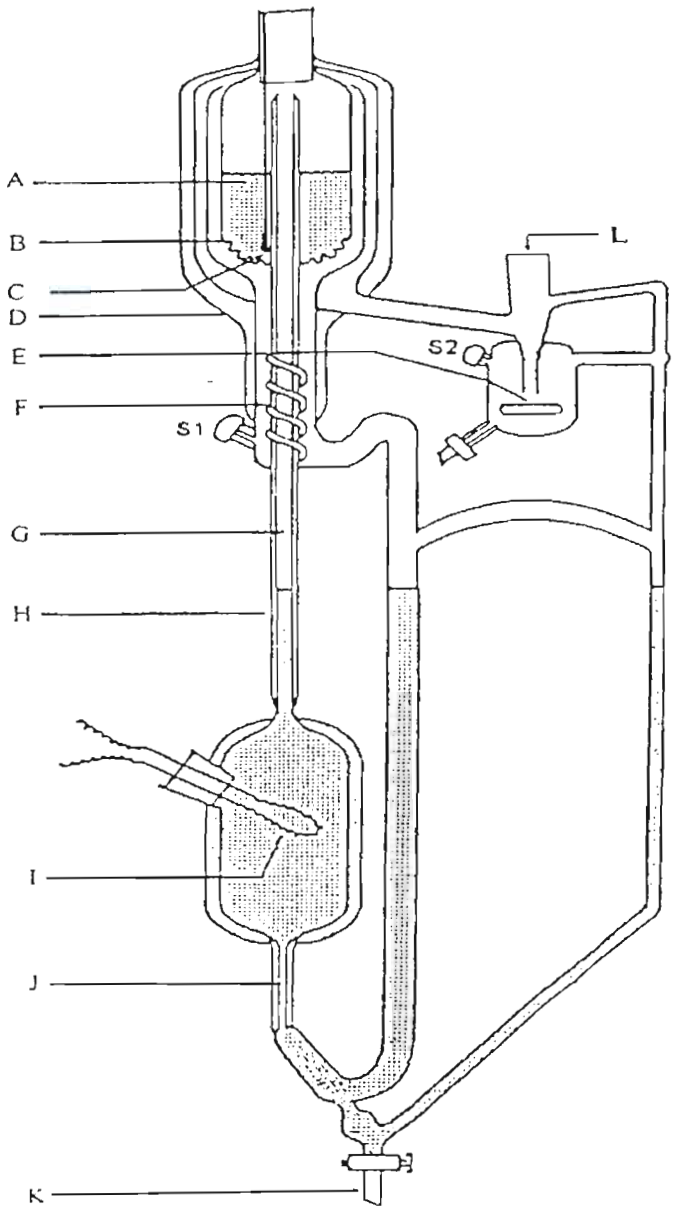

Figure 5-2: Schematic diagram of the VLE Still. *A: stainless steel wire mesh packing; B: drainage holes; C: PT-100 sensor; D: vacuum jacket; E: magnetic stirrer; F: stainless steel mixing spiral; G: insulated Cottrell pump; H: vacuum jacket; I: internal heater; J: capillary leg; K: drainage valve; L: condenser attachment; S1: liquid sampling septum; S2: vapour sampling septum.*

boiling and precise control of the circulation rate, while inducing rapid boiling. This boiling forced the liquid sample into the vacuum-jacketed equilibrium chamber via a vacuum-insulated Cottrell tube (to prevent heat transfer from the superheated mixture in the Cottrell pump to the equilibrium chamber). The mixture then flowed down through the packing that consisted of 3mm cylinders constructed from stainless-steel wire mesh. The packing provided a large interfacial surface area and ensured that there was significant contact between the liquid and vapour. This aided in achieving equilibrium rapidly within the still, even for species with a high relative volatility. The pressure drop through the packing was minimized due to its open structure (hollow, wire mesh cylinders). Within the packing, a PT-100 temperature sensing element was situated and this provided an accurate measure of the system's equilibrium temperature.

The equilibrium mixture exited from the equilibrium chamber via small holes placed at the bottom of the chamber and it was at this point that the liquid and vapour disengaged. The liquid flowed down into a small liquid trap (allowing sampling) and the overflow from this trap returned to the boiling chamber. The vapour flowed up and around the equilibrium chamber, and provided an essential thermal lagging role. The vapour then flowed down until contacting the condenser, and gathered in the condensate receiver from which the vapour samples were drawn. The vapour overflow returned to the boiling chamber via a standpipe leg.

A number of innovative features were incorporated into the VLE still design:

- Magnetic stirrers were included in the boiling chamber and the condensate receiver. The former served to provide a nucleation site for boiling (in addition to the internal heater) and also ensured that condensate returning from the condensate receiver overflow (at a lower temperature and rich in the more volatile component) was thoroughly mixed prior to evaporation, preventing flashing. The magnetic stirrer placed in the condensate receiver eliminated possible temperature and concentration gradients that might otherwise have existed in the vapour condensate. This aided in attaining equilibrium quickly and in allowing highly reproducible vapour sample concentrations when binary systems were being measured.

- Two heaters were integrated into the boiling chamber design. As mentioned above, the external heater helped to prevent heat losses to the environment while the internal heater provided the primary boiling driving force. This heater also resulted in brisk boiling within the boiling chamber. Simultaneously, the internal heater encouraged smooth boiling through the provision of nucleation sites and precise control of the circulation rate through the still.
- The central Cottrell pump resulted in the equilibrium chamber possessing angular symmetry. This prevented formation of gradients (either temperature or concentration) since no preferred radial direction existed for their development.
- The PT-100 temperature sensor rested within the packing. Thus, the returning liquid flowed around the sensor and this provided an extremely precise measure of the system temperature. Previous designs had the mixture being thrown onto the PT-100 bulb as it exited the Cottrell tube, which was clearly less accurate since the superheat was not permitted to dissipate.
- The still design was such that the packing was easily accessible through the top of the still. This enabled the packing height to be adjusted, which is a distinct advantage when dealing with highly volatile systems that may have difficulty in attaining equilibrium. Furthermore, in certain cases more inert glass packing may be required and the accessible equilibrium chamber allows for straightforward replacement of the packing.

5.1.1.1 Temperature Measurement and Control

The Hewlett-Packard multimeter was used to display the resistance of the PT-100 temperature sensor and this resistance was converted and displayed as a temperature on the computer interface using the simple linear relation: $T = m.R + c$ where T represented the temperature in degrees Celsius, R was the resistance of the PT-100 sensor and m and c were the gradient and y-intercept respectively (obtained from the temperature calibration – Section 6.2.2). The accuracy of the measured temperature was estimated to be within ± 0.02 °C, while the accuracy of the temperature control varied between 0.01 and 0.05 °C depending on the volatility of the species. The control strategy employed relied on pulse-width modulation of the solenoid valves in order to regulate the temperature and pressure.

5.1.1.2 Pressure Measurement and Control

The pressure was measured using a SENSOTEC Super TJE pressure transducer. The measured pressure accuracy was estimated at ± 0.03 kPa (the pressure calibration is discussed in Section 6.2.1) and when the still was being run isobarically, the pressure was controlled to within 0.01 kPa. Pulse-width modulation of the two solenoid valves was utilized in formulating the control strategy that was implemented with the aid of a computer.

5.1.1.3 Sampling

Both the liquid and vapour samples were withdrawn (through chemically-resistant septa) from the sampling points provided for that purpose (refer to Figure 5-2). Gas-tight syringes were utilized when taking the samples to ensure that no sample was lost during this process. This method of obtaining samples presents no problems provided that the suction pressure of the syringe is sufficient. Given that the volume of the sample withdrawn was small, operation of the still was unaffected. The septa needed to be replace once a week due to the harsh operating conditions (high temperatures and acidic mixtures).

5.1.1.4 Composition Analysis

A gas chromatograph was used to determine precise values for the liquid and vapour equilibrium compositions. According to Raal and Mühlbauer [1998], gas-liquid chromatography remains the most widely used procedure for analyzing multicomponent organic mixtures. A gas chromatograph operates by separating a mixture into its constituent components, which may then be analyzed to establish both the identity and the amount of each species present in the sample. In general, the two most popular GC detectors are:

1. A thermal conductivity difference (TCD) detector that provides a response to both hydrocarbons and non-hydrocarbons and, thus, is useful when water is suspected as a system impurity (e.g. if a hydrophilic substance such as ethanol is being studied).

2. A flame ionization detector (FID) that is only sensitive to species that contain a C-H bond i.e. hydrocarbons. They are, however, extremely responsive and are able to detect flows as low as 10^{-11} g/s (Raal and Mühlbauer [1998]).

Two gas chromatographs were employed in this project for the purpose of obtaining accurate composition measurements. The first was a Hewlett-Packard 5890 Series II gas chromatograph that was used when measuring VLE data for the cyclohexane (1) – ethanol (2) test system. The carboxylic acid binary systems could not be adequately separated using the column installed in the Hewlett-Packard GC. Thus, a Varian 3300 gas chromatograph was utilized instead. The Hewlett-Packard GC was operated using a TCD detector and a stainless-steel column (2.5m long with an inner diameter of 2.2mm) packed with 80 to 100 mesh Poropak Q. An FID was employed in the Varian 3300 gas chromatograph so that the acids could be accurately measured. A 30m megabore capillary column (diameter 0.53mm) with 007-FFAP on fused silica was employed in the Varian GC. These composition measurements are estimated to be accurate to within 10^{-3} of a mole fraction.

5.2 Molecular Simulation Equipment

The molecular simulation section of the project was conducted using a number of computers linked using a network hub. The linked computers (or *nodes*) are termed a *cluster*, and in this case a twenty node Linux-operated Beowulf cluster was utilized. One of the twenty nodes is known as the *master node* and was primarily concerned with allocating simulations (otherwise referred to as *jobs*) to the nineteen *slave nodes*. The actual computations took place on the slave nodes. The cluster could be accessed from a remote desktop computer, provided they were linked via a network and that the correct software (in this instance, SSH) had been installed.

Each node consisted of a 1.2 gigahertz AMD Athlon processor and 256 megabytes of RAM. Many versions of Linux are freely available as shareware and may be downloaded from the internet free of charge. The particular Linux version installed on the cluster was the Scyld Beowulf Scalable Distribution (modified from Redhat Linux 6.2). This version

was used as it allowed the cluster to be operated easily and efficiently with a minimum of maintenance. The simulations were performed using software developed by T. Vlught and modified by T. McKnight. The programme code (dubbed BIGMAC) was written in the programming language FORTRAN-77.

Jobs were submitted to the cluster (via the master node) through the package PBS Pro. It was possible to run simulations simultaneously over several nodes (parallel computation). Theoretically, this should have resulted in a significant decrease in computation times since the processing power should have increased considerably when the computers were linked. However, it was established that when two computers were linked, the computational speed-up was only around 1.7 times. Similarly, four computers running in parallel produced an increase of little more than two times. Hence, it was clear that it was more efficient to run jobs separately on individual nodes rather than to distribute the jobs over several nodes using the parallel software.

CHAPTER
6

EXPERIMENTAL PROCEDURE

The previous chapter was concerned with a description of the equipment used to produce the experimental data presented in this work. The current chapter focuses on the procedure followed in attaining those results. The VLE still can be operated in both isobaric and isothermal modes, and with each mode a specific (and different) procedure was necessary when measuring the VLE data. Before measurements could commence the still needed to be calibrated for both temperature and pressure, and the gas chromatographs needed to be calibrated for composition. It is vital that this phase of the work, the calibration of the equipment, be accomplished as accurately as possible since the accuracy of the measured data depends directly on the precision of the various calibrations. As was mentioned in chapter 5, the VLE still was previously utilized by Joseph et al. [2001], Joseph et al. [2002] and Sewnarain et al. [2002] in order to measure VLE data.

6.1 Cleaning of the VLE Still

Prior to calibration of the still and to the undertaking of any VLE measurements, the still must first be cleaned. It is essential that this cleaning be accomplished thoroughly as any contaminants in the system can have a considerable effect on the VLE data produced. The cleaning was achieved by rinsing the still systematically with acetone. The acetone was allowed to circulate under isobaric conditions for approximately forty-five minutes to an hour before being emptied from the still. This process was repeated two to three times

depending on the species. Chemicals such as the carboxylic acids were more difficult to remove than (for instance) ethanol and hence additional rinsing was required. Once the still had been satisfactorily cleaned, the vast majority of the acetone was drained using the drain valve installed on the still for this purpose. The vacuum pump was utilized to flash off the remaining acetone.

6.2 Equipment Calibration

6.2.1 Pressure Transducer Calibration

The SENSOTEC Super TJE pressure transducer was calibrated first because an accurate pressure reading is required in order to undertake the temperature sensor calibration. A mercury manometer attached to the still (Figure 5-1) was utilized in conjunction with a NIST certified electronic barometer in order to determine the actual pressure within the still. This was accomplished by first entering the set-point pressure (i.e. running the still in isobaric mode) using the graphical user interface (GUI) of the computer-controlled still and then accurately measuring the differential height of mercury within the manometer using a cathetometer. This height of mercury represented the pressure difference between atmospheric pressure (recorded by the barometer) and the pressure in the still, and hence a simple subtraction allowed calculation of the true system pressure:

$$P_{act} = P_{atm} - |\Delta mmHg| \tag{6-1}$$

This value was then compared to the pressure value displayed by the transducer. A series of pressures covering the range of anticipated experimental pressures was measured and a linear plot of 'displayed pressure' versus 'actual pressure' (Figure 6-1) completed the calibration.

6.2.2 Temperature Sensor Calibration

A PT-100 temperature sensor was used to measure the temperature of the system. The PT-100 resistance was displayed on a five-and-a-half digit Hewlett-Packard 34401 A model multimeter, with the GUI reflecting the true temperature calculated from the PT-100

resistance using the temperature versus resistance calibration curve (Figure 6-2). The temperature calibration was carried out in situ, using a pure component (purity >99.5%, Table 8-1). Two species (n-hexane [low boiling] and n-decade [high boiling]) were employed to ensure that the temperature calibration applied over the full experimental temperature range. To carry out the calibration, the still was operated isobarically over a range of pressures. For each pressure, the resistance of the sensor was recorded. Antoine's equation (readily available in literature, e.g. Reid et al. [1988]) for the respective pure component was then applied to determine the temperature corresponding to the system pressure. A plot of actual temperature versus resistance was generated and a least squares fit of the data to a straight line allowed determination of the slope and intercept of the line. These constants were then entered into the GUI and, thus, the actual system temperature was displayed by the computer during operation of the still.

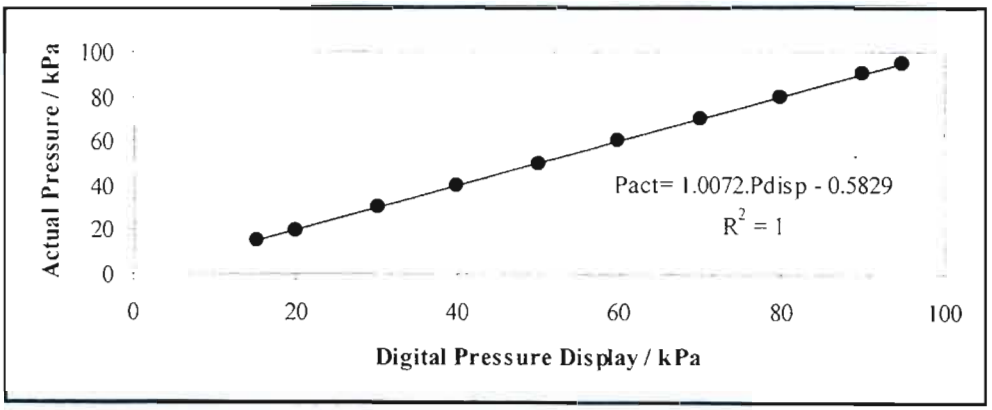

Figure 6-1: Pressure transducer calibration curve for VLE still.

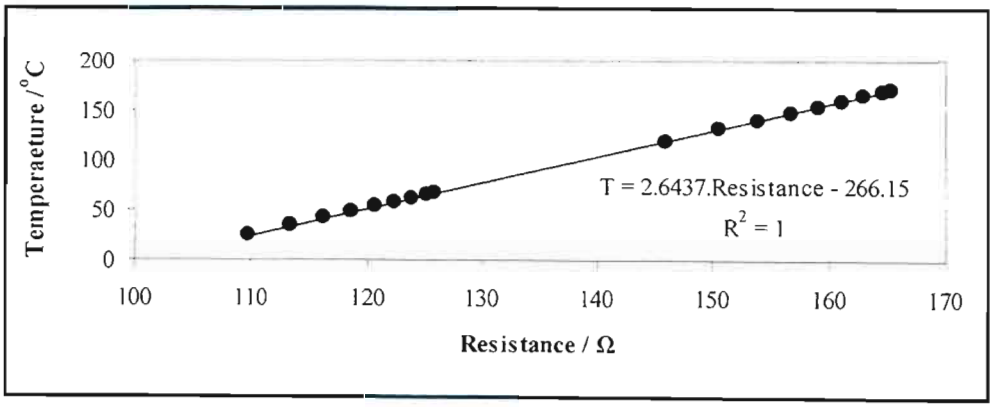

Figure 6-2: Temperature sensor calibration for VLE still.

6.2.3 Gas Chromatograph Calibration

Two gas chromatographs were utilized in this project in order to obtain accurate composition measurements. The cyclohexane (1) – ethanol (2) test system (refer to Section 8.3.1) was measured using a Hewlett-Packard 5890 Series II gas chromatograph, whereas the carboxylic acid systems were measured using a Varian 3300 gas chromatograph. The reason for this is that the response of the Hewlett-Packard detector (a thermal conductivity difference detector) to the acids was barely distinguishable from background noise and, thus, the errors incurred were unacceptably high. The Varian, however, had a flame ionization detector installed that gave an excellent response to the carboxylic acids. In addition, the retention times were far lower when using the Varian gas chromatograph since the Hewlett-Packard chromatograph had a packed column installed. The operating conditions for the two gas chromatographs are presented in Table 6-1.

The gas chromatograph (GC) calibration was carried out by following the area ratio method of Raal and Mühlbauer [1998]. This calibration is critical because a GC only produces peak areas and, hence, is no more accurate than the calibration used (Raal and Mühlbauer [1998]). In most cases, the area (A) of the peak generated by the electronic integrator is proportional to the number of moles (n) passing through the gas chromatograph. Introducing a response factor (F), the following general equation applies:

$$n_i = F_i . A_i \tag{6-2}$$

However, because of the difficulty in repeatedly injecting exactly the same volume of sample (and the area depends on the amount of sample injected), Raal and Mühlbauer [1998] suggest using ratios instead:

$$\frac{n_1}{n_2} = \frac{F_1}{F_2} \cdot \frac{A_1}{A_2} = \frac{x_1}{x_2} \tag{6-3}$$

The calibration is carried out by injecting standardized gravimetric samples of the system in question covering the entire composition range. The calibration is especially critical in the dilute regions as small errors will have a large effect on the compositions calculated from the calibration curve. In order to prevent detector overloading, sample volumes of 0.6 µl and 0.1 µl were used for the Hewlett-Packard and Varian gas chromatographs respectively.

Below, an example of a gas chromatograph detector calibration is given for the propionic acid (1) – valeric acid (2) system (Figures 6-3 and 6-4). The other calibrations are presented in the section titled "Experimental Results". A plot of x_1/x_2 versus A_1/A_2 provides the response factor ratio, F_1/F_2, since this ratio is merely the slope of the linear curve. The curve should naturally pass directly through the origin since when x_1 is zero, A_1 must also be zero. Ideally, the inverse of the slope of Figure 6-3, F_2/F_1 , should be equal to the slope of Figure 6-4, F_1/F_2, since this indicates that the response factor ratio is constant over the entire composition range. In the case of the carboxylic acids, the ratio was not constant since the inverse of F_1/F_2 was not exactly F_2/F_1. However, the percentage difference for both systems was only 1%. Since the ratios did differ, the F_2/F_1 slope was used in the valeric acid-rich region (i.e. in the dilute propionic acid region) and vice versa.

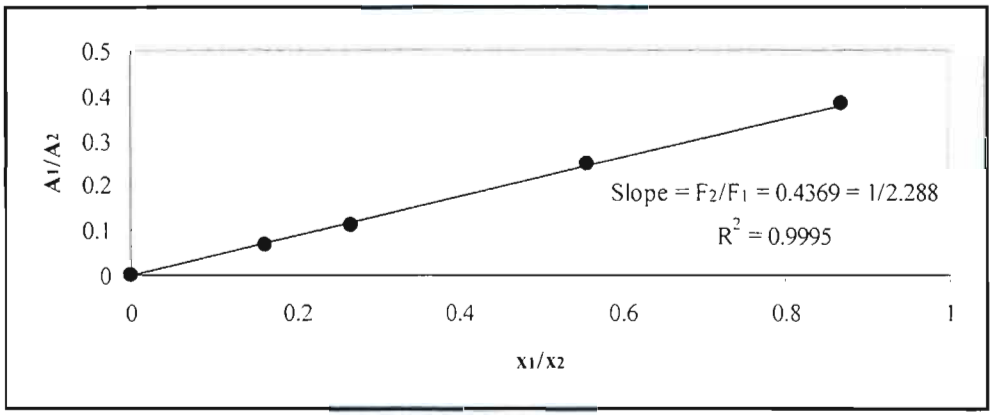

Figure 6-3: Calibration curve for the Varian 3300 gas chromatograph for the propionic acid (1) – valeric acid (2) system (dilute propionic acid region).

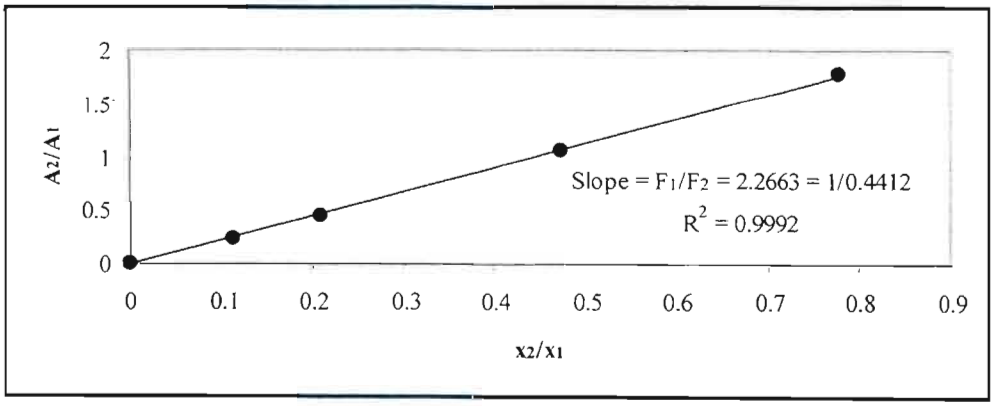

Figure 6-4: Calibration curve for the Varian 3300 gas chromatograph for the propionic acid (1) – valeric acid (2) system (dilute valeric acid region).

Table 6-1: Operating conditions for the Varian 3300 and Hewlett-Packard 5890 gas chromatographs.

Operating Condition	**Gas Chromatograph**	
Type	Hewlett-Packard	Varian 3300
Gas Flowrate (ml/min)	30	10
Oven Temperature Profile		
Initial Temperature (°C)	200	85
Hold Time (min)	-	0
Temperature Ramp (°C/min)	-	5
Final Temperature (°C)	-	140
Hold Time (min)	-	0
Detector Type	TCD	FID
Detector Profile		
Temperature (°C)	200	200
Attenuation	-	16
Range	-	10
Injector Profile		
Temperature (°C)	210	200
Auxiliary Profile		
Temperature (°C)	-	210
Hold Time (min)	-	0
Temperature Programme	-	No
Elution Time (min)		
Cyclohexane	10.34	
Ethanol	3.20	
Propionic Acid		4.26
Isobutyric Acid		4.72
Valeric Acid		8.36

6.3 Procedures for Isobaric and Isothermal Operation of the VLE Still

The VLE still was capable of being run in either isobaric or isothermal modes, with the still being controlled via a computer in both cases. Since the isothermal procedure relies initially on the isobaric mode, the isobaric procedure will be described first.

6.3.1 Isobaric Operation of the VLE Still

6.3.1.1 Initial Preparations

The computer, DC power supplies to the solenoid valves and stirrer motors, multimeter, pressure transducer and cooling water supply (Figure 5-1) were all switched on. The clean still was filled with one or other of the pure components that were to be studied (the second was added gradually as the experiment continued – refer to Section 6.3.1.3). The still was filled by injecting (with syringes) the component being added through the liquid and vapour sampling points alternately. Thus, both the liquid and vapour condensate receivers were full and, hence, the level to which the still must be filled could be accurately judged. As the temperature rose, the molar volume of the binary components increased and this had to be taken into account when filling the still. In general, the boiling chamber should be filled to a level approximately four centimeters above the top of the chamber. Once the boiling chamber was charged, the valve leading to the vacuum pump was opened and the vacuum pump was switched on. The GUI was then used to select the isobaric mode of operation from a drop-down menu and the set-point pressure was entered. At this point, the pressure within the still began to decrease towards this set-point pressure.

6.3.1.2 Heating Procedure

Two heaters were in operation on the VLE still: an external heater that served mainly to prevent loss of heat to the environment and an internal heater that provided the principal heating to bring the sample to the boil. It is essential that sufficient heating is applied to cause a high circulation rate (the circulation rate can be judged by counting the drop rate of

the vapour condensate) through the still and a vigorous pumping action through the Cottrell pump. Approximately one to one and a half hours of heating were required before the sample and the glass still attained thermal equilibrium. At this point, the power to the still was adjusted until the plateau region was found. It is critical that the VLE measurements be taken while in the plateau region since Kneisl et al. [1989] found the boiling point temperature to be a function of power input. The plateau region is the area of the temperature versus power input curve where the boiling temperature does not change with minor changes in the power input. If measurements are taken whilst outside this region, then certain errors will be incurred in the value recorded for the boiling point temperature. Ideally, the plateau region should be a flat line. However, in practice this is seldom the case and the plateau region often exhibits a slight slope.

6.3.1.3 Sampling and Analysis

Before the samples were taken, equilibrium had to be achieved i.e. both the temperature and composition of the system needed to be constant. For most systems, equilibrium will be attained within thirty minutes. However, this can vary depending on the system properties (particularly relative volatility) and on the circulation rate within the still (i.e. on the power input to the still. The binary systems in this study generally required between forty-five minutes and an hour to reach a stable equilibrium.

Once the system had reached equilibrium, the temperature was recorded and the samples were withdrawn. Both a liquid and a vapour sample were taken, from the liquid and vapour condensate receivers respectively (Figure 5-2). The samples were removed using syringes and were then stored in gas chromatograph sample bottles before being analyzed using the gas chromatograph. Each sample was injected into the chromatograph three times and the average was utilized in calculation of the liquid and vapour compositions. Once the samples had been removed, the second component was added to the still in order to adjust the system composition. Again, the system is brought to equilibrium and liquid and vapour samples are removed and analyzed. This process is then repeated until the halfway point in the VLE curve is reached. The still is then drained, cleaned and filled again with the second

pure component. The first component is now added to adjust the composition until the entire composition range has been covered and the VLE curve is complete. This method provides additional confirmation of the accuracy of the results because the two halves of the VLE curve must meet in order to complete the system measurements. Hence, any errors that may have occurred will show up if the curves do not match. In addition, this procedure allows a number of points to be measured in the dilute region on either side of the VLE envelope.

6.3.2 Isothermal Operation of the VLE Still

Isothermal operation relied on the isobaric operation for heating of the still. The pressure was set so that the system temperature, once thermal equilibrium was achieved, was close to the set-point temperature that was to be entered. The GUI was then used to switch isobaric mode off and switch isothermal mode on. The set-point temperature was then entered. The operation was very similar to that described above for the isobaric case, except that in isothermal mode it was the pressure that was constant at equilibrium.

6.4 Molecular Simulation Experimental Procedure

Although it would appear that the running of a simulation involves the relatively simple process of loading data into a computer and waiting for a result, this is not the case. A number of essential preparatory steps must be completed before the simulation may be submitted to the Beowulf cluster.

6.4.1 Literature Data

The first step towards the running of a simulation is the gathering of the necessary literature data. The pure component properties of the compound of interest must be obtained. This includes quantities such as molecular weight, vapour pressure data, enthalpy of vapourization, liquid and vapour densities, dipole moment and critical temperature, pressure and density. Naturally, when simulating the VLE data of a binary system

experimental data must be acquired for that particular system at the desired pressure or temperature (depending on whether the run is to be isobaric or isothermal). In general, systems with a very narrow phase envelope are avoided as it becomes difficult to find the correct starting conditions and, hence, a large proportion of the runs attempted will fail (refer to Section 4.1.2).

6.4.2 Simulation Box Sizes

The size of the simulation boxes is one of the critical parameters that must be ascertained prior to a simulation run. Clearly, the required volume (and, hence, size of the box) is dependent upon the number of molecules to be simulated. Therefore, the number of molecules must first be decided. The greater the number of molecules, the longer the system will take to reach equilibrium. However, a sufficient number of molecules are required to ensure that the simulation results are accurate. Since this depends on averages taken over all the molecules present in the simulation (Section 4.1.1; Equation (4-1)), too few molecules would yield unsatisfactory errors in the final results. Generally, between 200 and 500 molecules are used in a simulation.

It is preferable that the box volumes be similar in size at equilibrium. Since the density of the vapour must be far smaller than the corresponding liquid phase density, it becomes obvious that fewer molecules must be present in the vapour box when the system reaches equilibrium. The split of molecules between the two boxes is another variable that must be set by the researcher so that an optimal system configuration is attained. Once the number of molecules has been decided, the required liquid and vapour volumes may be calculated from the respective densities (at the system temperature). These two volumes are then added together to give the overall system volume. Halving this total volume and taking the cube root yields the starting box lengths that are entered as initial simulation conditions. The initial number of molecules in each box is also taken to be half of the total number of molecules. One of the two boxes will lose molecules to the other and become the vapour phase. This process occurs randomly and, thus, the researcher does not know beforehand which of the two boxes will simulate the respective phases.

6.4.3 Stockmayer Parameters

Once the number of molecules and the box sizes have been decided, the Stockmayer parameters must be determined. The critical temperature, dipole moment and liquid phase density at T_r = 0.75 are necessary before the ε and σ values can be evaluated. The procedure followed to calculate these parameters is covered in detail in Section 4.2.2.1 and will not be re-iterated here.

6.4.4 Ewald Parameters

The methodology of Ewald is covered in Section 4.3, so only the actual process by which the Ewald parameters are decided upon will be discussed in this section. The first step was to obtain a random starting molecular configuration. To achieve this, a run (the procedure for running a simulation is explained below, Section 6.4.5) was started and the spatial coordinates of each molecule in the simulation were printed to a file named *coordnew*. This simulation was allowed to run for 10000 cycles to ensure that the configuration was completely random. This configuration was then copied into another file named *coordold*. The input file (these files have the extension ".i"; e.g. *Acetic.i*) was then edited and *linit* was set to false. This ensured that the simulation looked for a file named *coordold* and not *coordnew* when searching for its configuration. Thus, the random molecular configuration was used to obtain the starting coordinates of each molecule in the simulation.

Next, the number of cycles was set to an extremely low figure (5 cycles were used in this work). Such a low number of cycles were required because only the initial system properties were of interest. Hence, whether the simulation continued for 5 cycles or 5000, the same data would be extracted (namely the initial external Coulombic energy). 5 cycles were chosen since this provided just sufficient time for the necessary changes to be made to the *forcefield* file before the current run was completed and the next simulation begun. The procedure consisted of selecting a value for α_E (e.g. 0.35) and then varying the number of k-vectors between 5 and 15. For each number of k-vectors, the initial external Coulombic energy was recorded. A plot of number of k-vectors versus external Coulombic energy was

then constructed for each value of α_E (on the same set of axes, see Figure 6-5 below). This graph allowed the researcher to select satisfactory values for α_E and the number of *k*-vectors (refer to Section 4.3.2). It is essential that these figures are determined together since the two parameters are intrinsically interrelated, with the required number of *k*-vectors increasing as α_E increases. However, as the number of *k*-vectors rises, so does the time required per simulation. Hence, there exists an optimum between the values for the two parameters and the time per run.

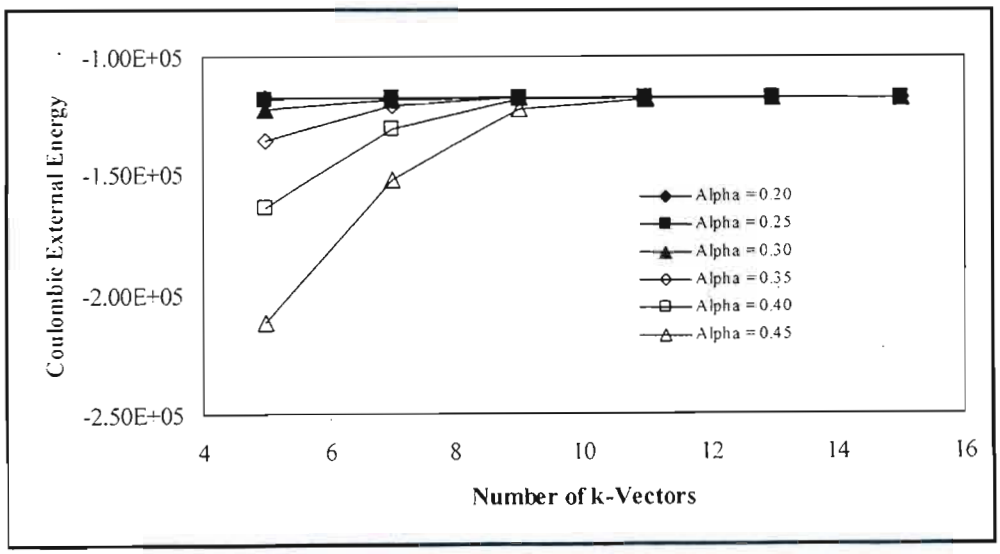

Figure 6-5: Plot of Coulombic external energy versus number of k-vectors showing the variation in energy over a range of α_E values.

6.4.5 Running a Simulation

The first step in running a simulation was to edit the input file (e.g. *Acetic.i*). If a new molecular configuration was desired, then the parameter *linit* was set to true. This told the simulation to generate a new coordination file, *coordnew*. Otherwise, *linit* is set to false and the programme then looks for a coordination file that has already been created called *coordold*.

It is necessary at this point to define what is meant by the term *cycle* in a simulation. A cycle consists of N attempts to modify the system in some manner (see below), where N is the number of molecules comprising the system. Therefore, it is obvious that by increasing the number of molecules in a simulation, the length of each cycle increases and, thus, the simulation time rises. The possible changes that may be tried are as follows:

1. molecular translation
2. molecular rotation
3. partial or full re-growth of a selected molecule
4. volume changes
5. molecule exchanges between boxes

The input file allowed the relative probabilities of these changes succeeding to be altered. These probabilities were set to be 0.222, 0.222, 0.222, 0.006 and 0.328 respectively.

In addition, the input file was configured so that the correct number of cycles etc. were performed. The number of cycles was set using the variable *nstep*. In general, 50000 to 80000 cycles are necessary to ensure equilibrium, although longer simulations may be necessary for complex systems. It is important to note that the starting configuration was further randomized by allowing a certain number of cycles to occur in which only molecular translations were allowed (i.e. no volume changes or molecule exchanges were permitted). This figure was set using the variable *nminit*.

The programme also allowed data to be printed to an output file and, hence, the programme had to be told how often this was to occur during a simulation. Clearly, printing the data each cycle would be unreasonable and would result in ridiculously large output files and slow simulation rates. At the same time, the data needed to be recorded often enough for the researcher to be able to graph the data effectively, thereby observing trends in the figures. Generally, a value between 100 and 500 (depending on the total number of cycles) was selected and entered using the variable *iprint*.

The final variable that must be set prior to running a simulation is *nsamp*. This variable set the number of cycles that were to pass before the programme began to calculate averages of

the system properties. Naturally, if the averages were evaluated from the first cycle, large standard deviations would have resulted as the system was purposefully initialized in a random configuration. Hence, a certain number of cycles (termed *equilibration cycles*) were necessary before the system began to approach equilibrium. This figure had to be estimated by the researcher based on experience and was generally set within the range 10000 to 25000 cycles. It is common practice to select *nsamp* such that *nsamp* > *nminit*. The number of cycles required for the simulation to proceed from the end of the equilibration period to the end of the simulation as a whole was designated as the number of *production cycles*. The system averages, standard deviations etc. were calculated during the production cycles.

The starting box sizes and number of molecules were also entered using the input file. The method by which the box lengths were calculated was discussed in Section 6.4.2. The total number of molecules was divided so that exactly half of the molecules were initially placed in each box. Equally vital for a Gibbs ensemble (i.e. NVT) simulation was the entering of the system temperature. Again, the input file was utilized for this purpose.

The final action of the input file was to copy certain necessary files from the directories in which they were stored to the directory in which the current simulation was to be run. The files were: *forcefield*, *topology* and *sequence*. These files were required by the programme so that the molecules comprising the system could be correctly specified. The Stockmayer parameters (refer to Section 4.2) and the Ewald parameters (refer to Section 4.3) were set within the *forcefield* file.

The final file requiring editing prior to beginning a simulation was the *Acetic.q* file. The correct path to the programme source code needed to be set within this file, as well as the name of the output file to which the simulation data was to be printed. It was essential that the output file name was changed before each simulation, to ensure that no data files were over-written. Once all of these steps had been carried out, the simulation could be submitted to the cluster and the run begun.

CHAPTER
7

CHOICE OF BINARY SYSTEMS

7.1 Test System: Cyclohexane (1) – Ethanol (2)

A test system is used in order to ensure that the experimental procedure and equipment are operating as expected and that accurate results may be obtained. This is accomplished by comparing data measured on the equipment with established literature data. If the measured data corresponds to the reported, reliable literature values, then the experimental method can be taken to be correct and the equipment functioning as expected. A suitable criterion is necessary for choosing the system and the following points were taken into consideration: the system must be non-ideal; consistent literature data should be available (Morachevsky and Zharov [1963], Joseph et al. [2001]); the test system chemicals should be available at a sufficiently high purity (>99%) and the chemicals should not be excessively expensive, toxic or unstable. All of these points were satisfied by the cyclohexane (1) – ethanol (2) system and, hence, this system was selected as the test system.

7.2 New Experimental VLE Systems: Carboxylic Acid Binaries

Since the focus of this project was carboxylic acids, the selected binary systems clearly had to incorporate acids. Previous work had been done in the department involving carboxylic acids by Sewnarain et al. [2002] and, hence, certain acid species were readily on hand for study. The available acids were propionic acid, butyric acid, isobutyric acid,

valeric acid, isovaleric acid, hexanoic acid and heptanoic acid. A search of the available literature revealed that VLE data pertaining to carboxylic acids is extremely scarce, with the Dortmund Data Bank (DDB) containing only three systems (butyric acid – propionic acid, butyric acid – isovaleric acid, propionic acid – isobutyric acid), all of which were at atmospheric pressure (760 mmHg). Thus, almost any choice for the binary systems would have constituted new data. The chemicals were checked for purity by injecting them into a gas chromatograph (Varian 3300 – refer to Section 6.2.3) and, thus, the elution times of the various acids were known. This allowed a choice of systems that would separate effectively when analyzed by gas chromatograph in order to determine experimental compositions. Other criteria considered included: the industrial significance of the chosen systems, the purity of the chemicals, cost of the chemicals, whether they were completely miscible and whether the vapour pressures lay within a reasonable range at the projected working temperatures.

As has been reported by Sewnarain et al. [2002], a local petrochemical company (SASOL Ltd.) is producing a waste acid stream as a byproduct of another process. The stream contains large amounts of carboxylic acids with the most prevalent acids being butyric acid, isobutyric acid and valeric acid. Therefore, the systems chosen were propionic acid (1) – valeric acid (2) and isobutyric acid (1) – valeric acid (2), since these two systems satisfied all of the criteria discussed above. Three isotherms at 120, 130 and 140 °C respectively and an isobar at 20 kPa were measured for each system and all of these systems represent new VLE data.

7.3 Molecular Simulation Systems

The central aim of this portion of the project was to investigate the molecular simulation of carboxylic acids. As such, a system containing at least one carboxylic acid needed to be chosen. Since the focus was not to develop a new potential model specific to the acids (one does not as yet exist), but rather to investigate the ability of current models to incorporate association effects through the addition of a dipole moment term, it was decided to minimize the complexity of the system by studying a binary containing only one carboxylic

acid. Acetic acid was selected for study as this acid had been previously simulated (using the Stockmayer potential model) by van Leeuwen [1994b] and, therefore, simulation parameters were available for acetic acid. Furthermore, there were large numbers of readily accessible systems incorporating acetic acid in literature. The DDB was utilized in obtaining good, consistent literature data to which the simulations could be compared.

The paper by van Leeuwen also contained Stockmayer parameters for another polar compound, methanol. In addition, the results of the pure component simulations for methanol were reproduced graphically allowing comparison with the simulations conducted in this work. Hence, methanol was selected as the second component of the binary VLE system to be predicted using molecular simulation.

CHAPTER
8

EXPERIMENTAL RESULTS

This chapter presents the experimental data measured during this project. The analysis and discussion of the data will be dealt with in Chapter 9. In order to satisfactorily ascertain the accuracy of the measured data, the purities of the components must be determined (Section 8.1). Thereafter, the carboxylic acid vapour pressure measurements are presented. To ensure that the VLE still was operating correctly and that the method used for obtaining data was satisfactory, a test system was measured. The system chosen was cyclohexane (1) – ethanol (2) since reliable literature data were easily attainable. Vapour-liquid equilibrium data were obtained for two binary carboxylic acid systems: propionic acid (1) – valeric acid (2) and isobutyric acid (1) – valeric acid (2). The reasons for these systems being chosen were laid out in Chapter 7. The final sets of results that are presented are from the molecular simulation portion of this project.

8.1 Chemical Purity

The carboxylic acids, n-hexane and cyclohexane were purchased through Capital Laboratory Supplies cc. The ethanol and n-decane were obtained from Merck. The reagents were used without further purification after gas chromatographic analysis revealed no significant impurities. The purities were confirmed via refractive index measurement; comparisons with literature values are presented in Table 8-1, along with the GC analysis.

Table 8-1: Chemical Purities and Refractive Indices.

Reagent	Refractive Index (293.15 K)		GC Analysis	Min. Purity
	Exp.	Lit.[a]	(mass%)	(mass%)[b]
n-Hexane	1.3749	1.3751	99.8	99.0
n-Decane	1.4105	1.4102	99.1	99.0
Cyclohexane	1.4265	1.4266	99.7	99.5
Ethanol	1.3612	1.3611	99.9	99.5
Propionic Acid	1.3810	1.3809	99.8	99.5
Butyric Acid	1.3978	1.3980	99.8	99.5
Isobutyric Acid	1.3933	1.3930	99.7	99.5
Valeric Acid	1.4087	1.4085	99.1	99.0
Isovaleric Acid	1.4029	1.4033	99.4	98.0
Hexanoic Acid	1.4156	1.4163	99.5	99.5
Heptanoic Acid	1.4175	1.4170	99.3	99.0

[a] Weast et al. . [b] As stated by the supplier

8.2 Carboxylic Acid Vapour Pressures

Vapour pressure data were measured for the following acids: propionic acid, butyric acid, isobutyric acid, valeric acid, isovaleric acid, hexanoic acid and heptanoic acid. The data are presented in Tables 8-2 to 8-8 and plotted in Figures 8-1 through 8-7. The pressures ranged between approximately 5 kPa and atmospheric pressure at sea level (which varied from 100.04 to 101.21 kPa according to the prevailing weather conditions). The equipment imposed a constraint on the upper bound of the temperature (and hence, pressure) range because the septa used on the still (for liquid and vapour sampling when obtaining VLE data) began to degrade at temperatures above 180 °C. Furthermore, the still itself was not designed for high temperature work. Thus, the temperatures ranged from approximately 85 °C to just over 180 °C. Due to this constraint on the maximum system temperature, fewer data points were measured for hexanoic and heptanoic acid since the temperatures rapidly exceeded 180 °C (even at low pressures). The VP data were regressed to obtain parameters for both the Antoine and Reid et al. [1988] equations (see Section 9.2). The differences between the experimentally measured pressures and the predicted pressures are given by:

$$|\Delta P_i| = P_{measured} - P_{calculated} \tag{8-1}$$

Table 8-2: Vapour pressure data for propionic acid.

P kPa	T °C	ΔP_{Reid} kPa	ΔP_{Ant} kPa
14.56	88.37	0.02	0.14
19.58	95.22	0.07	0.07
29.65	105.80	0.08	0.02
39.73	113.59	0.09	0.01
49.79	119.78	0.02	0.04
59.86	124.94	0.21	0.18
69.92	129.50	0.16	0.10
79.99	133.65	0.25	0.32
90.07	137.18	0.17	0.20
95.10	138.89	0.36	0.35
101.21	140.59	0.28	0.36

Table 8-3: Vapour pressure data for butyric acid.

P kPa	T °C	ΔP_{Reid} kPa	ΔP_{Ant} kPa
14.56	110.40	0.01	0.29
19.58	117.72	0.02	0.01
29.65	128.17	0.00	0.24
39.72	135.85	0.10	0.32
49.79	141.85	0.10	0.03
59.86	147.07	0.07	0.15
69.92	151.66	0.00	0.18
79.99	155.81	0.13	0.06
90.07	159.46	0.14	0.21
95.10	161.36	0.24	0.29
100.04	162.90	0.16	0.04

Table 8-4: Vapour pressure data for isobutyric acid.

P kPa	T °C	ΔP_{Reid} kPa	ΔP_{Ant} kPa
14.55	102.06	0.07	0.21
19.58	108.99	0.20	0.31
29.65	118.62	0.12	0.20
39.72	126.28	0.01	0.18
49.79	132.29	0.31	0.48
59.85	137.60	0.21	0.33
69.92	142.36	0.22	0.17
79.99	146.62	0.79	0.82
90.07	150.21	0.70	0.78
95.10	151.71	0.13	0.23
100.59	153.01	1.35	1.23

Table 8-5: Vapour pressure data for valeric acid.

P kPa	T °C	ΔP_{Reid} kPa	ΔP_{Ant} kPa
14.56	130.00	0.02	0.13
19.59	137.56	0.10	0.09
24.63	143.92	0.08	0.05
29.65	149.04	0.15	0.09
39.72	156.93	0.16	0.20
49.78	163.33	0.19	0.21
59.85	168.74	0.04	0.05
69.92	173.30	0.19	0.22
74.96	175.33	0.23	0.25
79.99	177.20	0.18	0.19
85.03	178.77	0.44	0.44

Table 8-6: Vapour pressure data for isovaleric acid.

P kPa	T °C	ΔP_{Reid} kPa	ΔP_{Ant} kPa
14.56	122.90	0.06	0.47
19.59	129.75	0.17	0.27
29.65	139.72	0.05	0.38
39.72	147.55	0.18	0.54
49.78	154.03	0.14	0.36
59.86	159.47	0.13	0.13
69.92	164.29	0.27	0.42
79.99	168.45	0.56	0.77
90.07	172.01	0.52	0.64
95.10	173.45	0.12	0.09
100.08	174.77	0.88	0.96

Table 8-7: Vapour pressure data for hexanoic acid.

P kPa	T °C	ΔP_{Reid} kPa	ΔP_{Ant} kPa
9.52	140.25	0.01	0.09
14.56	149.73	0.05	0.01
19.59	156.77	0.02	0.09
24.63	162.47	0.16	0.20
29.64	166.88	0.13	0.14
34.68	171.11	0.01	0.06
39.72	174.73	0.13	0.17
44.75	178.28	0.12	0.16

Table 8-8: Vapour pressure data for heptanoic acid.

P kPa	T °C	ΔP_{Reid} kPa	ΔP_{Ant} kPa
4.70	140.33	0.00	0.04
8.63	153.33	0.03	0.01
12.56	161.92	0.07	0.10
16.57	168.18	0.00	0.00
20.63	173.25	0.13	0.14
24.65	177.85	0.09	0.08
27.67	180.65	0.01	0.00

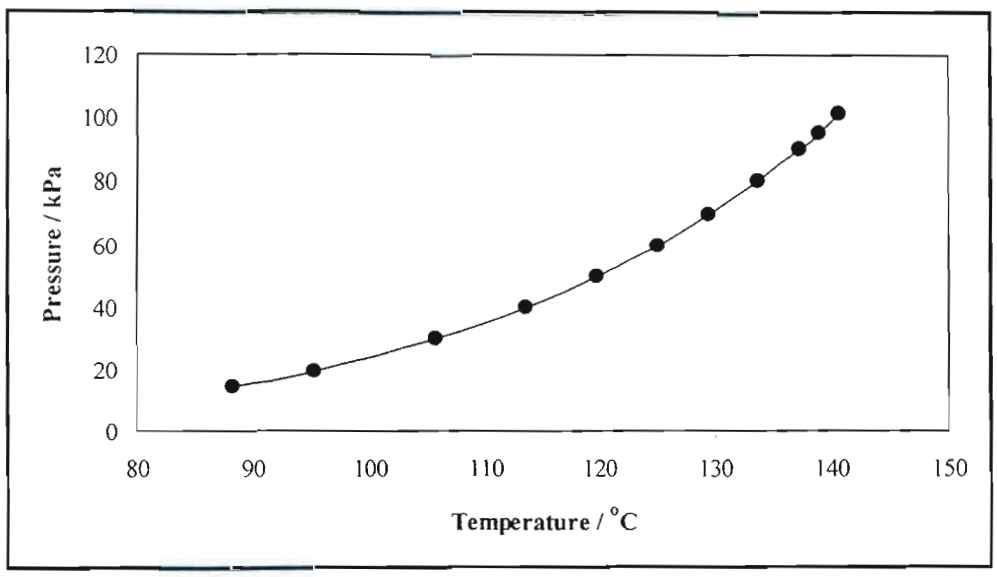

Figure 8-1: Vapour pressure curve for propionic acid.

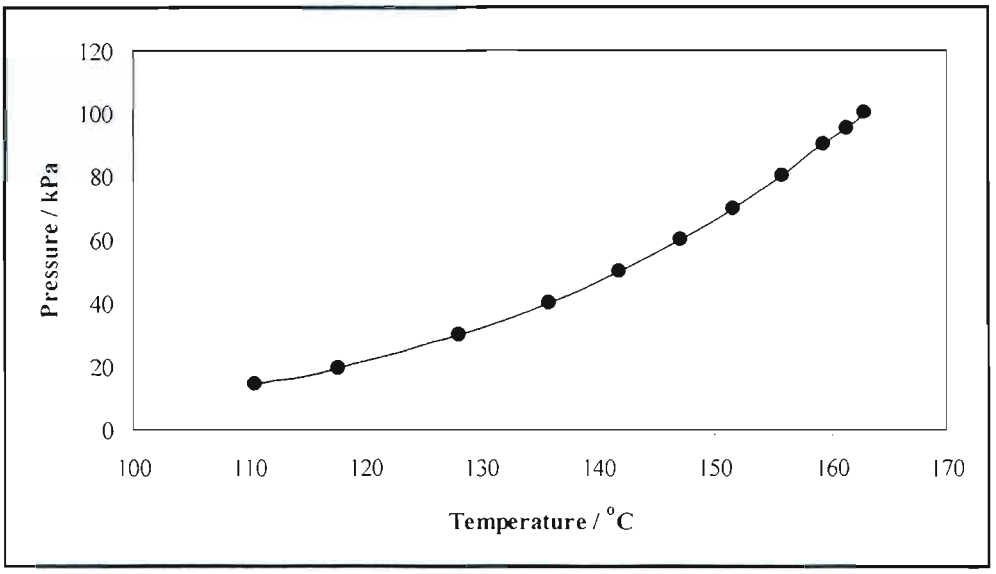

Figure 8-2: Vapour pressure curve for butyric acid.

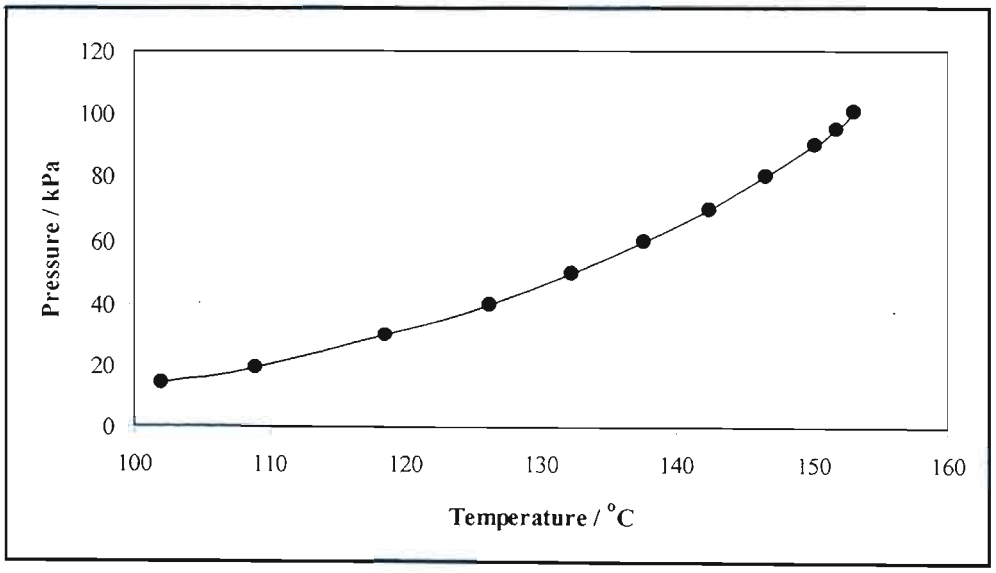

Figure 8-3: Vapour pressure curve for isobutyric acid.

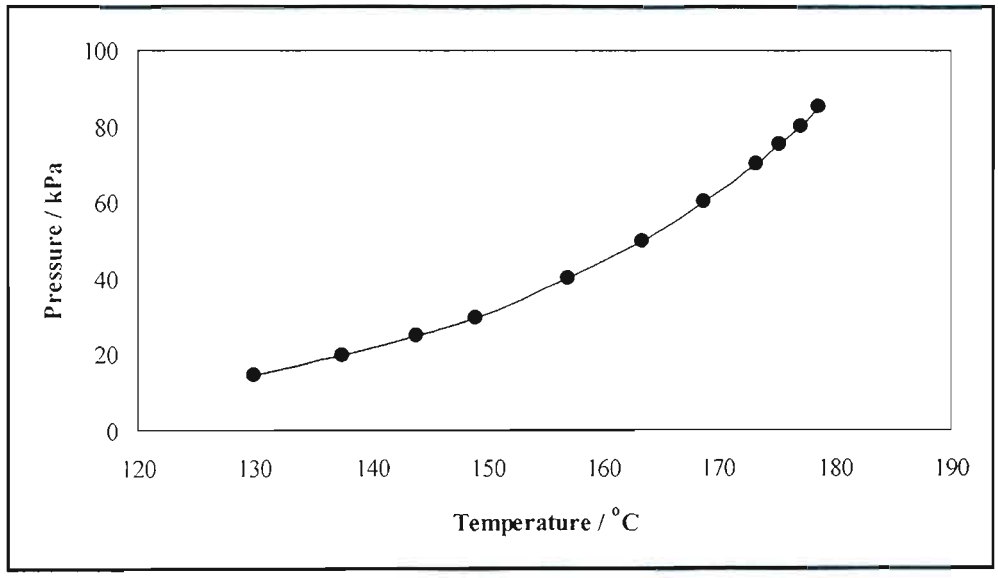

Figure 8-4: Vapour pressure curve for valeric acid.

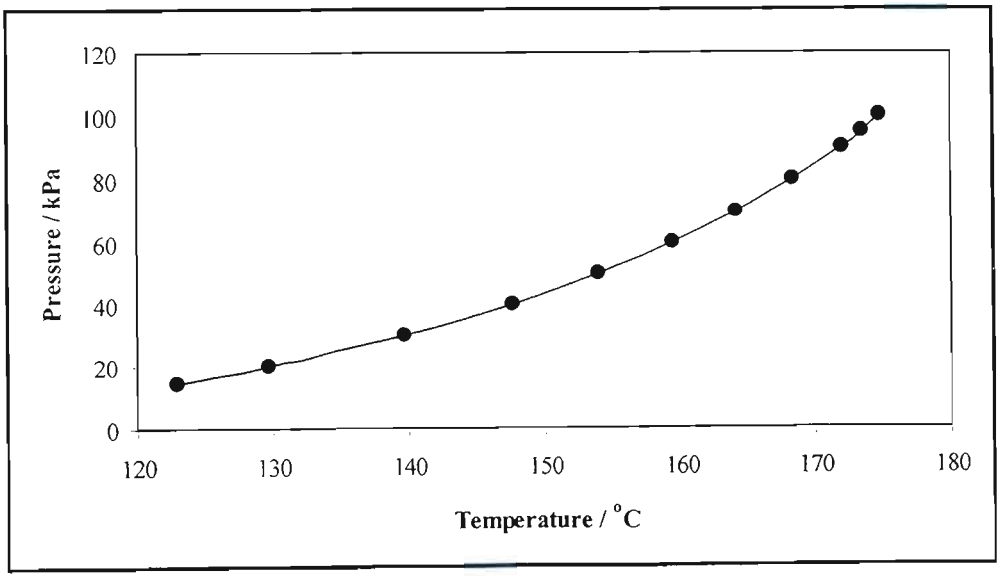

Figure 8-5: Vapour pressure curve for isovaleric acid.

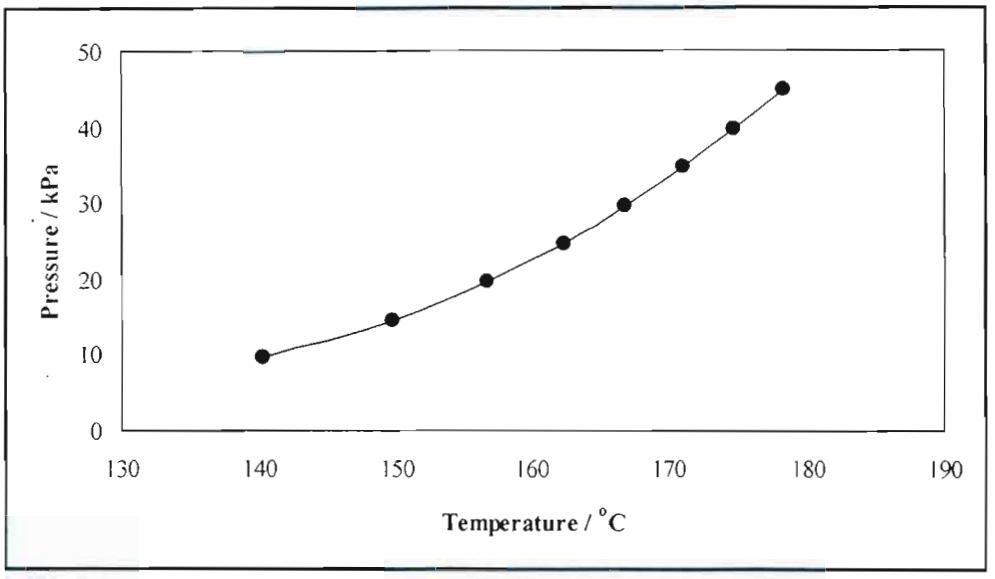

Figure 8-6: Vapour pressure curve for hexanoic acid.

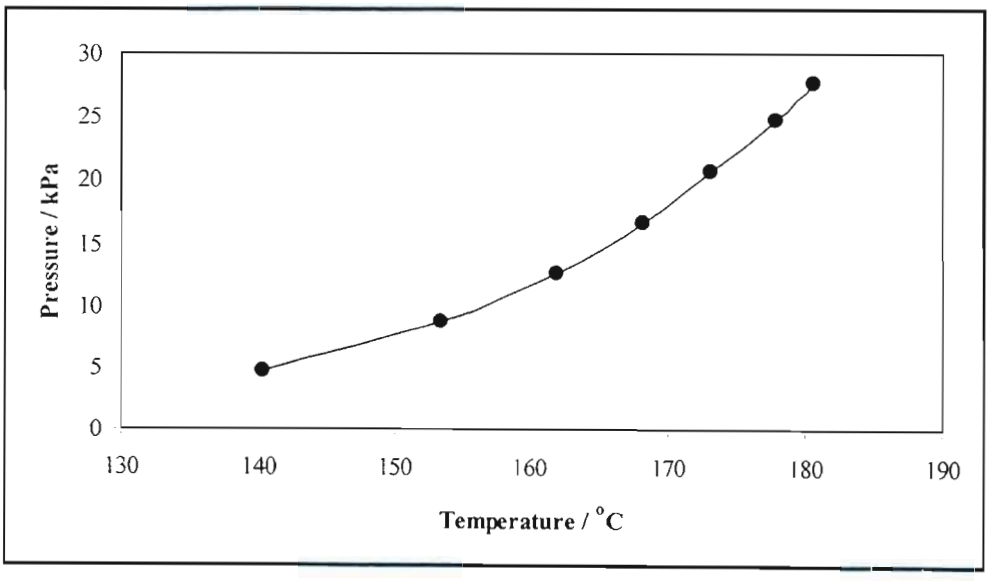

Figure 8-7: Vapour pressure curve for heptanoic acid.

8.3 Vapour-Liquid Equilibrium Results

8.3.1 Cyclohexane (1) – Ethanol (2) System

VLE data for the cyclohexane (1) – ethanol (2) system were measured at 40 kPa (since literature data at this pressure were readily available) to serve as a test system. In other words, it was never intended to be new data. Instead, these measurements allowed the researcher to ascertain whether the equipment being utilized was operating correctly, and also ensured that the method employed to obtain the experimental data was suitable. To accomplish this, reliable literature data was necessary. The data set measured by Morachevsky and Zharov [1963] and the data obtained by Joseph et al. [2001] at 40 kPa were used.

The experimental data, GC calibration curves and *x-y* and *T-x-y* plots are presented below. These results are discussed in Section 9.4.

Table 8-9: Vapour-liquid equilibrium data for the cyclohexane (1) – ethanol (2) system at 40 kPa.

T / K	x_1	y_1	T / K	x_1	y_1
325.89	1.000	1.000	315.13	0.306	0.580
317.56	0.964	0.732	315.36	0.270	0.573
315.18	0.891	0.658	317.31	0.161	0.494
314.64	0.740	0.625	318.07	0.138	0.468
314.59	0.662	0.620	319.93	0.087	0.399
314.58	0.595	0.611	321.37	0.062	0.346
314.6	0.525	0.608	322.87	0.040	0.277
314.67	0.474	0.606	324.17	0.029	0.227
314.73	0.432	0.601	329.69	0.000	0.000
314.93	0.353	0.588			

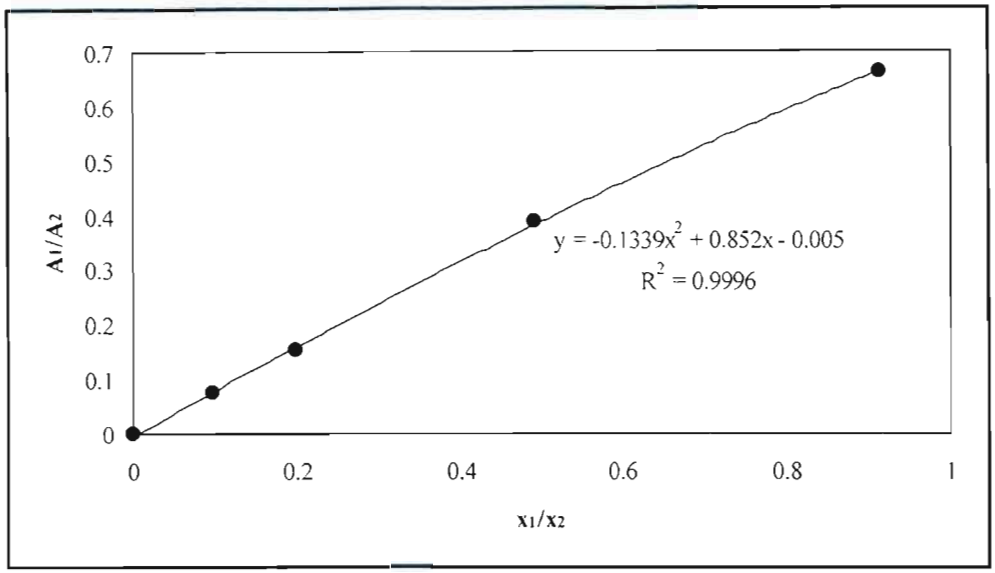

Figure 8-8: Calibration curve for the Hewlett-Packard 5890 gas chromatograph for the cyclohexane (1) – ethanol (2) system (dilute cyclohexane region).

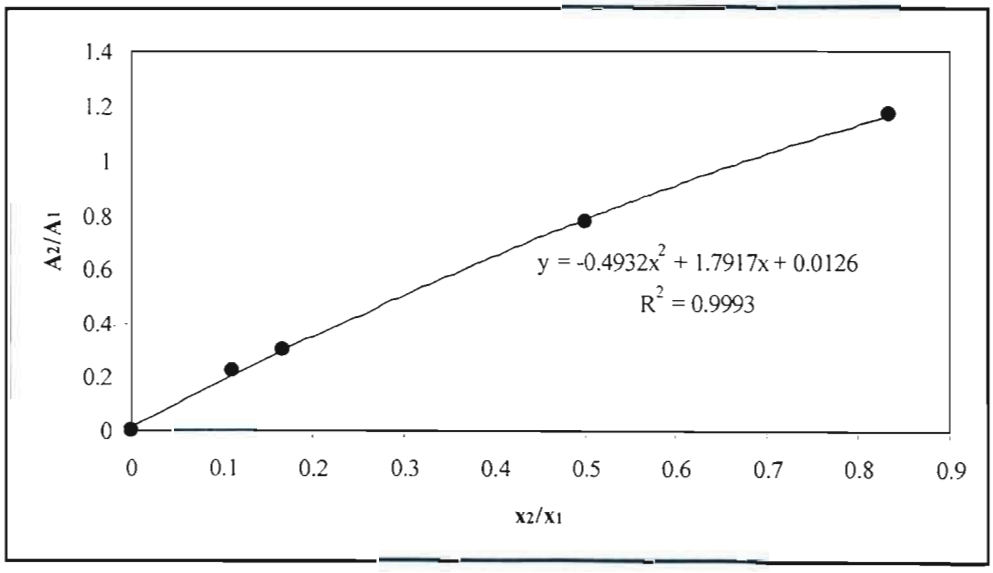

Figure 8-9: Calibration curve for the Hewlett-Packard 5890 gas chromatograph for the cyclohexane (1) – ethanol (2) system (dilute ethanol region).

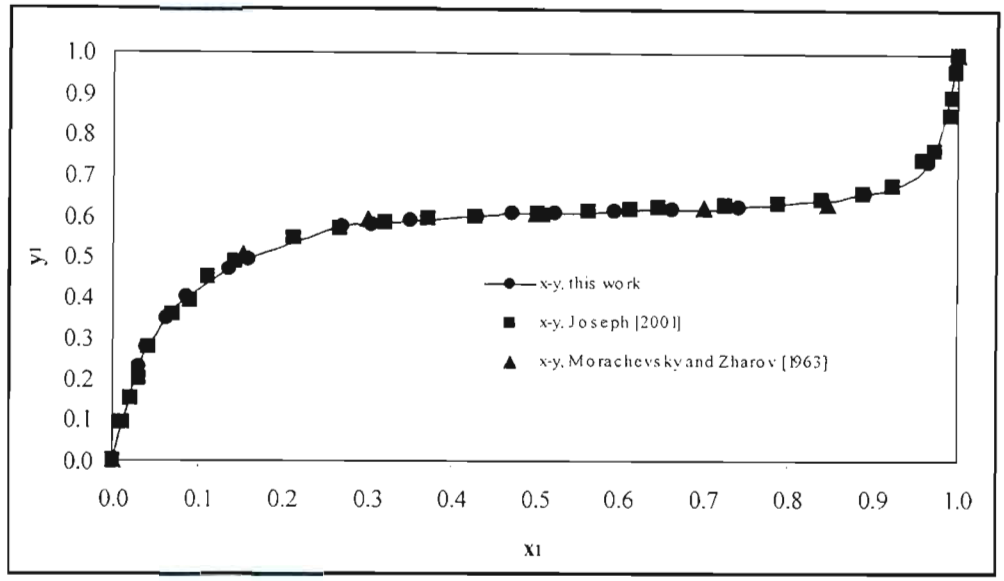

Figure 8-10: x-y curve for the cyclohexane (1) – ethanol (2) system at 40 kPa.

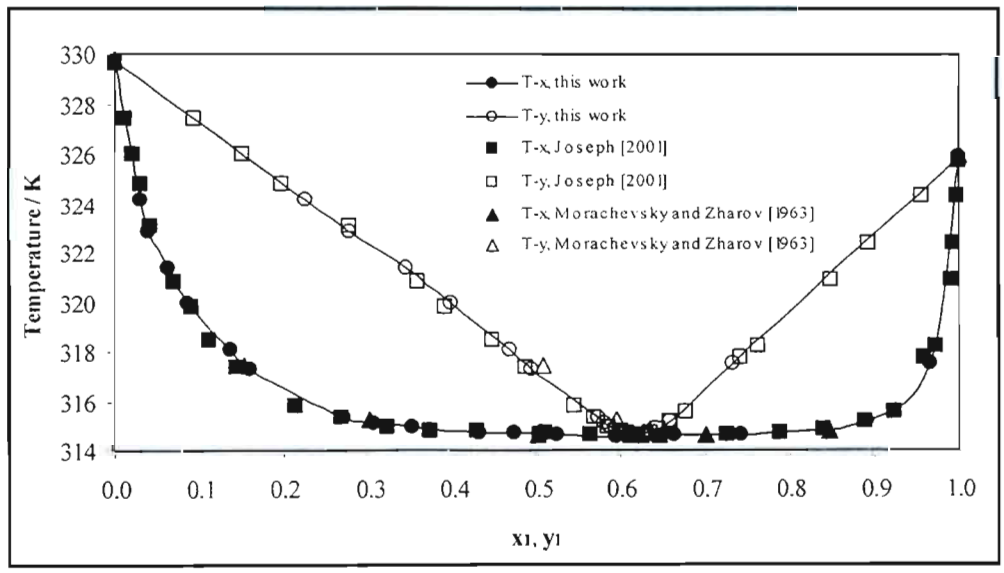

Figure 8-11: T-x-y curve for the cyclohexane (1) – ethanol (2) system at 40 kPa.

8.3.2 Propionic Acid (1) – Valeric Acid (2) System

The compositions for this system were determined using the Varian 3300 gas chromatograph, as opposed to the Hewlett-Packard 5890 used for the test system. The reason for this change is discussed in Section 6.2.3. This data represents new VLE data as this system has not been measured at these temperatures or pressure before. The experimental data, GC calibration curves and *x-y*, *P-x-y* and *T-x-y* plots are presented below. These results are discussed in Section 9.4.

Table 8-10: Vapour-liquid equilibrium data for the propionic acid (1) – valeric acid (2) system at 20 kPa.

T / K	x_1	y_1	T / K	x_1	y_1
368.98	1.000	1.000	385.79	0.516	0.821
370.01	0.969	0.992	390.14	0.380	0.718
370.82	0.951	0.987	393.63	0.287	0.628
371.90	0.922	0.979	397.85	0.201	0.498
373.45	0.880	0.967	402.30	0.121	0.351
376.69	0.787	0.941	408.19	0.045	0.133
380.23	0.673	0.904	411.39	0.000	0.000

Table 8-11: Vapour-liquid equilibrium data for the propionic acid (1) – valeric acid (2) system at 393.15 K.

P / kPa	x_1	y_1	P / kPa	x_1	y_1
50.13	1.000	1.000	31.56	0.588	0.859
49.48	0.989	0.997	24.49	0.418	0.761
48.76	0.980	0.994	18.73	0.264	0.615
48.16	0.965	0.990	15.21	0.151	0.457
46.92	0.926	0.978	12.05	0.072	0.235
43.13	0.849	0.956	10.78	0.039	0.111
37.51	0.726	0.916	10.01	0.000	0.000

Table 8-12: Vapour-liquid equilibrium data for the propionic acid (1) – valeric acid (2) system at 403.15 K.

P / kPa	x_1	y_1	P / kPa	x_1	y_1
71.02	1.000	1.000	34.64	0.417	0.756
69.87	0.990	0.998	26.20	0.258	0.613
68.85	0.979	0.994	21.31	0.153	0.472
65.80	0.928	0.975	18.78	0.084	0.334
60.04	0.847	0.953	16.51	0.029	0.152
52.25	0.728	0.911	15.23	0.009	0.033
44.90	0.598	0.854	14.68	0.000	0.000

Table 8-13: Vapour-liquid equilibrium data for the propionic acid (1) – valeric acid (2) system at 413.15 K.

P / kPa	x_1	y_1	P / kPa	x_1	y_1
98.95	1.000	1.000	48.71	0.403	0.714
97.72	0.990	0.998	38.41	0.261	0.568
96.10	0.979	0.995	30.85	0.147	0.382
88.90	0.897	0.967	27.33	0.086	0.255
78.93	0.794	0.930	23.35	0.030	0.093
65.90	0.634	0.861	22.24	0.010	0.029
54.24	0.483	0.769	21.35	0.000	0.000

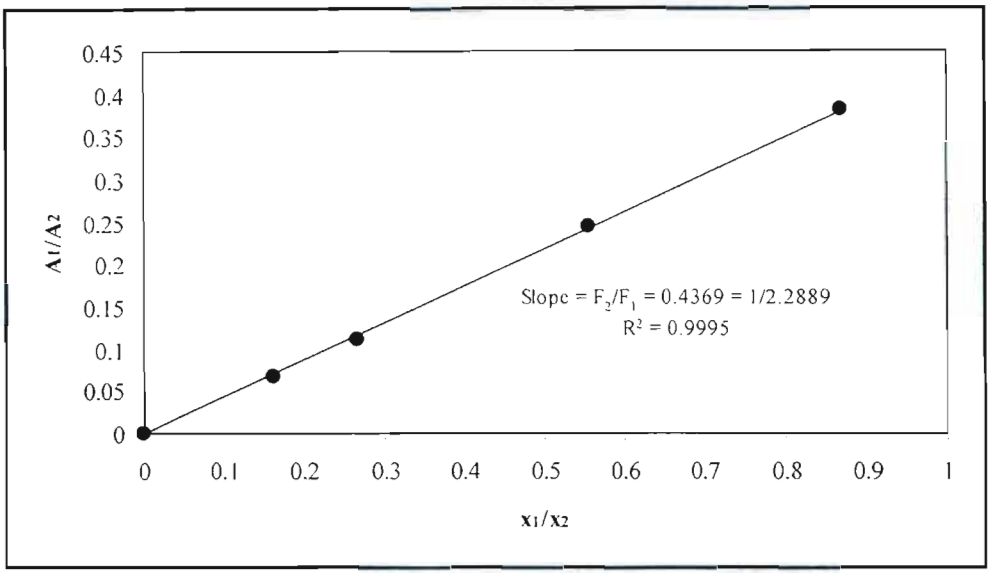

Figure 8-12: Calibration curve for the Varian 3300 gas chromatograph for the propionic acid (1) – valeric acid (2) system (dilute propionic acid region).

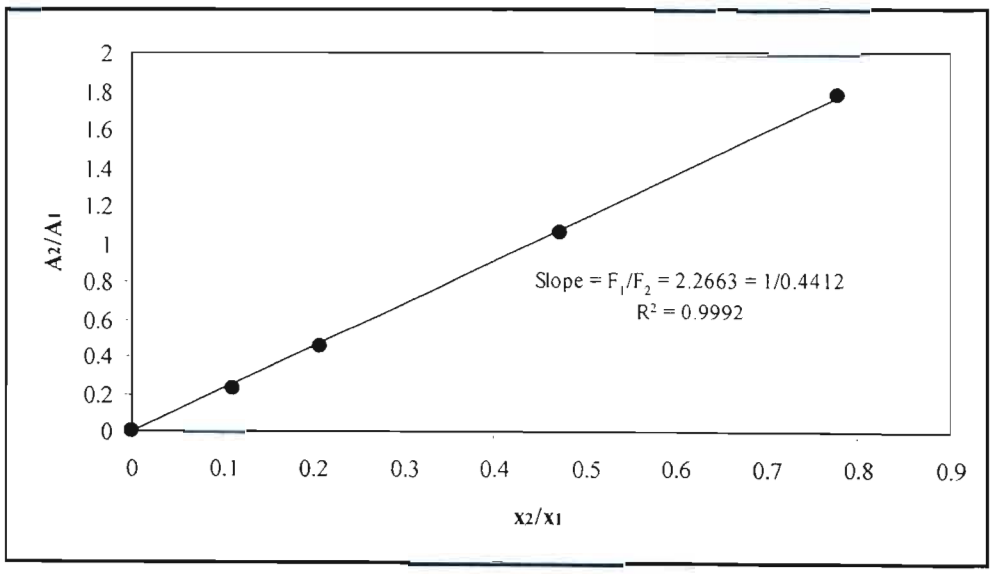

Figure 8-13: Calibration curve for the Varian 3300 gas chromatograph for the propionic acid (1) – valeric acid (2) system (dilute valeric acid region).

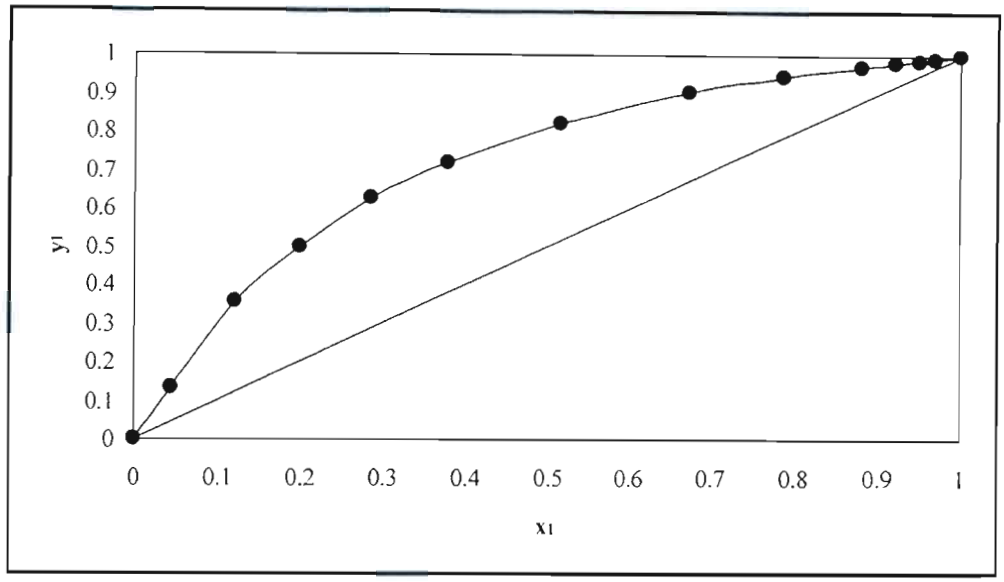

Figure 8-14: x-y curve for the propionic acid (1) – valeric acid (2) system at 20 kPa.

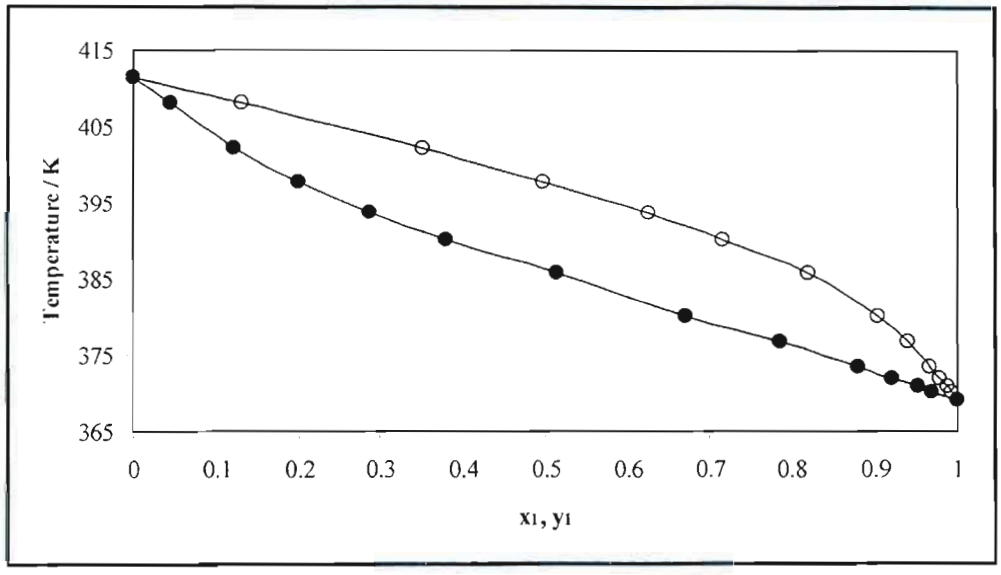

Figure 8-15: T-x-y curve for the propionic acid (1) – valeric acid (2) system at 20 kPa.

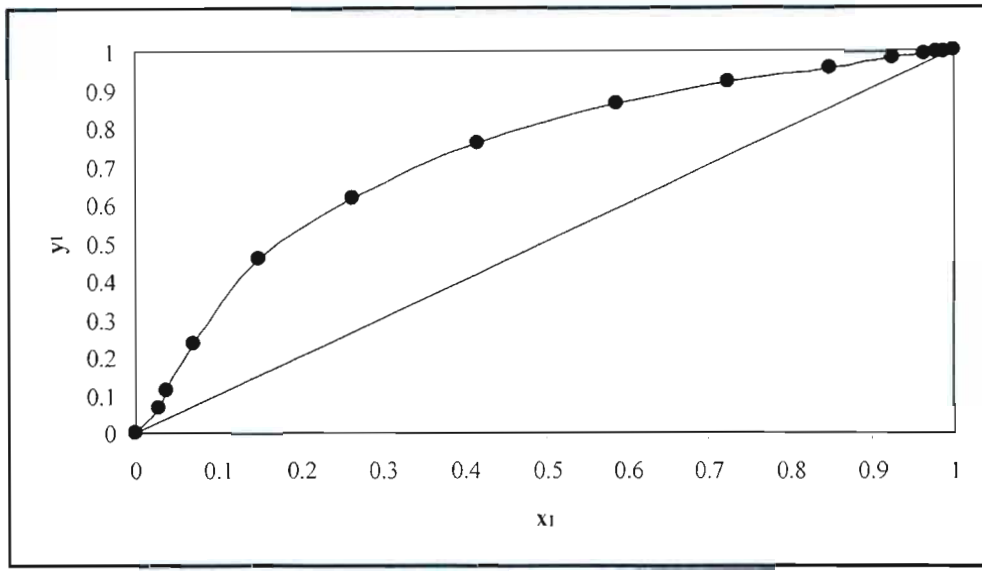

Figure 8-16: x-y curve for the propionic acid (1) – valeric acid (2) system at 393.15 K.

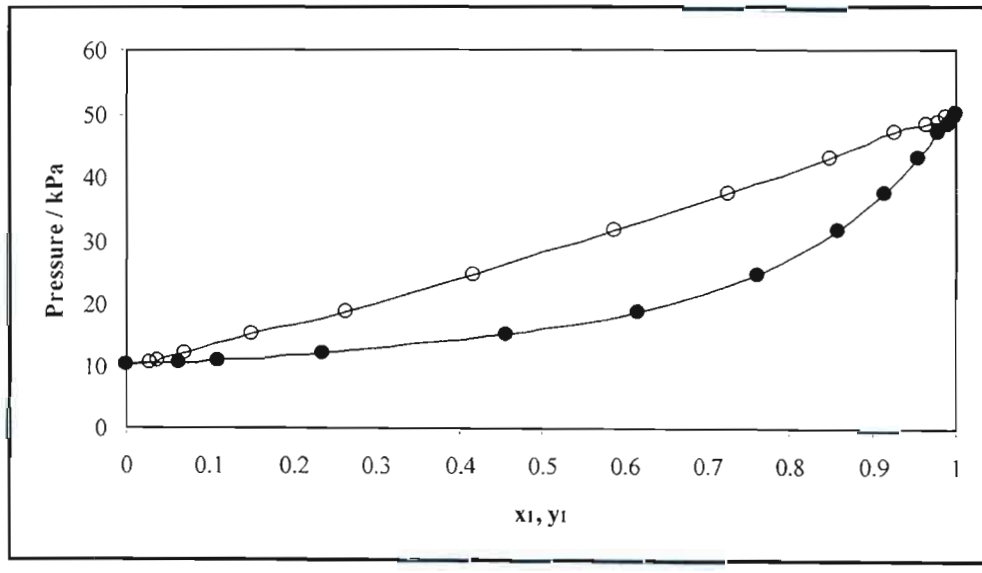

Figure 8-17: P-x-y curve for the propionic acid (1) – valeric acid (2) system at 393.15 K.

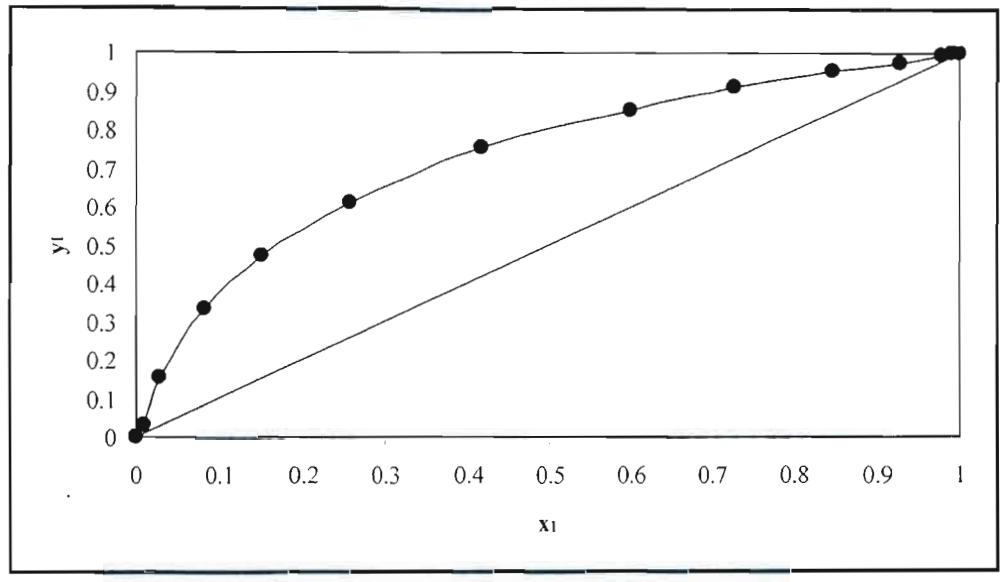

Figure 8-18: x-y curve for the propionic acid (1) – valeric acid (2) system at 403.15 K.

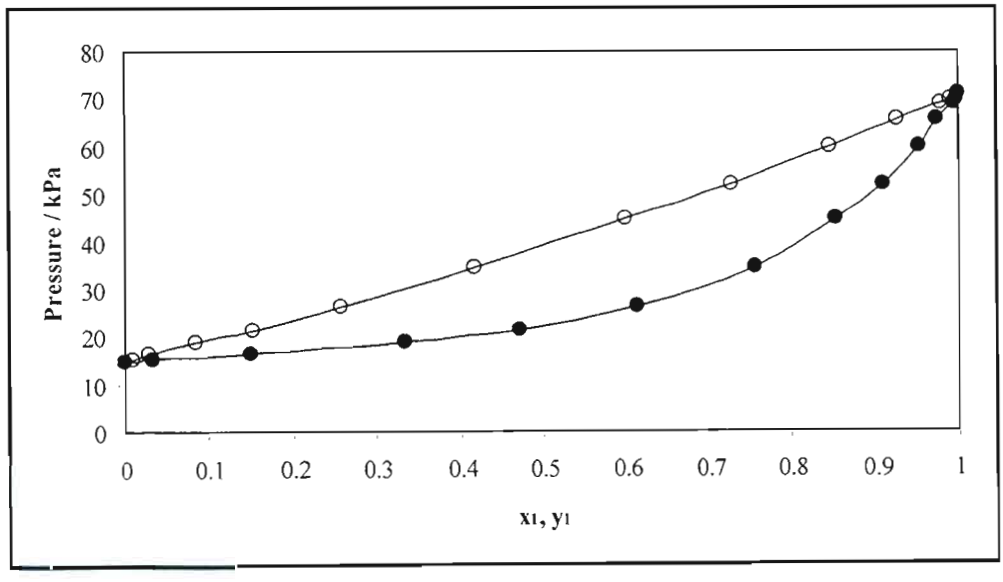

Figure 8-19: P-x-y curve for the propionic acid (1) – valeric acid (2) system at 403.15 K.

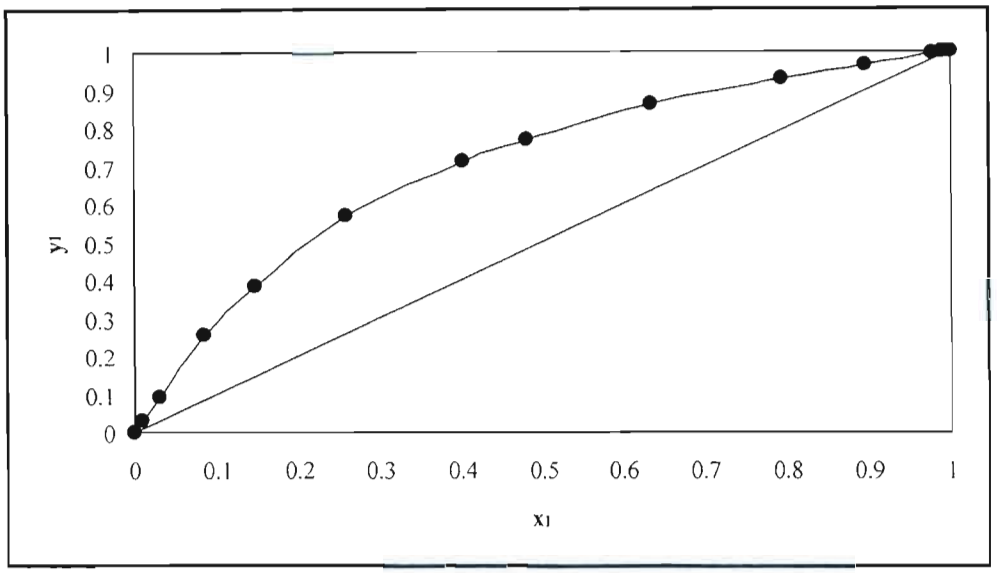

Figure 8-20: x-y curve for the propionic acid (1) – valeric acid (2) system at 413.15 K.

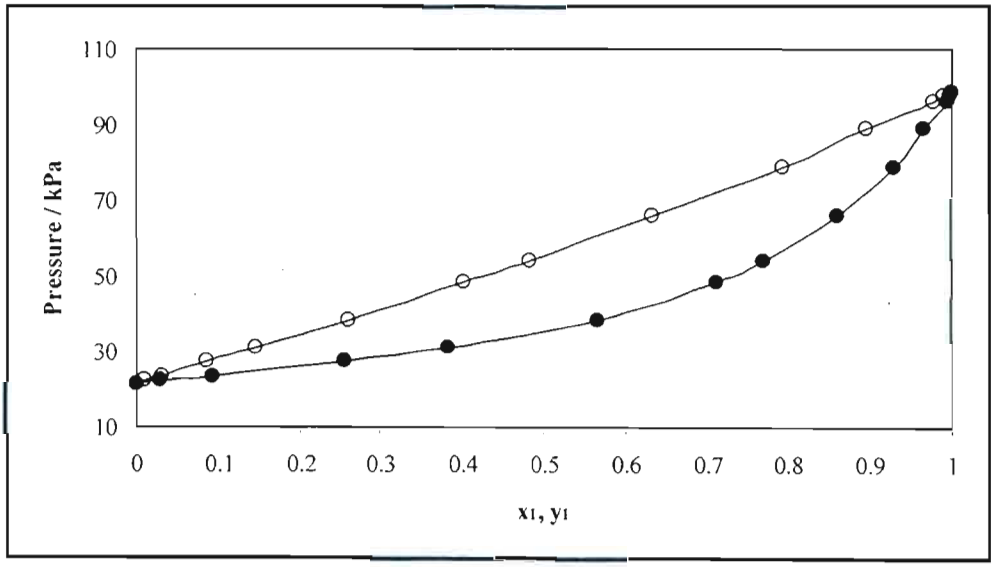

Figure 8-21: P-x-y curve for the propionic acid (1) – valeric acid (2) system at 413.15 K.

8.3.3 Isobutyric Acid (1) – Valeric Acid (2) System

The composition analysis of this system was again conducted using the Varian 3300 gas chromatograph. As for the previous carboxylic acid system, the data obtained represents new VLE data. The experimental data, GC calibration curves and *x-y*, *P-x-y* and *T-x-y* plots are presented below. These results are discussed later in Section 9.4.

Table 8-14: Vapour-liquid equilibrium data for the isobutyric acid (1) – valeric acid (2) system at 20 kPa.

T / K	x_1	y_1	T / K	x_1	y_1
382.27	1.000	1.000	396.75	0.445	0.683
382.66	0.992	0.995	402.85	0.221	0.424
383.05	0.982	0.992	406.53	0.120	0.256
383.68	0.964	0.985	409.11	0.056	0.123
384.85	0.924	0.969	410.48	0.023	0.054
387.52	0.820	0.926	410.95	0.012	0.034
392.76	0.593	0.800	411.39	0.000	0.000

Table 8-15: Vapour-liquid equilibrium data for the isobutyric acid (1) – valeric acid (2) system at 393.15 K.

P / kPa	x_1	y_1	P / kPa	x_1	y_1
31.01	1.000	1.000	16.79	0.371	0.628
30.68	0.992	0.995	13.80	0.226	0.445
30.25	0.968	0.987	11.79	0.110	0.244
29.04	0.898	0.958	10.82	0.048	0.115
27.07	0.816	0.925	10.38	0.025	0.061
23.67	0.678	0.856	10.14	0.011	0.024
20.46	0.557	0.779	10.02	0.000	0.000

Table 8-16: Vapour-liquid equilibrium data for the isobutyric acid (1) – valeric acid (2) system at 403.15 K.

P / kPa	x_1	y_1	P / kPa	x_1	y_1
45.23	1.000	1.000	24.39	0.371	0.615
44.83	0.991	0.996	20.32	0.226	0.429
44.04	0.966	0.985	17.24	0.106	0.229
41.82	0.897	0.957	15.84	0.047	0.112
38.98	0.819	0.925	15.22	0.024	0.058
33.60	0.670	0.850	14.94	0.010	0.024
29.74	0.556	0.775	14.68	0.000	0.000

Table 8-17: Vapour-liquid equilibrium data for the isobutyric acid (1) – valeric acid (2) system at 413.15 K.

P / kPa	x_1	y_1	P / kPa	x_1	y_1
64.44	1.000	1.000	34.70	0.367	0.590
64.02	0.991	0.996	29.36	0.222	0.405
61.66	0.927	0.969	24.95	0.104	0.216
59.13	0.873	0.944	23.03	0.048	0.107
54.19	0.772	0.903	22.09	0.024	0.054
48.74	0.673	0.847	21.66	0.009	0.021
42.34	0.554	0.764	21.32	0.000	0.000

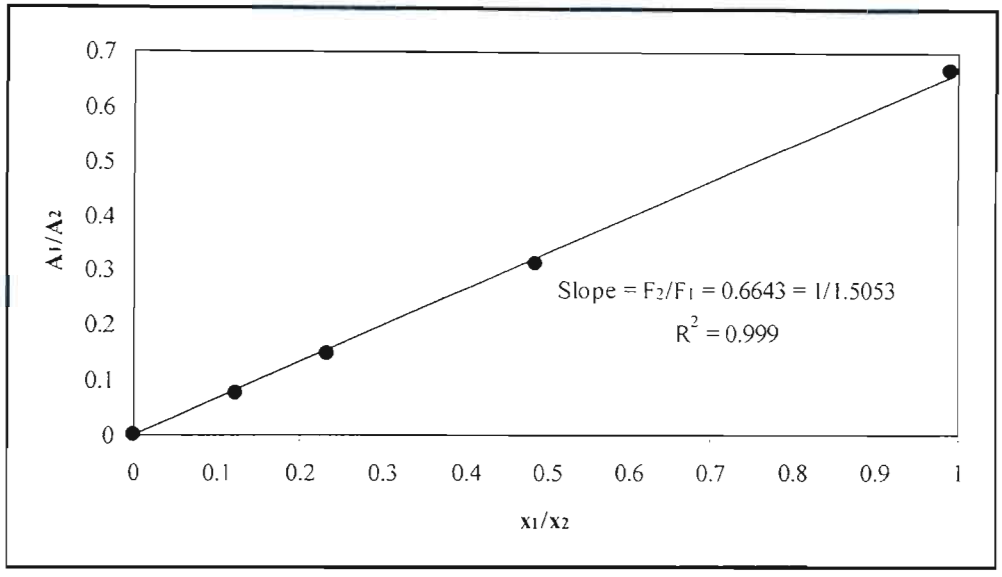

Figure 8-22: Calibration curve for the Varian 3300 gas chromatograph for the isobutyric acid (1) – valeric acid (2) system (dilute isobutyric acid region).

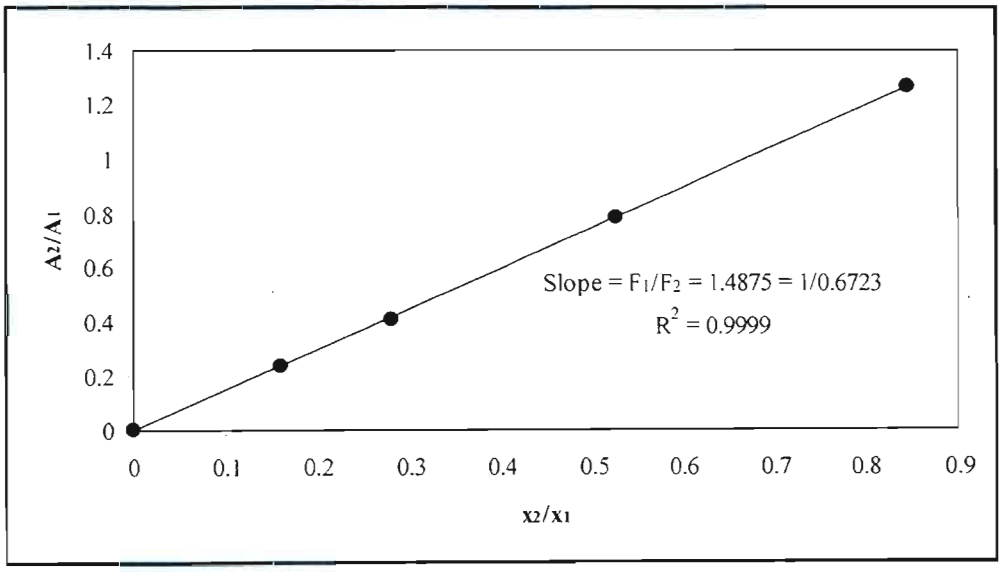

Figure 8-23: Calibration curve for the Varian 3300 gas chromatograph for the isobutyric acid (1) – valeric acid (2) system (dilute valeric acid region).

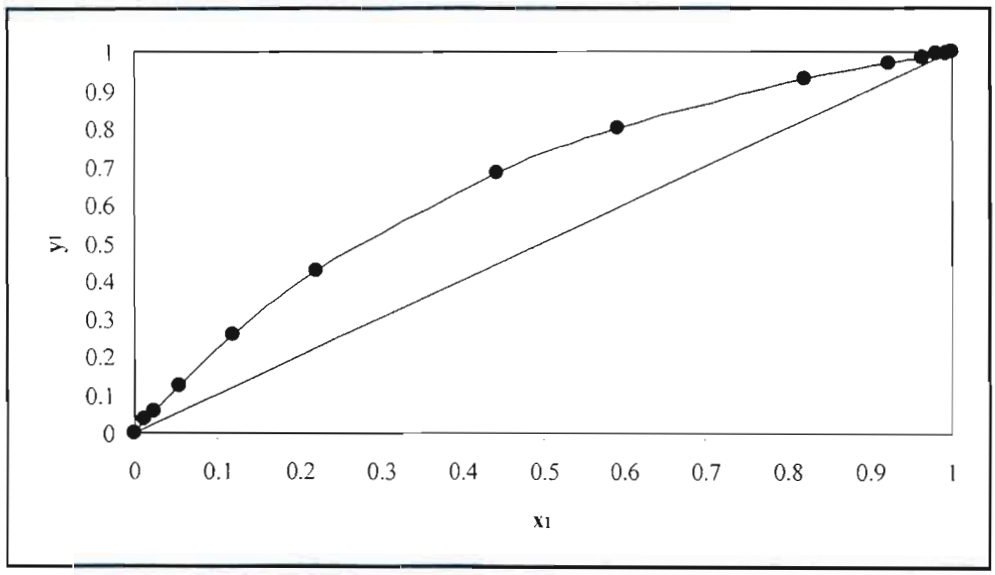

Figure 8-24: x-y curve for the isobutyric acid (1) – valeric acid (2) system at 20 kPa.

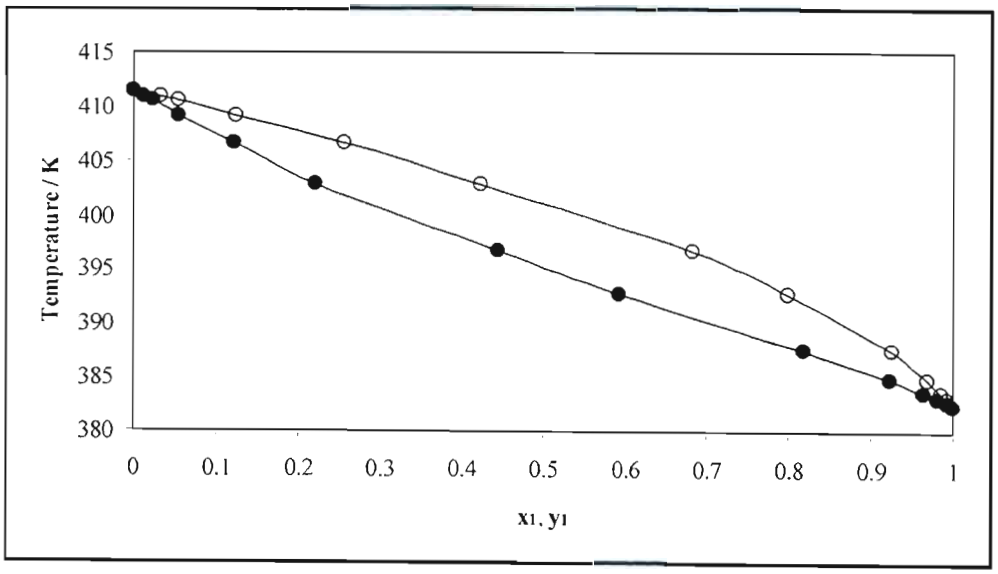

Figure 8-25: T-x-y curve for the isobutyric acid (1) – valeric acid (2) system at 20 kPa.

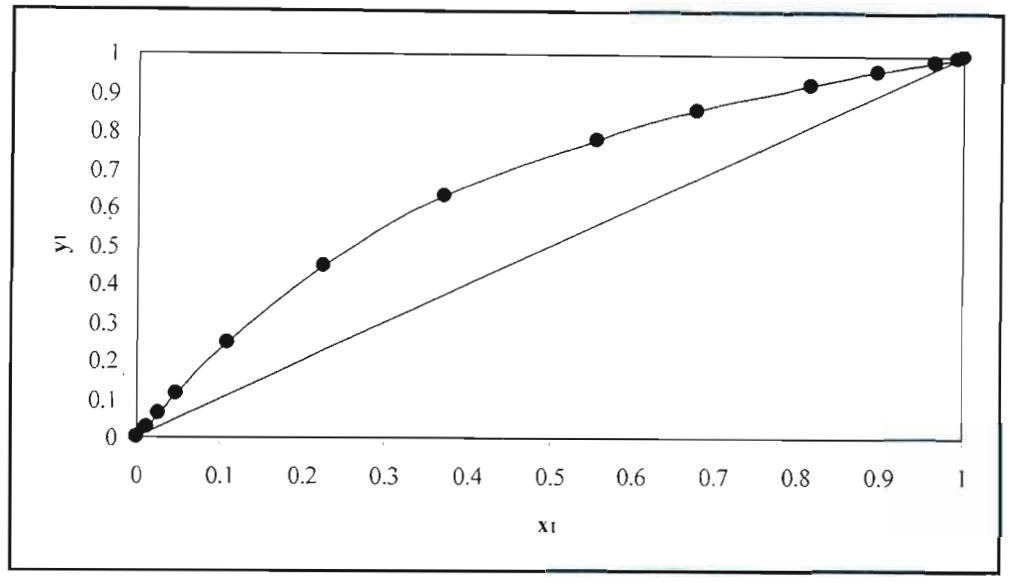

Figure 8-26: x-y curve for the isobutyric acid (1) – valeric acid (2) system at 393.15 K.

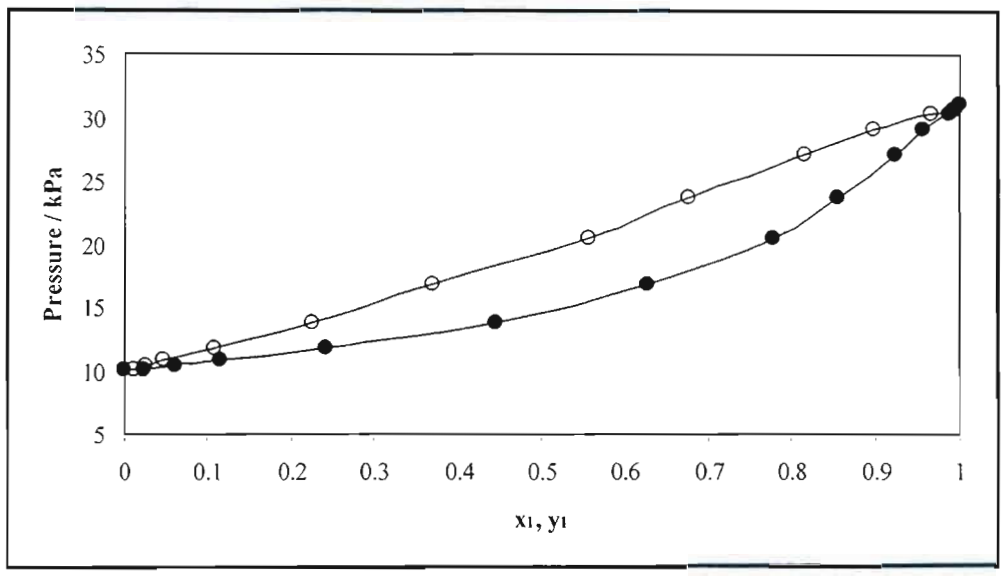

Figure 8-27: P-x-y curve for the isobutyric acid (1) – valeric acid (2) system at 393.15 K.

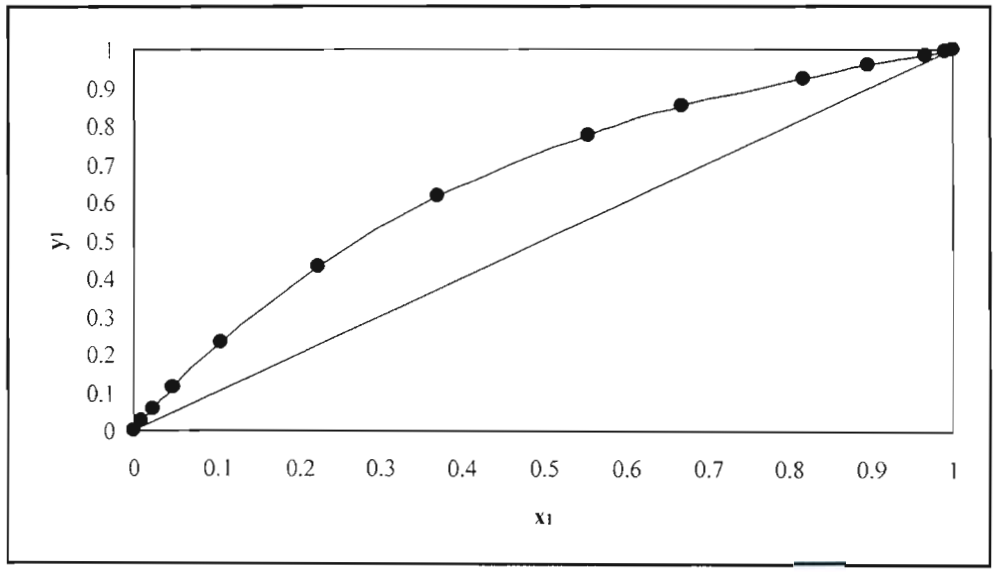

Figure 8-28: x-y curve for the isobutyric acid (1) – valeric acid (2) system at 403.15 K.

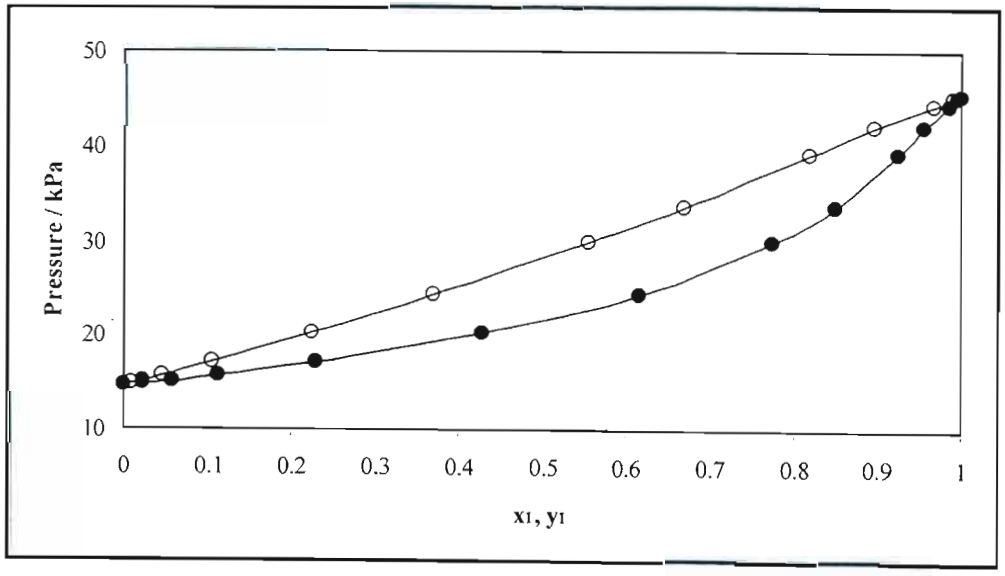

Figure 8-29: P-x-y curve for the isobutyric acid (1) – valeric acid (2) system at 403.15 K.

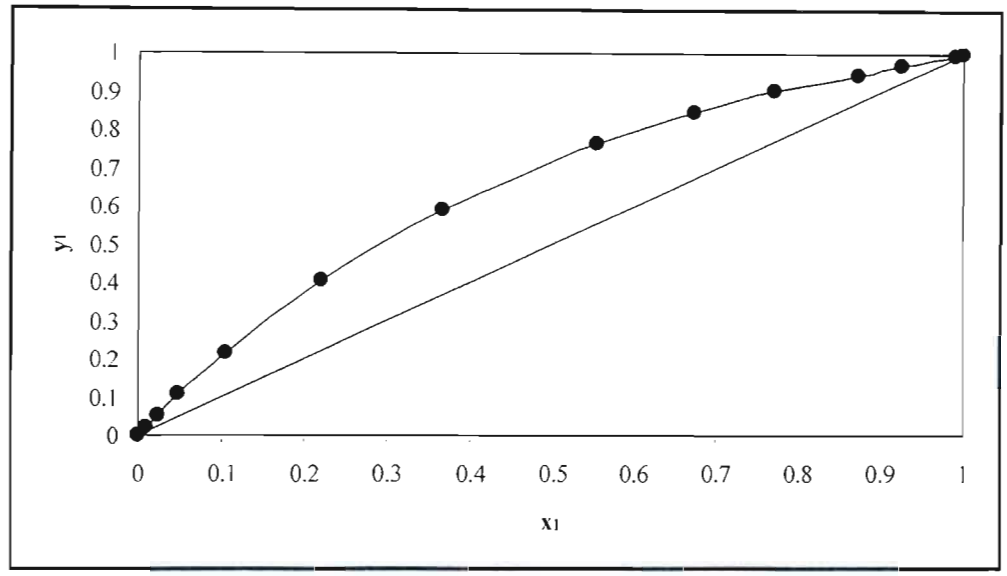

Figure 8-30: x-y curve for the isobutyric acid (1) – valeric acid (2) system at 413.15 K.

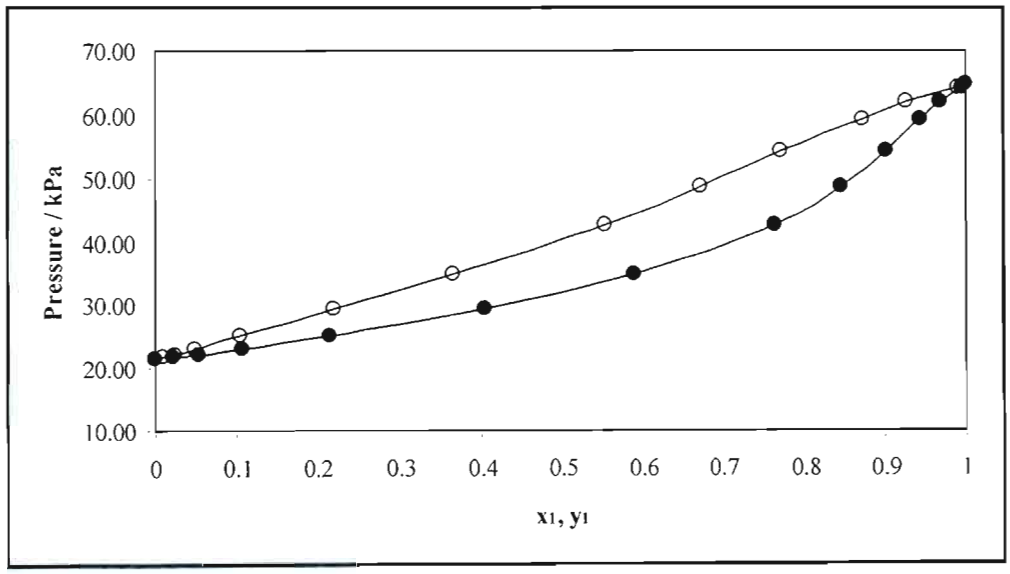

Figure 8-31: P-x-y curve for the isobutyric acid (1) – valeric acid (2) system at 413.15 K.

8.4 Molecular Simulation Results

8.4.1 Vapour Pressure Predictions

Three vapour pressure curves were predicted using molecular simulation. The first was for the straight-chain alkane n-pentane. The pentane vapour pressure measurements were used in order to become familiar with the simulation programmes and the procedure for submitting jobs to the Beowulf cluster (refer to Section 6.4). Thereafter, two polar compounds were selected: methanol and acetic acid. The Ewald parameters (see Sections 4.3 and 6.4.4) and vapour pressures of methanol were previously determined by van Leeuwen, which allowed for verification of the simulation results produced in this project. Along with the vapour pressure curves, the phase co-existence curves for the three pure components (viz. n-pentane, methanol and acetic acid) were also predicted and compared to experimental data obtained from literature. A more detailed analysis and discussion of these results is presented in Chapter 9 (Section 9.8.1). The density values that are quoted in the following tables (Tables 8-18 to 8-20) are in units of kg/m^3.

Table 8-18: Vapour pressure and phase-co-existence data for n-pentane.

T / K	P_{lit} / kPa	P_{sim} / kPa	$\rho_{l,lit}$	$\rho_{l,sim}$	$\rho_{v,lit}$	$\rho_{v,sim}$
284.00	39.19	44.23	617.27	599.55	1.19	1.36
291.00	52.02	55.44	610.60	593.03	1.55	1.63
299.00	70.55	74.44	602.94	586.39	2.06	2.18
313.00	115.20	115.30	589.16	572.88	3.26	3.32
328.00	184.60	185.14	573.88	558.56	5.09	5.01
343.00	282.60	274.66	557.95	544.35	7.64	7.43
358.00	415.60	414.49	541.12	529.09	11.10	10.83
365.00	491.70	492.93	532.89	520.82	13.09	12.85

Literature data taken from Smith and Srivastava [1986a].

Table 8-19: Vapour pressure and phase-co-existence data for methanol.

T / K	P_{lit} / kPa	P_{sim} / kPa	$\rho_{l,lit}$	$\rho_{l,sim}$	$\rho_{v,lit}$	$\rho_{v,sim}$
302.00	20.63	129.68353	782.84877	832.57	0.27	1.73
317.00	42.28	214.45326	767.84088	818.18	0.53	2.70
332.00	80.65	354.08591	752.68969	803.00	0.97	4.25
347.00	144.60	484.66963	737.10605	785.27	1.67	5.62
362.00	245.70	717.17613	720.85489	769.68	2.76	8.04
377.00	398.30	991.67735	704.06504	754.44	4.38	10.81

Literature data taken from Smith and Srivastava [1986b].

Table 8-20: Vapour pressure and phase-co-existence data for acetic acid.

T / K	P_{lit} / kPa	P_{sim} / kPa	$\rho_{l,lit}$	$\rho_{l,sim}$	$\rho_{v,lit}$	$\rho_{v,sim}$
323.15	7.49	47.77498	1017.50	1063.96	0.03	1.10
353.15	26.94	114.80271	983.50	1034.85	0.96	2.41
383.15	77.67	245.78821	948.30	996.70	2.47	4.84
413.15	184.10	482.07526	909.10	968.13	7.03	8.95
428.15	279.72	671.40452	892.72	946.04	10.35	12.13
443.15	407.60	902.73032	869.40	932.46	13.70	15.83

Literature data taken from Vargaftik [1975].

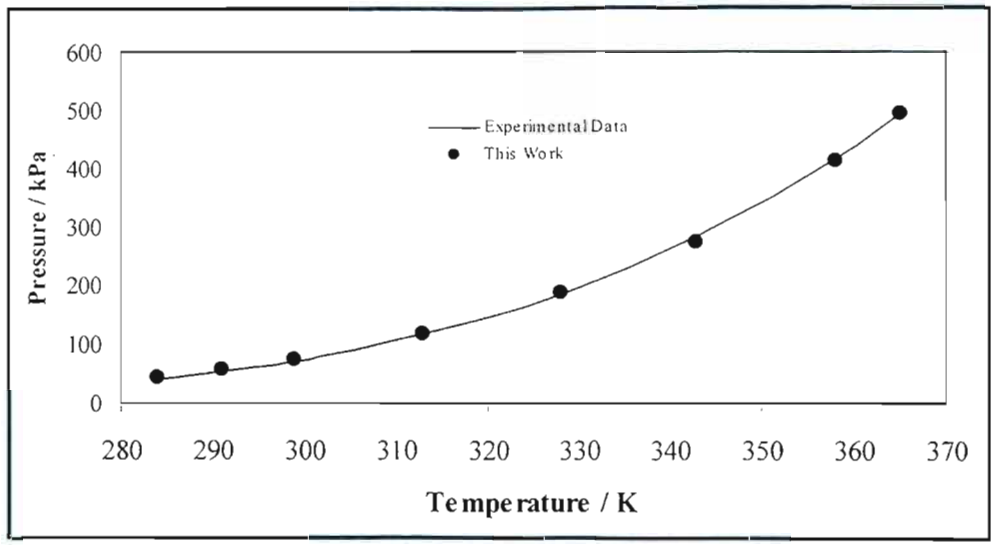

Figure 8-32: Vapour pressure curve for n-pentane.

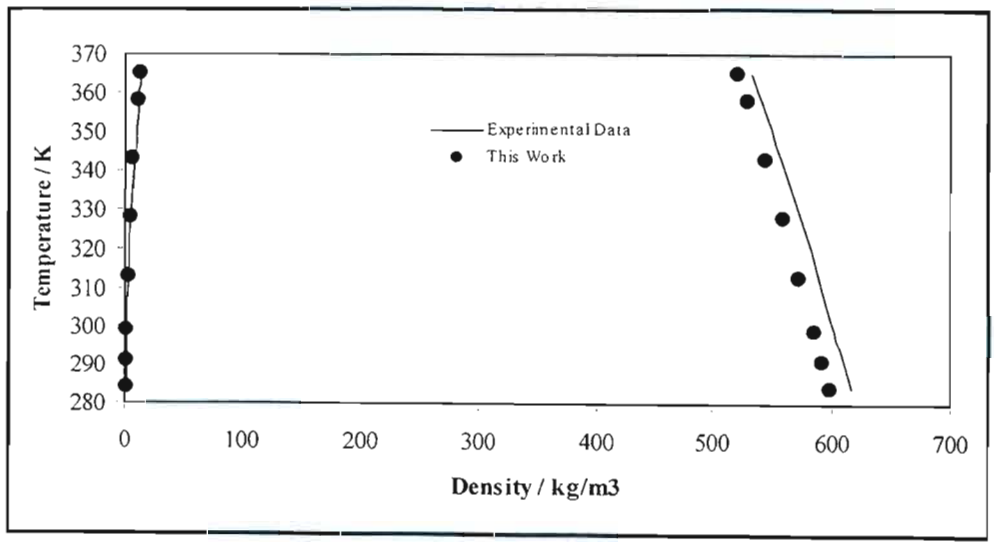

Figure 8-33: Phase-co-existence curve for n-pentane.

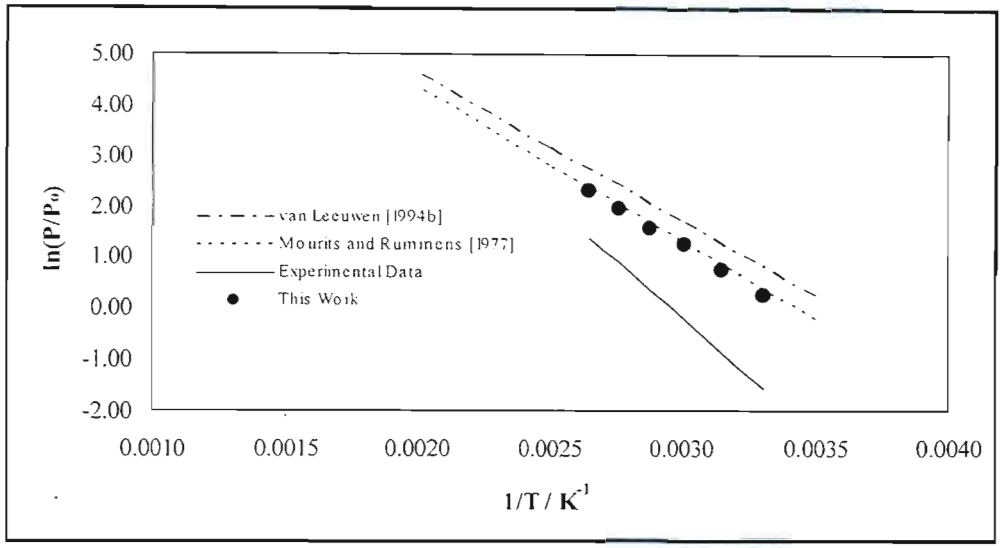

Figure 8-34: Vapour pressure curve for methanol (with literature data).

T represents temperature, P represents pressure and

P_o is a standard pressure (101.325 kPa).

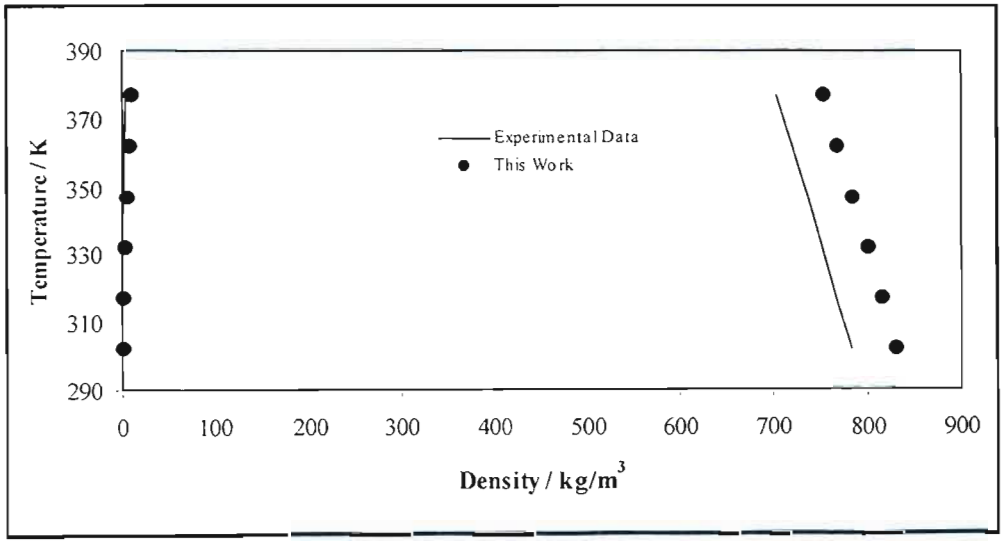

Figure 8-35: Phase-co-existence curve for methanol.

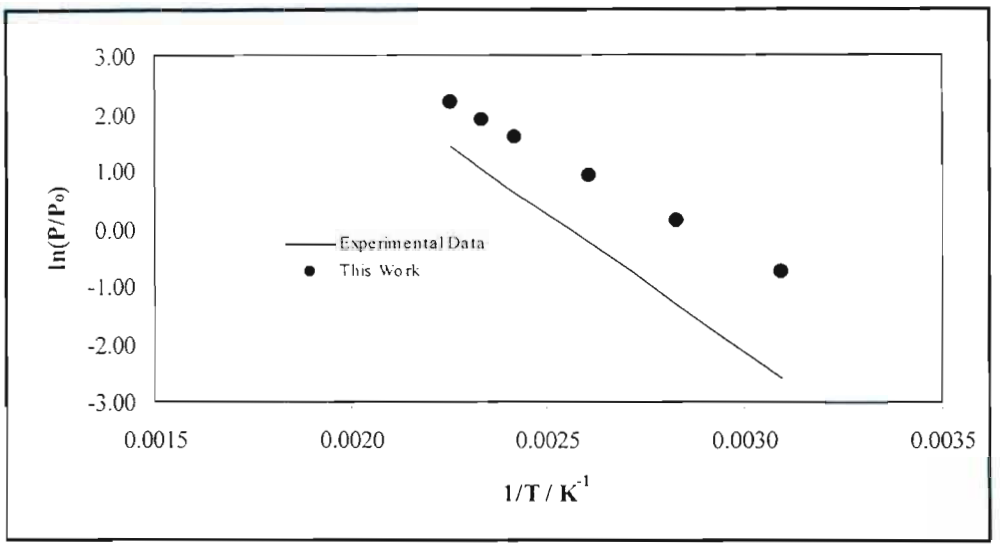

Figure 8-36: Vapour pressure curve for acetic acid.

T represents temperature, P represents pressure and

P_o is a standard pressure (101.325 kPa).

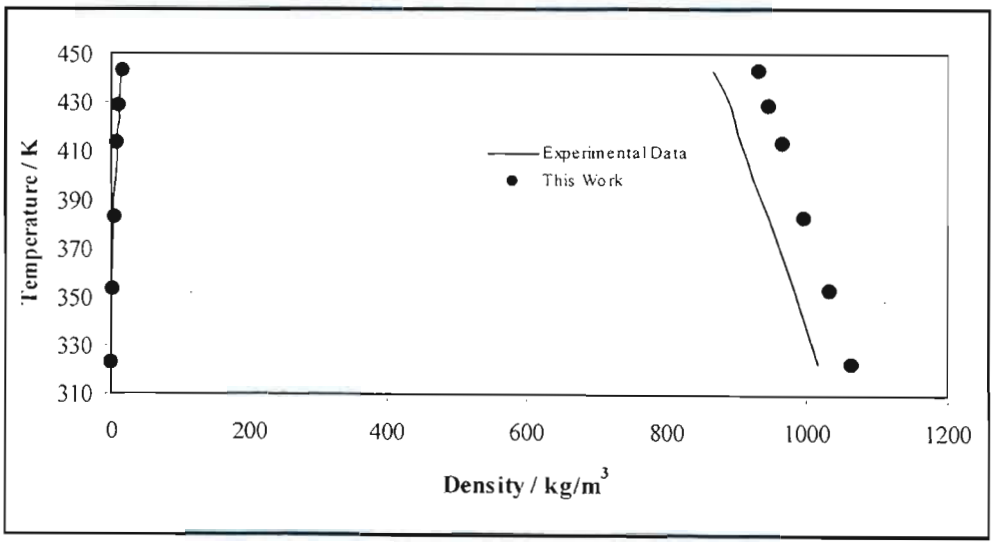

Figure 8-37: Phase-co-existence curve for acetic acid.

8.4.2 Binary Phase Diagram Prediction

The methanol (1) – acetic acid (2) system at atmospheric pressure (i.e. 101.325 kPa) was selected for the attempted prediction of a binary phase diagram. This particular system was chosen because the vapour pressures (this pure component data allows calculation of the end points of the phase envelope) of both methanol and acetic acid had already been predicted. In addition, both species comprising the system are polar compounds and, hence, the dipole programme utilized in the vapour pressure predictions could be used for this phase of the project as well. Finally, the system needed to include at least one carboxylic acid (in this case, acetic acid) in keeping with the nature of the project. The predicted phase diagram is displayed below, along with the experimental data (obtained from the DDB using the DDB software [1998]). A discussion of these results is given in Section 9.8.2.

Table 8-21: Predicted binary VLE data for the methanol (1) – acetic acid (2) system at 101.325 kPa.

T / K	z_1	x_1	y_1
368.10	0.000	0.000	0.000
358.00	0.100	0.070	0.340
350.00	0.200	0.131	0.540
333.00	0.400	0.308	0.796
322.00	0.600	0.474	0.909
313.00	0.800	0.699	0.964
309.00	0.900	0.875	0.990
307.30	1.000	1.000	1.000

z_1 represents the overall composition

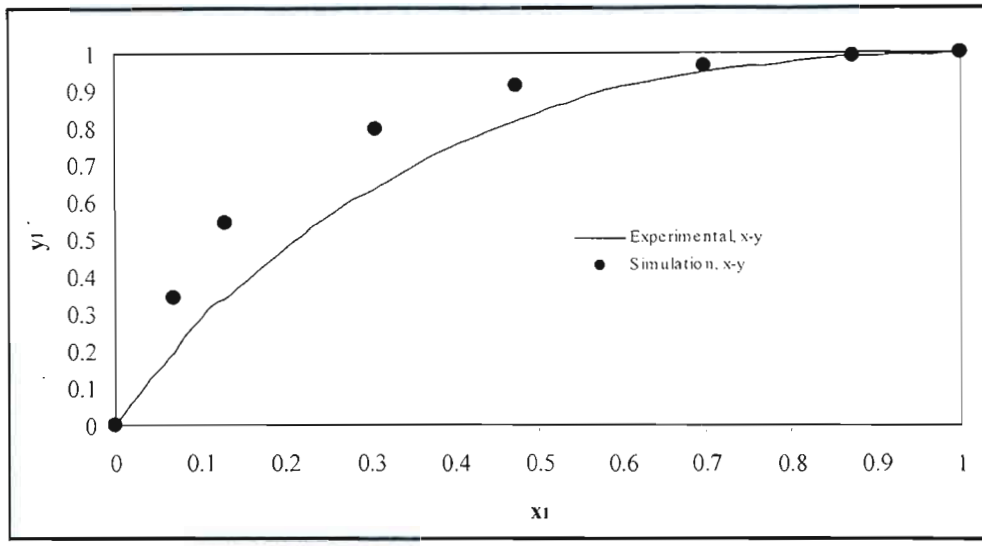

Figure 8-38: Graph showing the x-y simulation prediction versus the experimental for the methanol (1) – acetic acid (2) system at 101.325 kPa.

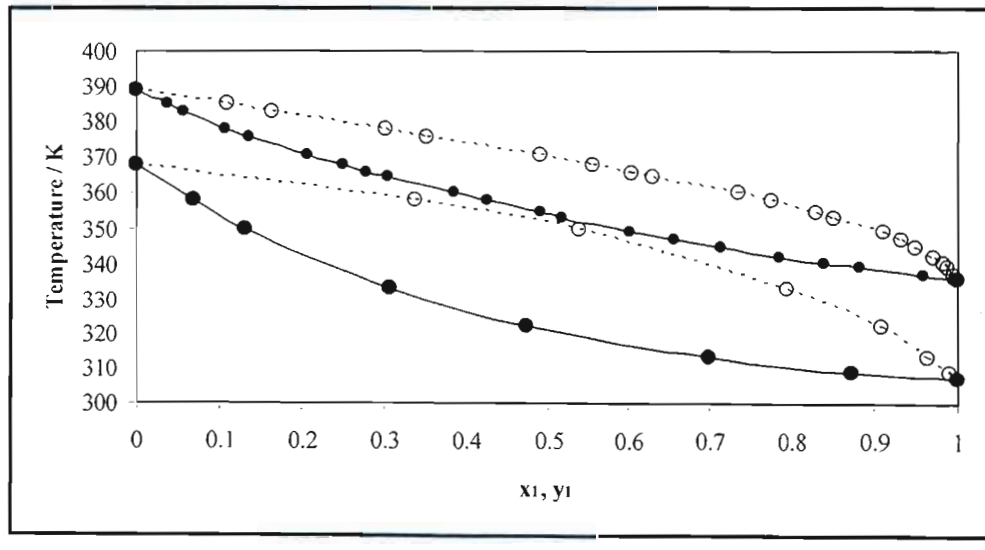

Figure 8-39: Graph showing the binary phase diagram prediction (bottom curve) versus the experimental data (top curve) for the methanol (1) – acetic acid (2) system at 101.325 kPa.

CHAPTER
9

DATA ANALYSIS AND DISCUSSION

The theoretical aspects of low-pressure vapour-liquid equilibrium (VLE) pertinent to this project were discussed in extensive detail in Chapter 3. This chapter deals with the results (and discussion thereof) of the VLE data analysis. This includes the regression of the data using both the combined and direct methods, infinite dilution activity coefficients and excess thermodynamic properties for the isothermal data. The vapour pressure curves measured are also discussed since the data were fitted to both the Reid et al. [1988] equation and the Antoine equation. Acentric factors for the carboxylic acids present in the VLE systems were also determined (these were used in the VLE regression programmes) and the methods by which this was accomplished are described. The final set of data that is discussed here pertains to the molecular simulation portion of this work.

9.1 Pure Component Properties

Pure component properties play a vital role when analyzing thermodynamic data. It is essential that accurate values are found or determined since certain techniques are particularly sensitive to these properties (e.g. the acentric factors in the direct method of VLE data regression). Quantities such as critical pressure, critical temperature, critical volume and critical compressibility are widely available and were easily obtained from the Dortmund Data Bank (DDB). The excellent compilation of McClellan [1974] (in conjunction with the text by Reid et al. [1988]) provided the dipole moments, whilst the

solvation and association parameters were acquired from Prausnitz et al. [1980]. The mean radius of gyration was determined using the group contribution method proposed by Reid et al. [1977] since they could not be located in the available literature. As was mentioned above, the acentric factors were calculated (Section 9.2.2) from the vapour pressure data measured as part of this project. The second virial coefficients were evaluated using the correlations discussed in Section 3.2.1 and the liquid molar volumes were obtained through application of the Rackett [1970] equation. All the pure component properties utilized in this work are presented in tabular form in Appendix A.

9.2. Experimental Vapour Pressure Data

At the outset of this project, the decision was made to measure the carboxylic acid vapour pressures because precise vapour pressure (VP) data are essential when modeling binary VLE systems. A literature survey was conducted initially and it was found that the only available vapour pressure measurements for carboxylic acids were those done by Sewnarain et al. [2002], and those provided in the form of equation parameters by the Dortmund Data Bank (DDB) and Korean Data Bank (KDB). As these differed from one another in most cases, the necessity of re-measuring this data to ensure accuracy became apparent. A comparison between these sources and the VP data measured in this work is presented in Table 9-3. The experimentally determined vapour pressure data were tabulated and graphed in Section 8.2.

9.2.1 Regression of the Vapour Pressure Data

The vapour pressure data were regressed to find parameters for both the Antoine equation:

$$\ln(P) = A' - \frac{B'}{T + C'} \tag{9-1}$$

and the Reid et al. [1988] equation:

$$\ln\left(\frac{P}{P_c}\right) = (1 - x_R)^{-1}[A' x_R + B' x_R^{1.5} + C' x_R^3 + D' x_R^6] \tag{9-2}$$

where

$$x_R = 1 - \frac{T}{T_c} \tag{9-3}$$

In both equations the pressure, P, is given in kPa and the temperature, T, in degrees Celsius. The parameters obtained are given in Tables 9-1 and 9-2 below.

Table 9-1: Parameters for the Antoine equation.

	Propionic	**Butyric**	**Isobutyric**	**Valeric**	**Isovaleric**	**Hexanoic**	**Heptanoic**
A	18.1057	14.5116	15.1762	36.4104	18.0849	13.4659	20.0521
B	5640.34	3164.47	3527.86	30029.23	5702.44	2642.20	7018.30
C	277.4614	156.5612	180.5140	760.4482	247.9884	95.2013	238.8097
$\Sigma(\Delta P^2)$	0.3568	0.4339	3.4342	0.4604	2.9935	0.1312	0.0368

Table 9-2: Parameters for the Reid et al. [1988] equation.

	Propionic	**Butyric**	**Isobutyric**	**Valeric**	**Isovaleric**	**Hexanoic**	**Heptanoic**
A	7.5182	-36.1019	0.9623	17.4844	33.0671	-54.5828	-19.8968
B	-37.6199	72.0808	-23.6343	-63.0365	-106.8467	118.0845	33.0734
C	58.7873	-145.5125	42.5490	97.2515	206.6594	-231.6407	-88.3811
D	-164.2785	470.1079	-200.7284	-244.7591	-813.6062	698.1327	298.2216
$\Sigma(\Delta P^2)$	0.2822	0.1424	3.1963	0.4141	1.5499	0.0769	0.0314

In all cases, the Reid et al. [1988] equation (Equation (9-2)) was found to give a superior correlation of the vapour pressure data when compared to the simpler Antoine equation (Equation (9-1)). This is clearly evidenced by the significantly lower $\Sigma(\Delta P^2)$ values for the Reid et al. [1988] equation presented in Tables 9-1 and 9-2. The fact that the Reid et al. [1988] equation provides a better fit to the VP data is not unexpected since this equation has four adjustable parameters as opposed to the three of the Antoine equation. Both equations, however, fitted the data exceedingly well.

Table 9-3 shows the comparison between the experimental data and the literature data obtained from the DDB and KDB. The average pressure difference per point and the average percentage pressure difference per point were both calculated for each carboxylic acid. The average pressure difference per point is determined using the following equation:

$$\Delta P_{avg} = \frac{|P_{ex} - P_{lit}|}{n_{ex}} \tag{9-4}$$

and the average percentage pressure difference per point from:

$$\%P_{avg} = \frac{\left|\left(P_{ex} - P_{lit}\right)/P_{ex}\right| x100\%}{n_{ex}} \tag{9-5}$$

where n_{ex} stands for the number of experimental points measured.

Table 9-3: Comparison between experimental and literature vapour pressure data.

Acid	ΔP_{avg} KDB	ΔP_{avg} DDB	$\%P_{avg}$ KDB	$\%P_{avg}$ DDB
	kPa	kPa		
Propionic	0.55	0.48	0.11	0.09
Butyric	4.22	0.42	0.56	0.12
Isobutyric	1.66	1.21	0.31	0.23
Valeric	0.98	0.77	0.16	0.16
Isovaleric	1.36	3.30	0.31	0.57
Hexanoic	0.70	0.92	0.29	0.31
Heptanoic	1.13	0.58	0.78	0.45

The average pressure differences (given in kPa) were small in general, with the exceptions being butyric and isovaleric acid. For butyric acid, the experimental results differed considerably from the KDB data (ΔP_{avg} = 4.2217), but the DDB data was extremely close to the experimental measurements (ΔP_{avg} = 0.4163). Conversely, for isovaleric acid, the

experimental data deviated fairly significantly from the DDB data (ΔP_{avg} = 3.3008), while the KDB data was fairly close to the measured data (ΔP_{avg} = 1.3637).

The percentage differences for each acid were generally smaller for the DDB data as compared to the KDB data; the only exceptions being isovaleric and hexanoic acid. In all cases, however, the percentage difference between the measured data and the literature data was less than 0.8% and in most cases was well below 0.5%.

9.2.2 Acentric Factor Evaluation

The parameter termed the *acentric factor* was first proposed by Pitzer et al. [1955]. Pitzer and co-workers defined the acentric factor (symbolized by ω) to be the parameter that represented the intermolecular forces that exist in a complex molecule between the various parts of that molecule and not just their centres. Hence, the parameter characterizes the non-sphericity or acentricity of a molecule, and, therefore, was given the name: acentric factor.

According to Reid et al. [1988], ω is essentially zero for monatomic gases, but increases for higher molecular weight hydrocarbons. This is clearly expected from the definition of the acentric factor, since the non-sphericity of a molecule will naturally increase as the complexity rises. The value of the acentric factor also increases with polarity. Thus, carboxylic acids have relatively large acentric factors. Reid et al. [1988] state that ω is widely used as a measure of the complexity of a molecule with respect to both geometry and polarity, but when ω reaches values above 0.4 it is no longer meaningful with regard to the original definition.

Pitzer et al. defined ω by:

$$\omega = -\log P_r - 1.000 \qquad (9\text{-}6)$$

where P_r is the reduced vapour pressure at the corresponding temperature $T_r = T/T_c = 0.7$. However, this equation does not always yield accurate values for ω, particularly for polar compounds. Therefore, in this work alternative correlations for determining ω (Reid et al.

[1988]) were employed when evaluating the acentric factor. The two correlations that were applied required the use of the term $\theta = T_b/T_c$, where T_b is the boiling point temperature (at atmospheric pressure) of the species of interest. The first correlation calculated ω from:

$$\omega = \frac{3}{7}\frac{\theta}{1-\theta}\log P_c - 1 \tag{9-7}$$

The second correlation was based on the Lee-Kesler vapour pressure relations and took the form:

$$\omega = \frac{\alpha}{\beta} \tag{9-8}$$

where

$$\alpha = -\ln P_c - 5.97214 + 6.09648\theta^{-1} + 1.28862\ln\theta - 0.169347\theta^6 \tag{9-9}$$

$$\beta = 15.2518 - 15.6875\theta^{-1} - 13.4721\ln\theta + 0.43577\theta^6 \tag{9-10}$$

Acentric factors were only evaluated for those carboxylic acids that were involved in the binary VLE systems, viz. propionic acid, isobutyric acid and valeric acid. These values are reported in Appendix A. Both correlations produced similar values for the acentric factor, with the Lee-Kesler equation yielding slightly larger values in all cases. The acentric factors calculated in this work corresponded well with those reported in the literature and databases such as the KDB and DDB.

9.2.3 Twu et al. [1991] Alpha Function

As was discussed above in Section 9.2.2, the acentric factors were calculated for the carboxylic acids involved in the binary VLE systems. This was necessary because the acentric factors were required in both the combined and direct regression procedures. However, in the direct method the acentric factors were utilized in the alpha function given by Peng and Robinson [1976] (Equation 3-106), which proved to be rather inaccurate. The same conclusion was reached by Stryjek and Vera [1986].They undertook a detailed study of the deviations in calculated vapour pressures for a range of compounds and acentric

factors. They found that large errors occurred at all temperatures for compounds with large acentric factors (such as carboxylic acids), even for the non-polar species hexadecane. Stryjek and Vera [1986] state that this error increases rapidly, even at low reduced temperatures. This led to Stryjek and Vera proposing a modified form of the expression for κ (Equation 3-111).

However, Twu et al. [1991] developed a correlation for alpha that superseded the Stryjek and Vera [1986] modification (Section 3.4.2.1). The expression for alpha is defined as:

$$\alpha(T) = T_r^{N'(M'-1)} e^{L'(1-T_r^{N'M'})} \tag{3-112}$$

The parameters in Equation (3-112) are particular to each chemical species and must be obtained via regression of experimental vapour pressure data. Thus, in this work the vapour pressure data measured during the initial phase of the project was used to determine L', M' and N' for the three carboxylic acids involved in the binary VLE systems (namely, propionic acid, isobutyric acid and valeric acid). The parameter N' is generally close to a value of two and is always positive (Twu et al. [1991]), whilst L' and M' may vary but usually lie within the range 0 to 1. The parameter N' was initially always set equal to two (Twu [1988]), however, Twu et al. [1991] decided to increase the flexibility of the correlation by allowing N' to alter. Twu et al. [1991] note that this improves the prediction of vapour pressures for highly polar substances with high normal boiling point temperatures. Since carboxylic acids fall into that category, Equation (3-112) was used in an effort to improve the results of the VLE data reduction (see Section 9.4.3.2 below).

As has been mentioned above, the three parameters found in Equation (3-112) must be determined by regressing measured vapour pressure data. This is accomplished by running a pure component regression using the equation of state (EOS) of interest. It is essential that the same EOS be used to find L', M' and N' as will be used in the binary VLE data reduction since the parameters differ depending on the EOS. The inputs to the regression programme are the temperatures recorded for the vapour pressure measurements and the initial guesses for the three parameters (along with the necessary pure component data such as critical properties). The values for the alpha function parameters are then optimized by

minimizing the deviation of the calculated pressures from the experimental vapour pressures. Thus, the alpha correlation of Twu et al. [1991] is uniquely specified (for each binary VLE system) to the chemicals and EOS that are employed in regressing that system.

Twu et al. [1996] state that it is crucial for accurate vapour-liquid calculations that the prediction of the pure-component vapour pressures be of high accuracy. They go on to say that the alpha given by Equation (3-112) in a cubic equation of state yields a very precise prediction of vapour pressure for all the pure components present in the VLE system. The L', M' and N' parameters calculated for propionic, isobutyric and valeric acid are presented in Appendix A and the improvements in accuracy that were obtained are discussed in Section 9.4.3.2.

9.3 Experimental Activity Coefficients

The established method of determining the experimental liquid-phase activity coefficients is to first evaluate the vapour phase correction term Φ_i from the second virial coefficients (calculated using one of the correlations discussed in Section 3.2.1), followed by substitution into:

$$y_i \Phi_i P = x_i \gamma_i P_i^{sat} \tag{3-37}$$

which yields the experimental activity coefficient (after minor re-arrangement). However, in the case of the carboxylic acids, this procedure produced extremely poor values for the experimental activity coefficients. An example of the sort of results that were obtained is provided in Figure 9-1 below.

These unusual curves generated for the experimental activity coefficients are as a result of the high degree of association that occurs in carboxylic acids, even at low pressures. The acids tend to dimerized in both the vapour and the liquid phase due to hydrogen bonding. This effect may be taken into account by considering the chemical theory description of dimerization and applying it to the liquid phase. (Chemical theory was discussed in Section 3.2.2; with reference to the vapour phase fugacity coefficients).

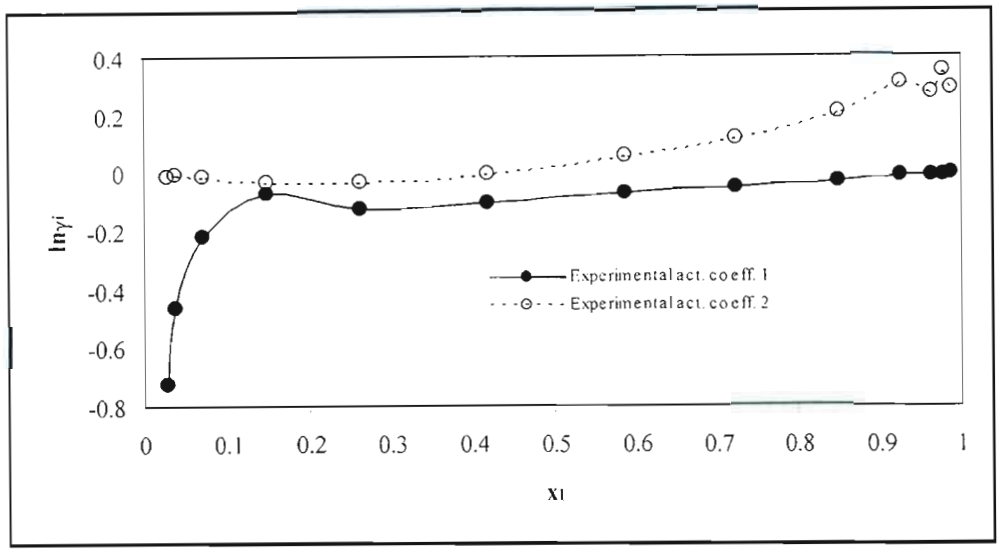

Figure 9-1: Experimental liquid-phase activity coefficients for the propionic acid (1) – valeric acid (2) system at 393.15 K using the traditional calculation method.

According to Prausnitz et al. [1999], the liquid-phase activity coefficients may be evaluated using the following equation:

$$\gamma_i = \frac{2k_i}{(2k_i - 1)x_i + k_i x_j + (x_i^2 + 2k_i x_i x_j + k_i x_j^2)^{1/2}} \tag{9-11}$$

where

$$k_i = 4K_{ij} + 1 \tag{9-12}$$

and K_{ij} is given by Equation (3-62). Using these equations to evaluate the experimental activity coefficients produces a remarkable improvement in the resultant curves. This is demonstrated graphically in Figure 9-2. The experimental liquid-phase activity coefficients determined using the chemical theory of associated solutions are presented in Tables 9-4 and 9-5; with comparisons to appropriate activity coefficient models given in Section 9.4.

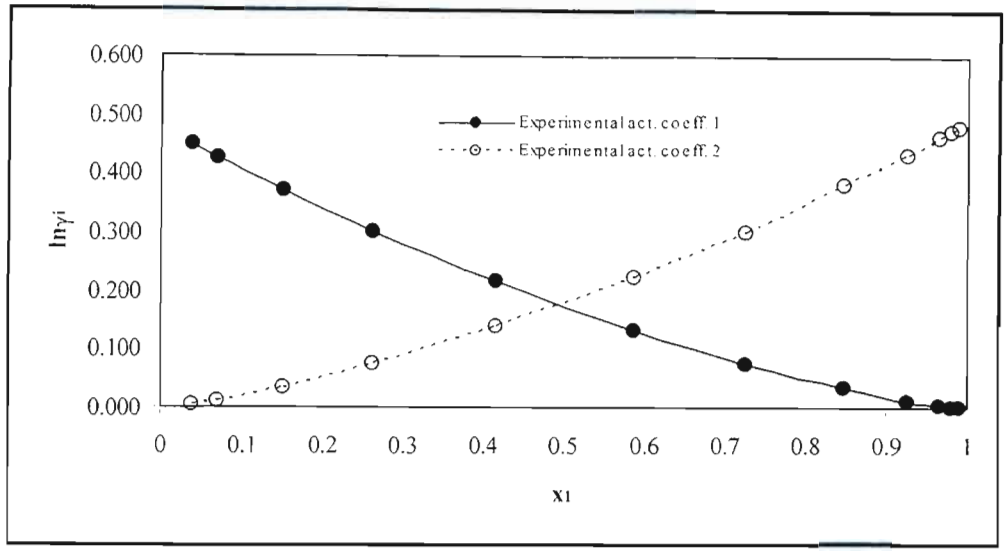

Figure 9-2: Experimental liquid-phase activity coefficients for the propionic acid (1) – valeric acid (2) system at 393.15 K using chemical theory in the liquid phase.

Table 9-4: Experimental liquid-phase activity coefficients for the propionic acid (1) – valeric acid (2) system calculated by taking chemical theory into account.

P = 20 kPa			T = 393.15 K		
x_1	γ_1	γ_2	x_1	γ_1	γ_2
0.045	1.460	1.003	0.039	1.566	1.004
0.121	1.426	1.021	0.072	1.529	1.011
0.201	1.379	1.048	0.151	1.448	1.035
0.287	1.328	1.086	0.264	1.350	1.077
0.380	1.273	1.135	0.418	1.239	1.150
0.516	1.197	1.222	0.588	1.142	1.251
0.673	1.120	1.352	0.726	1.078	1.352
0.787	1.070	1.470	0.849	1.033	1.462
0.880	1.034	1.586	0.926	1.011	1.542
0.922	1.019	1.646	0.965	1.003	1.586
0.951	1.010	1.690	0.980	1.001	1.604
0.969	1.005	1.720	0.989	1.000	1.615

T = 403.15 K			T = 413.15 K		
x_1	γ_1	γ_2	x_1	γ_1	γ_2
0.009	1.530	1.000	0.010	1.459	1.000
0.029	1.509	1.002	0.030	1.441	1.001
0.084	1.455	1.011	0.086	1.393	1.009
0.153	1.393	1.029	0.147	1.346	1.022
0.258	1.312	1.063	0.261	1.268	1.053
0.417	1.209	1.129	0.403	1.187	1.104
0.598	1.117	1.227	0.483	1.148	1.139
0.728	1.065	1.313	0.634	1.085	1.216
0.847	1.027	1.409	0.794	1.035	1.317
0.928	1.008	1.483	0.897	1.011	1.397
0.979	1.001	1.536	0.979	1.001	1.470
0.990	1.000	1.548	0.990	1.000	1.480

Table 9-5: Experimental liquid-phase activity coefficients for the isobutyric acid (1) – valeric acid (2) system calculated by taking chemical theory into account.

P = 20 kPa			T = 393.15 K		
x_1	γ_1	γ_2	x_1	γ_1	γ_2
0.012	1.493	1.000	0.011	1.614	1.001
0.023	1.486	1.001	0.025	1.597	1.002
0.056	1.463	1.005	0.048	1.570	1.006
0.120	1.419	1.018	0.110	1.502	1.022
0.221	1.353	1.050	0.226	1.392	1.062
0.445	1.219	1.156	0.371	1.278	1.125
0.593	1.145	1.254	0.557	1.163	1.229
0.820	1.049	1.458	0.678	1.102	1.313
0.924	1.015	1.584	0.816	1.046	1.429
0.964	1.005	1.639	0.898	1.019	1.509
0.982	1.002	1.667	0.968	1.003	1.588
0.992	1.000	1.683	0.992	1.000	1.617

T = 403.15 K			T = 413.15 K		
x_1	γ_1	γ_2	x_1	γ_1	γ_2
0.010	1.549	1.000	0.009	1.481	1.000
0.024	1.534	1.001	0.024	1.467	1.001
0.047	1.509	1.004	0.048	1.444	1.003
0.106	1.451	1.016	0.104	1.396	1.012
0.226	1.348	1.052	0.222	1.307	1.041
0.371	1.246	1.108	0.367	1.216	1.090
0.556	1.143	1.202	0.554	1.123	1.173
0.670	1.091	1.273	0.673	1.076	1.239
0.819	1.037	1.384	0.772	1.043	1.302
0.897	1.016	1.453	0.873	1.017	1.377
0.966	1.002	1.523	0.927	1.007	1.422
0.991	1.000	1.550	0.991	1.000	1.481

9.4 Experimental VLE Data Reduction

The techniques used in the reduction of binary VLE data were discussed extensively in Section 3.4. Both the combined and direct methods were utilized in regressing the experimental data. Three local-composition based, liquid-phase activity coefficient models were employed (viz. Wilson, NRTL and UNIQUAC), as well as the Peng-Robinson equation of state (Peng and Robinson [1976]). Two different mixing rules were used in conjunction with the Peng-Robinson EOS, namely the Wong-Sandler (Wong and Sandler [1992]) and the Twu-Coon (Twu and Coon [1996]) mixing rules (see Sections 3.4.2.3 and 3.4.2.4). In the case of the activity coefficient models, the vapour phase non-idealities were accounted for using two different methods. The first employed the Pitzer-Curl correlation (Pitzer and Curl [1957]) to determine the second virial coefficients which then allowed calculation of the fugacity coefficient. The second method involved application of the chemical theory of gas non-ideality in calculating the fugacity coefficients. This required the use of the Hayden and O'Connell (Hayden and O'Connell [1975]) correlation in

determining the dimerization equilibrium constants. These methods were discussed in detail in Section 3.2.

As was discussed in Section 3.4.1, the model parameters were optimized by minimizing the pressure deviations (or temperature deviations for the isobars) between the experimentally measured pressures (or temperatures) and those calculated by the model. Van Ness [1995] states that minimizing the pressure residuals (δP) provides a fit that is at least as good as any other that might be obtained by minimizing a different residual (e.g. δy). This postulation was investigated in this work by modelling each set of data using three residuals, namely pressure, vapour composition and Gibbs excess energy. The results confirmed that the objective function based on pressure ($S = \sum(\delta P)^2$) provided a fit that was at least as good as any other, as was put forward by Van Ness [1995]. The same result was found for the isobaric data – the temperature residuals (δT) yielded a superior fit. Hence, only the parameters resulting from the δP or δT regressions are reported here. The regression programmes were written in MATLAB, which offers a number of built-in optimization functions; one of which (*fminsearch*) was utilized in the data reduction carried out in this work.

The parameters obtained from the VLE data reduction for each model are presented, along with the average deviations between the experimental pressures and vapour compositions and those calculated from the model. The temperature dependence of the parameters was taken into account by including the RT term in the exponential expression of each model (e.g. for UNIQUAC: $\tau_{12} = \exp(-\Delta u_{12}/RT)$). For the purpose of thermodynamic consistency testing, the root mean square (RMS) value of the $\delta\ln(\gamma_1/\gamma_2)$ residual is also quoted. In addition, for each model the fit to the experimental data is displayed graphically. Since the regression was conducted using pressure residuals for the isothermal data (and temperature residuals in the case of isobaric data), the best fit was decided by choosing the model that provided the minimum pressure (or temperature) deviation.

As was discussed in Section 9.2.1; the measured carboxylic acid vapour pressures were fitted to both the Antoine and Reid et al. [1988] equations and the Reid et al. [1988]

equation proved to be slightly superior. However, the Antoine equation is far easier to work with when modelling VLE data because it may be conveniently rearranged to provide either saturated pressures or temperatures, depending upon which is required by the programme algorithm. In addition, the simpler Antoine equation provided a perfectly satisfactory representation of the data and, hence, very little is being sacrificed in terms of accuracy (refer to Tables 9-1 and 9-2). This benefit of being able to rearrange the Antoine equation is particularly useful during the bubblepoint temperature iterations, since if the Reid et al. [1988] equation was used, a separate, iterative loop would be required to converge on the saturated temperature.

9.4.1 Gas Chromatograph Calibration

The Hewlett-Packard 5890 gas chromatograph (GC) was used to determine the compositions of the cyclohexane (1) – ethanol (2) test system. The operating conditions that were employed are laid out in Table 6-1 and the gas chromatograph calibration curves are presented in Section 8.3.1 (Figures 8-8 and 8-9). Usually, GC calibration curves are linear. However, the calibration graphs for the cyclohexane – ethanol system displayed a slight curve and the best fit through the points was obtained using a quadratic equation (this is more common with TCD detectors than FID). This meant that the calibration could not be generalized to apply to the entire composition range by inverting the slopes of the curves and, thus, an average response factor ratio was not calculated. Instead, care had to be taken to ensure that the correct calibration curves were employed, depending on whether the samples were being taken in the dilute ethanol region or the dilute cyclohexane region. Although the calibration curves were atypical, the results obtained for the compositions were excellent and matched the literature data perfectly (Figures 8-10 and 8-11).

The carboxylic acid systems could not be measured using the Hewlett-Packard GC because the response factor for the acids was miniscule (Section 6.2.3). Instead, a Varian 3300 GC (with an FID detector) was utilized in determining the compositions of the carboxylic acid systems. Unlike the cyclohexane – ethanol GC calibration, the calibration curves generated for the acid systems were all linear. The propionic acid (1) – valeric acid

(2) calibration curves are presented in Figures 8-12 and 8-13, while Figures 8-22 and 8-23 apply to the isobutyric acid (1) – valeric acid (2) system. The inverses of the response factor ratios were not equal for either system; although the differences were small (the percentage difference in each case was less than 1%). Nevertheless, the response factor ratios were deemed not to be constant over the entire composition range. Thus, as for the test system, the correct calibration curve had to be applied in the correct region. For the propionic acid – valeric acid system, Figure 8-12 was employed in the valeric acid-rich (or dilute propionic acid) region and Figure 8-13 in the propionic acid-rich region. A similar procedure was followed for the isobutyric acid – valeric acid system.

This method ensured the accuracy of the composition measurements in the dilute regions on either side of the *x-y*, *T-x-y* and *P-x-y* curves. Clearly, in the middle of the curves the effect of the response ratios not correlating was negligible and either GC calibration could be employed. In general, the response factor ratio was switched when the composition reached a value of 0.5.

9.4.2 Phase Equilibrium Results for the Test System

As has been stated previously in Section 8.3.1, the cyclohexane (1) – ethanol (2) system was utilized as a test system to ensure that the VLE still was operating correctly and that the experimental procedure was accurate. To this end, experimental VLE data for the cyclohexane (1) – ethanol (2) system were measured at 40 kPa.

The measured data were then compared to accurate, reliable and consistent literature data. Two literature data sets were used: Morachevsky and Zharov [1963] and Joseph et al. [2001]. This comparison is presented in Figures 8-10 and 8-11 and it is clear that the experimental data matches the literature data exceedingly well. Thus, it was concluded that both the experimental setup and procedure were operating as desired.

The cyclohexane (1) – ethanol (2) system served a further purpose: the system was also used in ascertaining whether the techniques, equations and programmes developed to

analyze the experimental data were performing as desired. Accordingly, the test system data were regressed using the three liquid-phase activity coefficient models (Wilson, NRTL and UNIQUAC) in conjunction with the Hayden and O'Connell [1975] method for determining the second virial coefficients (used in determining the fugacity coefficients for the vapour phase correction term). The model parameters obtained from this regression are laid out in Table 9-6 below.

The three models all fitted the data well. The Wilson equation provided the best fit to the experimental data, whilst the UNIQUAC equation was the worst. This was rather unexpected since the Wilson [1964] equation is the simplest and oldest of the three models. However, this model yielded the lowest value for both ΔT and Δy; as is shown in Table 9-6. A similar trend was found by Joseph et al. [2002] for the cyclohexane (1) – ethanol (2) system, with UNIQUAC performing the worst of the liquid-phase activity coefficient models. Interestingly though, the modified UNIQUAC equation (Anderson and Prausnitz [1978]) performed far better and was in some cases preferable to the NRTL and Wilson models. The experimental data are presented, along with the fit provided by the respective models, in Figures 9-3 through 9-8. A comparison between the experimental activity coefficients and those calculated by each of the models is also given (Figures 9-9 to 9-11). Again, all three models provided a satisfactory fit to the experimental data. However, the NRTL and Wilson equations were clearly better once more.

Table 9-6: Model parameters and deviations from experimental values for the cyclohexane (1) – ethanol (2) system at 40 kPa.

Quantity	Wilson	NRTL	UNIQUAC
$\lambda_{12} - \lambda_{11}$ (J/mol)	1879.88	6327.33	-43.0794
$\lambda_{12} - \lambda_{22}$ (J/mol)	8670.09	4099.51	6311.49
α	-	0.47149	-
ΔT (K)	0.1696	0.1929	0.3537
Δy	0.0083	0.0087	0.0122
RMS $\delta\ln(\gamma_1/\gamma_2)$	0.0368	0.0414	0.0728

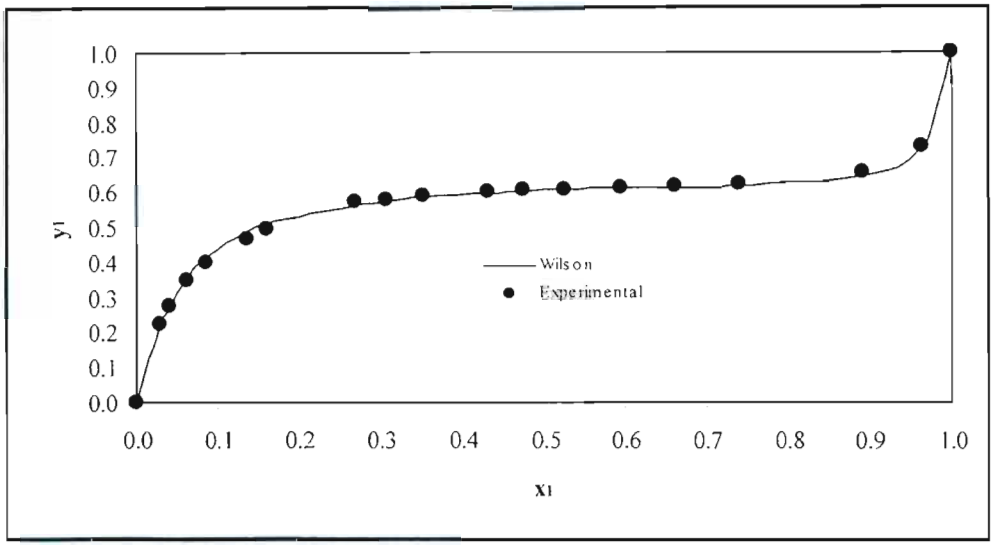

Figure 9-3: Wilson model fitted to x-y data for cyclohexane (1) – ethanol (2) system at 40 kPa.

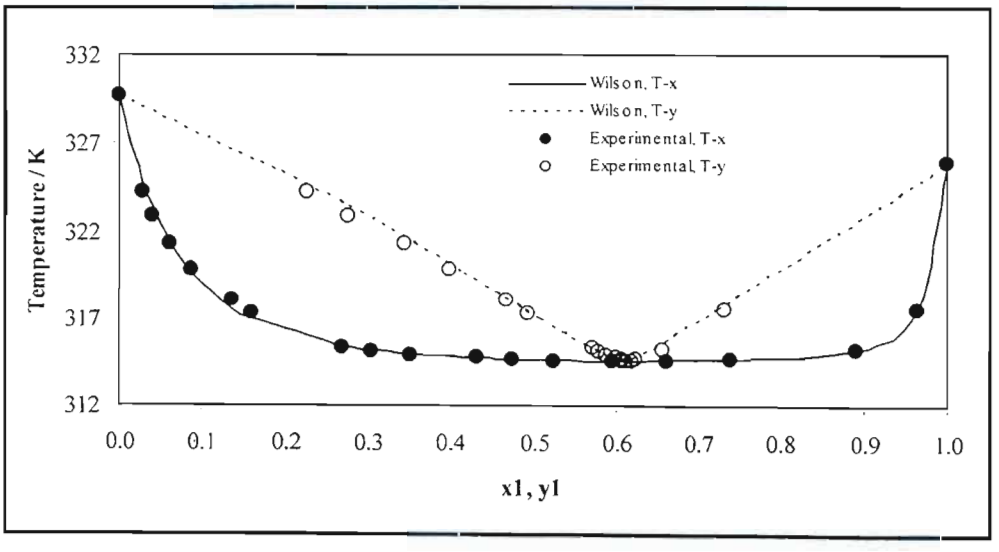

Figure 9-4: Wilson model fitted to T-x-y data for cyclohexane (1) – ethanol (2) system at 40 kPa.

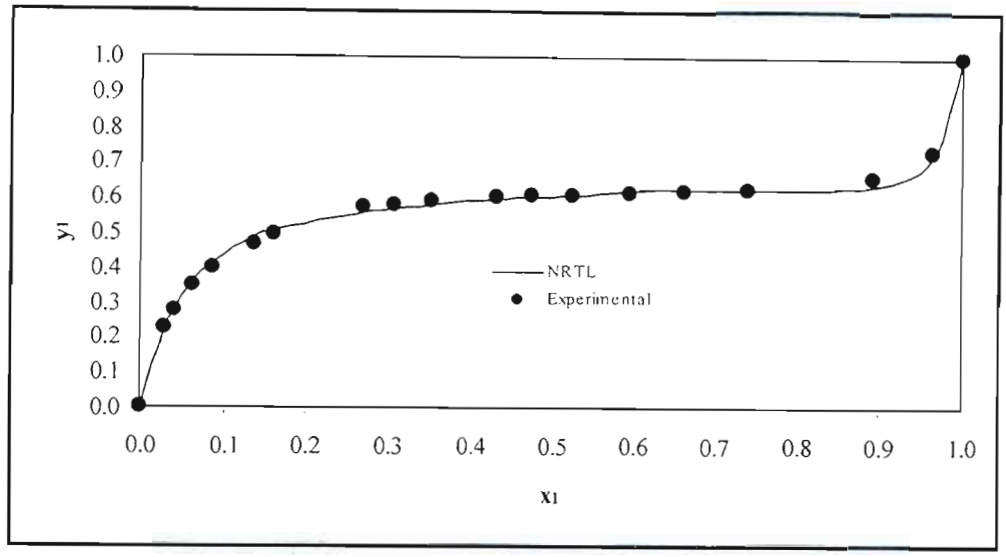

Figure 9-5: NRTL model fitted to x-y data for cyclohexane (1) – ethanol (2) system at 40 kPa.

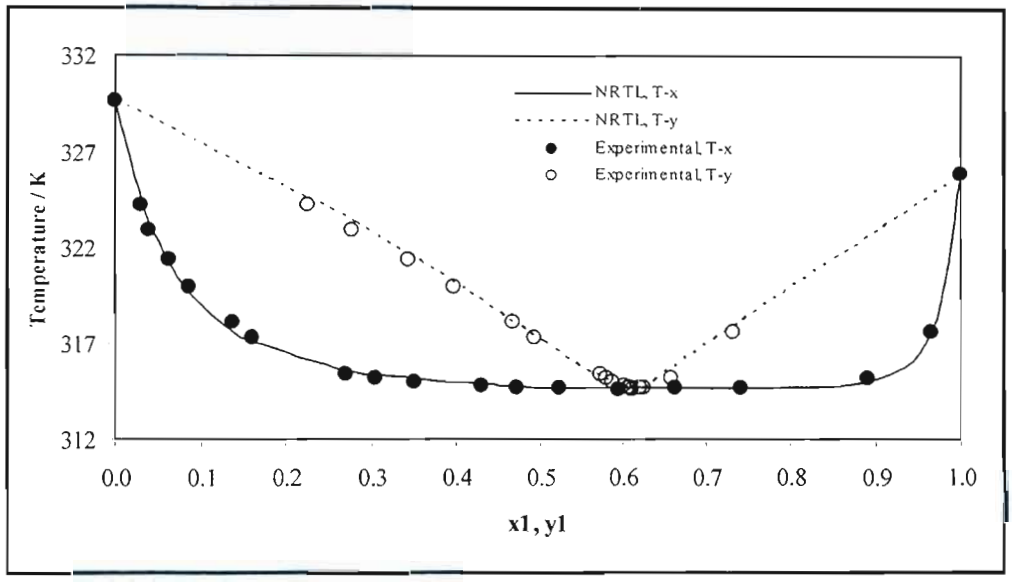

Figure 9-6: NRTL model fitted to T-x-y data for cyclohexane (1) – ethanol (2) system at 40 kPa.

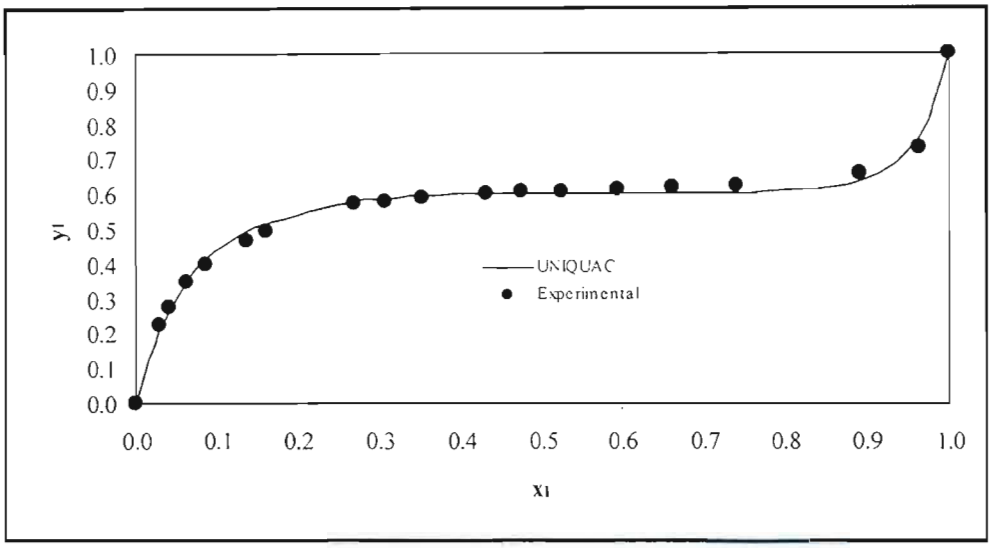

Figure 9-7: UNIQUAC model fitted to x-y data for cyclohexane (1) – ethanol (2) system at 40 kPa.

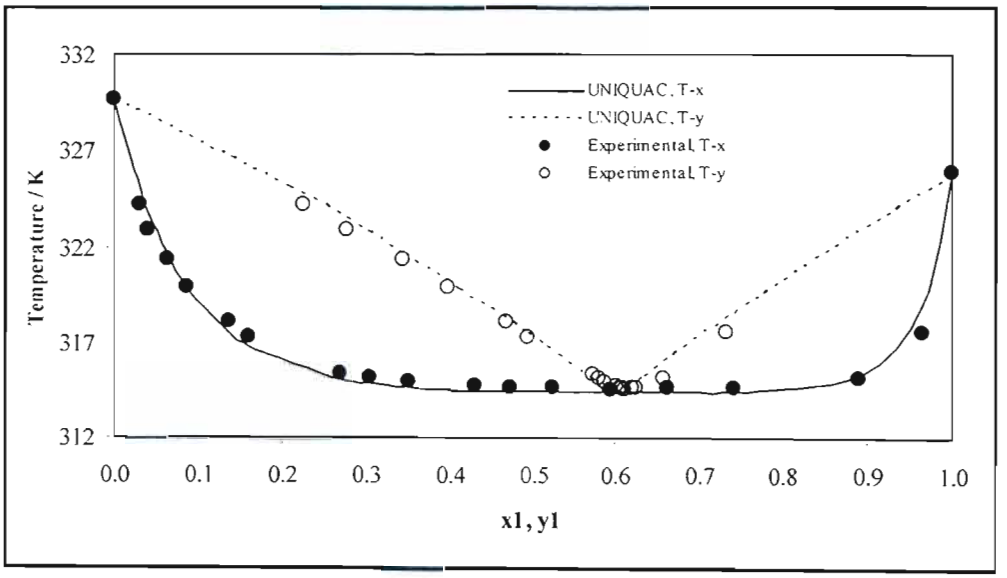

Figure 9-8: UNIQUAC model fitted to T-x-y data for cyclohexane (1) – ethanol (2) system at 40 kPa.

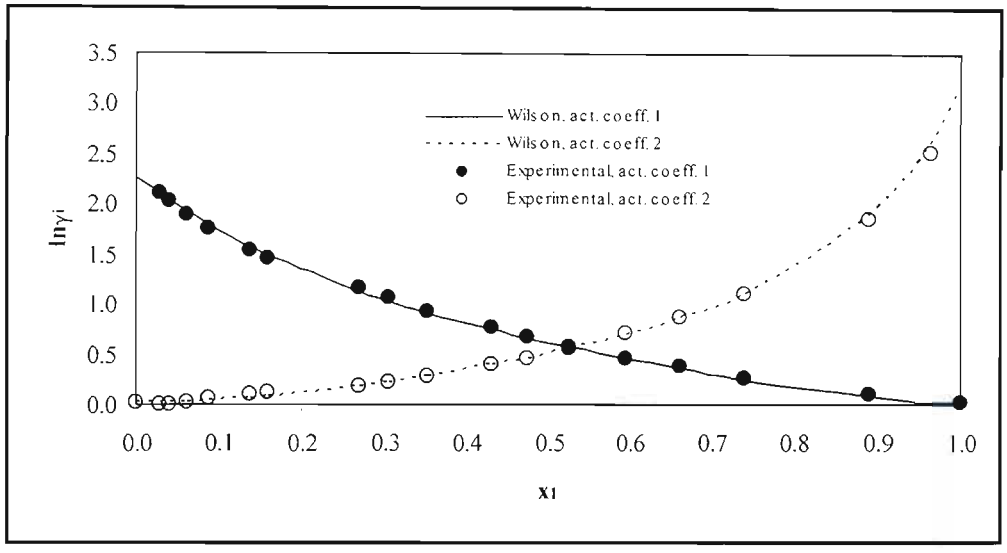

Figure 9-9: Comparison between the experimentally determined liquid-phase activity coefficients and those calculated from the Wilson model for the cyclohexane (1) – ethanol (2) system at 40 kPa.

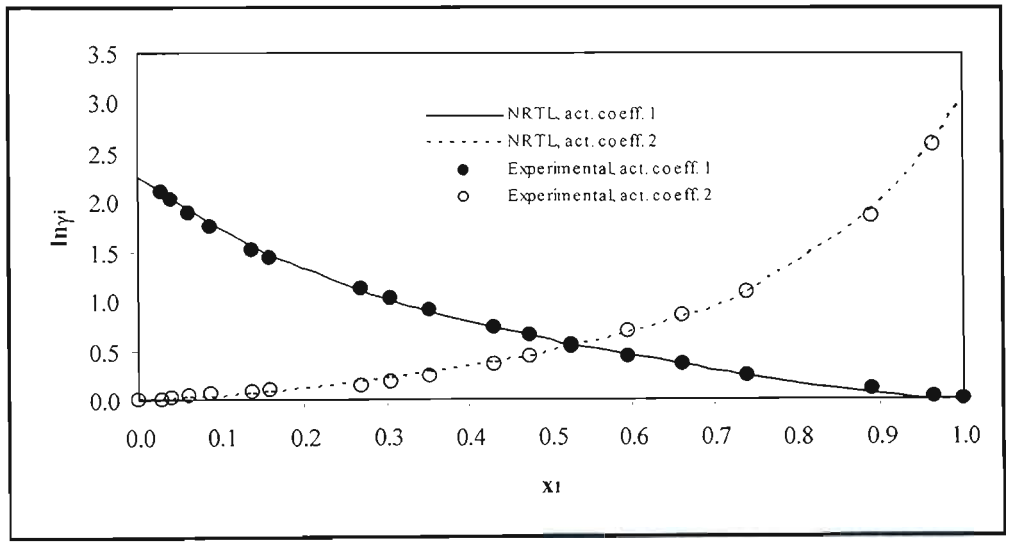

Figure 9-10: Comparison between the experimentally determined liquid-phase activity coefficients and those calculated from the NRTL model for the cyclohexane (1) – ethanol (2) system at 40 kPa.

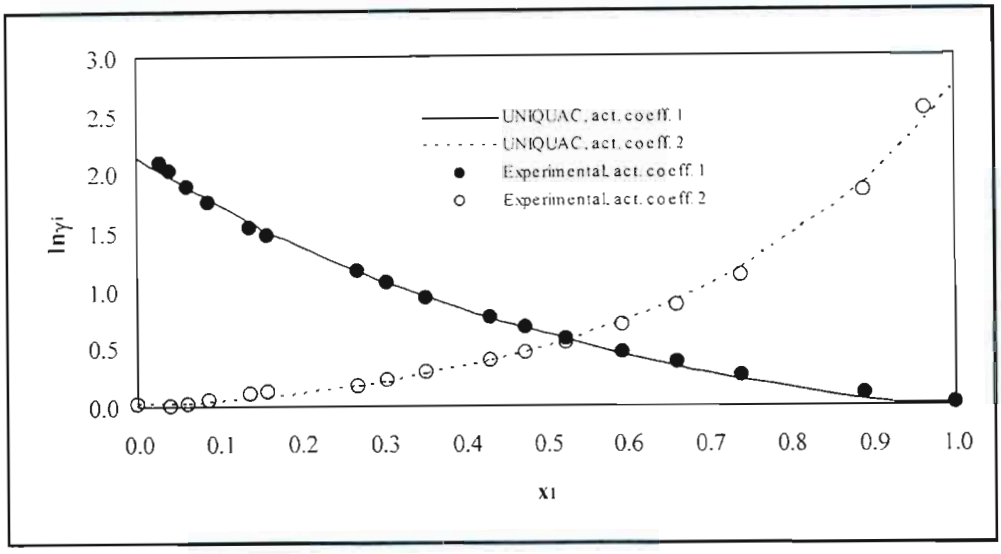

Figure 9-11: Comparison between the experimentally determined liquid-phase activity coefficients and those calculated from the UNIQUAC model for the cyclohexane (1) – ethanol (2) system at 40 kPa.

9.4.3 Phase Equilibrium Results for the Carboxylic Acid Systems

9.4.3.1 General Overview of Both Systems

As has been mentioned in previous sections, vapour-liquid equilibrium data have been measured for two binary carboxylic acid systems in this work: propionic acid (1) – valeric acid (2) and isobutyric acid (1) – valeric acid (2). For both systems, a single isobar at 20 kPa and three isotherms at 120, 130 and 140 °C respectively were measured. This gave a total of eight phase diagrams and, in each case, fourteen data points were experimentally determined. These curves were presented earlier in Sections 8.3.2 and 8.3.3 (Figures 8-14 to 8-21 and Figures 8-24 to 8-31) and the experimental T-x-y and P-x-y data are given in Tables 8-10 through 8-17.

As has often been noted in the literature, carboxylic acids are capable of forming strong hydrogen bonds. According to Prausnitz et al. [1980], two acid molecules have a tendency

to dimerize through the formation of two stable hydrogen bonds; and this may transpire even at very low pressures. Clearly, in a system consisting of two carboxylic acids, the opportunities for dimerization to occur are plentiful. However, the degree to which dimerization will take place is influenced by the system pressure. Prausnitz et al. [1980] state that dimerization decreases as pressure falls as a direct consequence of Le Chatelier's principle. This effect of pressure was noticed in this project and is discussed further below.

An examination of the experimental data shown in Figures 8-14 to 8-21 and Figures 8-24 to 8-31 reveals several characteristic trends. Firstly, the curves all display a slight "S"-shaped bend in their phase envelopes. This is most visible in the isobutyric acid – valeric acid system. This behaviour is also evident in the literature and may be observed in the experimental data measured by Kato et al. [1990] and Sewnarain et al. [2002]. Another characteristic feature of all the phase envelopes is the distinct narrowing that occurs in the dilute regions, giving the appearance of a bird's beak. This non-typical phase behaviour is most likely as a result of the association effects mentioned above. This is borne out by the fact that the effect is most evident in the propionic acid-rich and isobutyric acid-rich regions where the pressure is, obviously, higher at constant temperature. This leads directly (as was discussed in the previous paragraph) to increased dimerization according to Le Chatelier's principle and, consequently, more pronounced association effects. The isothermal data measured by Klekers and Scheller [1968] exhibits this narrowing effect particularly well. Again, the effect is most evident in the higher pressure area of the curve (in the formic acid-rich region).

Interestingly, though, aside from the hydrogen bonding effects that may be observed in the dilute regions, the curves as a whole are remarkably ideal. No large deviations occur in either the liquid or vapour phase. This is reflected in the fact that the experimental liquid-phase activity coefficients (refer to Section 9.3) are all fairly close to the ideal solution value of one. This unexpected ideality has been observed in the literature: Malijevská et al. [1986] state that "the system acetic acid – propionic acid is practically ideal". The same result was reported by Tamir and Wisniak [1975] who found that the activity coefficients were close to unity, indicating that the acetic acid – propionic acid system has only a slight

negative deviation from ideality. The data measured in this work displayed the same trend – a slight negative deviation from ideality. In addition, Miyamoto et al. [2001] measured eleven carboxylic acid systems consisting of various binary combinations of formic, acetic, propionic and butyric acid. The activity coefficients calculated for these systems were all approximately one, with the highest value for each system being (on average) 1.21. The figures reported by Miyamoto et al. for the experimental liquid-phase activity coefficients correspond well with those found in this project (see Tables 9-4 and 9-5 in Section 9.3).

Trends may also be observed in the experimental data with respect to the system temperature. For both systems, the phase envelopes broaden (but maintain the same general shape) as the temperature rises, whilst the *x-y* curves tend to become flatter (i.e. draw closer to the 45° line) with increasing temperature.

Comparing the two binary systems, it is readily noticeable that all the phase envelopes for the isobutyric acid – valeric acid system (Figures 8-25, 8-27, 8-29 and 8-31) are narrower than for the corresponding propionic acid – valeric acid curve (Figures 8-15, 8-17, 8-19 and 8-21). Furthermore, the *x-y* curves for the isobutyric acid – valeric acid data (e.g. Figure 8-26) are flatter than those produced by the propionic acid – valeric acid system (e.g. Figure 8-16). These differences are most likely a result of varying chain lengths. The greater the difference in the number of carbon atoms constituting the two species (in a binary carboxylic acid system), the wider the phase envelope and *x-y* curve will be at a specific temperature or pressure. Thus, the narrowest phase diagrams will be produced by systems consisting of two acids with the same number of carbon atoms in the hydrocarbon chain e.g. isobutyric acid – butyric acid or isovaleric acid – valeric acid. A literature search revealed that this observation is accurate. Kato et al. [1990] provide graphs of both the formic acid – acetic acid and formic acid – propionic acid systems at 100 kPa and it is plain to see that the former system exhibits a far narrower phase envelope. Moreover, Klekers and Scheller [1968] display their experimental data graphically for the formic acid – valeric acid system at 100 °C. From their plot, it is patently obvious that this system produces a far wider phase diagram than either of the VLE systems measured by Kato et al. [1990].

With regards to the VLE data reduction, the models provided a better fit to isobutyric acid – valeric acid data, in general. It is clear from the *x-y* and *P-x-y* (or *T-x-y*) plots shown in the sections that follow (Sections 9.4.3.2 and 9.4.3.3), that the models often struggled to accurately fit the experimental data in the dilute regions. This is, again, attributed to the unusual end effects that were discussed above. The inability of the models to match the experimental data in these areas is most apparent when the experimental and calculated activity coefficients are compared (Figures 9-34 to 9-40 and 9-63 to 9-69).

This deviation in the dilute regions resulted in the fairly large RMS values obtained for the $\delta\ln(\gamma_1/\gamma_2)$ residual during the direct test of thermodynamic consistency. Consequently, the direct test reflected rather poorly upon the experimental data. The end effects observed in the experimental measurements also had an effect on the figures obtained for the vapour composition deviations. Hence, the most logical conclusion to be drawn is that the models that have been used to date in order to fit the experimental data are incapable of accurately fitting carboxylic acid systems. Thus, the data are most likely consistent, despite the fact that the data (in particular, the propionic acid (1) – valeric acid (2) measurements) frequently performed badly in terms of both the point and direct tests. In future work, more complex associating models such as the SAFT EOS and the EOS developed specifically for carboxylic acids (refer to Section 3.4.2.2) will be used to model the data and should result in a considerable improvement in both the fit to the experimental measurements and the consistency tests.

The NRTL model was utilized frequently in regressing the experimental data, since the additional parameter incorporated into the model resulted in a good fit to the unusual "S"-shaped phase envelopes. This parameter is usually termed the *non-randomness parameter* and, as is suggested by the name, provides an indication of the deviation of the system from ideality. As has been mentioned previously, the systems studied in this work were practically ideal, except in the dilute regions. Nevertheless, in order to acquire a satisfactory fit to the experimental data, the non-randomness parameter, α, frequently lay outside of the conventional limits (-1 to 0.5). This was as a result of the model attempting to incorporate

the narrowing phenomenon discussed previously, as well as the "S"-shaped phase envelopes.

As was discussed in Section 9.4, the data reduction was conducted by minimizing the pressure (or temperature in the case of the isobars). Therefore, in the discussions of the individual systems that follow, the best fit model is judged based on the G^E model that exhibited the least deviation from the experimental pressures (or temperatures) i.e. the model with the lowest value for ΔP or ΔT was selected. In this project, eight different regressions were conducted for each phase diagram. The three liquid-phase activity coefficient models were utilized in conjunction with the Pitzer-Curl fugacity coefficient correlation and chemical theory, whilst the Peng-Robinson equation of state was used with two different mixing rules: the Wong-Sandler and the Twu-Coon. As it was difficult to qualitatively judge between these different methods, a best fit model is given for each case.

The consistency tests are discussed separately, in Section 9.7.

9.4.3.2 Propionic Acid (1) – Valeric Acid (2) System

The results of the VLE data reduction for the propionic acid (1) – valeric acid (2) system are given in Table 9-8, over the page. The best models are presented in the table that follows:

Table 9-7: Table showing the best fit models for the propionic acid (1) – valeric acid (2) system.

Procedure	P = 20 kPa	T = 393.15 K	T = 403.15 K	T = 413.15 K
Pitzer-Curl	NRTL	NRTL	NRTL	NRTL
Chemical Theory	-	Wilson	UNIQUAC	NRTL
Peng-Robinson	Twu-Coon	Twu-Coon	Twu-Coon	Wong-Sandler

Table 9-8: Model parameters and deviations from experimental values for the propionic acid (1) – valeric acid (2) system.

PC = Pitzer Curl correlation, CT = Chemical Theory correlation,
WS = Wong-Sandler mixing rule, TC = Twu-Coon mixing rule

Model	P = 20 kPa	T = 393.15 K	T = 403.15 K	T = 413.15 K
Wilson [PC]				
$\lambda_{12} - \lambda_{11}$ (J/mol)	-889.57	-889.40	-1188.84	-937.51
$\lambda_{12} - \lambda_{22}$ (J/mol)	505.57	889.40	1188.84	937.51
$\Delta P/\Delta T$ (kPa/K)	0.8922	0.1770	0.4253	0.5697
Δy	0.0084	0.0103	0.0213	0.0126
RMS $\delta\ln(\gamma_1/\gamma_2)$	0.1670	0.1479	0.1209	0.0936
NRTL [PC]				
$g_{12} - g_{11}$ (J/mol)	171.93	-987.34	-2345.99	-2211.22
$g_{12} - g_{22}$ (J/mol)	-609.88	-374.32	-447.19	-106.62
α	12.7569	-3.6246	-2.9816	-2.9366
$\Delta P/\Delta T$ (kPa/K)	0.2314	0.1713	0.2474	0.2037
Δy	0.0070	0.0099	0.0188	0.0142
RMS $\delta\ln(\gamma_1/\gamma_2)$	0.1681	0.1462	0.1196	0.0928
UNIQUAC [PC]				
$u_{12} - u_{11}$ (J/mol)	1814.50	-2083.02	1364.50	1209.50
$u_{12} - u_{22}$ (J/mol)	-1671.84	2775.64	-1364.50	-1209.50
$\Delta P/\Delta T$ (kPa/K)	0.8763	0.1926	0.4206	0.5606
Δy	0.0085	0.0108	0.0212	0.0126
RMS $\delta\ln(\gamma_1/\gamma_2)$	0.1963	0.1461	0.1195	0.0926
Wilson [CT]				
$\lambda_{12} - \lambda_{11}$ (J/mol)	-	-201.17	-4835.18	-599.62
$\lambda_{12} - \lambda_{22}$ (J/mol)	-	-1568.48	2742.46	-314.22
$\Delta P/\Delta T$ (kPa/K)	-	0.5967	1.0106	0.6915
Δy	-	0.0115	0.0103	0.0050
RMS $\delta\ln(\gamma_1/\gamma_2)$	-	0.1470	0.1210	0.0935

Model	P = 20 kPa	T = 393.15 K	T = 403.15 K	T = 413.15 K
NRTL [CT]				
$g_{12} - g_{11}$ (J/mol)	-	3647.03	-787.33	2333.50
$g_{12} - g_{22}$ (J/mol)	-	-2077.57	2615.85	-1373.33
α	-	0.2444	0.5874	0.3251
$\Delta P/\Delta T$ (kPa/K)	-	0.6750	1.0189	0.6906
Δy	-	0.0092	0.0107	0.0049
RMS $\delta\ln(\gamma_1/\gamma_2)$	-	0.1462	0.1198	0.0927
UNIQUAC [CT]				
$u_{12} - u_{11}$ (J/mol)	-	685.44	-1549.14	281.19
$u_{12} - u_{22}$ (J/mol)	-	-274.29	2665.02	-1.71
$\Delta P/\Delta T$ (kPa/K)	-	0.6789	1.0051	0.6983
Δy	-	0.0091	0.0113	0.0049
RMS $\delta\ln(\gamma_1/\gamma_2)$	-	0.1461	0.1205	0.0933
Peng-Robinson EOS [WS]				
$g_{12} - g_{11}$ (J/mol)	5419.46	-5974.65	3590.64	16265.6
$g_{12} - g_{22}$ (J/mol)	7752.86	8266.21	11522.9	7023.54
α	-1.3554	-0.7175	1.1125	0.3019
k_{ij}	-0.3175	-0.1348	-0.2701	-0.3277
$\Delta P/\Delta T$ (kPa/K)	0.6509	0.1856	0.4261	0.3026
Δy	0.0085	0.0103	0.0195	0.0136
Peng-Robinson EOS [TC]				
$g_{12} - g_{11}$ (J/mol)	-1163.39	6214.86	11499.7	239.35
$g_{12} - g_{22}$ (J/mol)	4480.62	3803.15	-2020.13	850.93
α	-0.4660	0.3053	-1.6567	-0.9505
k_{ij}	-0.0255	-0.0303	-0.0387	-0.0195
l_{ij}	0.0003	-0.0011	-0.0021	-0.0016
$\Delta P/\Delta T$ (kPa/K)	0.7314	0.1494	0.3217	0.6136
Δy	0.0101	0.0122	0.0180	0.0137

Although the models presented in Table 9-7 are the models that provided the best fit to the experimental data, there was frequently very little to choose between the various models. For instance, for the 393.15 K isotherm the difference between the Wilson equation and the NRTL equation (using the Pitzer-Curl correlation) amounts to 0.0057 kPa and 0.0004 of a mole fraction. These differences are so small that when the results are viewed graphically it is impossible to tell which model performed better.

The chemical theory of vapour imperfections had a marked effect on the vapour-phase compositions, with the deviation between the experimental and the calculated figures being considerably lessened in almost all cases. The differences between the three models used in conjunction with the chemical theory were, however, very slight with all the models fitting the data well. It is interesting to note, however, that the pressure deviations were usually far better when applying the Pitzer-Curl correlation. Thus, if it is imperative that the vapour-phase compositions be modelled accurately, then the chemical theory should be utilized. On the other hand, if the accuracy of the model pressures is crucial, then the Pitzer-Curl correlations would provide better results. The chemical theory, however, failed to converge to the correct temperature values for the 20 kPa isobar (although the vapour compositions agreed very well) and, hence, no parameters were reported in Tables 9-8 and 9-10.

In general, the results attained using the Peng-Robinson (Peng and Robinson [1976]) equation of state lay somewhere between the two combined methods discussed above. However, the equation of state modelled all of the experimental data well. The direct method modelling performed in this work was a precursor to more complicated associating equations of state, which are to be used in future work on the VLE data presented here. Thus, it is likely that the figures obtained using the direct method will become even better; possibly surpassing the combined method results.

Comparing the two mixing rules, it is clear that in most cases the Twu-Coon (Twu and Coon [1996]) mixing rules provided a better-quality fit to the experimental data. The 413.15 K isotherm was the only exception (Figures 9-32 and 9-33), and the Wong-Sandler (Wong and Sandler [1992]) mixing rules performed extremely well in this instance. The

fact that the Twu-Coon mixing rule proved to be superior to that of Wong-Sandler was anticipated, since the Twu-Coon rule has an additional parameter that may be varied during the optimization process.

The direct method was initially conducted using the alpha function proposed in the original paper (Peng and Robinson [1976]). However, the results were significantly improved when the alpha function of Twu et al. [1991] was employed instead. This is demonstrated by considering the propionic acid (1) – valeric acid (2) system at 393.15 K. Using the original function based on the acentric factors, the average pressure and vapour deviations are 0.4699 kPa and 0.0106 respectively. The alpha function proposed by Twu and co-workers yielded values of 0.1870 kPa and 0.0103 respectively. The improvement is self-evident, particularly in the case of the pressure deviations. According to Twu et al. [1991], the function based on the acentric factor works well for non-polar hydrocarbons. They go on to say that the function is generally not suitable for polar compounds.

The liquid-phase activity coefficients were calculated for each model and are compared to the experimental values (refer to Section 9.3) in Figures 9-34 to 9-40. The activity coefficients were not determined during the direct method regressions, since this method is based on fugacity coefficients in both the vapour and liquid phases. Thus, there are no model activity coefficients to which the experimental values may be compared. For the same reason, the direct test could not be performed for the Peng-Robinson EOS data reductions (the direct test is based on the deviations between the experimental and the model activity coefficients). However, the consistency was checked via the point test.

For the models that did permit calculation of the liquid-phase activity coefficients, the results are all fairly alike (as may be seen by the very similar RMS $\delta\ln(\gamma_1/\gamma_2)$ values reported in Tables 9-8 and 9-10). It is clear from the graphs shown below (Figures 9-12 through 9-40) that the dilute regions once again presented difficulties, with the models proving incapable of adequately matching the experimental data in these sections of the curves. As was mentioned in Section 9.4.3.1, this automatically meant that the results in terms of the direct test were rather poor.

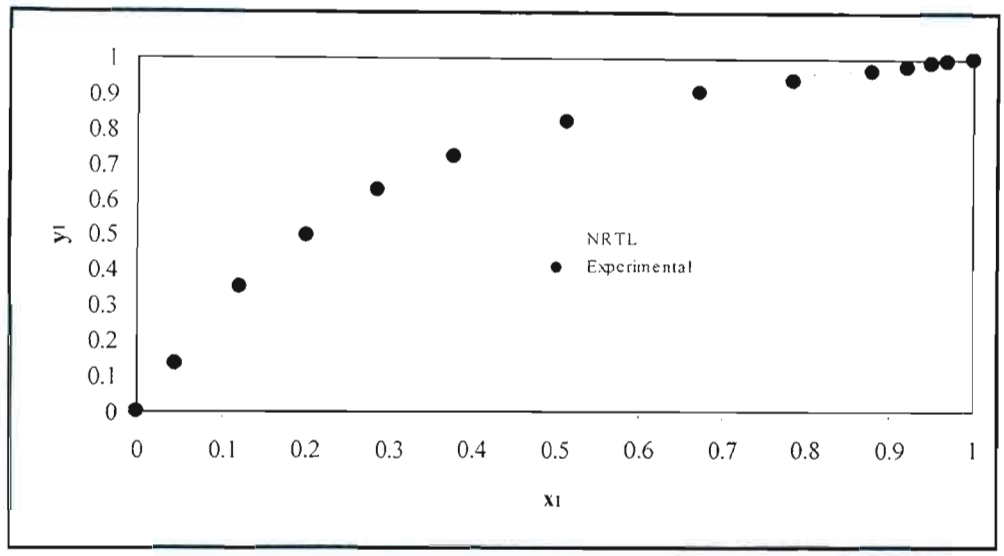

Figure 9-12: NRTL model fitted to x-y data using the Pitzer-Curl correlation for the propionic acid (1) – valeric acid (2) system at 20 kPa.

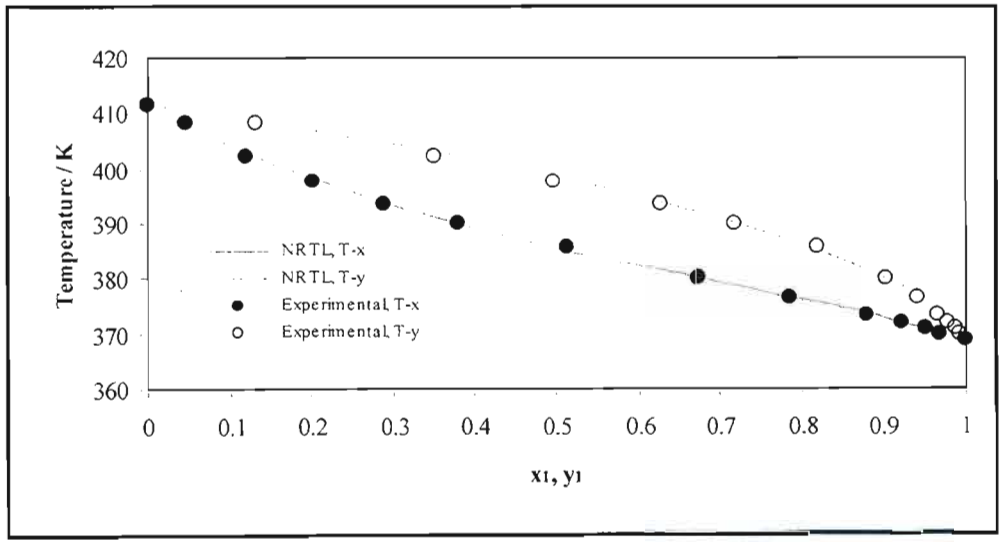

Figure 9-13: NRTL model fitted to T-x-y data using the Pitzer-Curl correlation for the propionic acid (1) – valeric acid (2) system at 20 kPa.

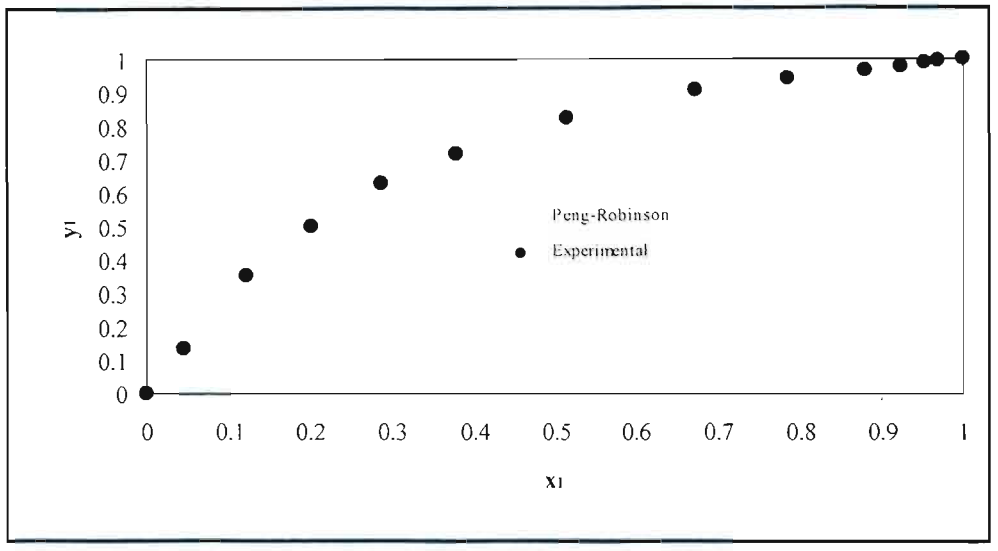

Figure 9-14: Peng-Robinson EOS fitted to x-y data using the Twu-Coon mixing rule for the propionic acid (1) – valeric acid (2) system at 20 kPa.

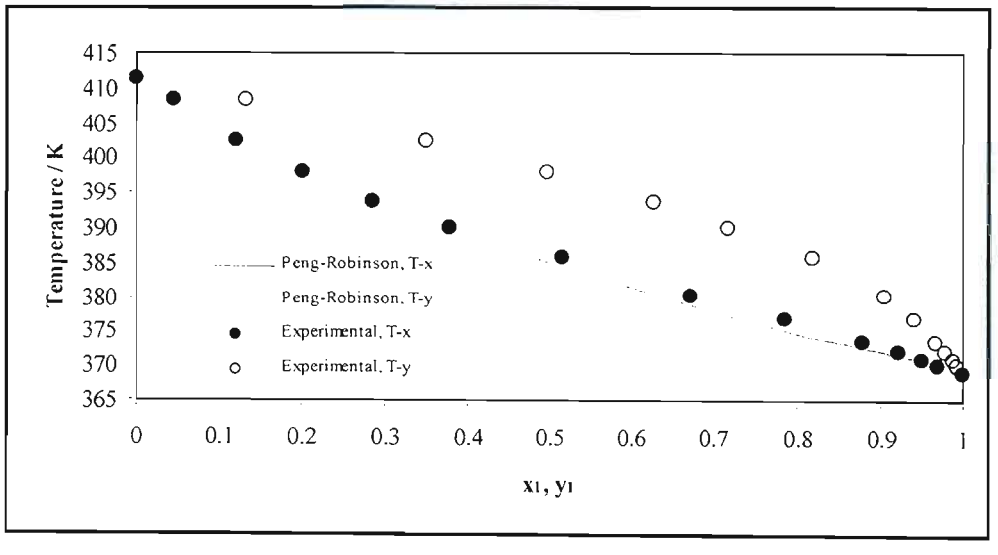

Figure 9-15: Peng-Robinson EOS fitted to T-x-y data using the Twu-Coon mixing rule for the propionic acid (1) – valeric acid (2) system at 20 kPa.

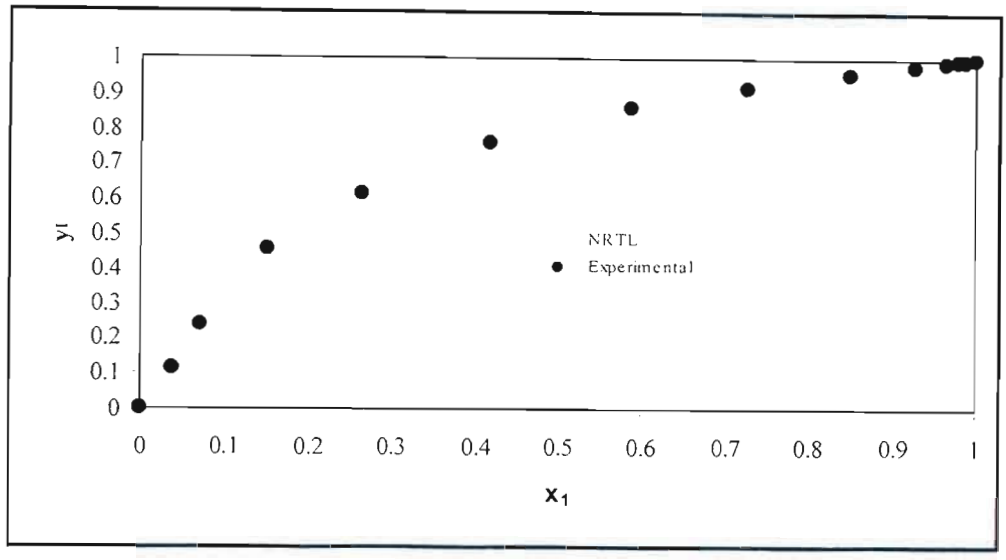

Figure 9-16: NRTL model fitted to x-y data using the Pitzer-Curl correlation for the propionic acid (1) – valeric acid (2) system at 393.15 K.

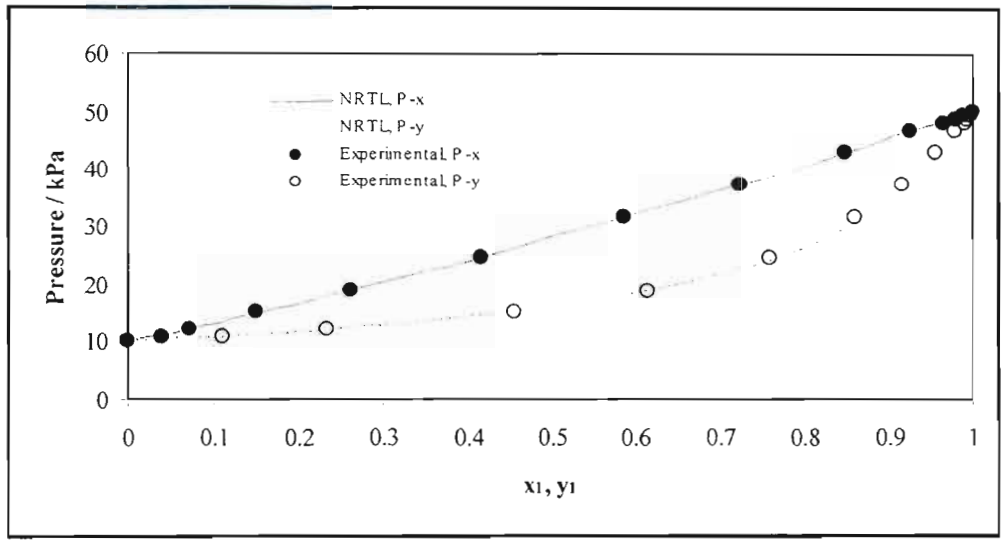

Figure 9-17: NRTL model fitted to P-x-y data using the Pitzer-Curl correlation for the propionic acid (1) – valeric acid (2) system at 393.15 K.

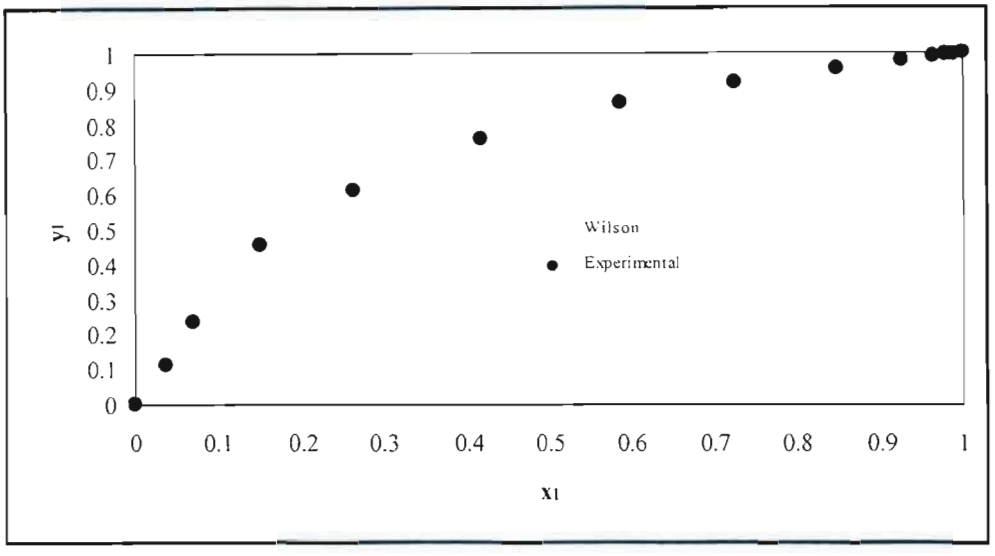

Figure 9-18: Wilson model fitted to x-y data using the chemical theory of vapour phase imperfections for the propionic acid (1) – valeric acid (2) system at 393.15 K.

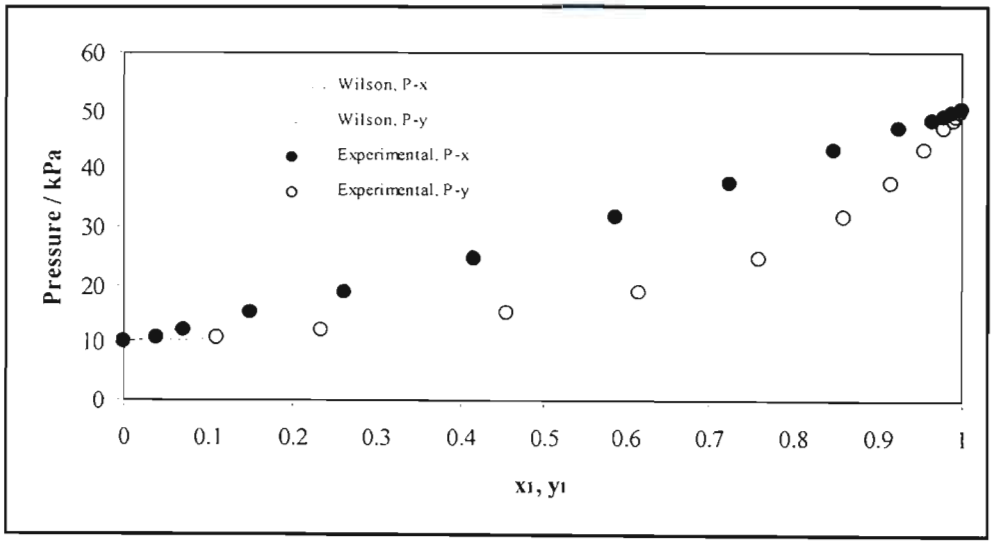

Figure 9-19: Wilson model fitted to P-x-y data using the chemical theory of vapour phase imperfections for the propionic acid (1) – valeric acid (2) system at 393.15 K.

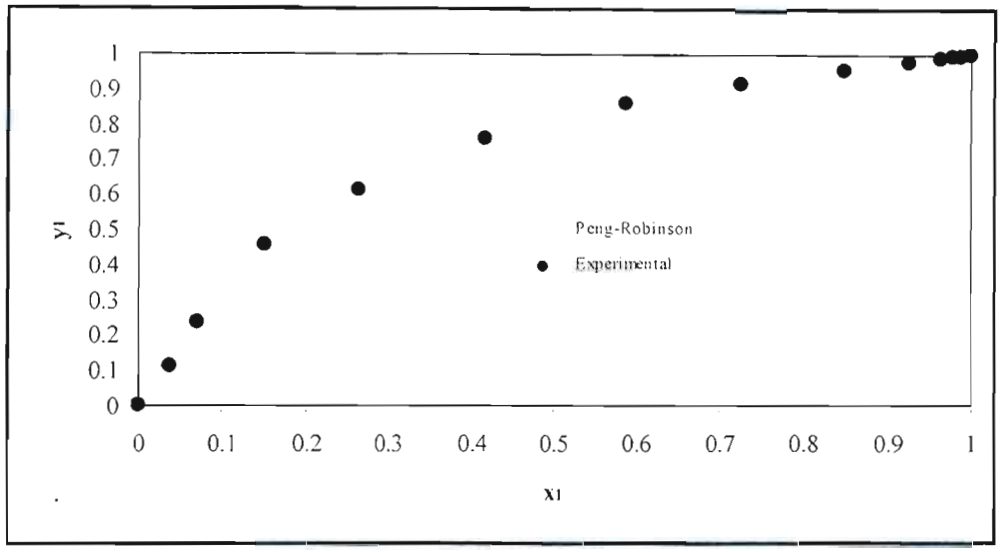

Figure 9-20: Peng-Robinson EOS fitted to x-y data using the Twu-Coon mixing rule for the propionic acid (1) – valeric acid (2) system at 393.15 K.

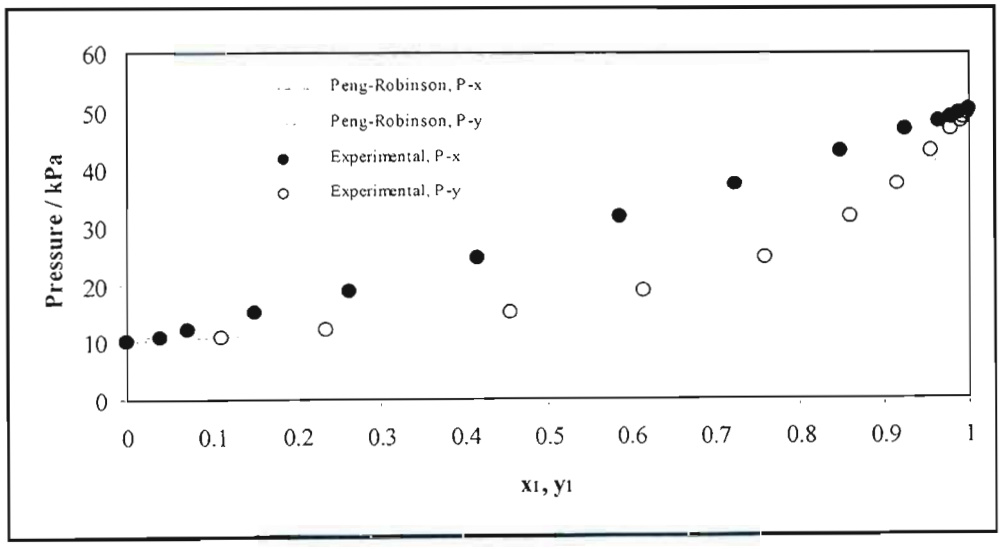

Figure 9-21: Peng-Robinson EOS fitted to P-x-y data using the Twu-Coon mixing rule for the propionic acid (1) – valeric acid (2) system at 393.15 K.

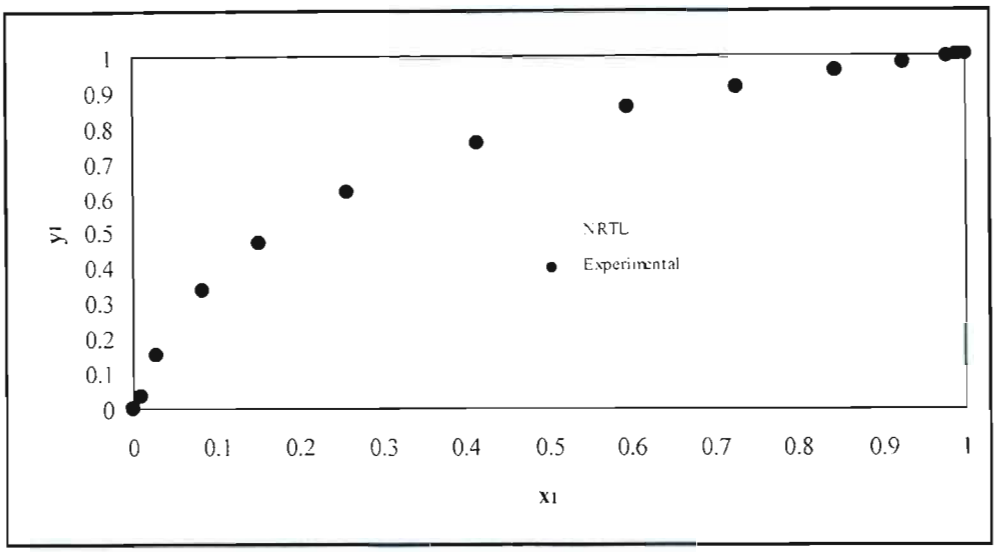

Figure 9-22: NRTL model fitted to x-y data using the Pitzer-Curl correlation for the propionic acid (1) – valeric acid (2) system at 403.15 K.

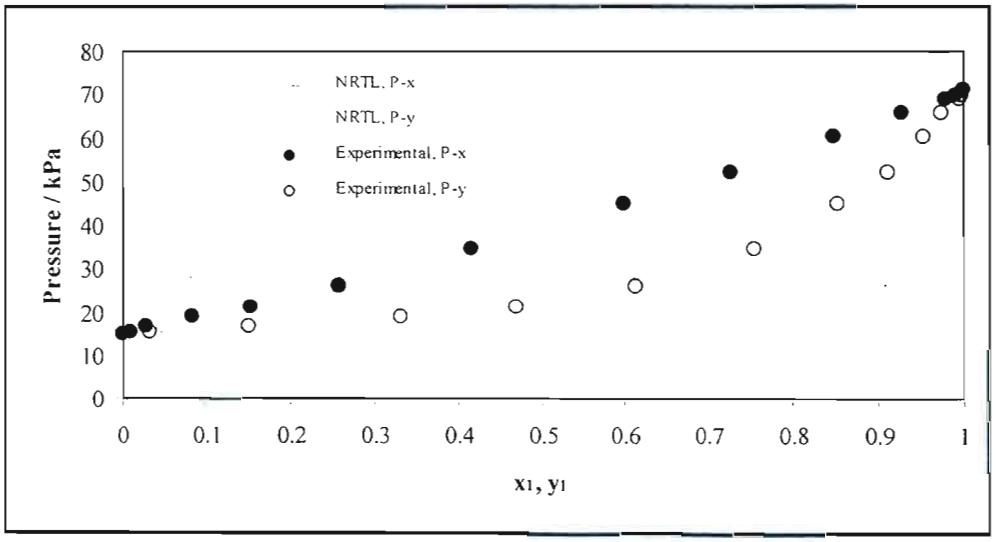

Figure 9-23: NRTL model fitted to P-x-y data using the Pitzer-Curl correlation for the propionic acid (1) – valeric acid (2) system at 403.15 K.

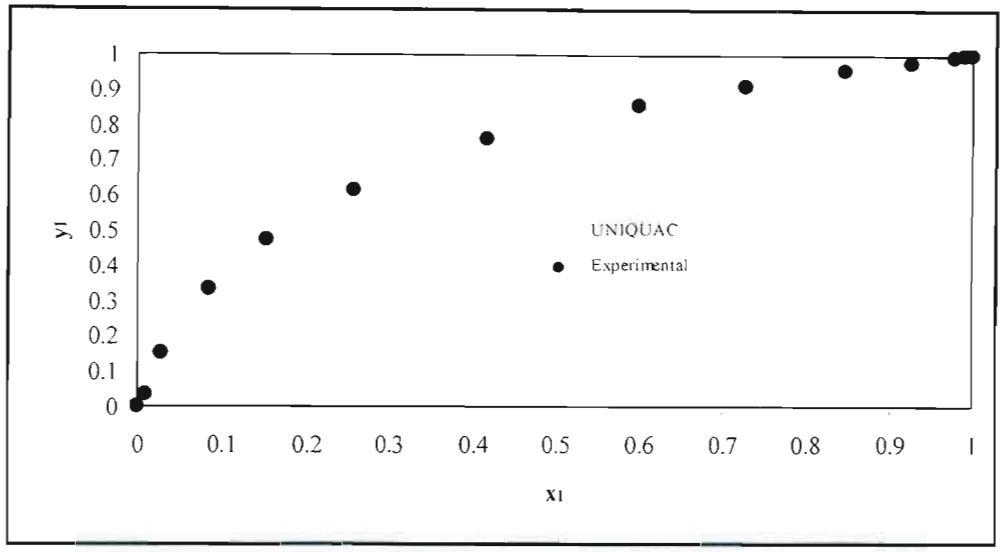

Figure 9-24: UNIQUAC model fitted to x-y data using the chemical theory of vapour phase imperfections for the propionic acid (1) – valeric acid (2) system at 403.15 K.

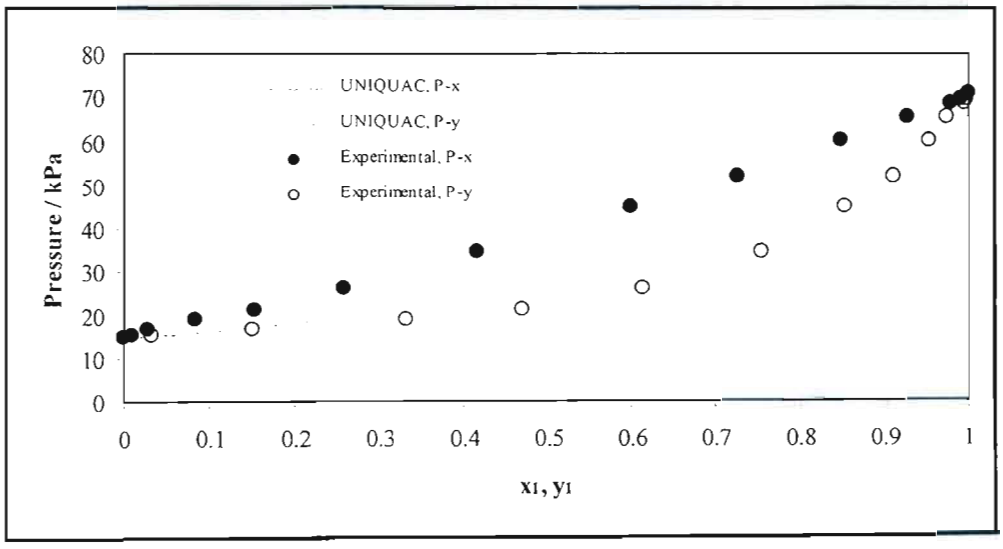

Figure 9-25: UNIQUAC model fitted to P-x-y data using the chemical theory of vapour phase imperfections for the propionic acid (1) – valeric acid (2) system at 403.15 K.

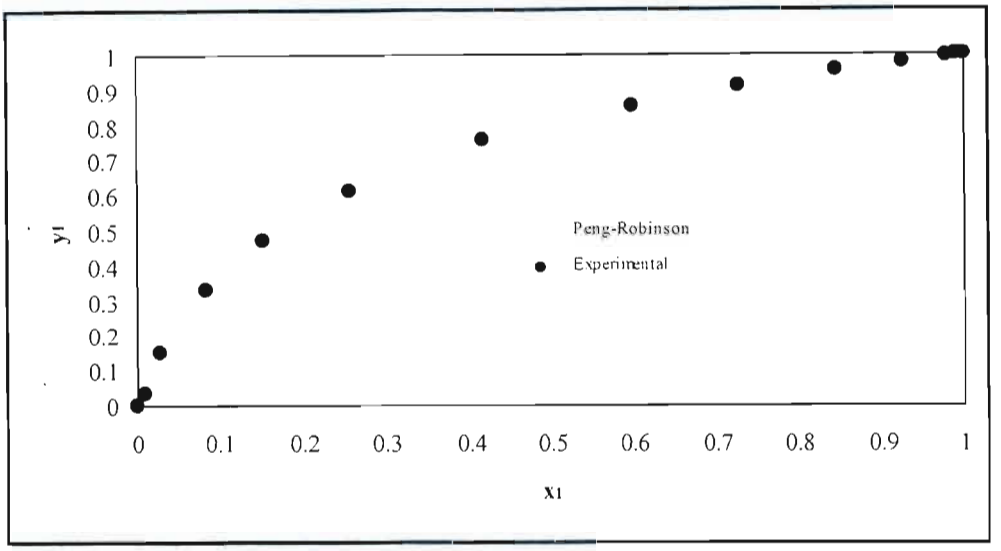

Figure 9-26: Peng-Robinson EOS fitted to x-y data using the Twu-Coon mixing rule for the propionic acid (1) – valeric acid (2) system at 403.15 K.

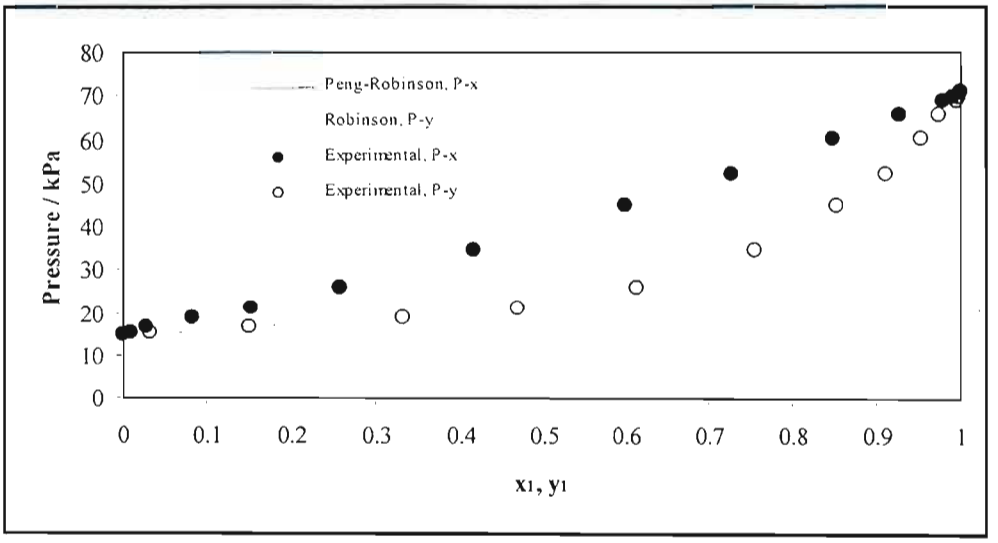

Figure 9-27: Peng-Robinson EOS fitted to P-x-y data using the Twu-Coon mixing rule for the propionic acid (1) – valeric acid (2) system at 403.15 K.

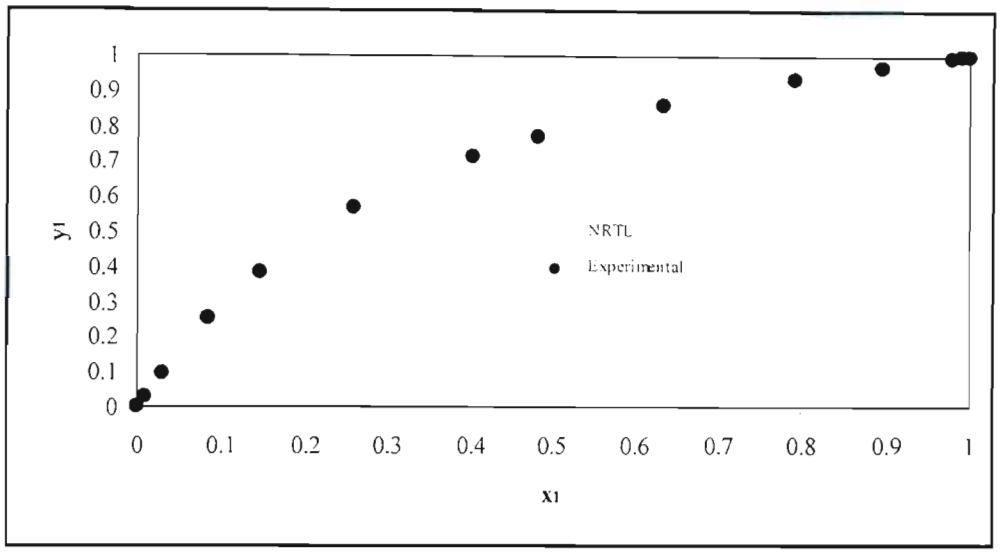

Figure 9-28: NRTL model fitted to x-y data using the Pitzer-Curl correlation for the propionic acid (1) – valeric acid (2) system at 413.15 K.

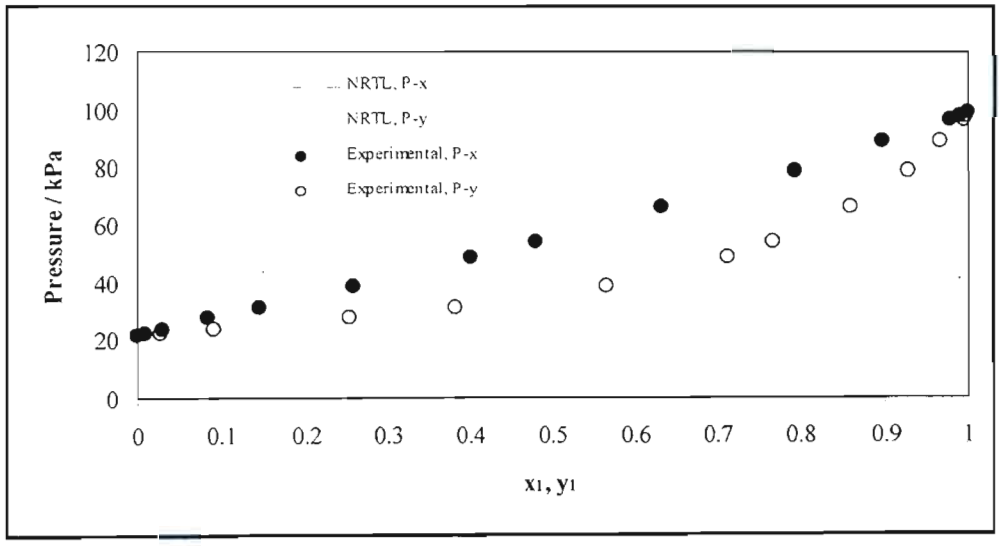

Figure 9-29: NRTL model fitted to P-x-y data using the Pitzer-Curl correlation for the propionic acid (1) – valeric acid (2) system at 413.15 K.

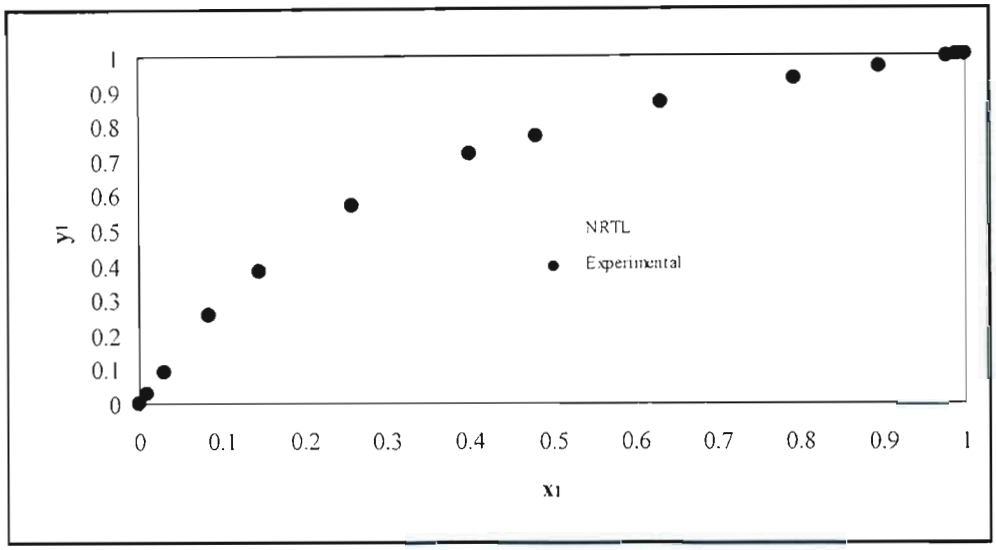

Figure 9-30: NRTL model fitted to x-y data using the chemical theory of vapour phase imperfections for the propionic acid (1) – valeric acid (2) system at 413.15 K.

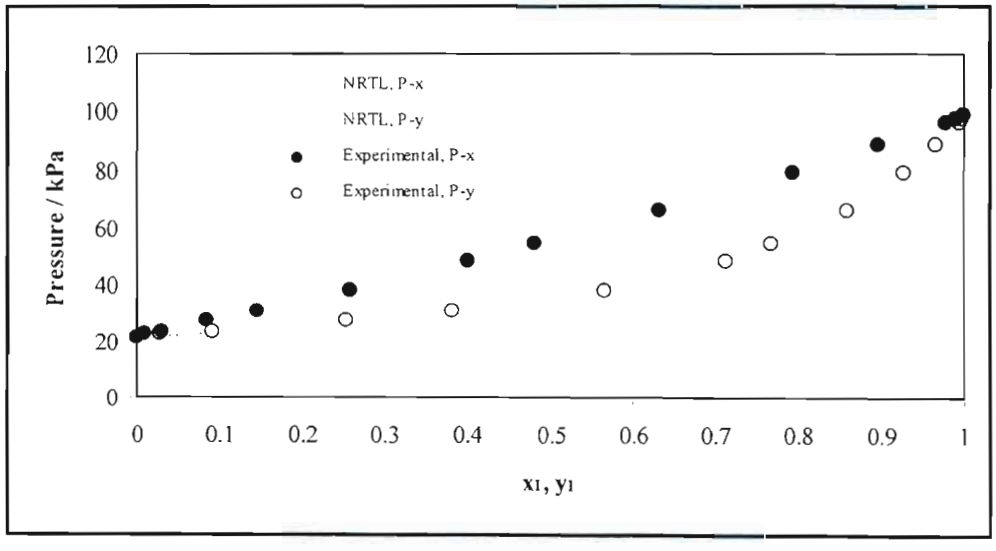

Figure 9-31: NRTL model fitted to P-x-y data using the chemical theory of vapour phase imperfections for the propionic acid (1) – valeric acid (2) system at 413.15 K.

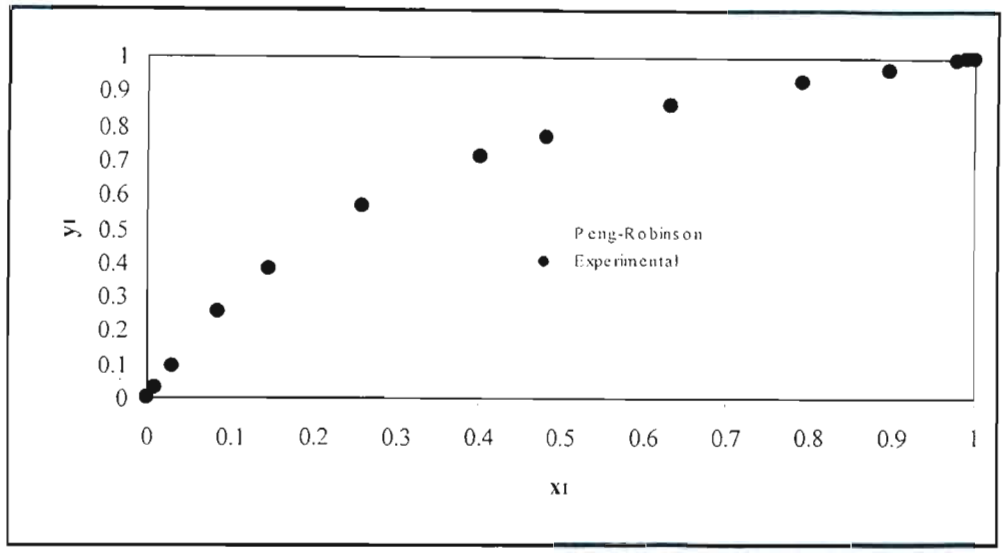

Figure 9-32: Peng-Robinson EOS fitted to x-y data using the Wong-Sandler mixing rule for the propionic acid (1) – valeric acid (2) system at 413.15 K.

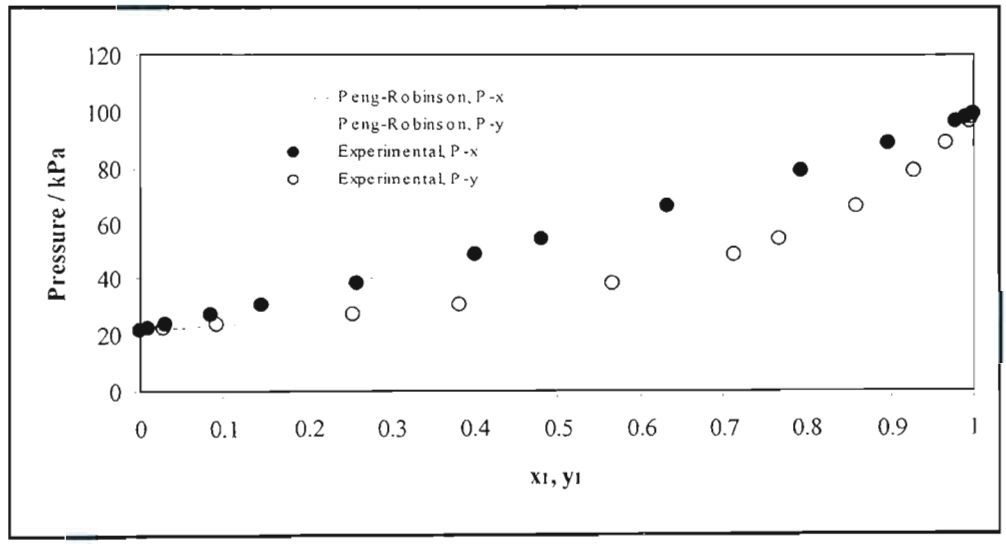

Figure 9-33: Peng-Robinson EOS fitted to P-x-y data using the Wong-Sandler mixing rule for the propionic acid (1) – valeric acid (2) system at 413.15 K.

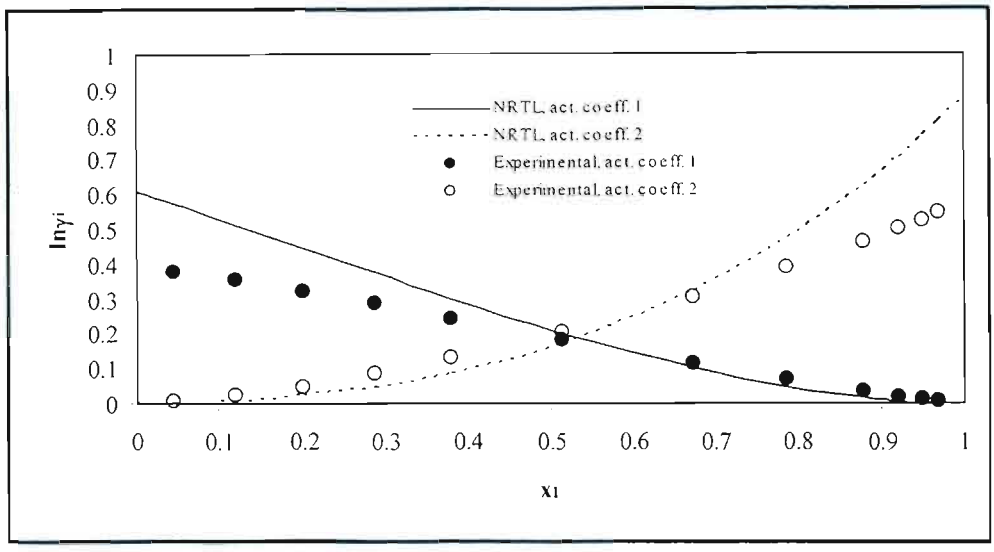

Figure 9-34: Comparison between the experimentally determined liquid-phase activity coefficients and those calculated from the NRTL model with the Pitzer-Curl correlation for the propionic acid (1) – valeric acid (2) system at 20 kPa.

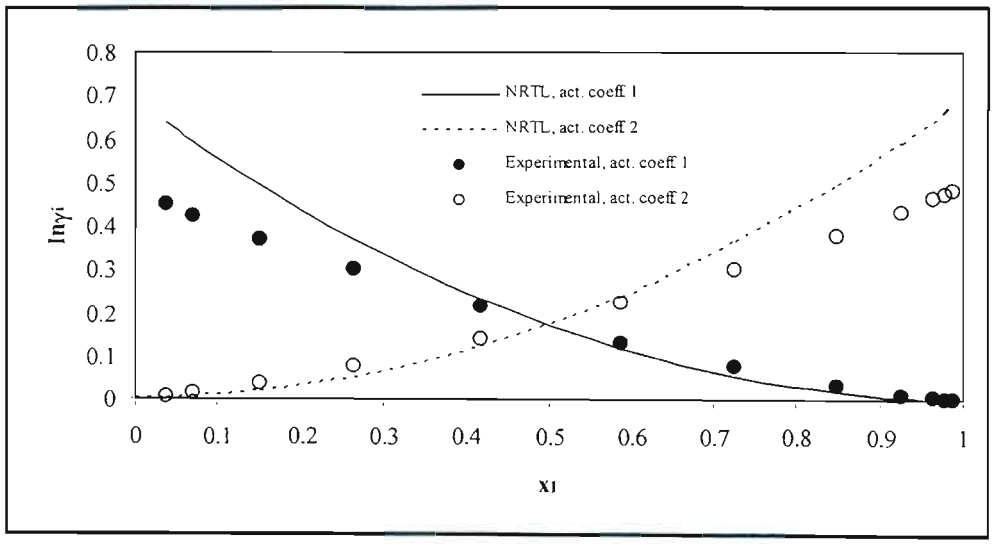

Figure 9-35: Comparison between the experimentally determined liquid-phase activity coefficients and those calculated from the NRTL model with the Pitzer-Curl correlation for the propionic acid (1) – valeric acid (2) system at 393.15 K.

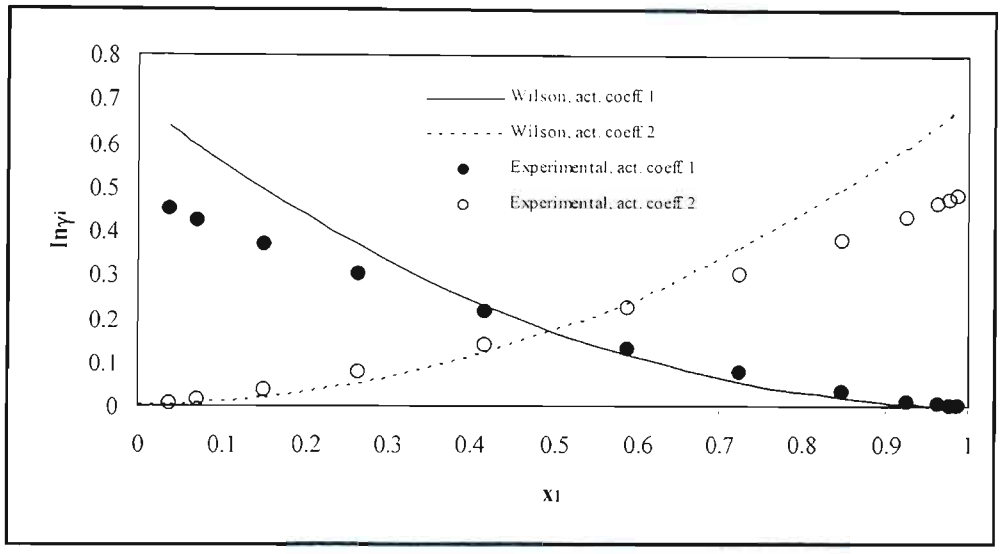

Figure 9-36: Comparison between the experimentally determined liquid-phase activity coefficients and those calculated from the Wilson model with chemical theory for the propionic acid (1) – valeric acid (2) system at 393.15 K.

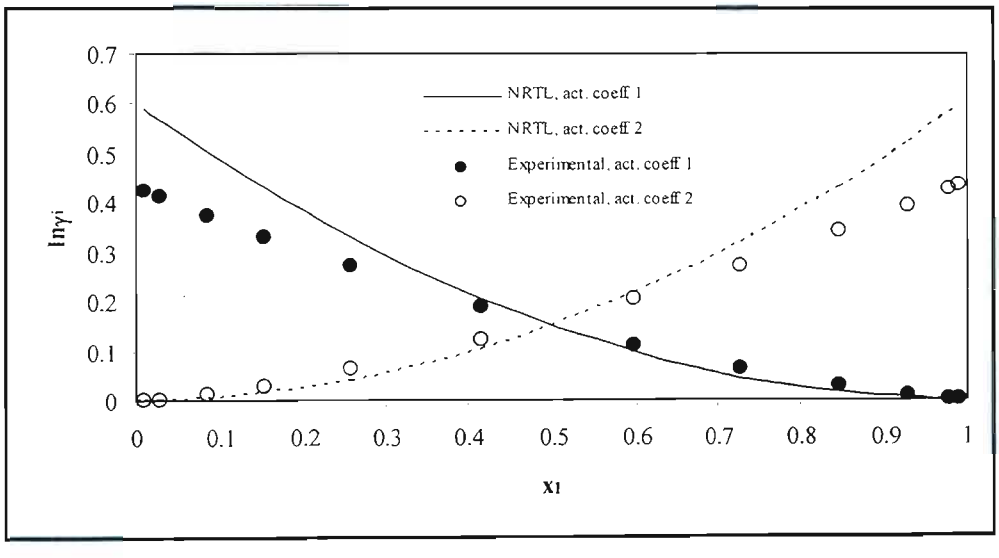

Figure 9-37: Comparison between the experimentally determined liquid-phase activity coefficients and those calculated from the NRTL model with the Pitzer-Curl correlation for the propionic acid (1) – valeric acid (2) system at 403.15 K.

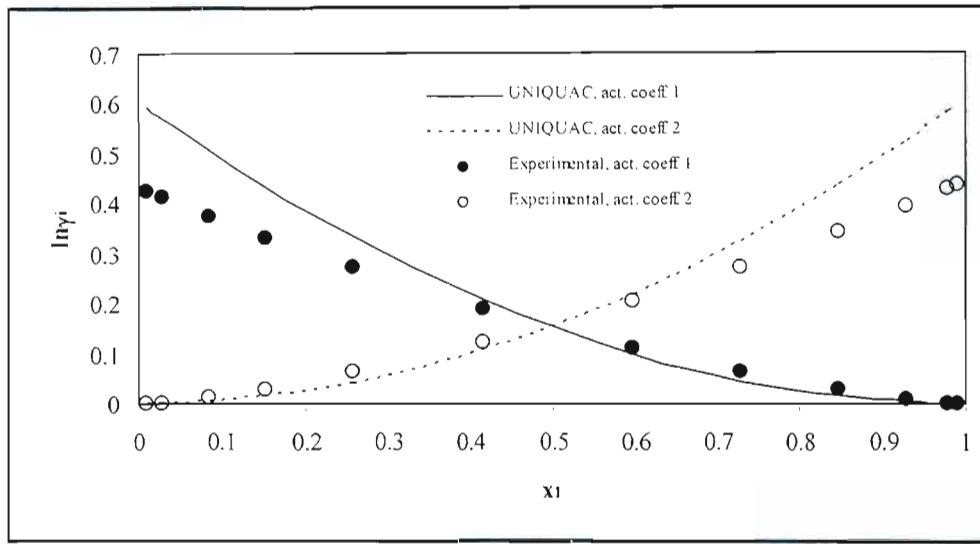

Figure 9-38: Comparison between the experimentally determined liquid-phase activity coefficients and those calculated from the UNIQUAC model with chemical theory for the propionic acid (1) – valeric acid (2) system at 403.15 K.

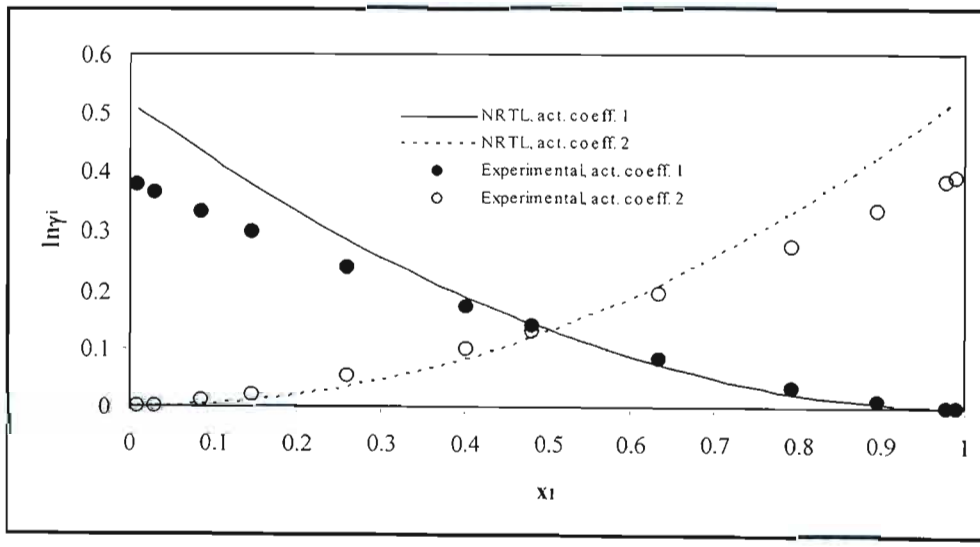

Figure 9-39: Comparison between the experimentally determined liquid-phase activity coefficients and those calculated from the NRTL model with the Pitzer-Curl correlation for the propionic acid (1) – valeric acid (2) system at 413.15 K.

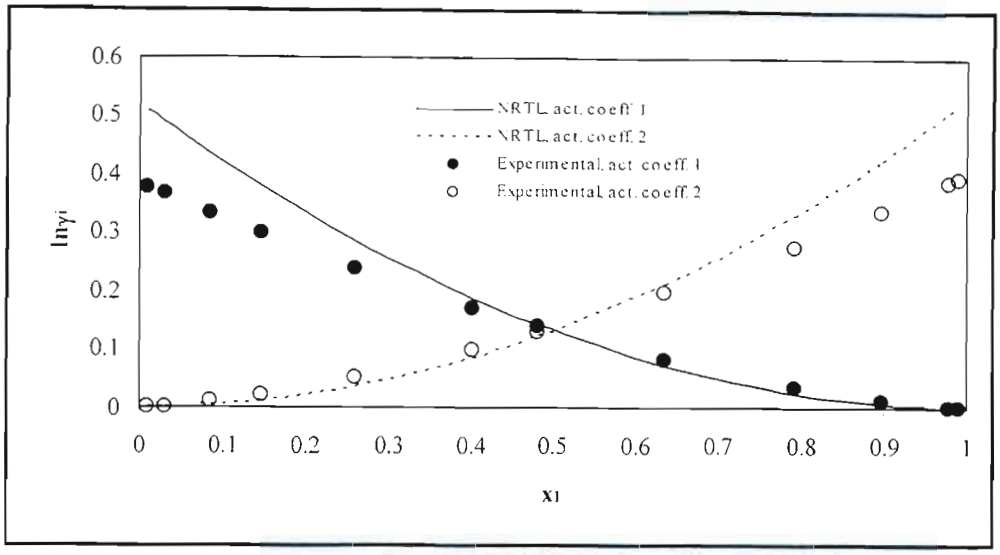

Figure 9-40: Comparison between the experimentally determined liquid-phase activity coefficients and those calculated from the NRTL model with chemical theory for the propionic acid (1) – valeric acid (2) system at 413.15 K.

9.4.3.3 Isobutyric Acid (1) – Valeric Acid (2) System

The parameters obtained through regression of the experimental VLE data for the isobutyric acid (1) – valeric acid (2) system are presented on the next page in Table 9-9. The models that provided the most appropriate fit to the measured data are laid out in the following table:

Table 9-9: Table showing the best fit models for the isobutyric acid (1) – valeric acid (2) system.

Procedure	P = 20 kPa	T = 393.15 K	T = 403.15 K	T = 413.15 K
Pitzer-Curl	NRTL	NRTL	NRTL	UNIQUAC
Chemical Theory	-	Wilson	UNIQUAC	Wilson
Peng-Robinson	Twu-Coon	Wong-Sandler	Twu-Coon	Wong-Sandler

All of the models fitted the isobutyric acid – valeric acid system well and, in general, the models performed better for this system than they did for the propionic acid – valeric acid system. This is self-evident when the deviations from the experimental data are considered. For the isobutyric acid system, it was rare for an isobar or isotherm to have a Δy greater than 0.01; whilst for the propionic acid system exactly the opposite trend was observed.

Again, there was often little to choose between the various models. Taking the 393.15 K isotherm (with the Pitzer-Curl correlation) as an example once more; the pressure deviations for all three models lay within 0.0027 kPa of each other and, likewise, the vapour compositions differed by a meagre 0.0006 mole fraction.

As was found for the propionic acid system, use of the chemical theory in accounting for the vapour phase imperfections resulted in a marked improvement in the vapour phase deviations. Again, however, the pressure deviations (ΔP) increased, although not considerably. The isobaric data again proved problematic when attempting to regress the experimental data using chemical theory for the vapour phase correction. As mentioned previously (in Section 9.4.3.2), the temperatures did not converge to the correct values and, thus, no parameters were acquired.

The results obtained from the Peng-Robinson EOS were good. In all cases the direct method was comparable to the combined method (which is usually considered superior for low pressure VLE) and, in some cases, even surpassed certain of the activity coefficient models (refer to Table 9-10). Comparing the two mixing rules, it was discovered that there was very little difference between them. This is evident in Table 9-9, where the best fit model designation was split evenly between the Wong-Sandler and Twu-Coon mixing rules. Furthermore, if the deviations between the calculated values and the experimental values are considered (see Table 9-10 above), it becomes clear that if one mixing rule produced a lower pressure deviation for a certain isotherm, then the other would generate a lower vapour mole fraction deviation. Evidently, for the isobutyric acid – valeric acid system the two mixing rules are very much on a par.

Table 9-10: Model parameters and deviations from experimental values for the isobutyric acid (1) – valeric acid (2) system.

PC = Pitzer Curl correlation, CT = Chemical Theory correlation,
WS = Wong-Sandler mixing rule, TC = Twu-Coon mixing rule

Model	P = 20 kPa	T = 393.15 K	T = 403.15 K	T = 413.15 K
Wilson [PC]				
$\lambda_{12} - \lambda_{11}$ (J/mol)	-2363.19	997.10	-1701.70	125.97
$\lambda_{12} - \lambda_{22}$ (J/mol)	2528.87	-1571.91	1701.70	-773.48
$\Delta P / \Delta T$ (kPa/K)	0.4512	0.1191	0.0909	0.2904
Δy	0.0071	0.0062	0.0074	0.0119
RMS $\delta \ln(\gamma_1/\gamma_2)$	0.1674	0.1553	0.1259	0.0955
NRTL [PC]				
$g_{12} - g_{11}$ (J/mol)	524.29	-1182.07	-3998.95	1649.03
$g_{12} - g_{22}$ (J/mol)	-516.18	629.88	2571.31	-2287.86
α	17.4758	0.46443	-0.2165	0.0213
$\Delta P / \Delta T$ (kPa/K)	0.1151	0.1189	0.0774	0.2901
Δy	0.0053	0.0062	0.0076	0.0119
RMS $\delta \ln(\gamma_1/\gamma_2)$	0.1651	0.1532	0.1245	0.0947
UNIQUAC [PC]				
$u_{12} - u_{11}$ (J/mol)	1712.76	-1090.84	1171.92	-572.77
$u_{12} - u_{22}$ (J/mol)	-1613.86	1090.84	-1171.92	429.13
$\Delta P / \Delta T$ (kPa/K)	0.4758	0.1216	0.0966	0.2898
Δy	0.0073	0.0056	0.0073	0.0119
RMS $\delta \ln(\gamma_1/\gamma_2)$	0.1640	0.1534	0.1246	0.0948
Wilson [CT]				
$\lambda_{12} - \lambda_{11}$ (J/mol)	-	1161.10	1054.60	1753.88
$\lambda_{12} - \lambda_{22}$ (J/mol)	-	-3611.68	-2956.15	-4872.68
$\Delta P / \Delta T$ (kPa/K)	-	0.2613	0.3366	0.3520
Δy	-	0.0059	0.0041	0.0059
RMS $\delta \ln(\gamma_1/\gamma_2)$	-	0.1553	0.1263	0.0959

Model	P = 20 kPa	T = 393.15 K	T = 403.15 K	T = 413.15 K
NRTL [CT]				
$g_{12} - g_{11}$ (J/mol)	-	3835.06	2541.33	2471.56
$g_{12} - g_{22}$ (J/mol)	-	249.54	179.01	-851.91
α	-	2.6827	4.0131	1.6322
$\Delta P/\Delta T$ (kPa/K)	-	0.3112	0.3559	0.3645
Δy	-	0.0032	0.0023	0.0065
RMS $\delta\ln(\gamma_1/\gamma_2)$	-	0.1532	0.1248	0.0951
UNIQUAC [CT]				
$u_{12} - u_{11}$ (J/mol)	-	2393.56	2092.96	3183.10
$u_{12} - u_{22}$ (J/mol)	-	-1528.32	-1415.13	-2034.18
$\Delta P/\Delta T$ (kPa/K)	-	0.2625	0.3355	0.3613
Δy	-	0.0059	0.0041	0.0063
RMS $\delta\ln(\gamma_1/\gamma_2)$	-	0.1533	0.1248	0.0951
Peng-Robinson EOS [WS]				
$g_{12} - g_{11}$ (J/mol)	9382.65	-3119.49	1335.32	-8847.77
$g_{12} - g_{22}$ (J/mol)	9259.88	-954.44	2904.26	975.79
α	-2.0298	-0.1400	-1.4809	0.2142
k_{ij}	-0.4753	-0.0472	-0.1690	-0.0092
$\Delta P/\Delta T$ (kPa/K)	0.4533	0.1199	0.0959	0.2941
Δy	0.0070	0.0065	0.0070	0.0120
Peng-Robinson EOS [TC]				
$g_{12} - g_{11}$ (J/mol)	4535.71	702.87	14160.6	1064.99
$g_{12} - g_{22}$ (J/mol)	10549.8	1064.72	11788.0	1105.97
α	3.9778	0.5852	-0.7488	-0.5805
k_{ij}	-0.0322	-0.0154	-0.0592	-0.0181
l_{ij}	-0.0023	0.0002	-0.0002	0.0010
$\Delta P/\Delta T$ (kPa/K)	0.4432	0.1247	0.0754	0.3006
Δy	0.0070	0.0063	0.0073	0.0115

As for the propionic acid – valeric acid system, the activity coefficients were calculated (where possible) and compared to the values determined directly from the experimental data (see Figures 9-63 to 9-69). Again, it is clear that the models could not effectively fit the experimental data in the dilute regions, leading to exaggerated RMS $\delta\ln(\gamma_1/\gamma_2)$ values.

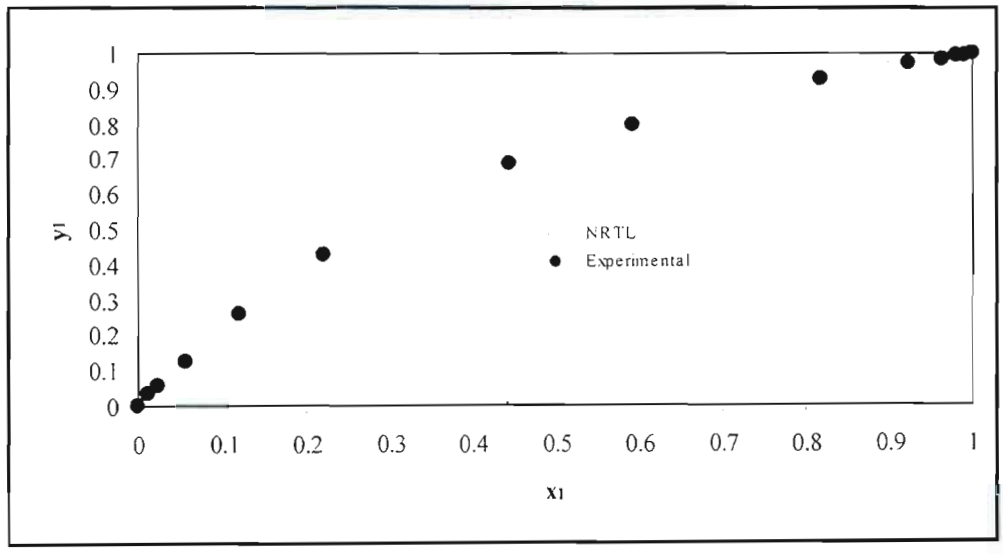

Figure 9-41: NRTL model fitted to x-y data using the Pitzer-Curl correlation for the isobutyric acid (1) – valeric acid (2) system at 20 kPa.

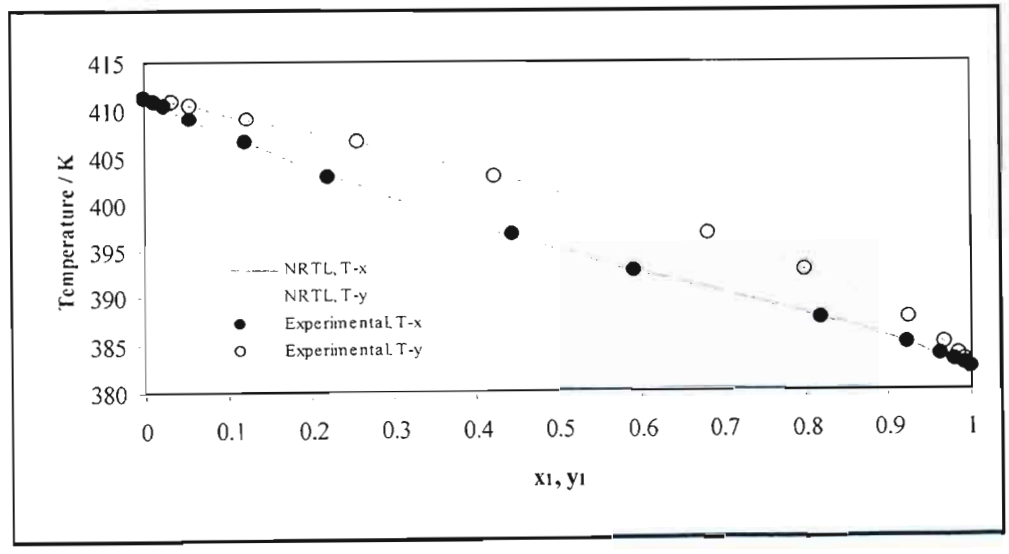

Figure 9-42: NRTL model fitted to T-x-y data using the Pitzer-Curl correlation for the isobutyric acid (1) – valeric acid (2) system at 20 kPa.

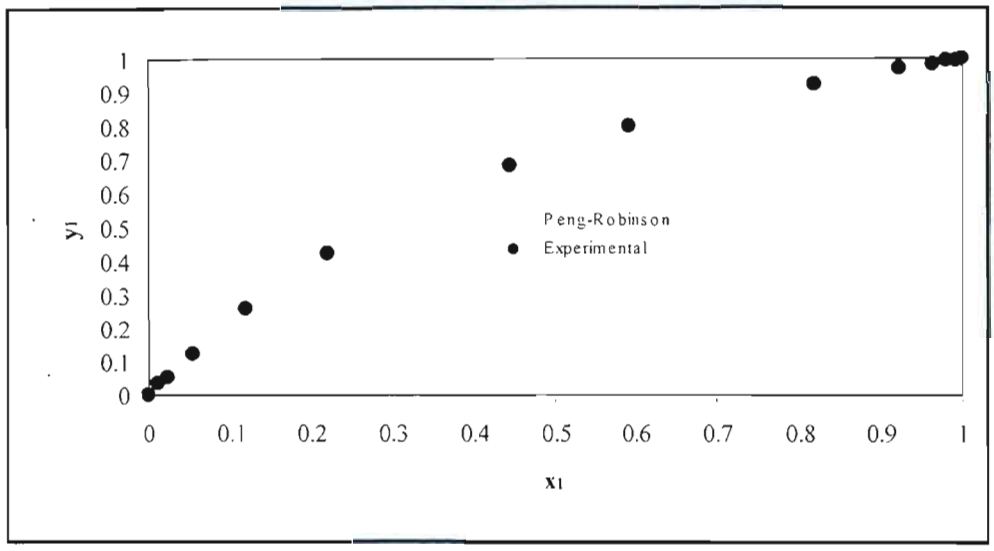

Figure 9-43: Peng-Robinson EOS fitted to x-y data using the Twu-Coon mixing rule for the isobutyric acid (1) – valeric acid (2) system at 20 kPa.

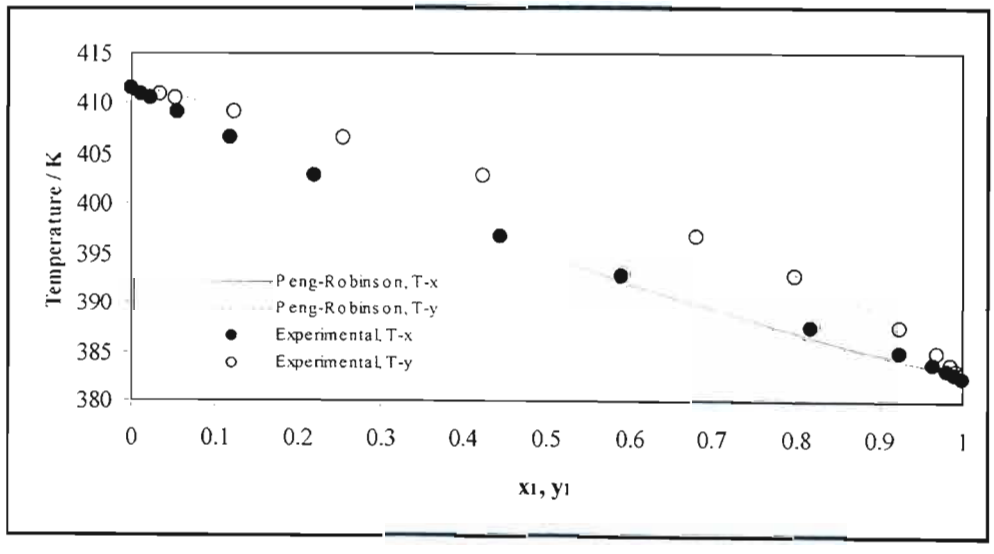

Figure 9-44: Peng-Robinson EOS fitted to T-x-y data using the Twu-Coon mixing rule for the isobutyric acid (1) – valeric acid (2) system at 20 kPa.

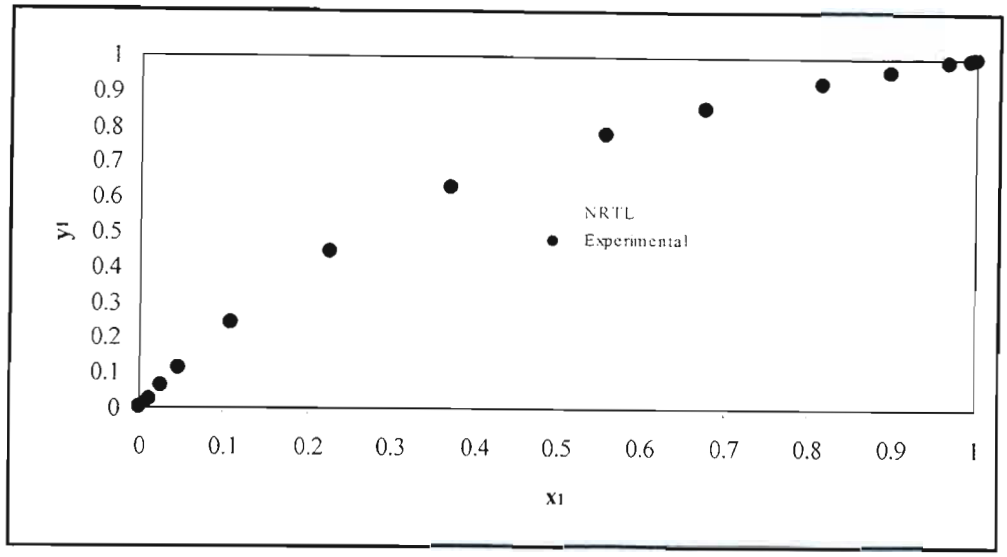

Figure 9-45: NRTL model fitted to x-y data using the Pitzer-Curl correlation for the isobutyric acid (1) – valeric acid (2) system at 393.15 K.

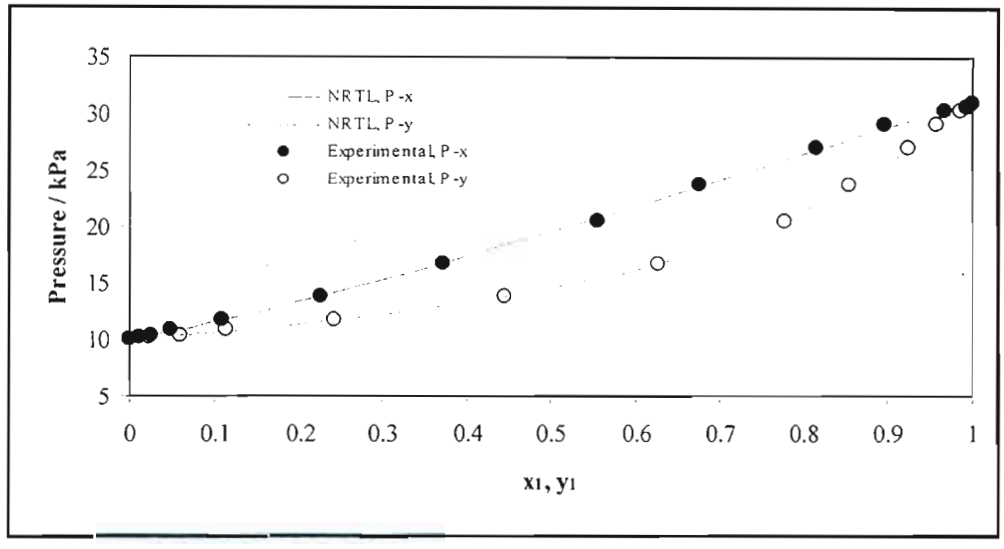

Figure 9-46: NRTL model fitted to P-x-y data using the Pitzer-Curl correlation for the isobutyric acid (1) – valeric acid (2) system at 393.15 K.

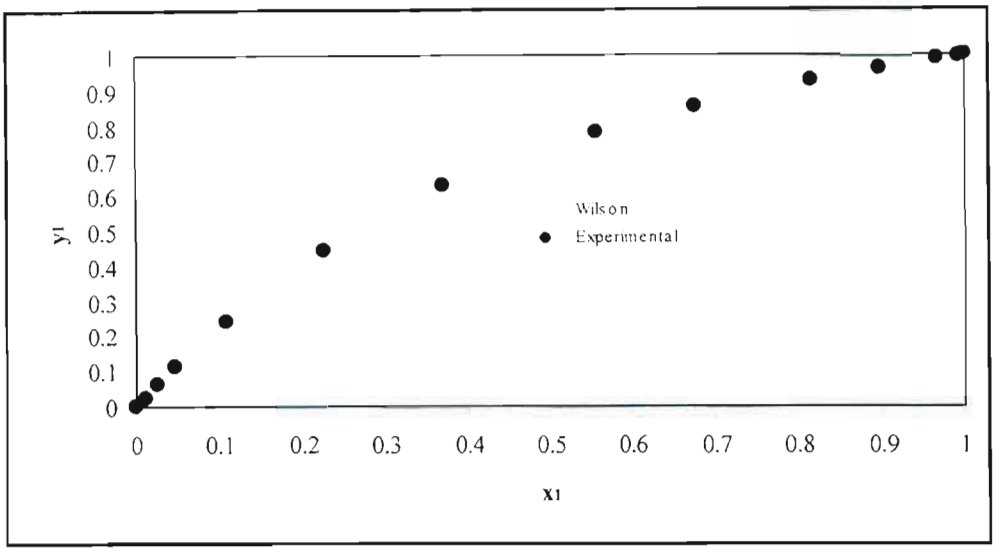

Figure 9-47: Wilson model fitted to x-y data using the chemical theory of vapour phase imperfections for the isobutyric acid (1) – valeric acid (2) system at 393.15 K.

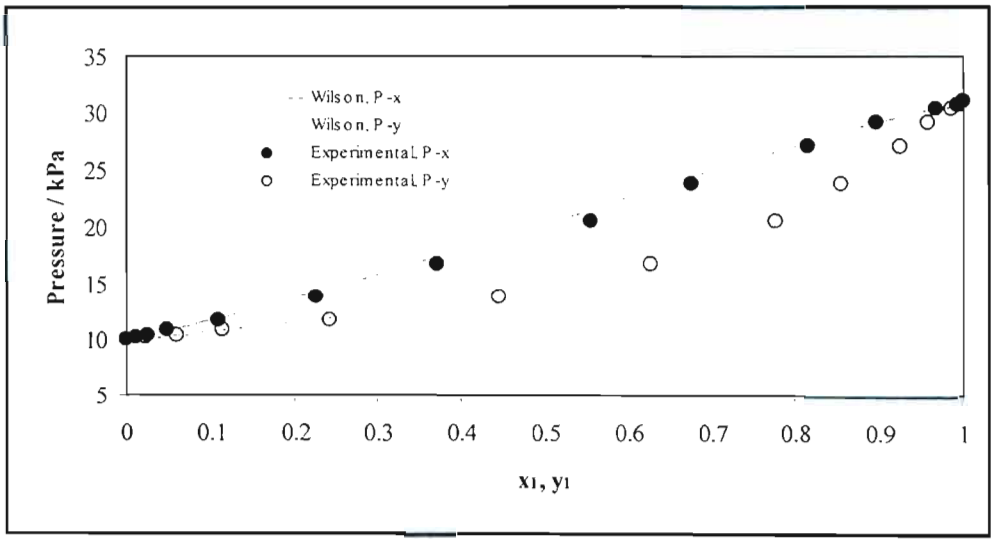

Figure 9-48: Wilson model fitted to P-x-y data using the chemical theory of vapour phase imperfections for the isobutyric acid (1) – valeric acid (2) system at 393.15 K.

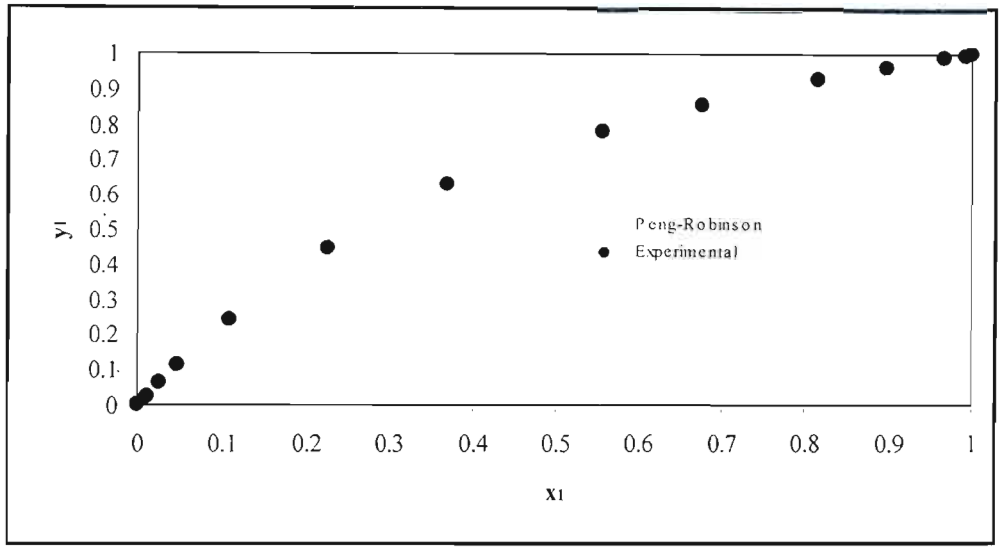

Figure 9-49: Peng-Robinson EOS fitted to x-y data using the Wong-Sandler mixing rule for the isobutyric acid (1) – valeric acid (2) system at 393.15 K.

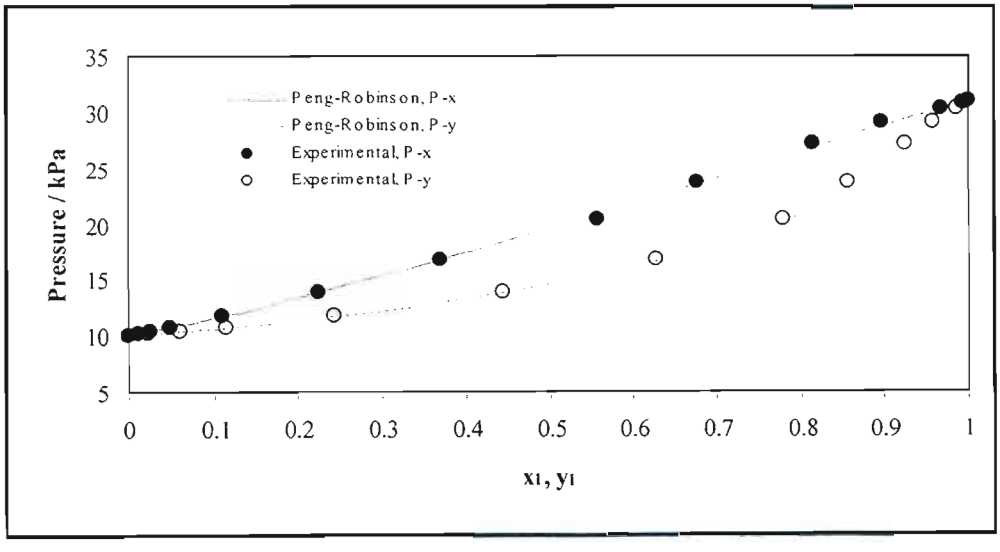

Figure 9-50: Peng-Robinson EOS fitted to P-x-y data using the Wong-Sandler mixing rule for the isobutyric acid (1) – valeric acid (2) system at 393.15 K.

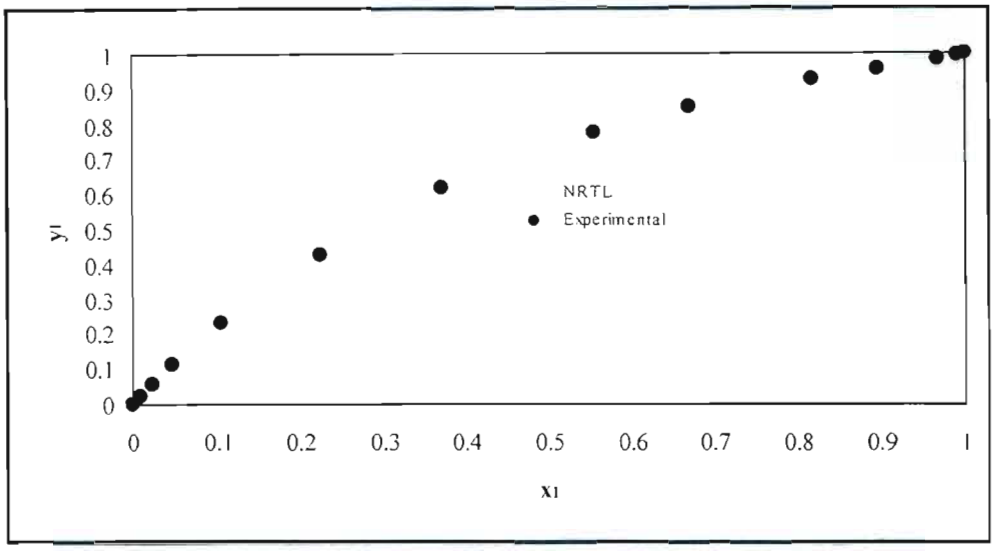

Figure 9-51: NRTL model fitted to x-y data using the Pitzer-Curl correlation for the isobutyric acid (1) – valeric acid (2) system at 403.15 K.

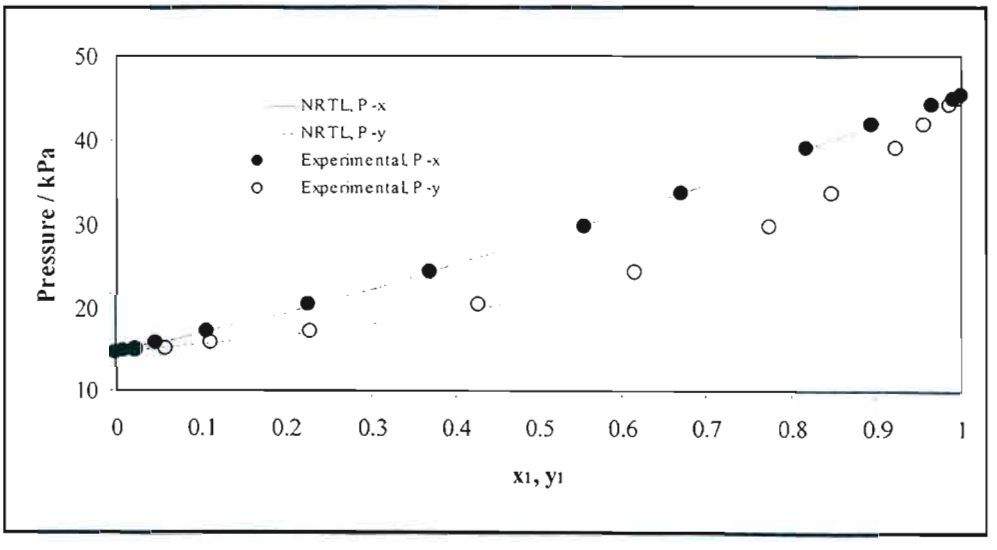

Figure 9-52: NRTL model fitted to P-x-y data using the Pitzer-Curl correlation for the isobutyric acid (1) – valeric acid (2) system at 403.15 K.

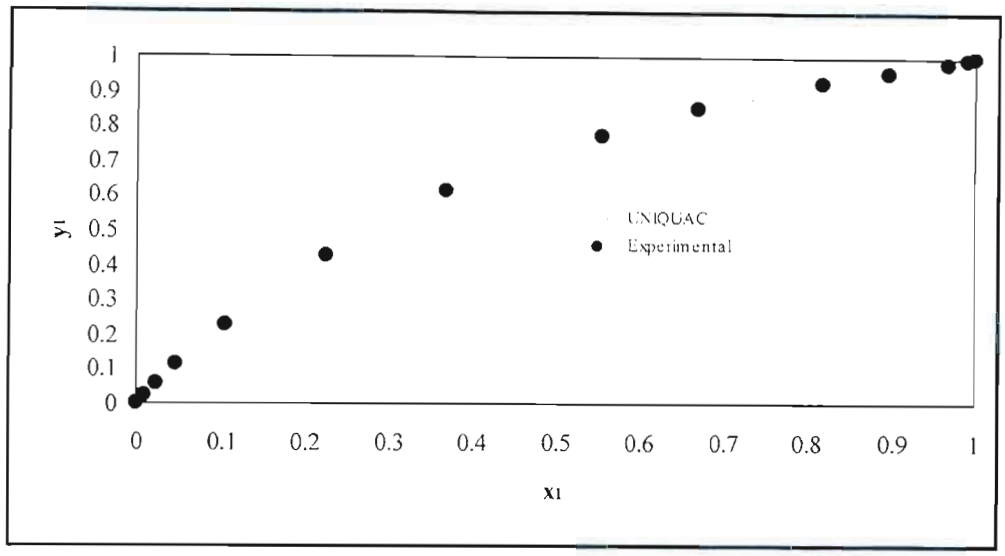

Figure 9-53: UNIQUAC model fitted to x-y data using the chemical theory of vapour phase imperfections for the isobutyric acid (1) – valeric acid (2) system at 403.15 K.

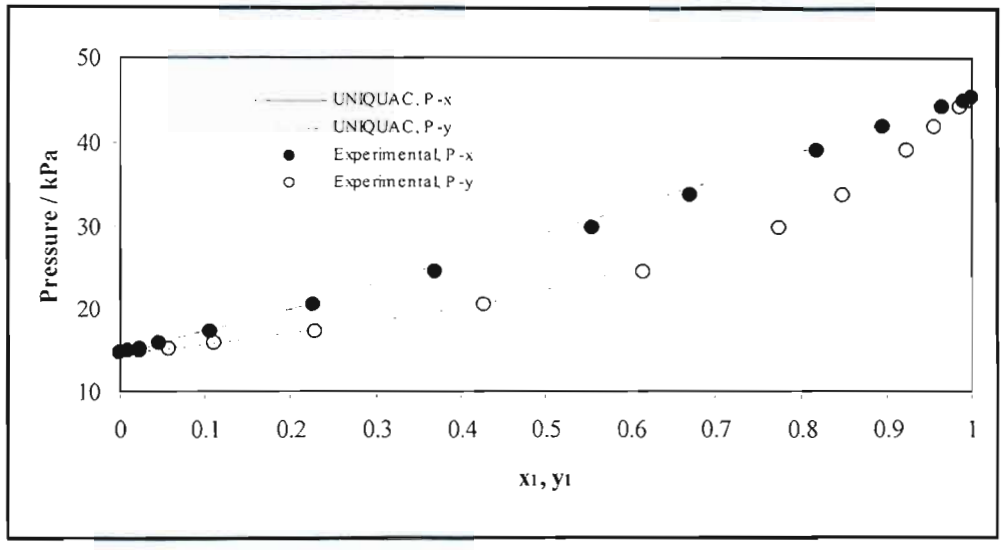

Figure 9-54: UNIQUAC model fitted to P-x-y data using the chemical theory of vapour phase imperfections for the isobutyric acid (1) – valeric acid (2) system at 403.15 K.

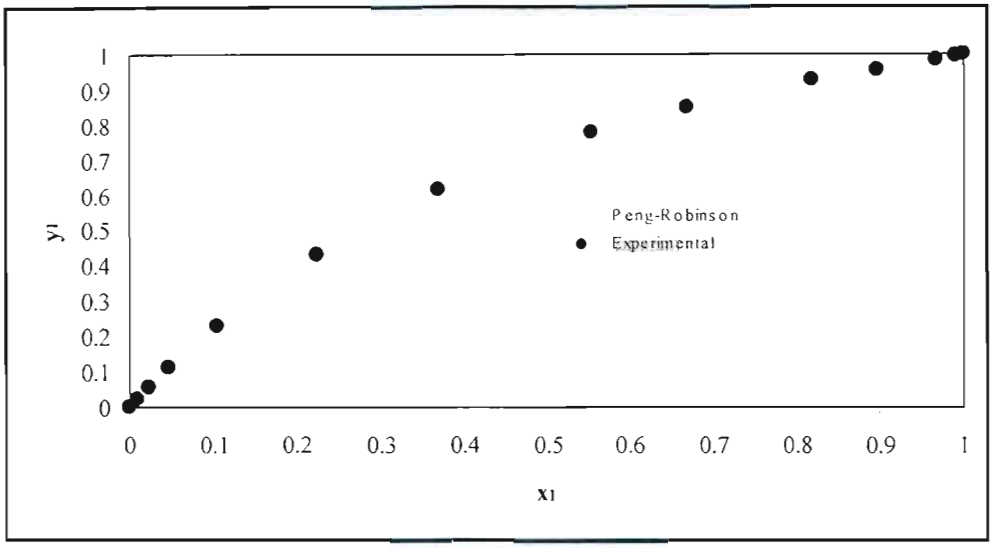

Figure 9-55: Peng-Robinson EOS fitted to x-y data using the Twu-Coon mixing rule for the isobutyric acid (1) – valeric acid (2) system at 403.15 K.

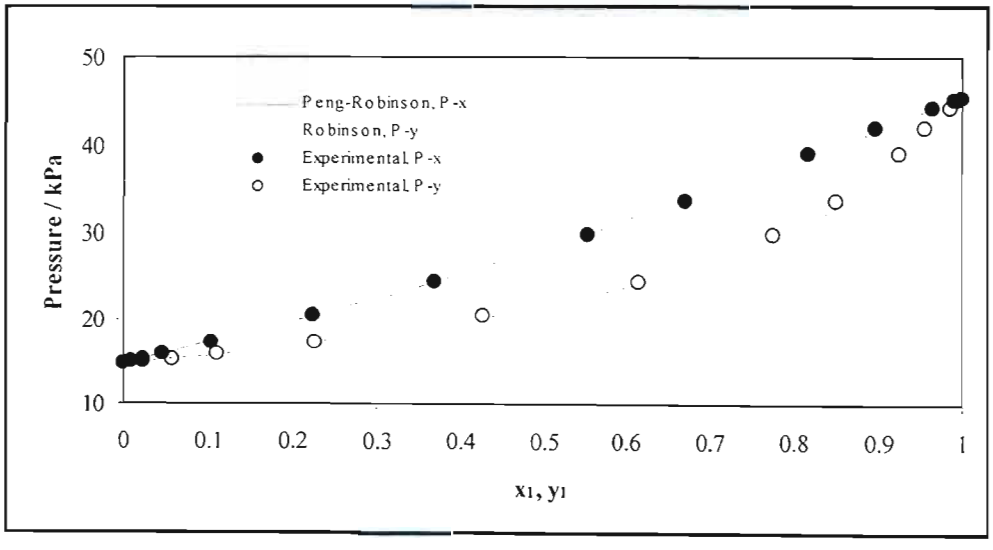

Figure 9-56: Peng-Robinson EOS fitted to P-x-y data using the Twu-Coon mixing rule for the isobutyric acid (1) – valeric acid (2) system at 403.15 K.

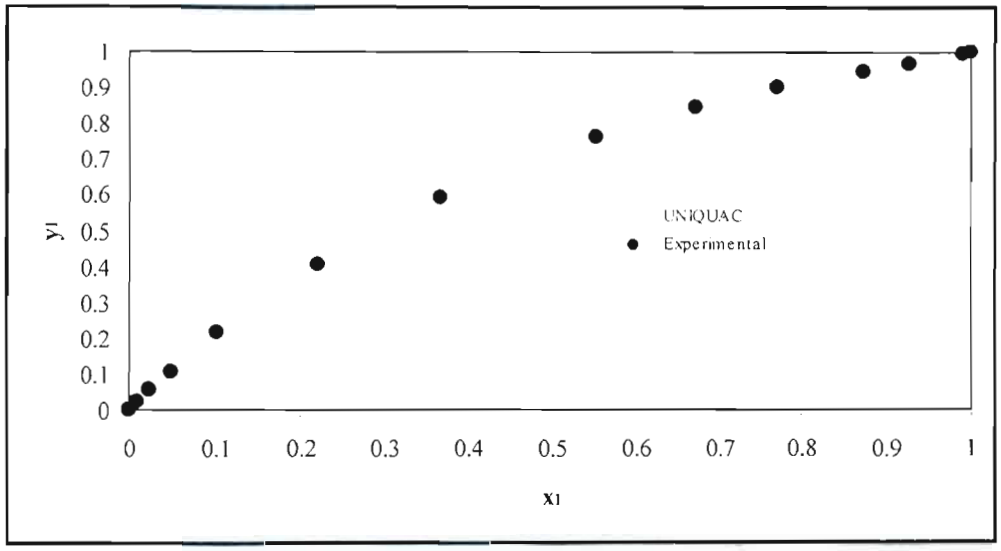

Figure 9-57: UNIQUAC model fitted to x-y data using the Pitzer-Curl correlation for the isobutyric acid (1) – valeric acid (2) system at 413.15 K.

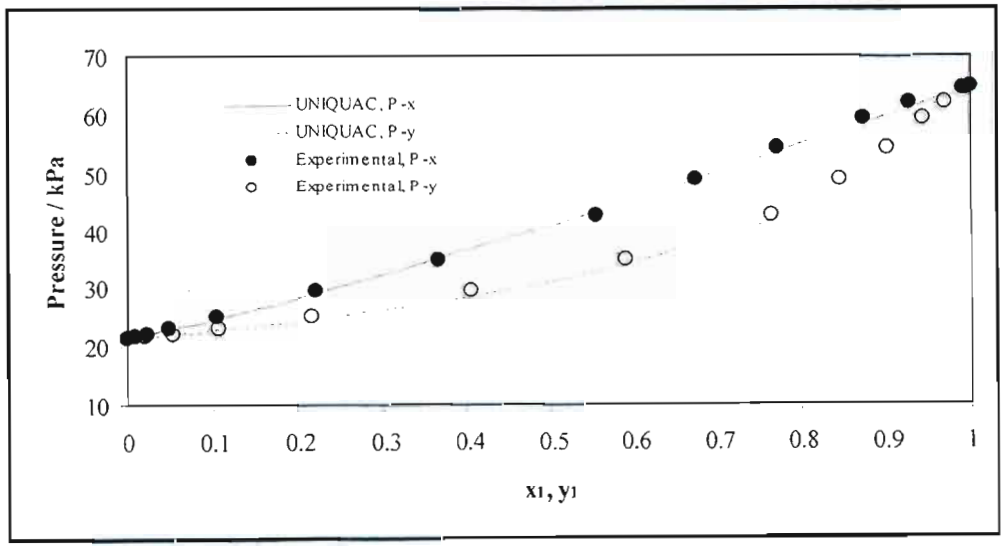

Figure 9-58: UNIQUAC model fitted to P-x-y data using the Pitzer-Curl correlation for the isobutyric acid (1) – valeric acid (2) system at 413.15 K.

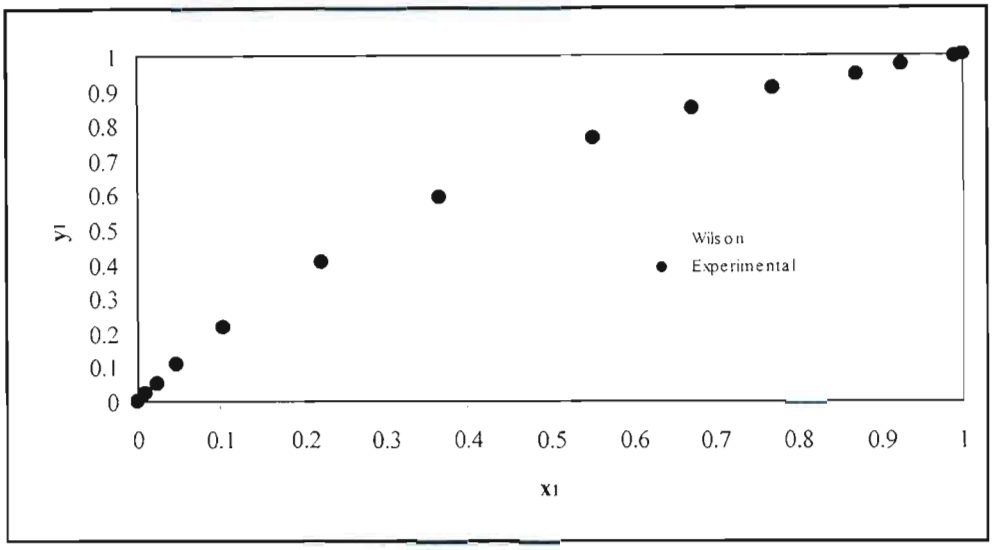

Figure 9-59: Wilson model fitted to x-y data using the chemical theory of vapour phase imperfections for the isobutyric acid (1) – valeric acid (2) system at 413.15 K.

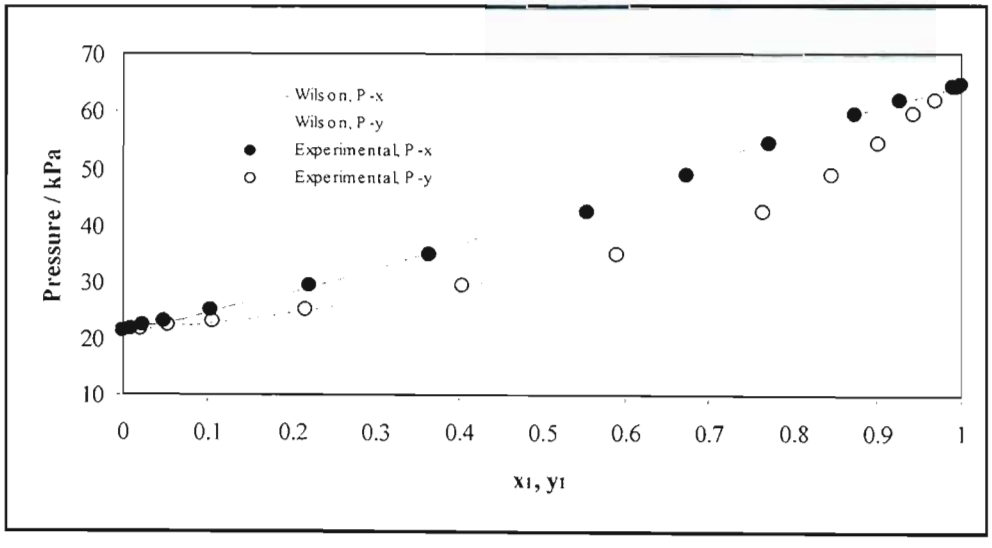

Figure 9-60: Wilson model fitted to P-x-y data using the chemical theory of vapour phase imperfections for the isobutyric acid (1) – valeric acid (2) system at 413.15 K.

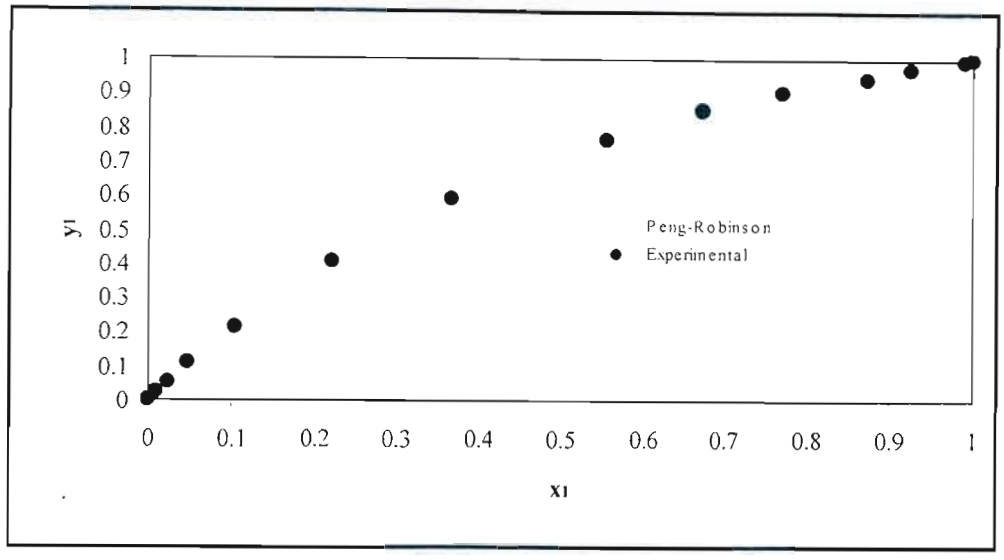

Figure 9-61: Peng-Robinson EOS fitted to x-y data using the Wong-Sandler mixing rule for the isobutyric acid (1) – valeric acid (2) system at 413.15 K.

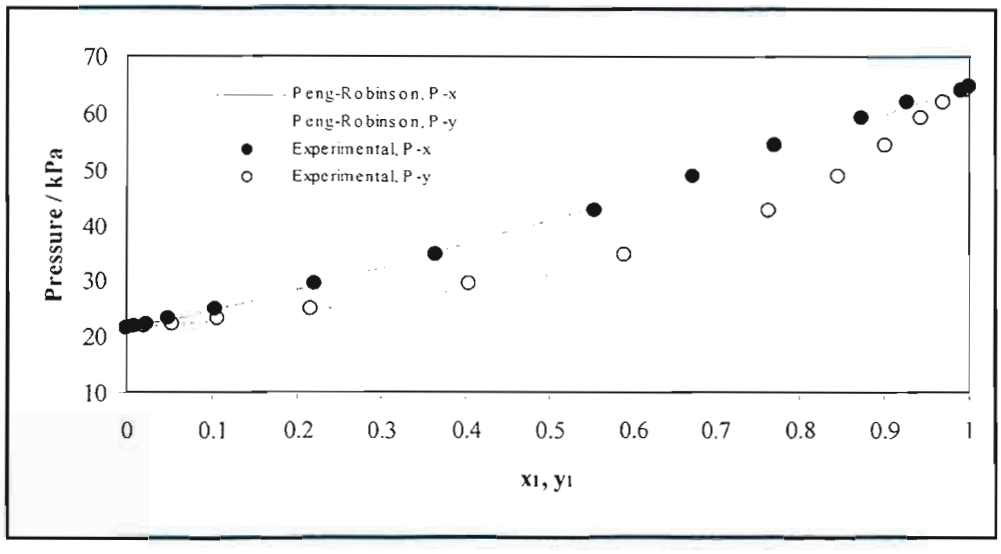

Figure 9-62: Peng-Robinson EOS fitted to P-x-y data using the Wong-Sandler mixing rule for the isobutyric acid (1) – valeric acid (2) system at 413.15 K.

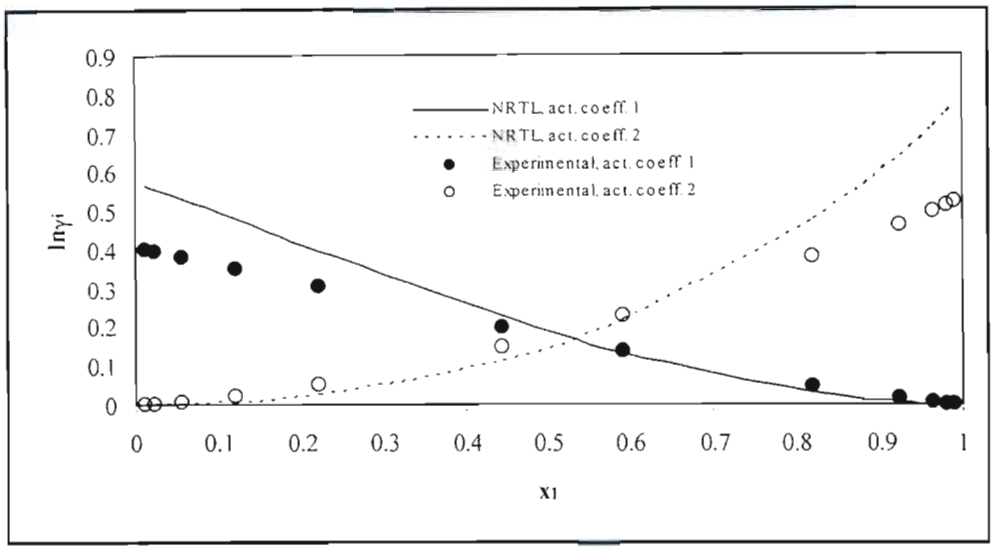

Figure 9-63: Comparison between the experimentally determined liquid-phase activity coefficients and those calculated from the NRTL model with the Pitzer-Curl correlation for the isobutyric acid (1) – valeric acid (2) system at 20 kPa.

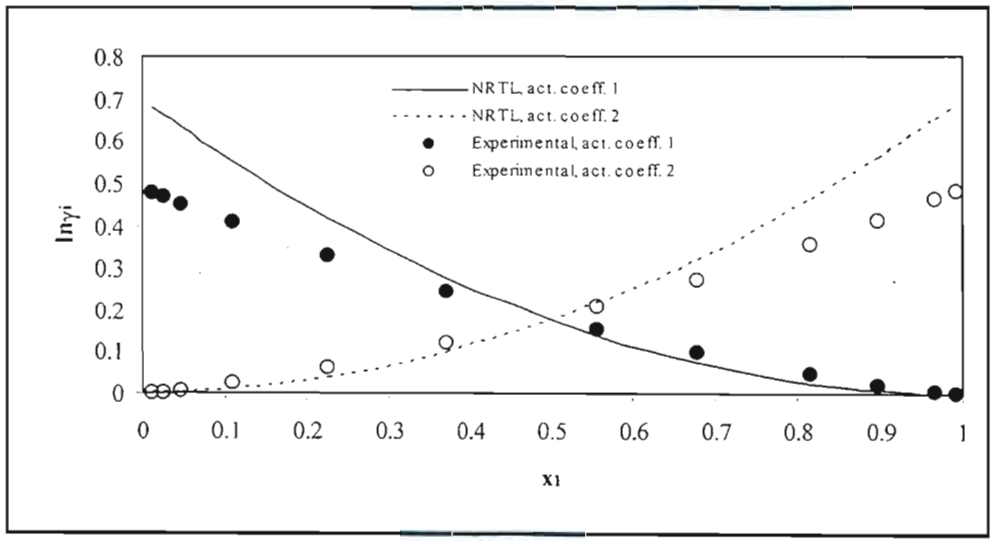

Figure 9-64: Comparison between the experimentally determined liquid-phase activity coefficients and those calculated from the NRTL model with the Pitzer-Curl correlation for the isobutyric acid (1) – valeric acid (2) system at 393.15 K.

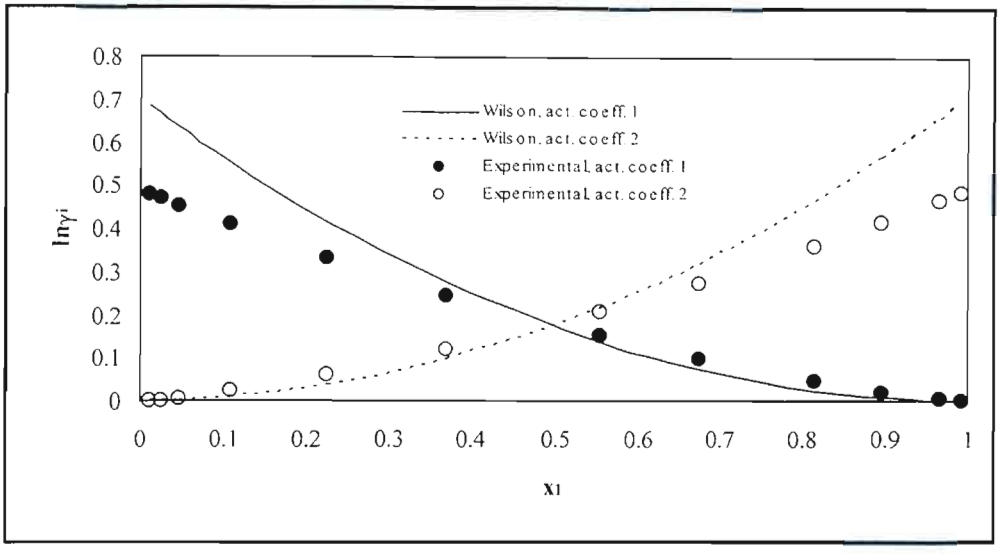

Figure 9-65: Comparison between the experimentally determined liquid-phase activity coefficients and those calculated from the Wilson model with chemical theory for the isobutyric acid (1) – valeric acid (2) system at 393.15 K.

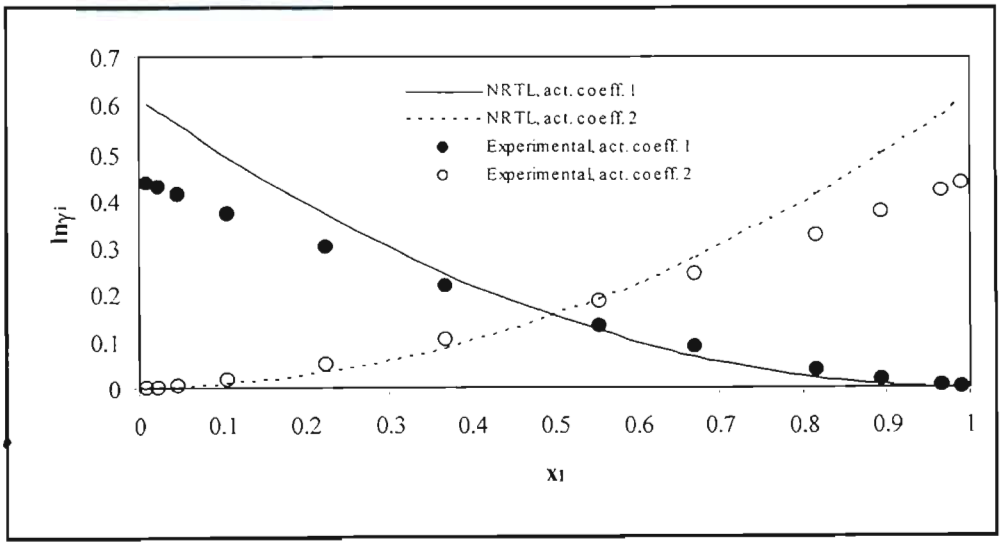

Figure 9-66: Comparison between the experimentally determined liquid-phase activity coefficients and those calculated from the NRTL model with the Pitzer-Curl correlation for the isobutyric acid (1) – valeric acid (2) system at 403.15 K.

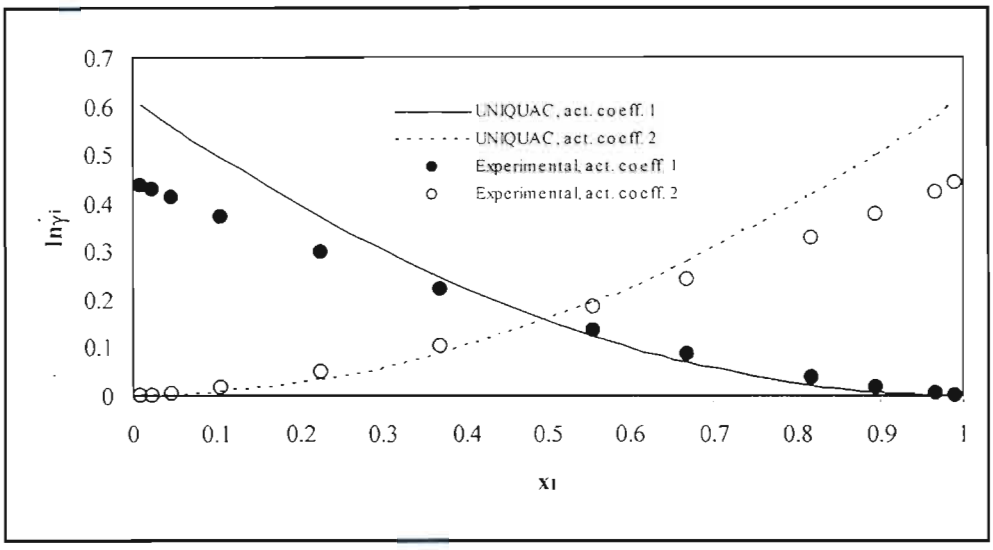

Figure 9-67: Comparison between the experimentally determined liquid-phase activity coefficients and those calculated from the UNIQUAC model with chemical theory for the isobutyric acid (1) – valeric acid (2) system at 403.15 K.

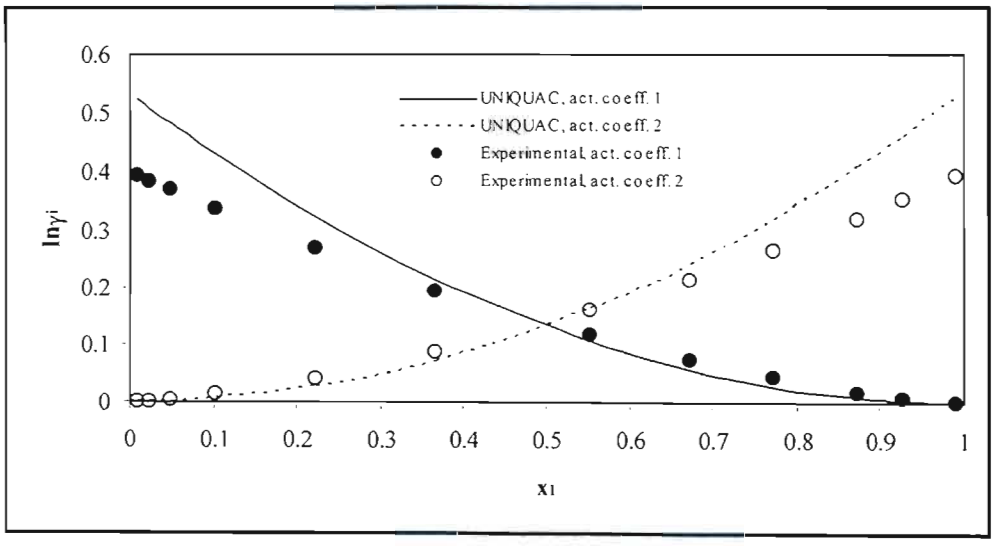

Figure 9-68: Comparison between the experimentally determined liquid-phase activity coefficients and those calculated from the UNIQUAC model with the Pitzer-Curl correlation for the isobutyric acid (1) – valeric acid (2) system at 413.15 K.

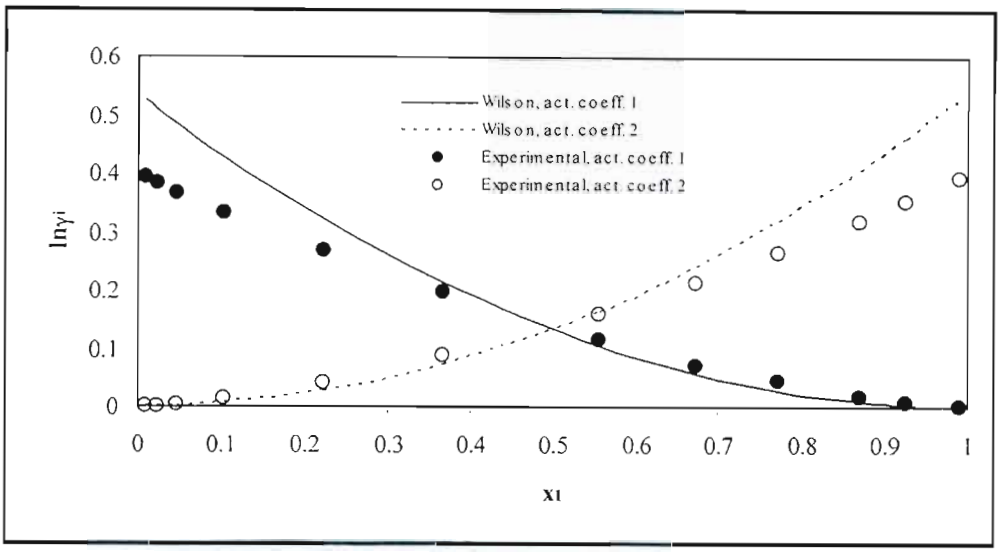

Figure 9-69: Comparison between the experimentally determined liquid-phase activity coefficients and those calculated from the Wilson model with chemical theory for the isobutyric acid (1) – valeric acid (2) system at 413.15 K.

9.5 Thermodynamic Consistency Testing

9.5.1 Cyclohexane (1) – Ethanol (2) Test System

An analysis of the data measured for the cyclohexane – ethanol test system with respect to thermodynamic consistency revealed that the measured data are extremely consistent. Yet again, the UNIQUAC equation faired poorest (for this system) and failed to pass the point test of Van Ness et al. [1973] (Section 3.7.1). It is clear that the UNIQUAC equation does not suit this system particularly well and is not capable of adequately representing the measured data. Since the consistency tests rely on an appropriate model being employed for the regression; the UNIQUAC equation was always likely to produce results that fail the tests for thermodynamic consistency.

On the other hand, both the NRTL and the Wilson equations produce results that easily pass both the point test (Van Ness et al. [1973]) and the direct test of thermodynamic

consistency (Van Ness [1995]). As was discussed in Section 3.7.1, the point test requires that the vapour compositions display an average absolute deviation less than 0.01, if the data are to be deemed consistent. The NRTL and Wilson models easily comply with this requirement, yielding an average absolute deviation of 0.0087 and 0.0083 respectively.

In terms of the direct test, the Wilson model gave a slightly lower figure for the RMS value of the residual ($\delta\ln(\gamma_1/\gamma_2)$), but both models fell into the range 0.025 – 0.050 (as is shown in Table 9-6). This indicates a consistency index of 2 (refer to Table 3-1) and according to Van Ness [1995] signifies that the data are very good. The scatter around zero is shown graphically (for both tests) for the best-fit model viz. the Wilson model in Figures 9-70 and 9-71. The remaining graphs (i.e. those for the NRTL and UNIQUAC equations) are presented in Appendix B.

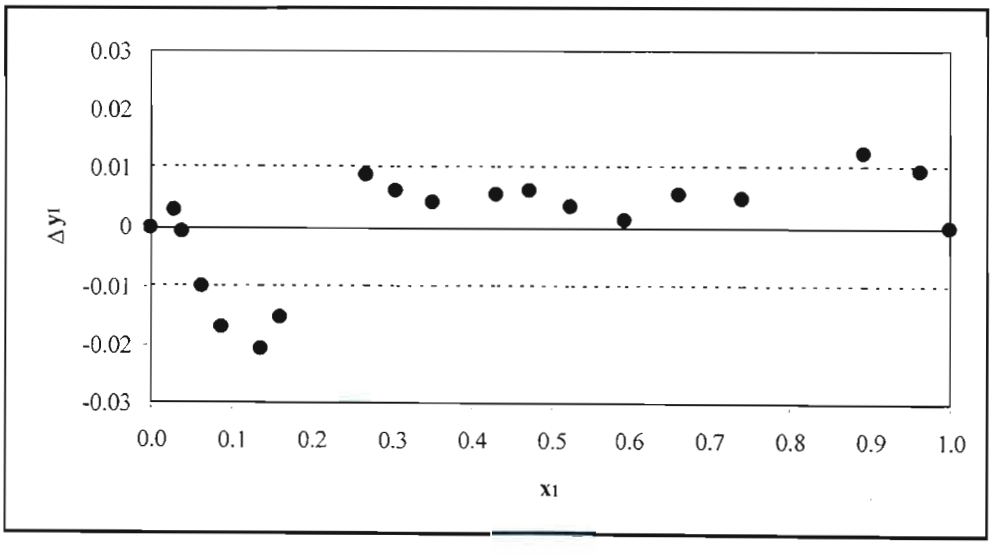

Figure 9-70: Graph showing the deviation of the vapour compositions calculated using the Wilson model from the experimental vapour compositions for the cyclohexane (1) – ethanol (2) system at 40 kPa.

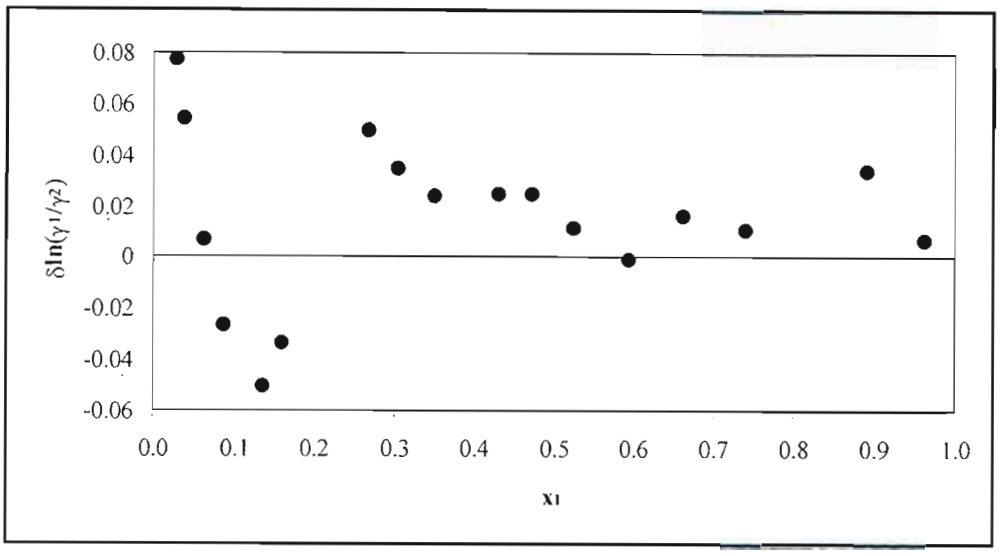

Figure 9-71: Graph showing the deviation of the activity coefficients calculated using the Wilson model from the experimental activity coefficients for the cyclohexane (1) – ethanol (2) system at 40 kPa.

9.5.2 Propionic Acid (1) – Valeric Acid (2) System

The Δy values obtained for the propionic acid – valeric acid system are given in Table 9-8. As was noted in Section 9.4.3.1, the deviations of the vapour compositions (for this system in particular) were adversely influenced by the association effects exhibited in the dilute regions of the carboxylic acid systems. Thus, the Δy residuals were (for the most part) greater than 0.01 for the propionic acid – valeric acid system. The only major exception was the isobaric data, which easily complied with the point test criterion ($\Delta y < 0.01$). For both the 393.15 K and 413.15 K data sets, at least one of the best fit models complied with the point test (even though some of the other models did not) in each case, and hence, the data are considered to be consistent. Only the 403.15 K isotherm did not pass the point test, although the reasons for this have been mentioned above (as well as discussed in detail in Section 9.4.3.1).

With regards to the direct test, the isobar at 20 kPa achieved an index of 7, and the isotherms at 393.15 K, 403.15 K and 413.15 K received indices of 6, 5 and 4 respectively. Thus, although the experimental data sets all passed the direct test, only the isotherm measured at 413.15 K achieved an index indicating satisfactory data. The reason for the relatively high RMS $\delta\ln(\gamma_1/\gamma_2)$ values has already been discussed in both Sections 9.4.3.1 and 9.4.3.2 and need not be re-iterated here. However, it should be noted that the indices obtained for the direct test are not a true reflection of the thermodynamic consistency of the propionic acid – valeric acid data.

This is also clearly illustrated in the plots utilized in calculating the RMS $\delta\ln(\gamma_1/\gamma_2)$ figures. These exhibit a definite trend (for example, refer to Figure 9-74) and do not scatter about zero as would be expected if the models provided a good fit to the experimental activity coefficient data. Hence, it is obvious that the large values calculated for the $\delta\ln(\gamma_1/\gamma_2)$ residuals are as a result of the activity coefficient models proving incapable of accurately matching the experimental data and is not an indication of inconsistent VLE data. Thus, in the case of carboxylic acid binary VLE systems, the point test apparently provides a far better indication of thermodynamic consistency than the highly recommended direct test.

The graphs presented below show the degree of scatter about zero of the various deviations, namely Δy, ΔP and $\delta\ln(\gamma_1/\gamma_2)$. The ΔP deviations do not form (at least not directly) part of the thermodynamic consistency tests used in this work. However, they do give a good indication of the quality of the fit attained by the various models employed in this project. Only the deviations evaluated from the model that performed best in each case are given here, the remaining plots may be viewed in Appendix B.

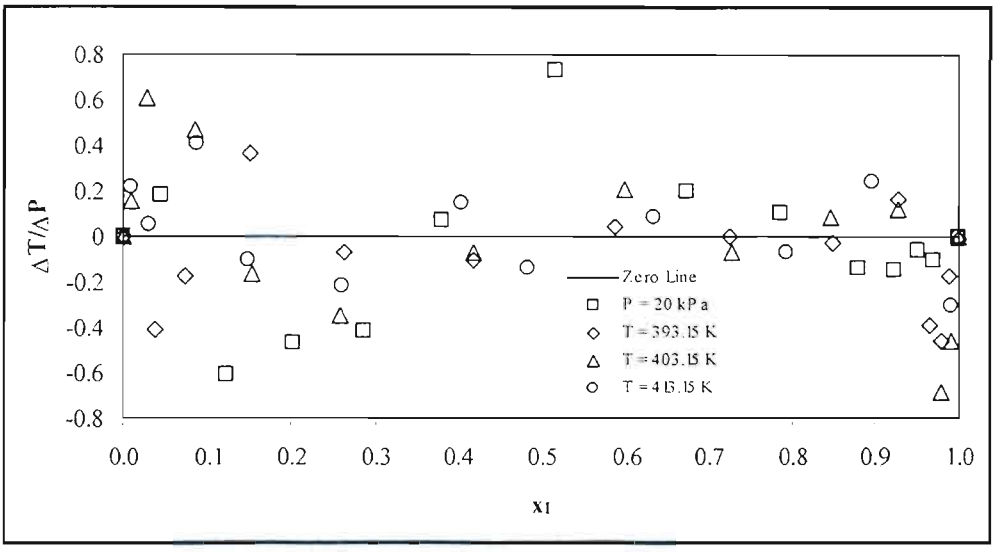

Figure 9-72: Graph of the deviation of the best fit models pressures and temperatures from the experimental values for the propionic acid (1) – valeric acid (2) system.

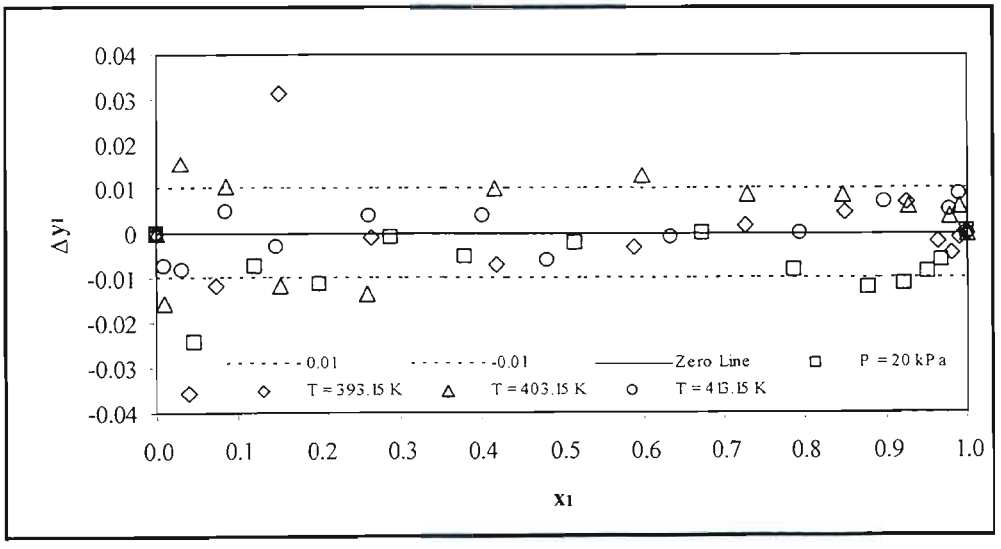

Figure 9-73: Graph showing the deviation of the best fit models vapour compositions from the experimental values for the propionic acid (1) – valeric acid (2) system.

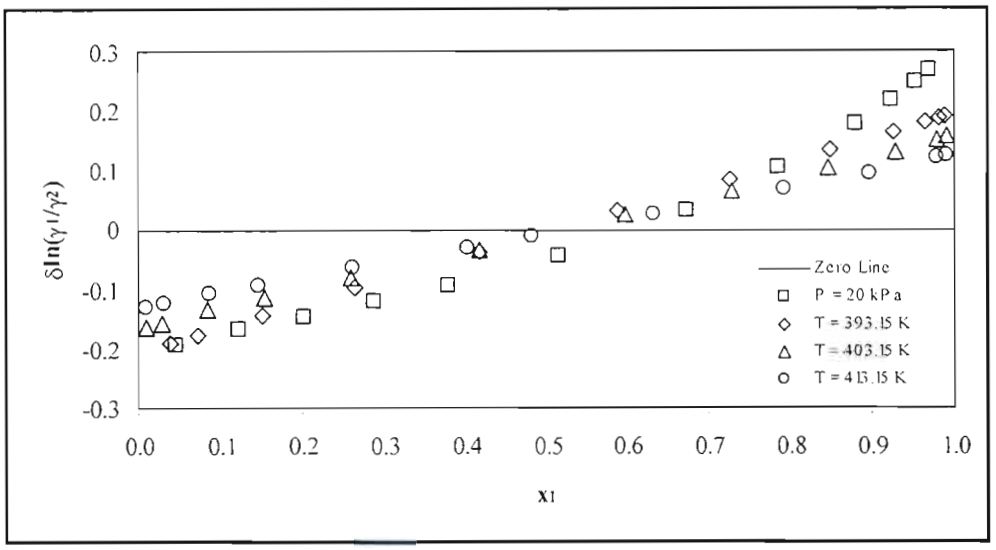

Figure 9-74: Graph showing the deviation of the best fit models activity coefficients from the experimental values for the propionic acid (1) – valeric acid (2) system.

9.5.3 Isobutyric Acid (1) – Valeric Acid (2) System

The models provided a far better fit to the isobutyric acid system than to the propionic acid system. Consequently, the Δy figures for the isobutyric acid – valeric acid system are remarkably good. All of the experimental data sets passed the point test, in most cases with ease. The only data set that struggled was the isotherm at 413.15 K, which only achieved an average vapour phase deviation less than 0.01 when the chemical theory of gas non-ideality was utilized to account for the vapour phase imperfections.

Again, the direct test results are unsatisfactory, but (as has already been mentioned in Section 9.4.3.1 and 9.4.3.2) this was anticipated since the models did not adequately fit the experimental activity coefficients. The 20 kPa isobar attained an index of 7, as did the 393.15 K isotherm. The remaining isotherms (403.15 K and 413.15 K) achieved indices of 6 and 4 respectively. As was discovered for the propionic acid – valeric acid system, the plots of $\delta\ln(\gamma_1/\gamma_2)$ versus x_1 display a distinct trend, again indicating that the models were

not able to satisfactorily model the liquid-phase activity coefficients and that the point test is preferable as a means of determining thermodynamic consistency for carboxylic acids.

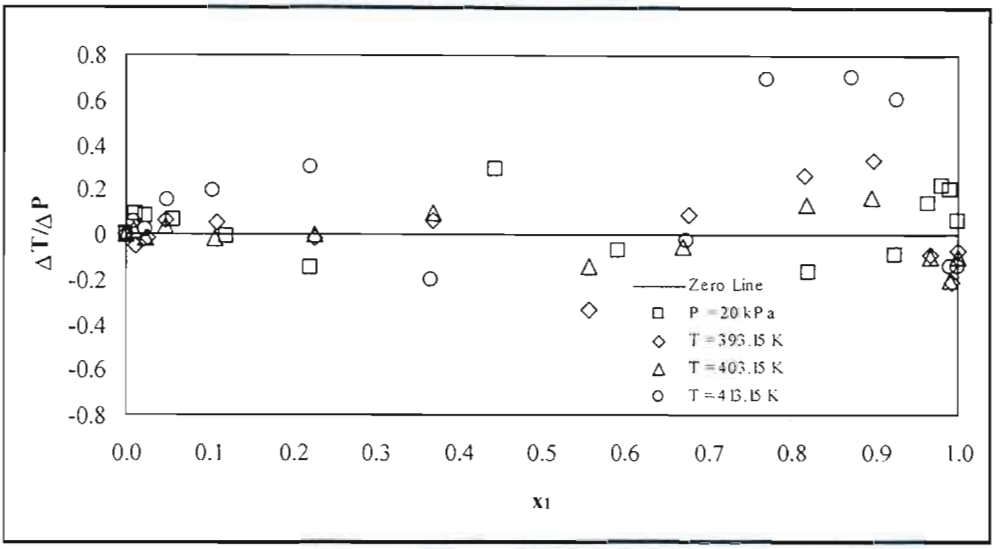

Figure 9-75: Graph of the deviation of the best fit models pressures and temperatures from the experimental values for the isobutyric acid (1) – valeric acid (2) system.

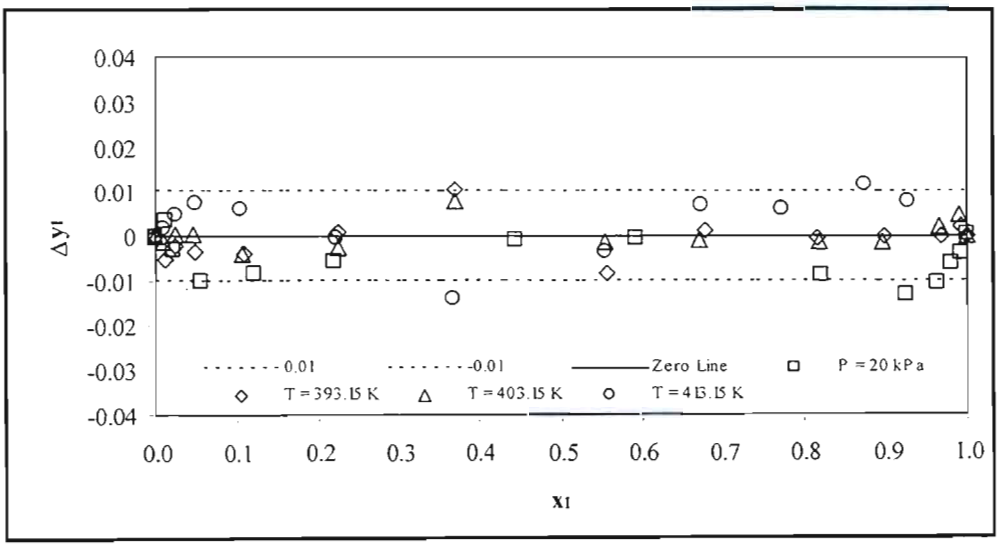

Figure 9-76: Graph showing the deviation of the best fit models vapour compositions from the experimental values for the isobutyric acid (1) – valeric acid (2) system.

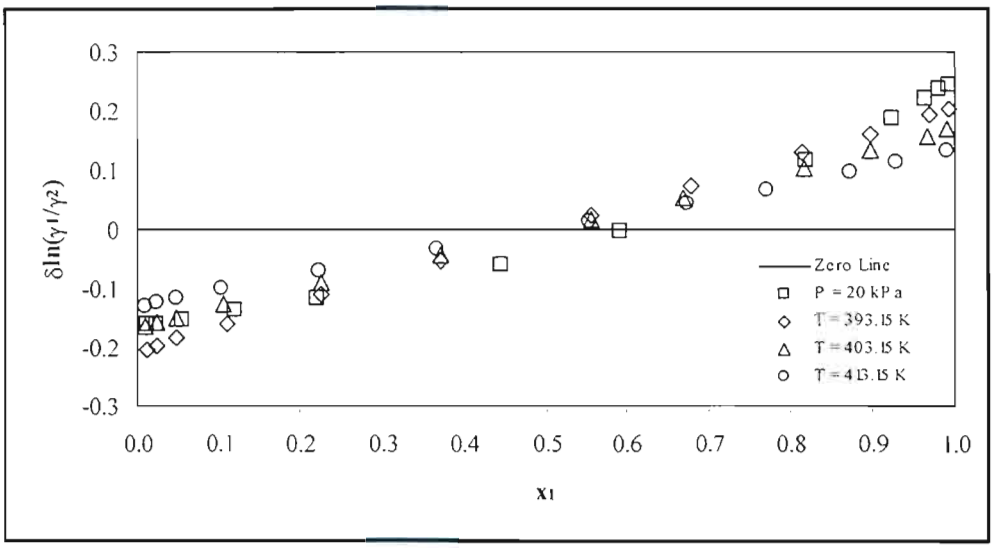

Figure 9-77: Graph showing the deviation of the best fit models activity coefficients from the experimental values for the isobutyric acid (1) – valeric acid (2) system.

9.6 Infinite Dilution Activity Coefficients

The concept of infinite dilution activity coefficients was introduced in Section 3.5. The method that was employed in this work was based on the equation of Gautreaux and Coates [1955], Equation (3-147). The partial derivative of pressure with respect to liquid mole fraction was calculated using the procedure of Maher and Smith [1979] (as modified from the Ellis and Jonah [1962] method). The steps involved in this evaluation are clearly laid out and discussed in detail in Section 3.5.1.

Unfortunately, it proved impossible to accurately determine the infinite dilution activity coefficients from the experimental data measured in this work. Two reasons exist for this:

1. The deviation from ideality for much of the data was extremely small, as has already been pointed out in Section 9.4.3.1. Hence, the values calculated for the deviation pressure, P_D, were all relatively small, which inevitably meant that any

slight errors in the pressure measurements would have a significant effect. This is clearly evident in the degree of scatter which is visible in Figure 9-78 below.

2. This scattering effect is exacerbated by the hydrogen bonding evident in the dilute regions. It is obvious that the dilute regions are critical in accurate determination of the infinite dilution activity coefficients, and the method proposed by Maher and Smith [1979] does not differ in this regard. Thus, the end effects caused by the carboxylic acid association (discussed in Section 9.4.3.1) have a detrimental effect on the plots utilized to evaluate the infinite dilution activity coefficients. This may be viewed in the example given below, Figure 9-78.

Thus, no values for the infinite dilution activity coefficients could be calculated from the carboxylic acid binary VLE data. When dealing with carboxylic acid systems, it is recommended that the infinite dilution activity coefficients be measured experimentally e.g. via inert gas stripping or differential static (and/or dynamic) methods.

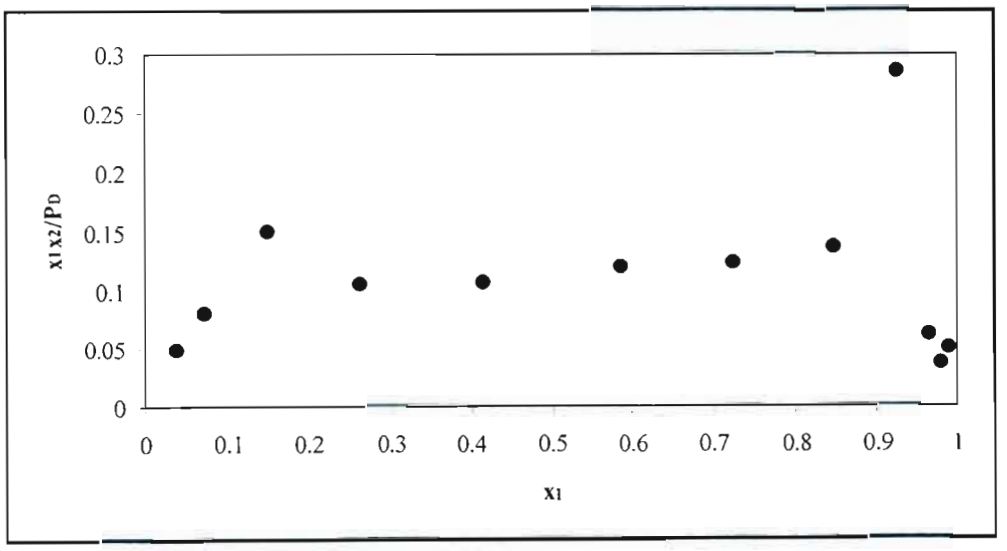

Figure 9-78: Plot showing the scatter in the infinite dilution activity coefficient data for the propionic acid (1) – valeric acid (2) system at 393.15 K.

9.7 Excess Thermodynamic Properties

The excess thermodynamic properties were discussed earlier in this work in Section 3.6. The method employed in calculating these properties was laid out in detail and, thus, only the points salient to the discussion of these properties will be repeated here. The Gibbs-Hermholtz equation (Equation (3-157)) allows evaluation of the molar excess enthalpy (H^E), provided that the excess Gibbs energy (G^E) has been calculated at a number of temperatures. In this project, three isotherms were measured for each of the carboxylic acid systems studied. Hence, a plot of G^E/RT versus temperature enabled the partial derivative in Equation (3-157) to be evaluated. These plots are shown in Figures 9-79 and 9-83, but only half of the G^E/RT plots are shown to avoid cluttering the graphs (which would lead to confusion). Thereafter, it became a simple matter of substitution to determine H^E.

Once the molar excess enthalpy and excess Gibbs energy were known, the fundamental relation given in Equation (3-158) yielded the excess entropy, S^E. This process was carried out over the entire composition range, permitting these properties to be plotted against the liquid mole fraction. These graphs are presented below (Figures 9-80 to 9-82 and 9-84 to 9-86) and the excess enthalpy data are given in Tables 9-11 and 9-12. It should be noted that the excess Gibbs energy values used to determine H^E were calculated during the VLE data reduction (refer to Section 9.4). The objective function used in this reduction was based on the excess Gibbs energy, as this was found to give far better results than if the pressure residuals were used.

The interesting behaviour exhibited by the excess properties calculated for the propionic acid – valeric acid system is often found in associating systems. Examples of similar curves may be found in the literature in the excellent texts of Walas [1985] and Smith et al. [1996]. The isobutyric acid – valeric acid system displayed more conventional excess thermodynamic behaviour. Comparing the two sets of results, it was discovered that the G^E values were very similar for both systems. However, the H^E and TS^E values differed considerably. The values determined for the isobutyric acid system were far larger than the corresponding values for the propionic acid system.

Table 9-11: Molar excess enthalpy (J/mol) values for the propionic acid (1) – valeric acid (2) system.

x_1	T = 393.15 K	T = 403.15 K	T = 413.15 K
0.0	0.00	0.00	0.00
0.1	-205.62	-216.22	-227.08
0.2	-295.58	-310.81	-326.42
0.3	-295.58	-310.81	-326.42
0.4	-257.03	-270.27	-283.84
0.5	-167.07	-175.68	-184.50
0.6	-70.68	-74.32	-78.06
0.7	12.85	13.51	14.19
0.8	70.68	74.32	78.06
0.9	77.11	81.08	85.15
1.0	0.00	0.00	0.00

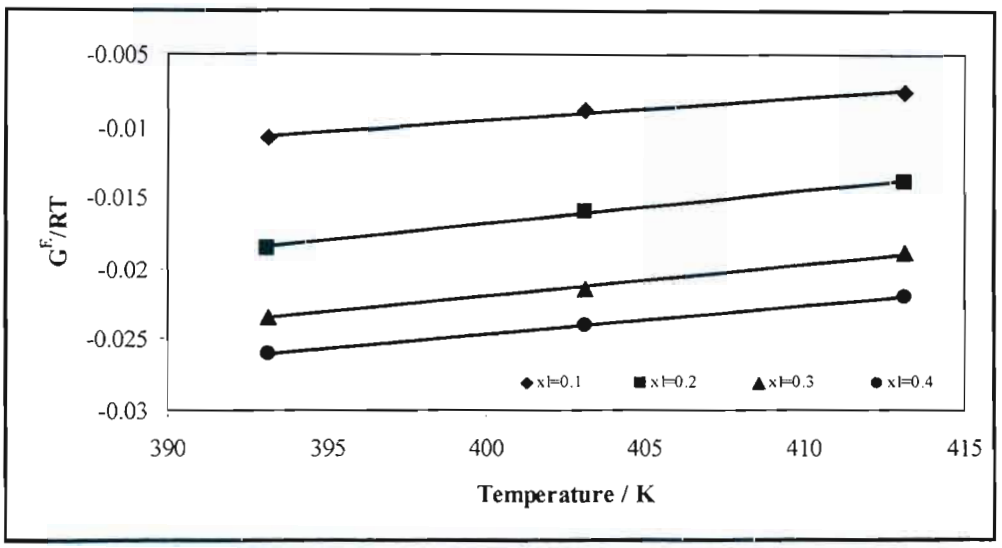

Figure 9-79: Plot utilized in determining the molar excess enthalpy values for the propionic acid (1) – valeric acid (2) system.

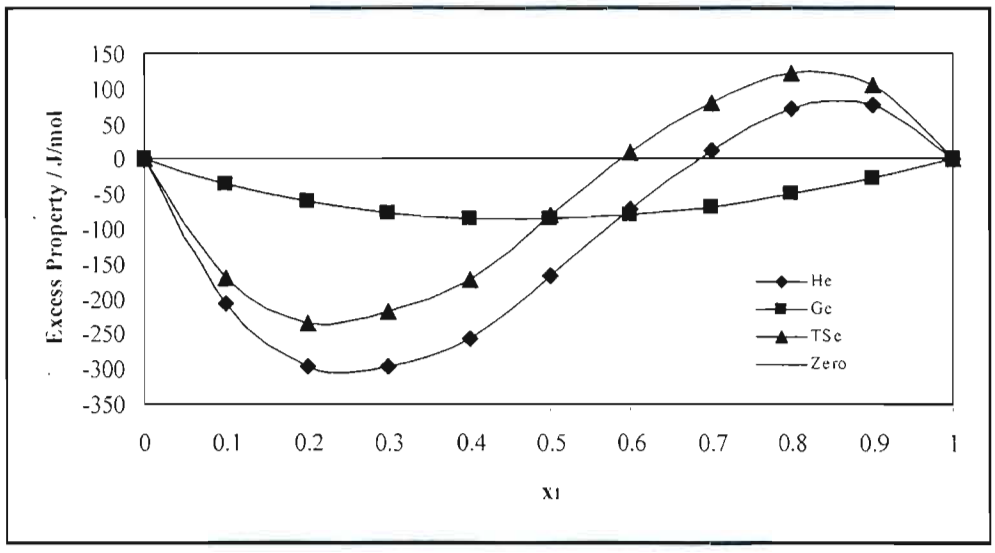

Figure 9-80: Excess thermodynamic properties for the propionic acid (1) – valeric acid (2) system at 393.15 K.

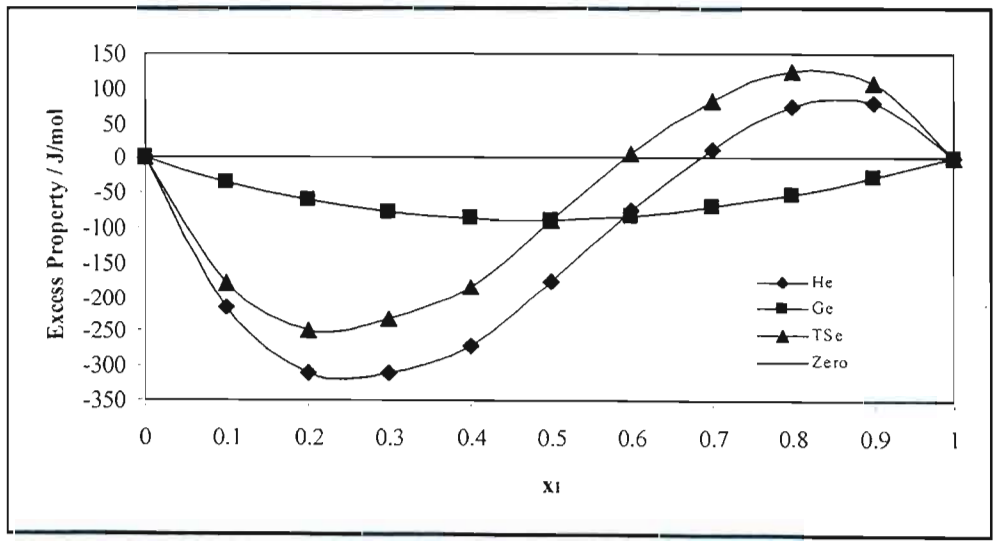

Figure 9-81: Excess thermodynamic properties for the propionic acid (1) – valeric acid (2) system at 403.15 K.

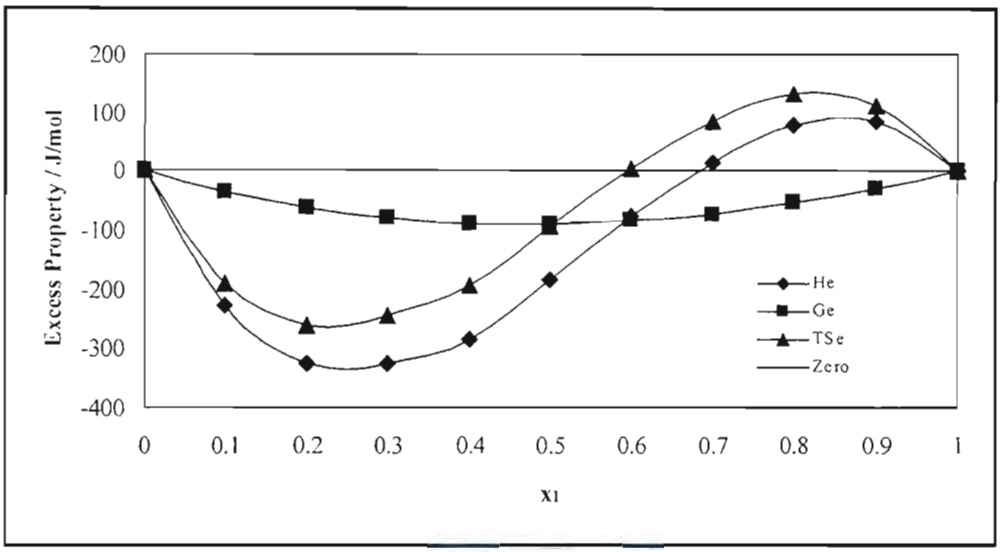

Figure 9-82: Excess thermodynamic properties for the propionic acid (1) – valeric acid (2) system at 413.15 K.

Table 9-12: Molar excess enthalpy (J/mol) values for the isobutyric acid (1) – valeric acid (2) system.

x_1	T = 393.15 K	T = 403.15 K	T = 413.15 K
0.0	0.00	0.00	0.00
0.1	417.67	439.19	461.25
0.2	777.51	817.57	858.63
0.3	1073.09	1128.38	1185.05
0.4	1291.57	1358.11	1426.32
0.5	1413.66	1486.49	1561.14
0.6	1439.36	1513.51	1589.53
0.7	1342.97	1412.16	1483.09
0.8	1085.95	1141.89	1199.24
0.9	649.00	682.43	716.71
1.0	0.00	0.00	0.00

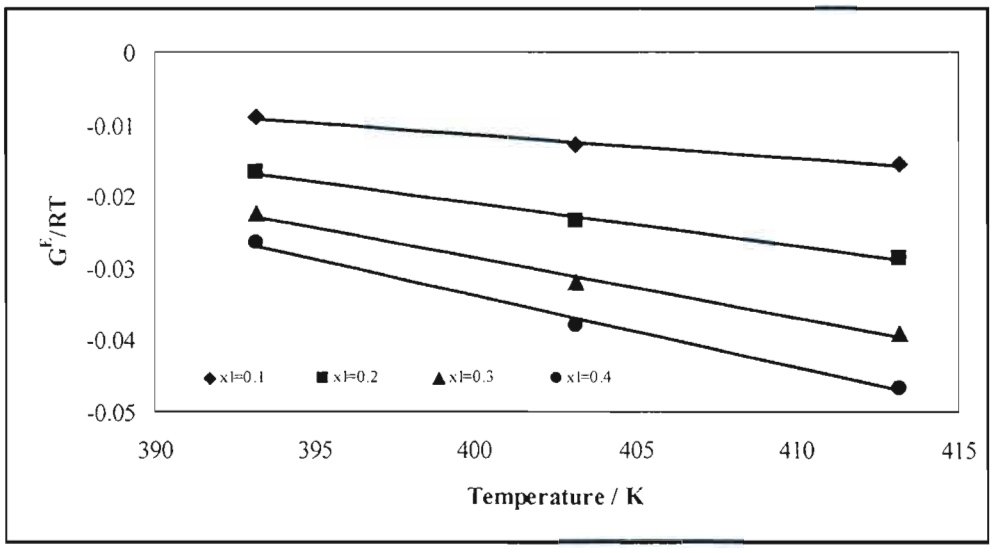

Figure 9-83: Plot utilized in determining the molar excess enthalpy values for the isobutyric acid (1) – valeric acid (2) system.

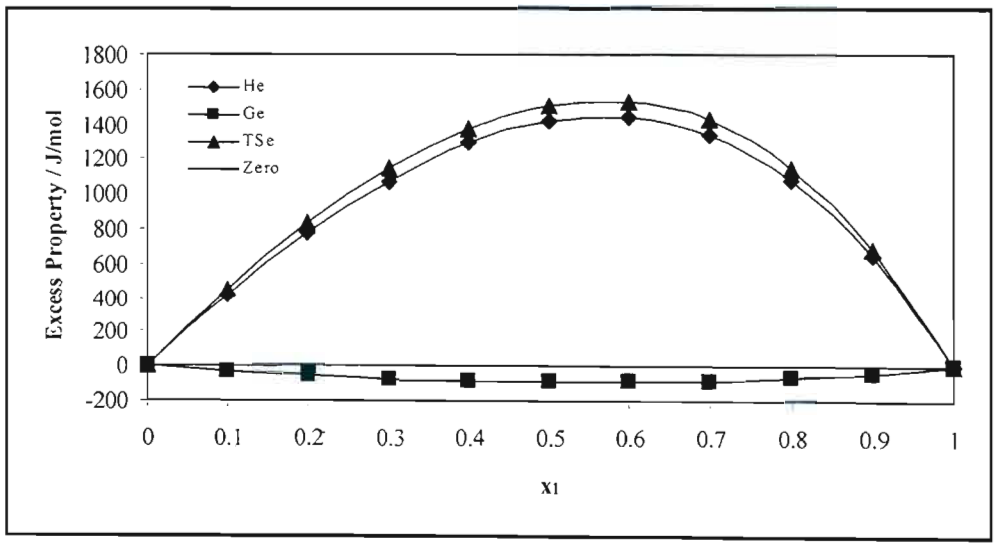

Figure 9-84: Excess thermodynamic properties for the isobutyric acid (1) – valeric acid (2) system at 393.15 K.

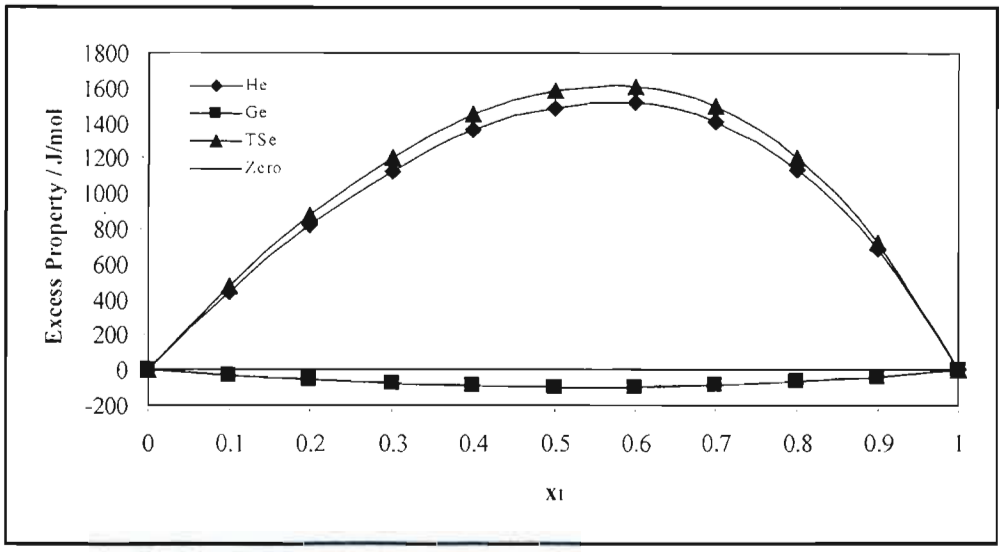

Figure 9-85: Excess thermodynamic properties for the isobutyric acid (1) – valeric acid (2) system at 403.15 K.

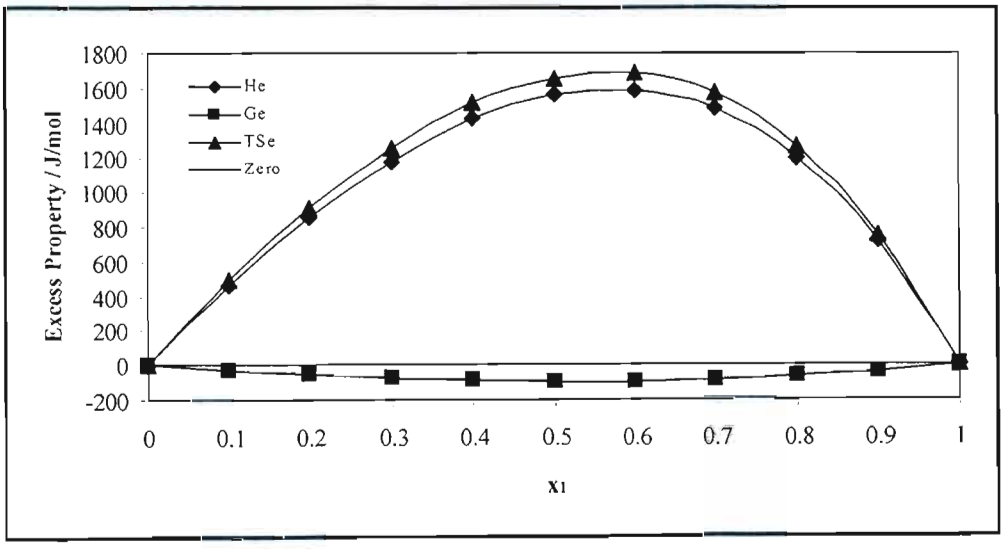

Figure 9-86: Excess thermodynamic properties for the isobutyric acid (1) – valeric acid (2) system at 413.15 K.

9.8 Molecular Simulation Results

9.8.1 Pure Component Predictions

9.8.1.1 n-Pentane

The initial phase of this portion of the project was concerned with becoming familiar with the software and procedures utilized when running simulations on the Beowulf cluster. To this end, a simple straight-chain alkane (n-pentane) was selected for simulation. n-Pentane was chosen because it had been previously established that simulation of simple alkanes was straightforward and accurate results could be easily obtained. The simulations were run using 500 molecules with 70 000 cycles overall. Due to the exceedingly ideal behaviour of straight-chain alkanes, it was found that only 1 500 equilibrium cycles were necessary. Even with the large number of molecules and cycles, the simulations were still relatively short (just a few hours) compared to the amount of time required to finish a job involving polar compounds (refer to the sections that follow).

The simulated vapour pressure curve was presented earlier in Figure 8-32. It is clear that the simulation data matches the experimental data (Smith and Srivastava [1986a]) very well, with an average percentage difference of only 3.58 %. The phase co-existence data predicted for n-pentane was also good (Figure 8-33). The liquid phase simulation densities were slightly smaller than the experimental values, whereas the vapour phase densities were somewhat larger. Thus, the phase co-existence curve calculated using molecular simulation lies just inside the experimental curve. The average percentage deviations were 2.606 % and 4.508 % for the liquid and vapour phase densities respectively.

9.8.1.2 Methanol

The first step in simulating methanol was to determine the Stockmayer parameters using the method of van Leeuwen [1994b]. The necessary experimental inputs are the dipole moment, the critical temperature and the liquid density at $T_r = 0.75$. An iterative calculation

procedure was then followed using an Excel spreadsheet set up for the express purpose of determining the Stockmayer parameters (refer to Section 4.2.2.1). The values that were found for methanol were as follows: ε/k_B = 359.00 K, σ = 3.804 Å^3 and μ^* = 1.035. These values corresponded extremely well with those obtained by van Leeuwen [1994b], which were ε/k_B = 359.0 K, σ = 3.803 Å^3 and μ^* = 1.036.

The Ewald parameters were also evaluated using the procedure laid out in Section 6.4.4. The values eventually selected for the Ewald parameters provided the optimum between relatively short simulation times (the average simulation times were between 15 and 25 hours) and accurate results. The Gaussian distribution parameter, α_E, was taken to be 0.20 and the corresponding number of k-vectors was set to a value of 8 (refer to Section 6.4.4). The methanol simulations were conducted using 400 molecules. Each simulation ran for 80 000 cycles with 25 000 equilibration cycles, leaving 55 000 production cycles during which averages were collected for the various thermodynamic properties of the system (Section 4.1.1). The experimental data were taken from Smith and Srivastava [1986b].

It is obvious from Table 8-19 that the saturated vapour pressures that were predicted from the simulations were far too high. This is reflected by the fact that that the simulation data lie well above the experimental values in Figure 8-34. Furthermore, the slope of the simulation data is too low when compared with the experimental data slope. However, the methanol saturated vapour pressures have been simulated previously by van Leeuwen [1994b] and Mourits and Rummens [1977] (one of the main reasons for selecting methanol for simulation was that the results could be compared to these literature values). The values simulated in this work lie close to both sets of literature data (see Figure 8-34) and, in particular, are almost identical to the values reported by Mourits and Rummens [1977]. This is interesting because Mourits and Rummens [1977] used the gas-viscosity method (see Section 4.2.2) to evaluate their Stockmayer parameters. All three sets of simulated vapour pressure data have approximately the same slope, and all the slopes are not steep enough when compared with the experimental data. The fact that the simulation results produced in this project closely match the values reported in the literature indicates that both the programme code and the simulation procedures are operating correctly.

The phase co-existence curve for methanol is presented in Figure 8-35. The simulated values (both liquid and vapour) are clearly larger than the experimentally measured values. In effect, the simulated coexistence curve is shifted to the right of the experimental curve. The liquid phase density differed from the experimental values by (on average) 6.676 %, with the largest disparity occurring at 377.00 K (7.155 %). Considering the vapour phase densities, it is clear from Table 8-19 that the values determined using molecular simulation were considerably larger than those reported by Smith and Srivastava [1986b]; with the simulation values being between 1.5 and 5 times greater than the experimental figures. Intriguingly, the relative errors decreased as the system temperature increased (i.e. the largest errors were incurred at the lower temperatures), whilst the opposite trend was observed in the liquid phase density measurements with the observed errors increasing with temperature. The reasons for the poor comparison between the simulation results and the experimental values for the polar compounds are discussed in Section 9.8.3.

9.8.1.3 Acetic Acid

Using a similar spreadsheet to that employed for methanol, the Stockmayer parameters were evaluated for acetic acid: ε/k_B = 435.57 K, σ = 4.356 Å^3 and μ^* = 0.7805. Again, these values are almost identical to those reported by van Leeuwen [1994b]: ε/k_B = 435.6 K, σ = 4.356 Å^3 and μ^* = 0.781. The same Ewald parameters were used for the acetic acid simulations as was discussed for methanol in Section 9.8.1.2. However, for the acetic acid system a longer equilibration time was necessary (i.e. the number of cycles required for the system properties to stop fluctuating excessively was higher). Hence, 55 000 equilibration cycles were permitted before the simulation began to gather system averages.

The total number of cycles was kept at 80 000 cycles in the interest of keeping the simulations as short as possible. This allowed 25 000 production cycles during which averages were collected for the various system properties. This did not effect the accuracy of the final result at all since such a long equilibration time ensured that by the time the programme began to calculate averages, the system was at equilibrium and the system properties were hardly varying. In fact, by increasing the equilibration time the accuracy

was improved because no significantly incorrect figures were incorporated into the system averages. This was reflected in the pronounced reduction in the standard deviations determined for each quantity (e.g. pressure, number of molecules in each phase, box volumes) reported by the simulation.

The number of molecules was lowered to 300 molecules for acetic acid in an effort to lessen the required simulation time. Despite this significant reduction in the number of interactions that needed to be calculated during each cycle, a single simulation still took approximately 20 hours to run to completion. The thermodynamic property compilation of Vargaftik [1975] was consulted when obtaining the pure component vapour pressures and densities for acetic acid.

As was found for the methanol simulations, the vapour pressures predicted were considerably higher than the experimental values. This fact is borne out in Figure 8-36, with the simulation data lying above the experimental data and, again, it is obvious that the simulation data have a gentler slope. Figure 8-36 also indicates that the relative difference between the experimental values and those predicted via simulation is decreasing as temperature increases. The data presented in Table 8-20 backs up this observation: at 323.15 K the simulation vapour pressure is approximately six times larger than the corresponding experimental figure, but by the time the temperature reaches 443.15 K this disparity has diminished to the point that the predicted value is little more than twice the experimental value.

Table 8-20 contains the phase co-existence data predicted for acetic acid and these figures are portrayed graphically in Figure 8-37. As was observed for methanol, the simulated values (in both phases) are as a rule larger than those determined via experimentation. The liquid phase densities exhibited an average percentage difference of 5.768 %, with the maximum error of 7.254 % occurring at the highest temperature (443.15 K). Considering the vapour phase densities, it is again clear that the predicted values are considerably higher than the experimental values quoted in the literature. However, the disparity between the simulated and experimental values is lower than was observed for methanol. Once again, a

trend is observed between the system temperature and the percentage errors: in the vapour phase the error diminishes as temperature increases, whereas for the liquid phase the exact opposite trend occurs with the errors becoming steadily larger.

It is clear from the pure component simulation data that have been presented here for methanol and acetic acid that Stockmayer fluids are not capable of accurately predicting real polar fluids. The vapour pressures are characteristically too high and the predicted densities tend to be too large. Probable reasons for these short-comings are discussed in Section 9.8.3. A viable means of improving these results is the development of a superior potential model (see the recommendations proposed in Chapter 11). This possibility is to be the focus of further research in the area of molecular simulation.

9.8.2 Binary System Simulation

The pure component simulations were conducted using the *NVT* version of the Gibbs ensemble in which the number of molecules, total system volume and system temperature were held constant. However, for the methanol (1) – acetic acid (2) binary system the *NPT* version of the Gibbs ensemble had to be employed. Thus, while the number of molecules and system temperature were still constant, now the volume of each box could fluctuate independently. Thus, a good initial guess for the liquid and vapour phase box sizes was necessary. If these initial values were too inaccurate then the simulations would usually fail.

The system temperature was another crucial input parameter. If the temperature was set too high, the simulation would produce two vapour boxes because it attempted to predict a superheated vapour situation i.e. the predicted point would lie above the phase envelope. Similarly, if the system temperature was set too low, a sub-cooled liquid condition arose and two liquid boxes would result. Analogous constraints held for the overall initial composition. This value had to be such that (combined with the temperature) the starting point for the simulation lay within the system phase envelope; allowing the simulation to separate into distinct liquid and vapour phases. Since these input values are typically rather

uncertain, it becomes difficult to simulate narrow phase envelopes. Thus, it is generally preferable to attempt to predict systems that exhibit broad phase boundaries. This allows for considerable leeway in the initial temperature and composition set-points and avoids the frustration of having simulation after simulation fail due to imprecise starting conditions.

The results of the binary phase diagram simulation are given in Table 8-21 and are presented graphically in Figures 8-38 and 8-39. The simulated system was methanol (1) – acetic acid (2) at atmospheric pressure i.e. 101.325 kPa. The experimental data was taken from the Dortmund Data Bank (DDB) and was selected so that the end-point temperatures fell within the temperature range of the predicted vapour pressure curves (see Sections 8.4.1 and 9.8.1). In general, the simulations were run for 80 000 cycles overall with 30 000 equilibrium cycles. This allowed 50 000 cycles for the system averages to be collected, ensuring that the results were as precise as possible. The system consisted of 400 molecules, with the split between methanol and acetic acid molecules being determined by the overall mole fraction.

It is clear from Figure 8-39 that the predicted phase diagram corresponds poorly with the experimental data. The phase envelope does exhibit the appropriate shape; however, the temperature range is approximately 20 °C too low. Moreover, the phase envelope is too broad i.e. the liquid-phase mole fractions are smaller and the vapour-phase mole fractions larger than they ought to be. This is again apparent in the *x-y* curve shown in Figure 8-38, where this leads to the simulated data lying above the experimental curve. These difficulties again emphasize the shortcomings of the current potential model (refer to Section 9.8.3 below for a more detailed discussion of these limitations) being used to attempt to simulate polar compounds.

9.8.3 Overview

From the results that have been presented in this section, several conclusions may be drawn. Firstly, it is apparent that the technique of molecular simulation is quite capable of producing accurate data for simple hydrocarbons that do not contain complex functional

groups or branched structures (such as n-pentane). Furthermore, more complex, polar compounds may also be simulated. The phase co-existence data produced was satisfactory, and (according to van Leeuwen [1994b]), the method used in this project provides a better approximation of the phase co-existence behaviour of a polar system than the other methods discussed in Section 4.1.1. However, the predicted saturated vapour pressure curves disagreed with the experimental figures: the vapour pressures were too high, with the slope being too gentle (Figures 8-34 and 8-36).

van Leewen [1994b] states that the vapour-pressures of hydrogen bonding species (such as methanol and acetic acid) cannot be accurately accounted for by the dipole moment. This indicates that the Stockmayer potential is too simple for the modelling of real fluids, and in particular, fluids that exhibit hydrogen bonding. These association effects may be better represented if the potential incorporated other electrostatic interactions e.g. higher multipoles, off-centred dipoles and hydrogen-bonding. In addition, non-sphericity of a molecule also contributes towards deviations from corresponding-states behaviour (refer to Section 4.2) and these configurational properties are not taken into account in the Stockmayer potential (van Leeuwen [1994b]). Furthermore, the deviation from corresponding-states behaviour for a real polar fluid differs quantitatively from that for a Stockmayer fluid. This is clearly demonstrated by the discrepancies visible between the predicted and experimental data of the two polar compounds (methanol and acetic acid).

An interesting point raised by van Leeuwen [1994b] is that the deviation from the experimental data is of the same order of magnitude for different substances. This implies that there is a systematic and consistent error that is introduced when using the Stockmayer potential to simulate polar compounds. Thus, it is likely that the procedure used in this work may be combined with an improved potential model for polar fluids to produce highly accurate results.

The physical significance of the reduced dipole moment should also be mentioned. This quantity gives an indication of the ratio between polar and non-polar interactions. Thus, a low value for μ^* implies that a compound is weakly polar e.g. carbon monoxide (μ^* =

0.137) and a high value for μ^* indicates a strongly polar compound such as water (μ^* = 1.560) or acetonitrile (μ^* = 2.838). Methanol and acetic acid lie somewhere between these two extremes; with values for the reduced dipole moment of 1.036 and 0.781 respectively.

The parameters used during the simulations were selected so as to ensure that the best possible results were obtained for a given run. At the outset of this portion of the project, several problems existed for the dipole simulations. Initially, energy drifts were occurring during the simulation which resulted in errors when the final energy balancing was undertaken. This problem was solved through selection of the correct Ewald parameters (α_E = 0.20 with 8 *k*-vectors). The cut-off radius needed to be set at 14 Å in order to produce satisfactory saturated vapour pressures. However, this led to complications in that the programme ends and reports an error if the box length reaches a length of twice the cut-off radius. This is due to the fact that if the box length is less than this distance then certain molecules will be reflected more than once in the mirror images used by the simulation code to generate the thermodynamic properties of the system in question. As a result, the starting box volumes had to be carefully selected to ensure that the liquid box length would not be too small at equilibrium. Despite an effort to avoid this occurrence, a number of simulations crashed due to this problem with the cut-off radius. However, the starting volumes could not be made too large because then the simulations would not form a liquid phase. Thus, there was a delicate balance that had to be found between the starting box volumes, the final box volumes and the cut-off radius.

A further complication that became apparent was that the vapour phase box would frequently empty completely; clearly resulting in erroneous system averages. The pressure would instantly become zero while the heat of vapourization would return a value of positive infinity. To avoid this situation, the box volumes were again called into play. Increasing the overall (i.e. combined) box volume tended to draw molecules across from the liquid phase into the vapour phase, producing the desired configuration i.e. a few molecules in the vapour box to allow the vapour properties to be determined and the majority of the molecules in the smaller liquid box to generate the correct liquid density.

CHAPTER
10

CONCLUSION

10.1 Measurement of Experimental Data

A glass, re-circulating vapour-liquid equilibrium (VLE) still was utilized in this project to determine experimental data pertaining to carboxylic acids. The still was previously used to obtain VLE data by Joseph et al. [2001] and Joseph et al. [2002] and is described in exacting detail by Joseph et al. [2001]. The still was computer controlled in both isobaric and isothermal operating modes using a pulse-width modulation control strategy. This permitted a fine degree of control over the temperature and pressure. In isobaric mode, the pressure was controlled to within 0.01 kPa, and in isothermal mode the temperature control was maintained to within a limit of 0.01 to 0.05 °C (depending on species volatility). A full description of the VLE still is presented in Chapter 5.

The initial phase of the project involved the measurement of vapour pressure data for seven carboxylic acids: propionic, butyric, isobutyric, valeric, isovaleric, hexanoic and heptanoic acids. Thereafter, the binary VLE systems were measured, starting with the cyclohexane (1) – ethanol (2) system at 40 kPa. This system served as a test system, ensuring the correct functioning of the equipment and procedures employed in this project. The test system data were in excellent agreement with two sets of published literature data and, hence, a high degree of confidence was placed, not only in the methods and equipment being used, but also in the new data that were measured. The new VLE data were acquired

for two carboxylic acid systems: propionic acid (1) – valeric acid (2) and isobutyric acid (1) – valeric acid (2). For each system, an isobar at 20 kPa and three isotherms (at 120, 130 and 140 °C respectively) were measured.

The molecular simulation portion of the work was carried out using a Linux-operated, Beowulf cluster consisting of a master node and nineteen slave nodes (i.e. computers). Pure component vapour pressure and phase-coexistence data were simulated for three species, namely n-pentane, methanol and acetic acid. A single binary phase diagram was also predicted for the methanol (1) – acetic acid (2) system at 101.325 kPa.

10.2 Experimental Data Analysis

10.2.1 Vapour Pressure Data

The vapour pressure data measured for the carboxylic acids were regressed to obtain parameters for both the Antoine and the Reid et al. [1988] equations. These parameters are tabulated in Section 9.2.1. In addition, acentric factors and parameters for the alpha function of Twu et al. [1991] were acquired through regression of the vapour pressure data. This pure component data was then utilized in the VLE data regression discussed below.

10.2.2 VLE Data Regression

The experimental VLE data were regressed using two different reduction methods. The first method is commonly referred to as the combined method because liquid-phase activity coefficients are utilized to account for the liquid phase non-idealities, whilst fugacity coefficients serve the same purpose in the vapour phase. The combined method data reduction was conducted using Barker's method of optimization, in conjunction with three local-composition based activity coefficient models: the Wilson [1964], NRTL (Renon and Prausnitz [1968]) and UNIQUAC (Abrams and Prausnitz [1975]) models. The vapour-phase deviations from ideality were accounted for using second virial coefficients determined from various methods: the Pitzer-Curl [1957] correlation, the Hayden and

O'Connell [1975] approach and the chemical theory of gas imperfections. The second modeling technique used in this work is generally termed the direct method, since the liquid and vapour non-idealities are described using fugacity coefficients. The Peng-Robinson equation of state (Peng and Robinson [1976]) was employed, in combination with the Wong-Sandler [1992] and Twu-Coon [1996] mixing rules.

The parameters obtained for the various models are presented in tabular form in Section 9.4. All the models provided (in general) an acceptable fit to the experimental data, with only minor deviations between the calculated and measured pressures (or temperatures) and compositions. The pressure and temperature deviations were generally minimized when using the combined method with the Pitzer-Curl correlation, whereas the vapour phase composition deviations were lowest for the combined method with the chemical theory of vapour imperfections. The equation of state deviations lay, by and large, between those attained by the two combined methods.

The liquid-phase activity coefficients were evaluated from the experimental VLE data, but the established method for calculating these quantities produced exceedingly poor results (see Section 9.3). This difficulty was eliminated by applying the chemical theory to the liquid phase. However, the models used in this work proved incapable of adequately fitting the experimental activity coefficients.

10.2.3 Thermodynamic Consistency Testing

Two thermodynamic consistency tests were applied in order to determine whether the binary VLE data were consistent or not: the point test (Van Ness at al. [1973]) and the direct test of Van Ness [1995]. As was mentioned in Section 10.2.2, the models used in this work to fit the liquid-phase activity coefficients could not satisfactorily match the experimental activity coefficients. Thus, the crucial root mean square values calculated from the $\delta\ln(\gamma_1/\gamma_2)$ residuals as part of the direct test were adversely effected. This was discussed in greater detail in Sections 9.4.3.1 and 9.4.3.2 and meant that the results of the

direct test proved to be inconclusive with regards to determining the thermodynamic consistency of the experimental VLE data.

However, the point test gave a far more reliable indication of the consistency of the measured data. All of the experimental VLE data gathered in this project proved to be consistent according to the point test. In addition, the systems all passed the direct test, although the results were not always good (for the reason discussed above). Thus, it is concluded that the VLE data measured in this project are all thermodynamically consistent.

10.2.4 Infinite Dilution Activity Coefficients

The isothermal VLE data were analyzed using the method of Ellis and Jonah [1962] (as modified by Maher and Smith [1979]) in an attempt to determine the infinite dilution activity coefficients. Unfortunately, the required plots displayed too much scatter in the dilute regions for the infinite dilution activity coefficients to be evaluated with any degree of accuracy. This is discussed more extensively in Section 9.6.

10.2.5 Excess Thermodynamic Properties

The excess thermodynamic properties were calculated for both acid systems using the Gibbs-Hermholtz equation. The molar excess enthalpy, excess Gibbs energy and excess entropy were evaluated and plotted against the liquid mole fraction. The heat-of-mixing data (i.e. excess enthalpy) constitutes new data.

10.2.6 Molecular Simulation

The pure component vapour pressures and density data predicted for n-pentane showed an excellent agreement with the experimental data obtained from literature. This was expected since straight-chain alkanes are relatively easy to simulate. The pure component data of the two polar compounds (namely, methanol and acetic acid) were then predicted. The method proposed by van Leeuwen [1994b] using the Stockmayer potential to simulate polar

molecules was employed. This required that Stockmayer and Ewald parameters be determined for both methanol and acetic acid. The simulation results showed a significant deviation from the experimental data. However, the same results were previously reported for methanol by van Leeuwen [1994b]. These discrepancies between the experimentally measured data and that predicted using molecular simulation highlights the inadequacy of the currently available potential models for predicting the behaviour of polar compounds.

A binary system consisting of methanol and acetic acid was also predicted. As expected, the simulation data did not correspond well with the literature data. The temperatures predicted were too low and the phase envelope was too broad. However, the general shape of the phase diagram agreed well with that exhibited by the experimental data.

CHAPTER
11

RECOMMENDATIONS

The work completed in this project has revealed several areas that warrant greater investigation. These areas are highlighted below, along with various recommendations pertaining to the study of carboxylic acids:

1. The modeling of the carboxylic acid systems needs to be improved. Several cubic equations of state exist that incorporate association (see Section 3.4.2.2) and should be investigated as a means of improving the fit to the experimental data. In addition, more complicated equations of state such as SAFT (statistical associated fluid theory, developed by Chapman et al. [1989, 1990]), the ERAS (extended real-associated-solution) model proposed by Heintz [1985] and the lattice-fluid-association (LFAS) model of Panayiotou [1991] have been used (amongst others) to obtain good agreement between calculated and measured data for systems containing highly polar compounds. The equation of state modeling carried out in this project serves as a precursor to these more complicated equations of state, which are to be used in future work.
2. An investigation into alternative methods for calculating the infinite dilution activity coefficients from experimental VLE data should be conducted. One possibility is the inclusion of chemical theory to account for the association effects exhibited by the carboxylic acids.
3. Another option available (if the infinite dilution activity coefficients cannot be determined from the VLE data) is to measure the infinite dilution activity

coefficients directly. A number of methods exist by which such data may be obtained, with the principle techniques according to Raal and Mühlbauer [1998] being differential ebulliometry, use of a differential static apparatus, gas chromatographic methods and inert gas stripping. These methods are covered in greater detail in the excellent text of Raal and Mühlbauer [1998].

4. The Stockmayer potential used in this work to simulate polar compounds was found to be inadequate. It is therefore recommended that other potential models, such as the OPLS (Jorgensen [1986]), AMBER94 (Cornell et al. [1995]) and MMFF94 (Halgren [1996]) models should be researched and implemented in an effort to improve the simulation predictions. The OPLS force field (Jorgensen [1986]) in particular has been used previously to simulate alcohols and may well prove applicable to carboxylic acids.
5. An additional possibility is to develop a new force field or potential model that applies specifically to carboxylic acids and carboxylic acid systems. This would allow the model to be designed in such a way that it produces highly accurate results for carboxylic acids, although its generality and transferability to other systems might suffer.
6. It is also recommended that the effect of varying the Ewald parameters (α_E and the number of k-vectors) should be explored. It is possible that increasing the value of these parameters could result in more accurate results. However, this would carry the disadvantage of greatly increased simulation times.

REFERENCES

Abrams, D S and Prausnitz, J M, (1975), "Statistical Thermodynamics of Liquid Mixtures: A New Expression for the Excess Gibbs Energy of Partly or Completely Miscible Systems", *American Institute of Chemical Engineering Journal*, Vol. 21, pp. 116-127.

Allen, M P and Tildesley, D J, (1987), "Computer Simulation of Liquids", Oxford Science Publications, Oxford.

Anderson, T F and Prausnitz, J M, (1978), "Application of the UNIQUAC Equation to Calculation of Multicomponent Phase Equilibria. 1: Vapour-Liquid Equilibria; 2: Liquid-Liquid Equilibria", *Industrial and Engineering Chemistry. Process Design and Development*, Vol. 17, pp. 552-567.

Barker, J A, (1953), "Determination of Activity Coefficients from Total Pressure Measurements", *Australian Journal of Chemistry*, Vol. 6, pp. 207-210.

Black, C, (1958), "Vapour Phase Imperfections in Vapour-Liquid Equilibria", *Industrial and Engineering Chemistry*, Vol. 50, pp. 391-402.

Bruice, P Y, (1998), "Organic Chemistry", 2nd edition, Prentice-Hall, Inc., New Jersey.

Chapman, W G, Gubbins, K E, Jackson, G and Radosz, M, (1989), "SAFT: Equation-of-State Solution Model for Associating Fluids", *Fluid Phase Equilibria*, Vol. 52, pp. 31-38.

Chapman, W G, Gubbins, K E, Jackson, G and Radosz, M, (1990), "New Reference Equation of State for Associating Fluids", *Industrial and Engineering Chemistry Research*, Vol. 29, pp. 1709-1721.

Cholinski, J, Szafranski, A and Wyrzykowska-Stankiewicz, D, (1986), "Computer Aided Second Virial Coefficient Data for Organic Individual Compounds and Binary Systems", PWN-Polish Scientific Publishers, Warsaw.

Cornell, W D, Cieplak, P, Bayly, C I, Gould, I R, Merz, K M, Ferguson, D M, Spellmeyer, D C, Fox, T, Caldwell, J W and Kollman, P A, (1995), "A Second Generation Force Field for the Simulation of Proteins, Nucleic Acids, and Organic Molecules", *Journal of the American Chemical Society*, Vol. 117, pp. 5179-5197.

Danner, R P and Gess M A, (1990), "A Data Base Standard for the Evaluation of Vapour-Liquid Equilibrium Models", *Fluid Phase Equilibria*, Vol. 56, pp. 285-301.

de Leeuw et al., S W, Perram, J W and Smith, E R, (1980), "Simulation of Electrostatic Systems in Periodic Boundary Conditions. I. Lattice Sums and Dielectric Constants", *Proceedings of the Royal Society of London*, Vol. A373, pp. 26-56.

Dortmund Data Bank Software, purchased 1998.

Dymond, J H and Smith, E B, (1980), "The Virial Coefficients of Gases and Gaseous Mixtures", Clarendon Press, Oxford.

Ellis, S R M and Jonah, D A, (1962), "Prediction of Activity Coefficients at Infinite Dilution", *Chemical Engineering Science*, Vol. 17, pp. 971-976.

Errington, J R and Panagiotopoulos, A Z, (1999), "A New Intermolecular Potential for the n-Alkane Homologous Series", *Journal of Physical Chemistry B*, Vol. 103, pp. 6314-6322.

Fredunslund, A, Gmehling, J and Rasmussen, P, (1977), "Vapour-Liquid Equilibria using UNIFAC", Elsevier, Amsterdam.

Frenkel, D and Smit, B, (1996), "Understanding Molecular Simulation: From Algorithms To Applications", Academic Press, San Diego.

Gao, G, Wang, W and Zeng, X C, (1997), "Vapour-Liquid Equilibria for Pure HCFC/HFC Substances by Gibbs Ensemble Simulation of Stockmayer Potential Molecules", *Fluid Phase Equilibria*, Vol. 137, pp. 87-98.

Gautreaux, M F and Coates, J, (1955), "Activity Coefficients at Infinite Dilution", *American Institute of Chemical Engineers. Journal*, Vol. 1, pp. 496-500.

Gess, M A, Danner, R P and Nagvekar, M, (1991), "Thermodynamics Analysis of Vapour-Liquid Equilibria: Recommended Models and a Standard Data Base", Design Institute for Physical Property Data, American Institute of Chemical Engineers.

Gmehling, J and Onken, U, (1977), "Vapour-Liquid Equilibrium Data Collection", DECHEMA Chemistry Data Series, Frankfurt/Main.

Halgren, T A, (1996), "Merck Molecular Force Field. I. Basis, Form, Scope, Parameterization, and Performance of MMFF94", *Journal of Computational Chemistry*, Vol. 17, pp. 490-519.

Harlacher, E A and Braun, W G, (1970), "A Four-Parameter Extension of the Theorum of Corresponding", *Industrial and Engineering Chemistry., Process Design and Development*, Vol. 9, pp. 479-483.

Hartwick, R P and Howat, C S, (1995), "Infinite Dilution Activity Coefficients of Acetone in Water. A New Experimental Method and Verification", *Journal of Chemical and Engineering Data*, Vol. 40, pp. 738-745.

Hayden, J G and O'Connell, J P, (1975), "A Generalized Method for Predicting Second Virial Coefficients", *Industrial and Engineering Chemistry., Process Design and Development*, Vol. 14, pp. 209-216.

Heidemann, R A and Prausnitz, J M, (1976), "A van der Waals-type Equation of State for Fluids with Associating Molecules", *Proc. Natl. Acad. Sci.*, Vol. 73, pp. 1773-1776.

Heintz, A, (1985), "A New Theoretical Approach for Predicting Excess Properties of Alkanol/Alkane Mixtures", *Berichte der Bunsen-Gesellschaft – Physical Chemistry*, Vol. 89, pp. 172-181.

Herington, E F G, (1947), "A Thermodynamic Consistency Test for the Internal Consistency of Experimental Data of Volatility Ratios", *Nature*, Vol. 160, pp. 610-611.

Huron, M J and Vidal, J, (1977), "New Mixing Rules in Simple Equations of State for Representing Vapour-Liquid Equilibria in Strongly Non-Ideal Mixtures", *Fluid Phase Equilibria*, Vol. 3, pp. 255-271.

Jorgensen, W L, (1986), "Optimized Intermolecular Potential Functions for Liquid Alcohols", *Journal of Physical Chemistry*, Vol. 90, pp. 1276-1284.

Joseph, M A, Raal, J D and Ramjugernath, D, (2001), "Phase Equilibrium Properties of Binary Systems with Diacetyl from a Computer Controlled Vapour-Liquid Equilibrium Still", *Fluid Phase Equilibria*, Vol. 182, pp. 157-176.

Joseph, M A, Raal, J D and Ramjugernath, D, (2002), "Computer-aided Measurement of Vapour-Liquid Equilibria in a Dynamic Still at Sub-Atmospheric Pressures", *Developments in Chemical Engineering Mineral Processes*, Vol. 10, pp. 615-637.

Kato, M, Yoshikawa, H and Yamaguchi, M, (1990), "Vapour-Liquid Equilibrium Measurements of Three Binary Systems Made of Formic Acid, Acetic Acid and Propionic Acid by the Dew-Point Temperature Method", *Fluid Phase Equilibria*, Vol. 54, pp. 47-56.

Klekers, A J and Scheller, W A, (1968), "Isothermal Vapour-Liquid Equilibrium Data for the System Formic Acid – Valeric Acid at 50 °, 75 °, and 100 °C", *Journal of Chemical Engineering Data*, Vol. 13, pp. 480-482.

Kneisl, P, Zondlo, J W and Wallace, B W, (1989), "The Effect of Fluid Properties on Ebulliometer Operation", *Fluid Phase Equilibria*, Vol. 46, pp. 85-94.

Kreglewski, A, (1969), "Second Virial Coefficients of Real Gases", *Journal of Physical Chemistry*, Vol. 73, pp. 608-615.

Maher, P J and Smith, B D, (1979), "Infinite Dilution Activity Coefficient Values from Total Pressure VLE Data. Effect of Equation of State Used", *Journal of Chemical and Engineering Data*, Vol. 24, pp. 16-22.

Malijevská, I, Sýsová, M and Vlčková, D, (1986), "Vapour-Liquid Equilibrium in Strongly Associated Systems. The Systems Acetic Acid – Propionic Acid and Acetic Acid – Trifluoroacetic Acid", *Collection Czechoslovak Chem. Commun*, Vol. 51, pp. 194-205.

Marquadt, D W, (1963), "An Algorithm for Least-Squares Estimation of Non-Linear Parameters", *Journal. Society of Industrial and Applied Mathematics*, Vol. 11, pp. 431-441.

Martin, M G and Siepmann, J I, (1998), "Transferable Potentials for Phase Equilibria. 1. United-Atom Description of n-Alkanes", *Journal of Physical Chemistry B*, Vol. 102, pp. 2569-2577.

McClellan, A L, (1963-1974), "Tables of Experimental Dipole Moments", W. H. Freeman, San Francisco.

Metropolis, N, Rodenbluth, A W, Rosenbluth, M N, Teller, A H and Teller, E, (1953), "Equation of State Calculations by Fast Computing Machines", *Journal of Chemical Physics*, Vol. 21, pp. 1087-1092.

Miyamoto, S, Nakamura, S, Iwai, Y and Arai, Y, (2001), "Measurement of Isothermal Vapour-Liquid Equilibria for Monocarboxylic Acid + Monocarboxylic Acid Binary Systems with a Flow-Type Apparatus", *Journal of Chemical Engineering Data*, Vol. 46, pp. 405-409.

Morachevsky, A G and Zharov, V T, (1963), *Zhurnal Prikladnoi Khimii*, Vol. 36, pp 2771 as reported by Gmehling, J and Onken, U, (1977), "Vapour Liquid Equilibrium Data Collection, Organic Hydroxy Compounds:Alcohols", Vol. 1, Part 2a, 429, DECHEMA, Frankfurt/Main.

Mourits, F M and Rummens, F H A, (1977), "A Critical Evaluation of Lennard-Jones and Stockmayer Potential Parameters and of Some Correlation Methods", *Canadian Journal of Chemical Engineering*, Vol. 55, pp. 3007-3020.

Münsch, E, (1979), "Calculation of the Enthalpy of Mixing from Vapour-Liquid Equilibria", *Thermochimica Acta*, Vol. 32, pp.151-164.

Nath, S K, Escobedo, F A and de Pablo, J J, (1998), "On the Simulation of Vapour-Liquid Equilibria for Alkanes", *Journal of Chemical Physics*, Vol. 108, pp. 9905-9911.

Nath, S K, Banaszak, B J and de Pablo, J J, (2001), "A New United Atom Force Field for α-Olefins", *Journal of Chemical Physics*, Vol. 114, pp. 3612-3616.

Nothnagel, K-H, Abrams, D S and Prausnitz, J M, (1973), "Generalized Correlation for Fugacity Coefficients in Mixtures at Moderate Pressures", *Industrial and Engineering Chemistry., Process Design and Development*, Vol. 12, pp. 25-35.

O'Connell, J P and Prausnitz, J M, (1967), "Empirical Correlation of Second Virial Coefficients for Vapour-Liquid Equilibrium Calculations", *Industrial and Engineering Chemistry., Process Design and Development*, Vol. 6, pp. 245-250.

Orbey, H and Sandler, S I, (1996), "A Comparison of Various Cubic Equation of State Mixing Rules for the Simultaneous Description of Excess Enthalpies and Vapour-Liquid Equilibria", *Fluid Phase Equilibria*, Vol. 121, pp. 67-83.

Panagiotopoulos, A Z, (1987), "Direct Determination of Phase Coexistence Properties of Fluids by Monte Carlo Simulation in a New Ensemble", *Molecular Physics*, Vol. 61, pp. 813-826.

Panagiotopoulos, A Z, Quirke, N, Stapleton, M and Tildesley, D J, (1988), "Phase Equilibria by Simulation in the Gibbs Ensemble. Alternative Derivation, Generalization and Application to Mixture and Membrane Equilibria", *Molecular Physics*, Vol. 63, pp. 527-545.

Panayiotou, C and Sanchez, I C, (1991), "Hydrogen Bonding in Fluids: Equation of State Approach", *Journal of Physical Chemistry*, Vol. 95, pp. 10090-10097.

Peng, D. Y. and Robinson, D. B. (1976), "A New Two Constant Equation of State", *Industrial and Engineering Chemistry Fundamentals*, Vol. 15, pp. 59-64.

Pitzer, K S, Lippmann, D Z, Curl, R F, Huggins, C M and Petersen, D E, (1955), "The Volumetric and Thermodynamic Properties of Fluids. II. Compressibility Factor, Vapour Pressure and Entropy of Vapourization", *Journal of the American Chemical Society*, Vol. 77, pp. 3433.

Pitzer, K S and Curl, R F, (1957), "Empirical Equation for the Second Virial Coefficient", *Journal of the American Chemical Society,* Vol. 79, pp. 2369-2370.

Pividal, K A, Britigh, A and Sandler, S I, (1992), "Infinite Dilution Activity Coefficients for Oxygenate Systems Determined Using a Differential Static Celll", *Journal of Chemical and Engineering Data*, Vol. 37, pp. 484-487.

Polak, J and Lu, B C-Y, (1972), "Second Virial Coefficients of Polar Gases – a Correlation with Stockmayer Potential Function", *Canadian Journal of Chemical Engineering*, Vol. 50, pp. 553-556.

Prausnitz, J M, (1969), "Molecular Thermodynamics of Fluid-Phase Equilibria", Prentice-Hall, Englewood Cliffs, NJ.

Prausnitz, J M, Anderson, T F, Grens, E A, Eckert, C A, Hseih, R, O' Connell, J P, (1980), "Computer Calculations for Multicomponent Vapour-Liquid and Liquid-Liquid Equilibria", Prentice-Hall, Englewood Cliffs, NJ.

Prausnitz, J M, Lichtenthaler, R N and de Azevedo, E G, (1986), "Molecular Thermodynamics of Fluid-Phase Equilibria", 2nd edition, Prentice-Hall, Englewood Cliffs, NJ.

Prausnitz, J M, Lichtenthaler, R N and de Azevedo, E G, (1999), "Molecular Thermodynamics of Fluid-Phase Equilibria", 3rd edition, Prentice-Hall, Upper Saddle River, New Jersey.

Raal, J D, (2000), "Characterization of Differential Ebulliometers for Measuring Activity Coefficients", *American Institute of Chemical Engineers. Journal*, Vol. 46, pp. 210-220.

Raal, J D and Mühlbauer, A L, (1998), "Phase Equilibria: Measurement and Computation", Taylor and Francis, Bristol, PA.

Raal, J D and Naidoo, P, (1990), "Excess Enthalpy Measurements Using a Novel Highly Refined Microflow Calorimeter and the Prediction of Vapour Liquid Equilibria From Such Data", *Fluid Phase Equilibria*, Vol. 57, pp 147-160.

Rackett, H G, (1970), "Equation of State for Saturated Liquids", *Journal of Chemical and Engineering Data*, Vol. 15, pp. 514-517.

Redlich, O and Kister, A T, (1948), "Algebraic Representation of Thermodynamic Properties and the Classfication of Solutions", *Industrial Engineering Chemistry*, Vol. 40, pp. 345-348.

Redlich, O and Kwong, J, (1949), "On the Thermodynamics of Solutions. V. An Equation of State. Fugacities of Gaseous Solutions" *Chemical Reviews*, Vol. 44, pp. 233-244.

Reid, C R, Prausnitz, J M and Polling, B E, (1977), "The Properties of Gases and Liquids", 3rd edition, McGraw-Hill Book Company, Singapore.

Reid, C R, Prausnitz, J M and Polling, B E, (1988), "The Properties of Gases and Liquids", 4th edition, McGraw-Hill Book Company, Singapore.

Renon, H and Prausnitz, J M, (1968), "Local Compositions in Thermodynamic Excess Functions for Liquid Mixtures", *American Institute of Chemical Engineers. Journal*, Vol. 14, pp. 135-144.

Sandler, S I, Orbey, H and Lee, B, (1994), "Models fro Thermodynamic and Phase Equilibria Calculations", Marcel Dekker, New York.

Scatchard, G, (1949), "Equilibrium in Non-Electrolyte Mixtures", *Chemical Reviews*, Vol. 44, pp. 7-35.

Sewnarain, R, Raal, J D and Ramjugernath, D, (2002), "Isobaric Vapour-Liquid Equilibria for the Systems Propionic Acid + Butyric Acid, Isobutyric Acid + Butyric Acid, Butyric Acid + Isovaleric Acid, and Butyric Acid + Hexanoic Acid at 14 kPa", *Journal of Chemical Engineering Data*, Vol. 47, pp. 603-607.

Siepmann, J I, (1990), "A Method for the Direct Calculation of Chemical Potentials for Dense Chain Systems", *Molecular Physics*, Vol. 70, pp. 1145-1158.

Siepmann, J I and Frenkel, D, (1991), "Configurational Bias Monte Carlo: A New Sampling Scheme for Flexible Chains", *Molecular Physics*, Vol. 75, pp. 59-70.

Smith, B D and Srivastava, R, (1986a), "Thermodynamic Data for Pure Components. Part A: Hydrocarbons and Ketones", Elsevier, Oxford.

Smith, B D and Srivastava, R, (1986b), "Thermodynamic Data for Pure Components. Part B: Halogenated Hydrocarbons and Alcohols", Elsevier, Oxford.

Smith, J M, Van Ness, H C and Abbott, M M, (1996), "Introduction to Chemical Engineering Thermodynamics", 5th edition, McGraw-Hill International Editions, New York.

Smith, W, (1982), "Point Dipoles in the Ewald Summation", *CCP5 Quarterly*, Vol. 4, pp. 13-25.

Smyth, C P, (1955), "Dipole Moment and Molecular Structure", McGraw-Hill, New York.

Soave, G, (1972), "Equilibrium Constants from a Modified Redlich-Kwong Equation of State", *Chemical Engineering Science*, Vol. 27, pp, 1197-1203.

Stryjek, R and Vera, J H, (1986), "PRSV: An Improved Peng-Robinson Equation of State for Pure Compounds and Mixtures", *The Canadian Journal of Chemical Engineering*, Vol. 64, pp. 323-333.

Tamir, A and Wisniak, J, (1975), "Vapour-Liquid Equilibria in Associating Solutions", *Chemical Engineering Science*, Vol. 30, pp. 335-342.

Tsonopoulos, C, (1974), "An Empirical Correlation of Second Virial Coefficients", *American Institute of Chemical Engineers Journal*, Vol. 20, pp. 263-272.

Tsonopoulos, C and Prausnitz, J M, (1970), "Fugacity Coefficients in Vapour-Phase Mixtures of Water and Carboxylic Acids", *Chemical Engineering Journal*, Vol. 1, pp. 273-278.

Tsuboka, T and Katayama, T, (1975), *Journal of Chemical Engineering Japan*, Vol. 8, pp. 181. (As given in Raal and Mühlbauer [1998].)

Twu, C H, (1988), "A Modified Redlich-Kwong Equation of State for Highly Polar, Supercritical Systems", International Symposium on Thermodynamics in Chemical Engineering and Industry, pp. 148-169.

Twu, C H, Bluck, D, Cunningham, J R and Coon, J E, (1991), "A Cubic Equation of State with a New Alpha Function and a New Mixing Rule", *Fluid Phase Equilibria*, Vol. 69, pp. 33-50.

Twu, C H, Coon, J E and Cunningham, J R, (1993), "An Equation of State for Carboxylic Acids", *Fluid Phase Equilibria*, Vol. 82, pp. 379-388.

Twu, C H and Coon, J E, (1996), "CEOS/A^E Mixing Rules Constrained by vdW Mixing Rule and Second Virial Coefficient", *American Institute of Chemical Engineers Journal*, Vol. 42, pp. 3212-3222.

Van Laar, J J, (1910), "The Vapour Pressure of Binary Mixtures", *Zeitschrift feur Physik Chemie*, Vol. 72, pp. 723-751. (As given in Walas [1985].)

van Leeuwen, M E, (1994a), "Deviation from Corresponding States Behaviour for Polar Fluids", *Molecular Physics*, Vol. 82, pp. 383-392.

van Leeuwen, M E, (1994b), "Derivation of Stockmayer Potential Parameters for Polar Fluids", *Fluid Phase Equilibria*, Vol. 99, pp. 1-18.

Van Ness, H C, Byer, S M and Gibbs, R E, (1973), "Vapour-Liquid Equilibrium: Part I. An Appraisal of Data Reduction Methods", *American Institute of Chemical Engineers Journal*, Vol. 19, pp. 238-244.

Van Ness, H C, (1995), "Thermodynamics in the Treatment of Vapour/Liquid Equilibrium (VLE) Data", *Pure and Applied Chemistry*, Vol. 67, No. 6, pp. 859-872.

Van Ness, H C and Abbott, M M, (1982), "Classical Thermodynamics of Nonelectrolyte Solutions: With Applications to Phase Equilibria", McGraw-Hill, New York.

Van Ness, H C and Abbott, M M, (1997), "Perry's Chemical Engineers' Handbook", Section 4, McGraw-Hill Book Company, Singapore.

Van Ness, H C, Pedersen, F and Ramussen, P, (1978), "Part V. Data Reduction by Maximum Likelihood", *American Institute of Chemical Engineers Journal*, Vol. 24, pp. 1055-1063.

Vargaftik, N B, (1975), "Tables on the Thermophysical Properties of Liquids and Gases", 2nd edition, Hemisphere Publishing Corporation, London.

Walas, S M, (1985), "Phase Equilibrium in Chemical Engineering", Butterworth, Boston.

Weast, R C, Astle, M J and Beyer, W H, (1983-1984), "Handbook of Chemistry and Physics", 64th edition, CRC Press: Boca Raton, FL.

Wick, C D, Martin, M G and Siepmann, J I, (2000), "Transferable Potentials for Phase Equilibria. 4. United Atom Description of Linear and Branched Alkenes and Alkylbenzenes", *Journal of Physical Chemistry B*, Vol. 104, pp. 2415-2423.

Wilson, G M, (1964), "Vapour-Liquid Equilibrium. XI: A New Expression for the Excess Free Energy of Mixing", *Journal of the American Chemical Society*, Vol. 86, pp. 127-130.

Wisniak, J and Tamir, A, (1978), "Mixing and Excess Thermodynamic Properties", Elsevier Scientific Publishing Company, Netherlands.

Wong, D S and Sandler, S I, (1992), "A Theoretically Correct Mixing Rule for Cubic Equations of State", *American Institute of Chemical Engineers. Journal*, Vol. 38, No.5, pp. 671-680.

Yerazunis, S, Plowright, J D and Smola, F M, (1964), " Vapour-Liquid Equilibrium Determination by a New Apparatus", *American Institute of Chemical Engineers. Journal*, Vol. 10, pp. 660-665.

APPENDIX

A

PURE COMPONENT PROPERTIES

The pure component properties used in this project are included in this appendix. The critical pressure, temperature, volume and compressibility were easily obtained from the Dortmund Data Bank (DDB). The dipole moments were found in the compilation of McClellan [1974] and the text of Reid et al. [1988], whilst the solvation and association parameters were acquired from Prausnitz et al. [1980]. The mean radius of gyration was determined using the group contribution method proposed by Reid et al. [1977]. The second virial coefficients were calculated using the correlations discussed in Section 3.2.1 and the liquid molar volumes were evaluated via the Rackett [1970] equation (presented in Tables A-2 and A-3).

The acentric factors of the carboxylic acids were determined from the vapour pressure data measured in this work (see Section 9.2.2), as were the parameters (viz. L', M' and N') for the Twu et al. [1991] alpha correlation (refer to Section 9.2.3) and are presented in Table A-1.

The pure component properties that are presented here for carboxylic acids are only for the three acids that comprised the binary vapour-liquid equilibrium systems, since only the acids that were modeled required this data. In addition, certain pure component properties were necessary in order to successfully complete the test system (comprised of cyclohexane and ethanol) modeling, and these figures are also included in Table A-1. The data for the test system was obtained from the DDB and Smith et al. [1996].

Table A-1: Pure component properties used in this project.

Pure component Property	Propionic Acid	Isobutyric Acid	Valeric Acid	Cyclo-hexane	Ethanol
T_c / K	604.0	605.0	639.9	553.5	513.9
P_c / atm	44.70	36.50	35.82	41.24	62.21
V_c / cm^3/mol	230.0	292.0	340.0	308.0	167.1
Z_c	0.2003	0.2148	0.2253	0.2730	0.2400
Dipole Moment / debye	1.76	1.34	1.81	0.30	1.70
Solvation & Association	4.5	4.5	4.5	0.0	1.4
Radius of Gyration / Å	2.682	3.115	3.541	3.261	2.250
Acentric Factor	0.5397	0.6321	0.7165	0.2120	0.6450
L′	0.2636	0.2926	0.7040	-	-
M′	0.7412	0.7176	0.9225	-	-
N′	2.3367	2.3244	2.0869	-	-

Table A-2: Liquid molar volumes and second virial coefficients for the propionic acid (1) – valeric acid (2) system.

Temperature	B_{11} cm^3/mol	B_{22} cm^3/mol	B_{12} cm^3/mol	V_1^L cm^3/mol	V_2^L cm^3/mol
393.15 K	-1429.2	-1916.0	-2552.0	69.932	109.255
403.15 K	-1326.4	-1772.2	-2353.3	71.089	110.722
413.15 K	-1233.9	-1643.1	-2175.3	72.308	112.255

Table A-3: Liquid molar volumes and second virial coefficients for the isobutyric acid (1) – valeric acid (2) system.

Temperature	B_{11} cm^3/mol	B_{22} cm^3/mol	B_{12} cm^3/mol	V_1^L cm^3/mol	V_2^L cm^3/mol
393.15 K	-1814.7	-2150.9	-2552.0	93.414	109.255
403.15 K	-1679.2	-1986.8	-2353.3	94.886	110.722
413.15 K	-1557.5	-1839.6	-2175.3	96.436	112.255

APPENDIX
B

THERMODYNAMIC CONSISTENCY

This appendix contains the graphs utilized in the determination of the thermodynamic consistency of the measured VLE data. Two consistency tests were conducted for each set of experimental data, namely the point test and the direct test. The deviation of the model pressures and temperatures from this experimental data are also presented.

B.1 Cyclohexane (1) – Ethanol (2) Test System

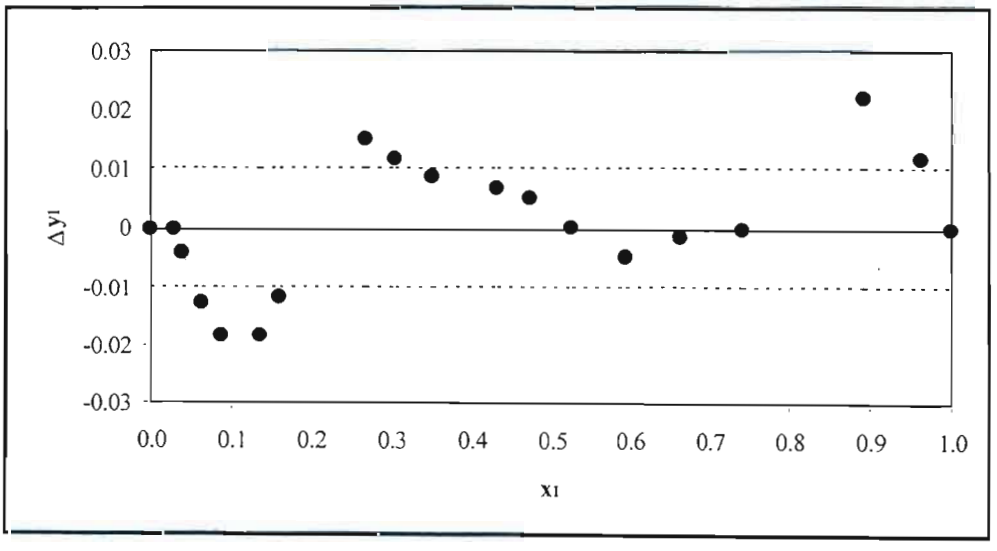

Figure B-1: Graph showing the deviation of the vapour compositions calculated using the NRTL model from the experimental vapour compositions for the cyclohexane (1) – ethanol (2) system at 40 kPa.

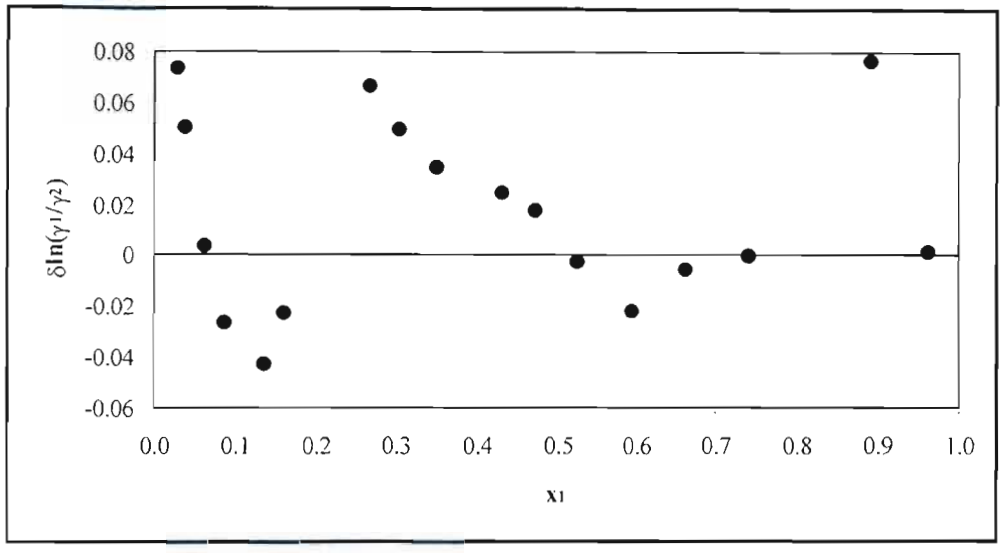

Figure B-2: Graph showing the deviation of the activity coefficients calculated using the NRTL model from the experimental activity coefficients for the cyclohexane (1) – ethanol (2) system at 40 kPa.

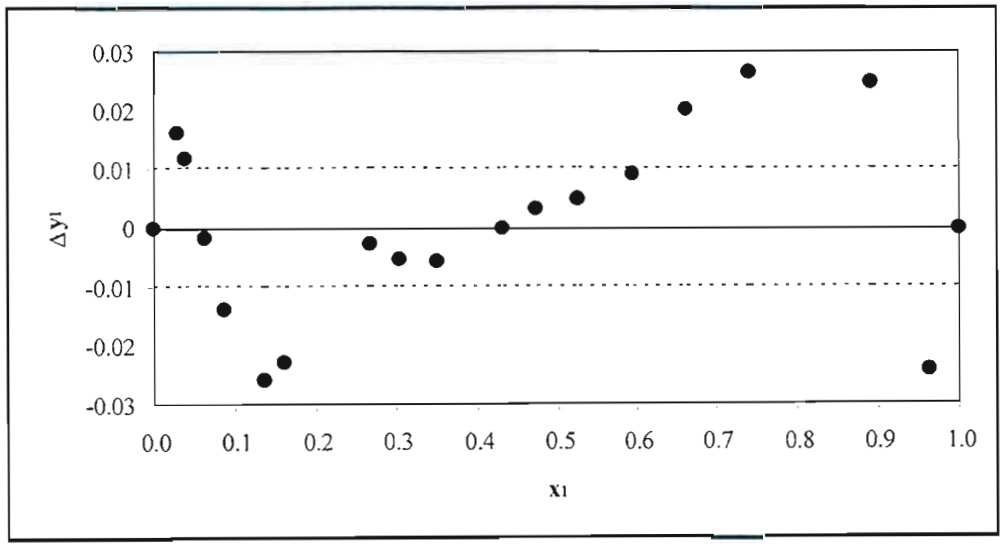

Figure B-3: Graph showing the deviation of the vapour compositions calculated using the UNIQUAC model from the experimental vapour compositions for the cyclohexane (1) – ethanol (2) system at 40 kPa.

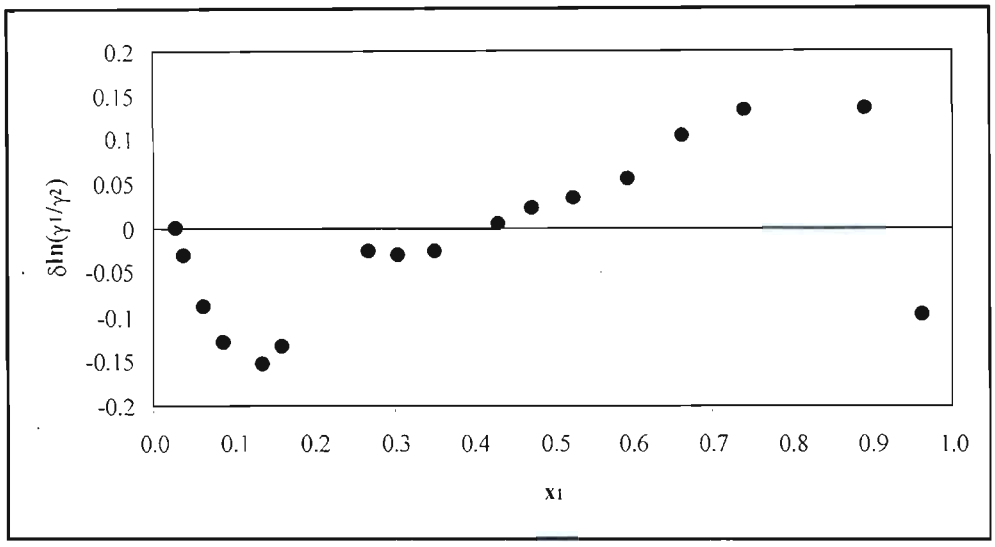

Figure B-4: Graph showing the deviation of the activity coefficients calculated using the UNIQUAC model from the experimental activity coefficients for the cyclohexane (1) – ethanol (2) system at 40 kPa.

B.2 Propionic Acid (1) – Valeric (2) System

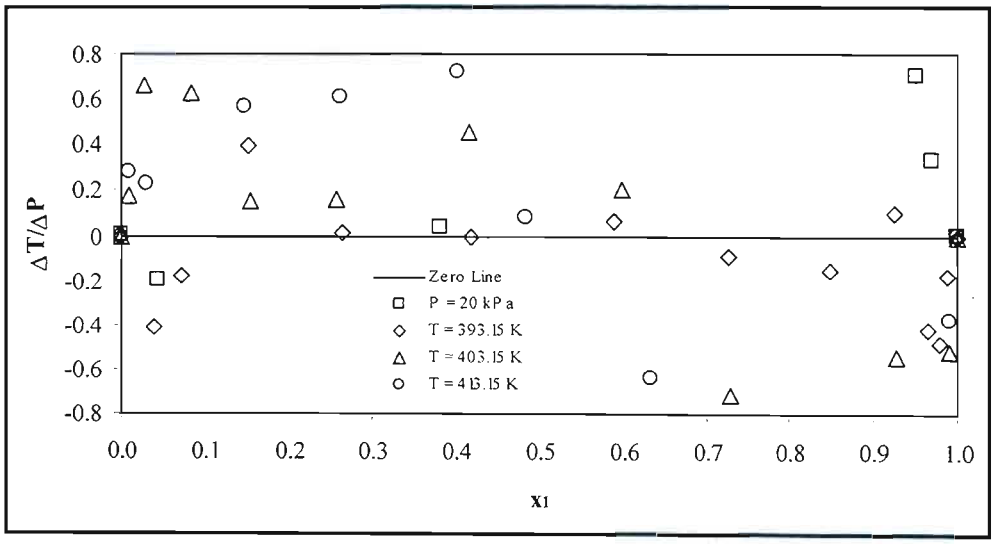

Figure B-5: Graph showing the deviation of the Wilson model (with Pitzer-Curl correlation) pressures and temperatures from the experimental values for the propionic acid (1) – valeric acid (2) system.

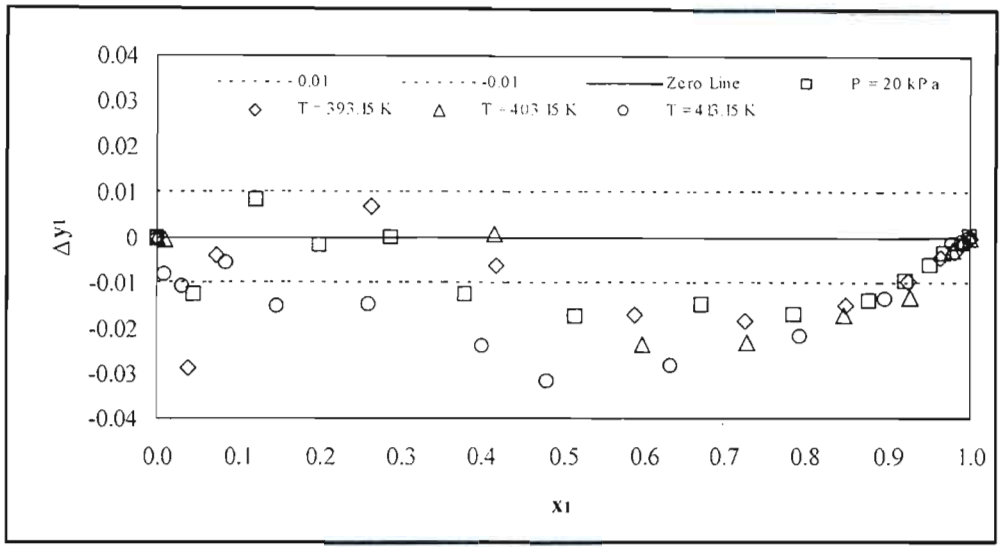

Figure B-6: Graph showing the deviation of the Wilson model (with Pitzer-Curl correlation) vapour compositions from the experimental values for the propionic acid (1) – valeric acid (2) system.

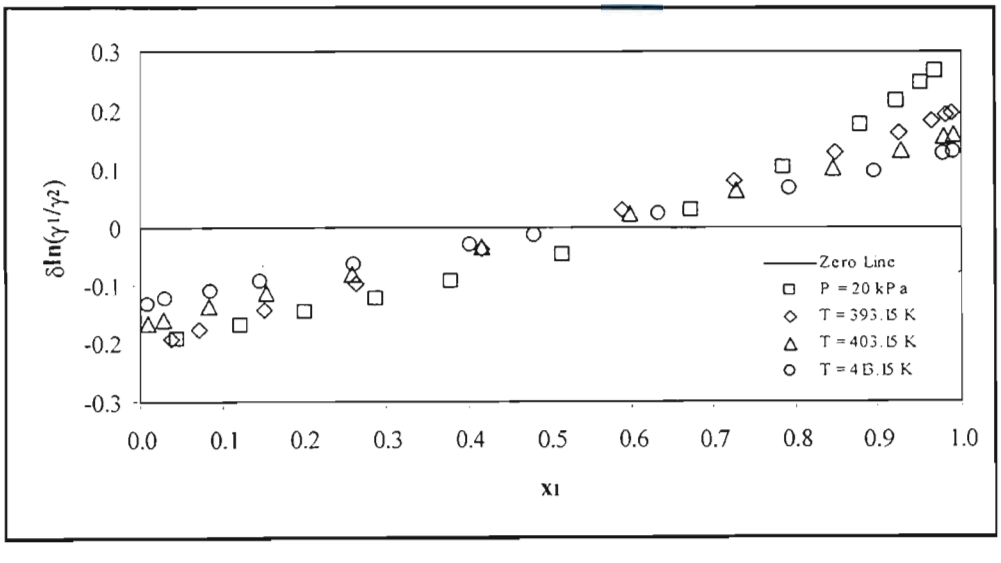

Figure B-7: Graph showing the deviation of the Wilson model (with Pitzer-Curl correlation) activity coefficients from the experimental values for the propionic acid (1) – valeric acid (2) system.

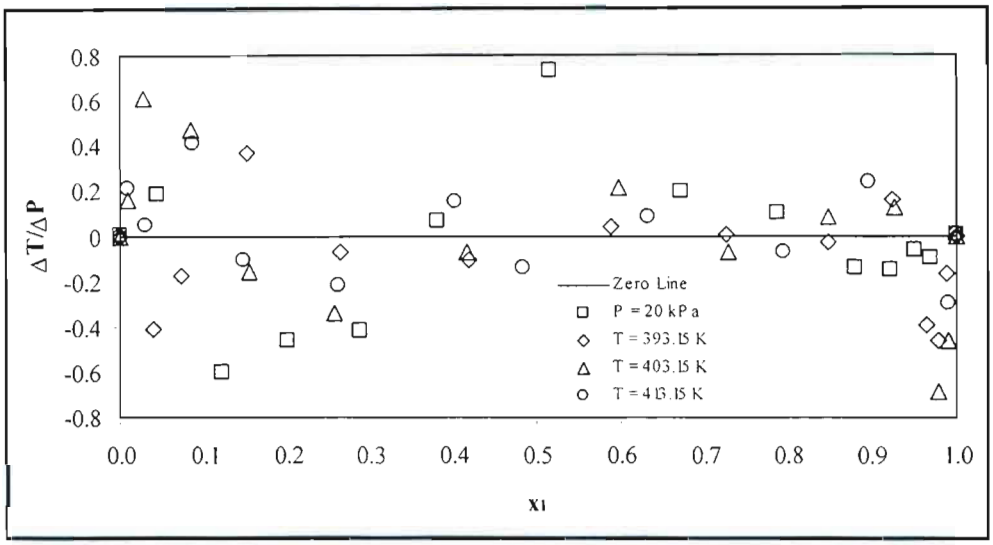

Figure B-8: Graph showing the deviation of the NRTL model (with Pitzer-Curl correlation) pressures and temperatures from the experimental values for the propionic acid (1) – valeric acid (2) system.

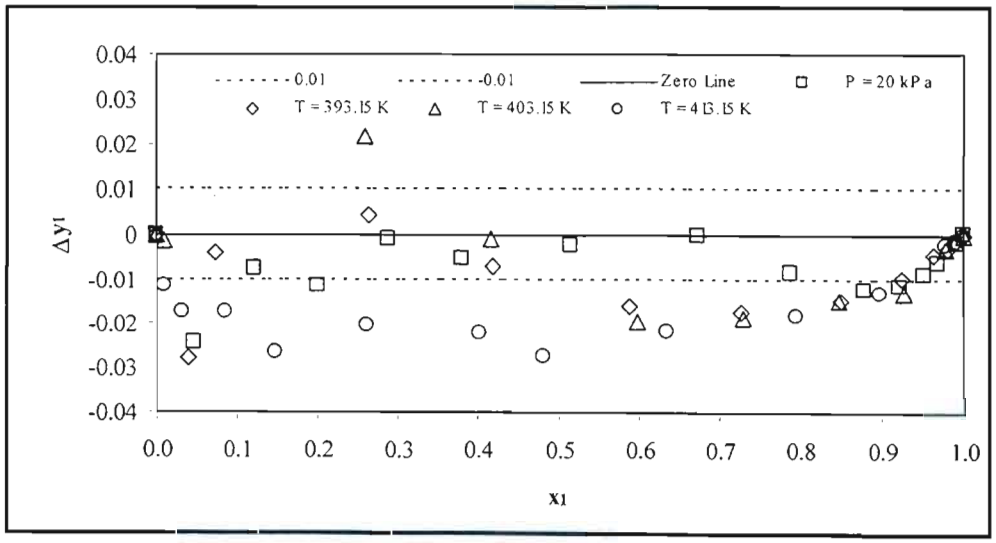

Figure B-9: Graph showing the deviation of the NRTL model (with Pitzer-Curl correlation) vapour compositions from the experimental values for the propionic acid (1) – valeric acid (2) system.

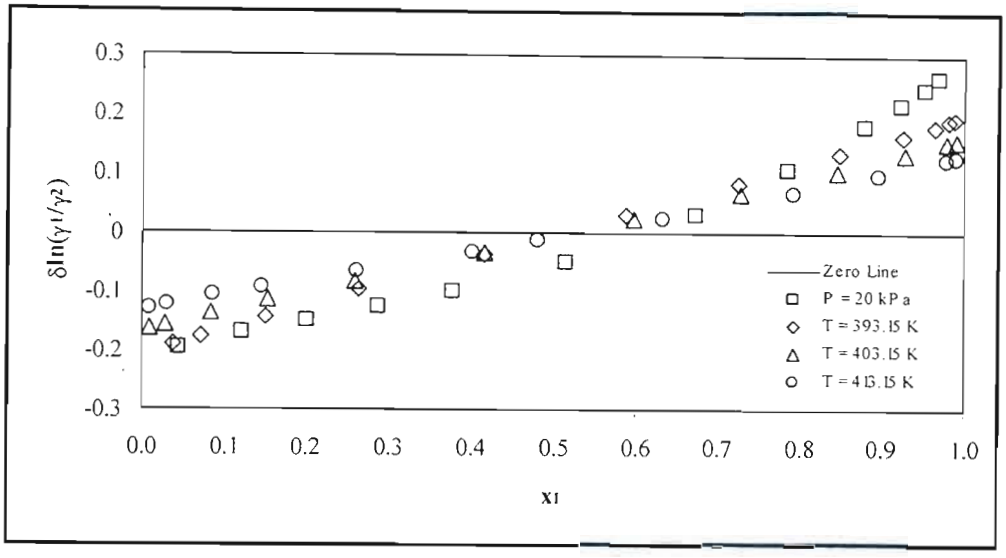

Figure B-10: Graph showing the deviation of the NRTL model (with Pitzer-Curl correlation) activity coefficients from the experimental values for the propionic acid (1) – valeric acid (2) system.

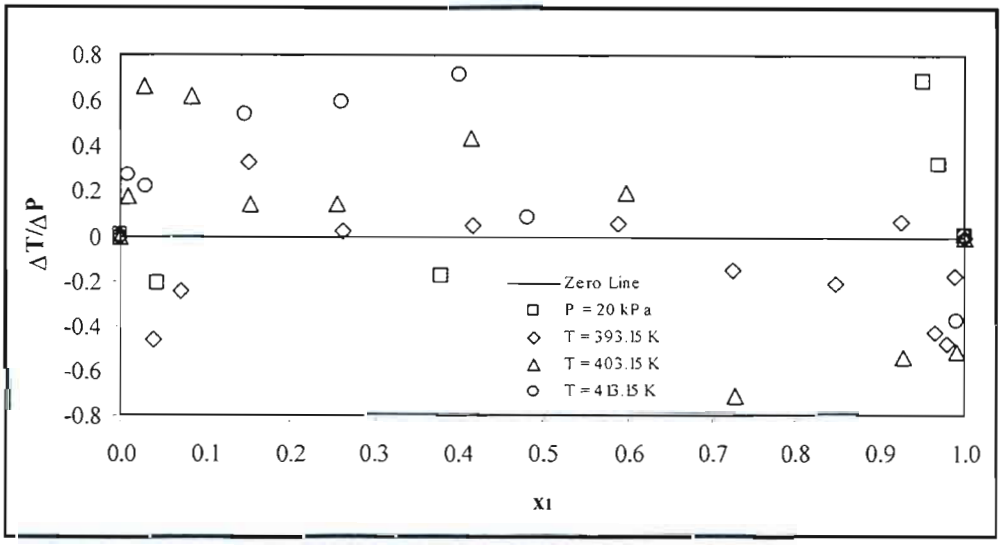

Figure B-11: Graph showing the deviation of the UNIQUAC model (with Pitzer-Curl correlation) pressures and temperatures from the experimental values for the propionic acid (1) – valeric acid (2) system.

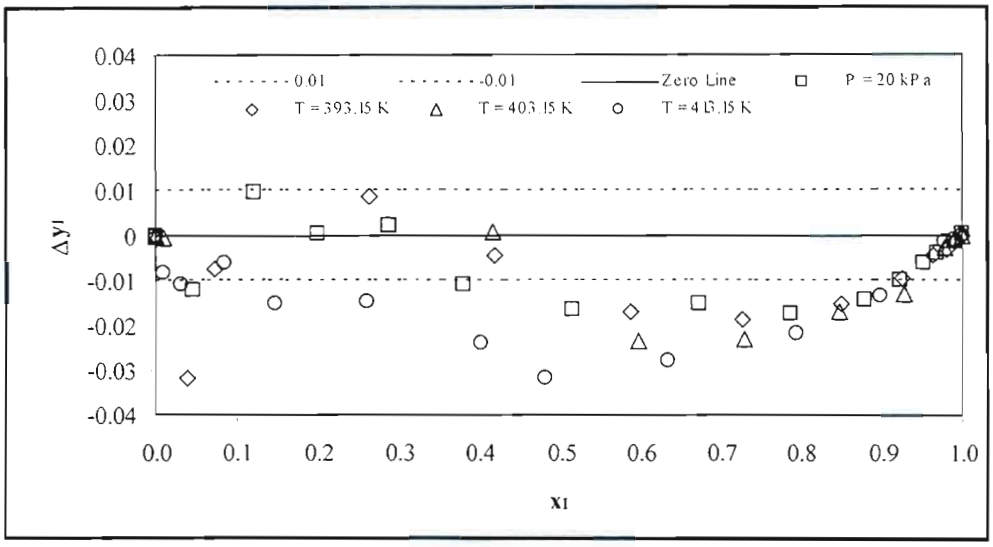

Figure B-12: Graph showing the deviation of the UNIQUAC model (with Pitzer-Curl correlation) vapour compositions from the experimental values for the propionic acid (1) – valeric acid (2) system.

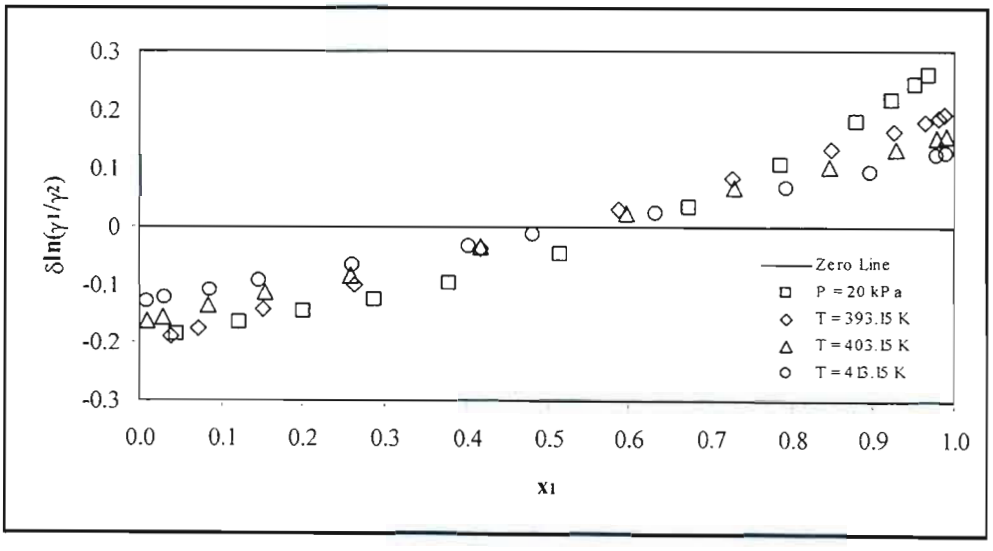

Figure B-13: Graph showing the deviation of the UNIQUAC model (with Pitzer-Curl correlation) activity coefficients from the experimental values for the propionic acid (1) – valeric acid (2) system.

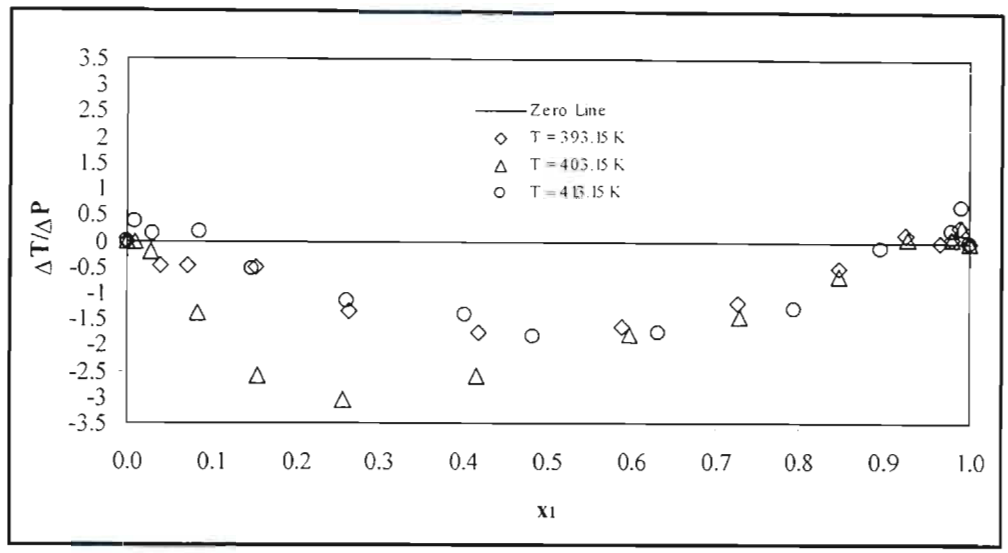

Figure B-14: Graph showing the deviation of the Wilson model (with chemical theory) pressures and temperatures from the experimental values for the propionic acid (1) – valeric acid (2) system.

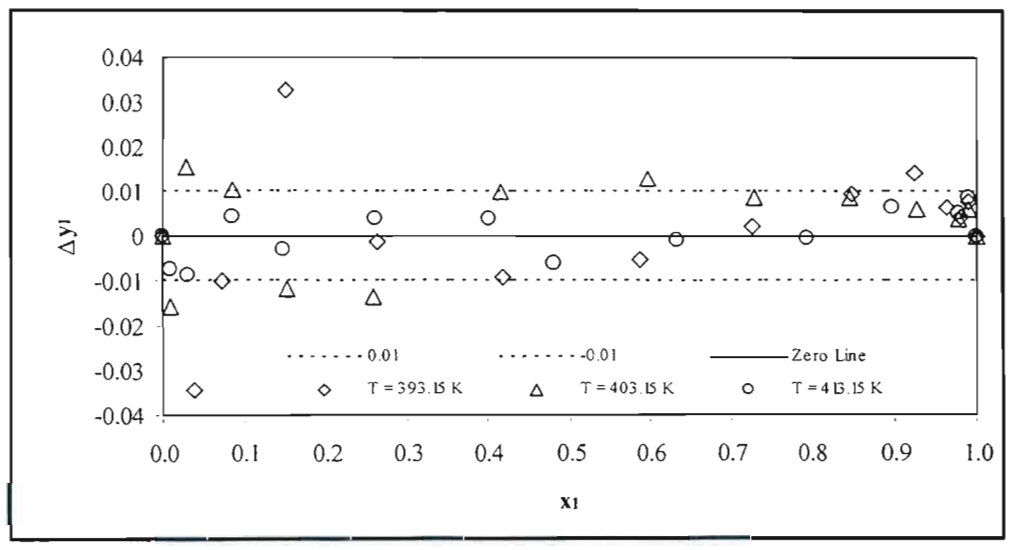

Figure B-15: Graph showing the deviation of the Wilson model (with chemical theory) vapour compositions from the experimental values for the propionic acid (1) – valeric acid (2) system.

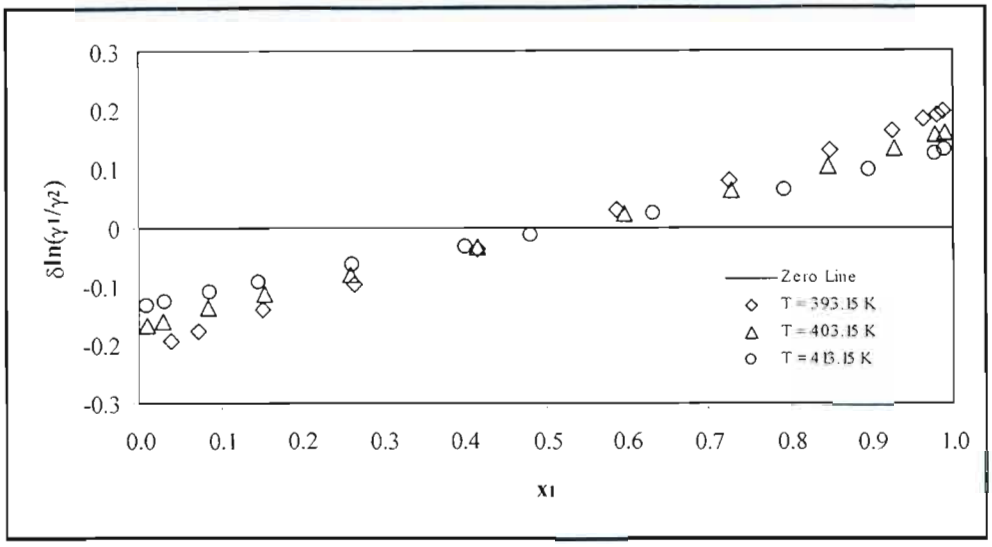

Figure B-16: Graph showing the deviation of the Wilson model (with chemical theory) activity coefficients from the experimental values for the propionic acid (1) – valeric acid (2) system.

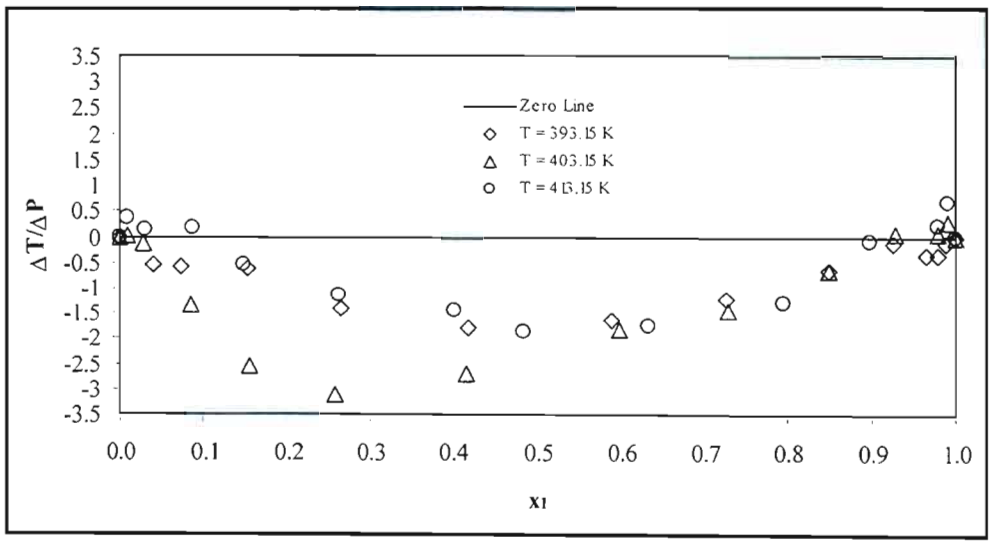

Figure B-17: Graph showing the deviation of the NRTL model (with chemical theory) pressures and temperatures from the experimental values for the propionic acid (1) – valeric acid (2) system.

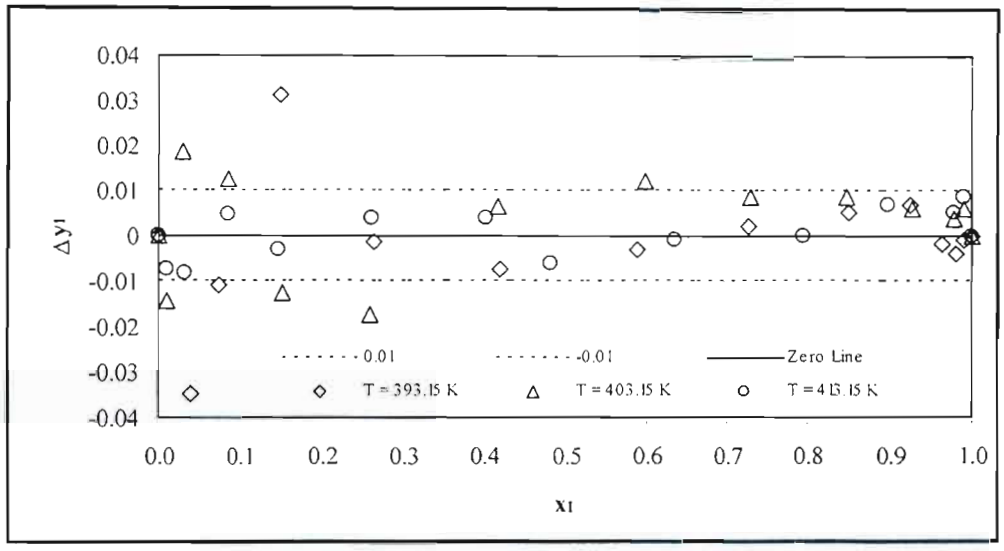

Figure B-18: Graph showing the deviation of the NRTL model (with chemical theory) vapour compositions from the experimental values for the propionic acid (1) – valeric acid (2) system.

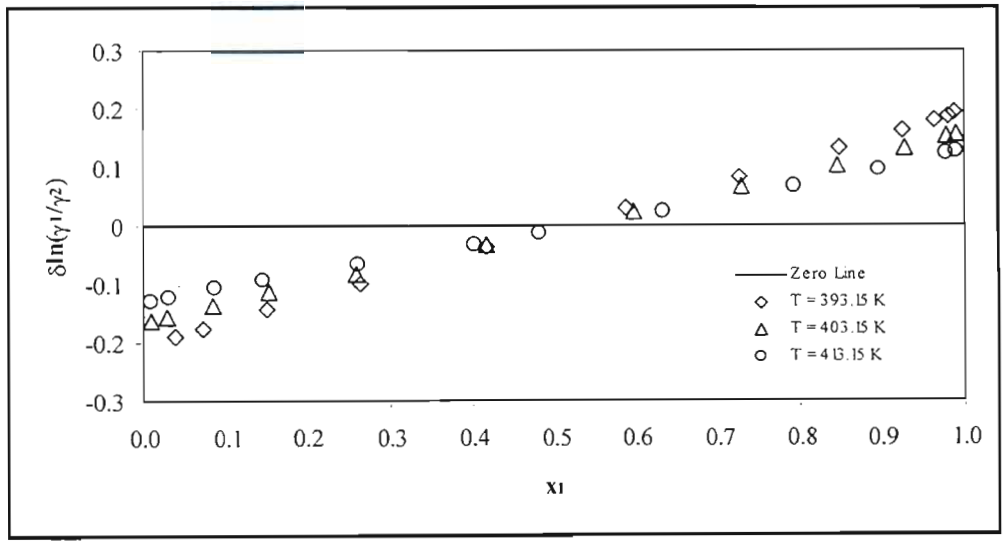

Figure B-19: Graph showing the deviation of the NRTL model (with chemical theory) activity coefficients from the experimental values for the propionic acid (1) – valeric acid (2) system.

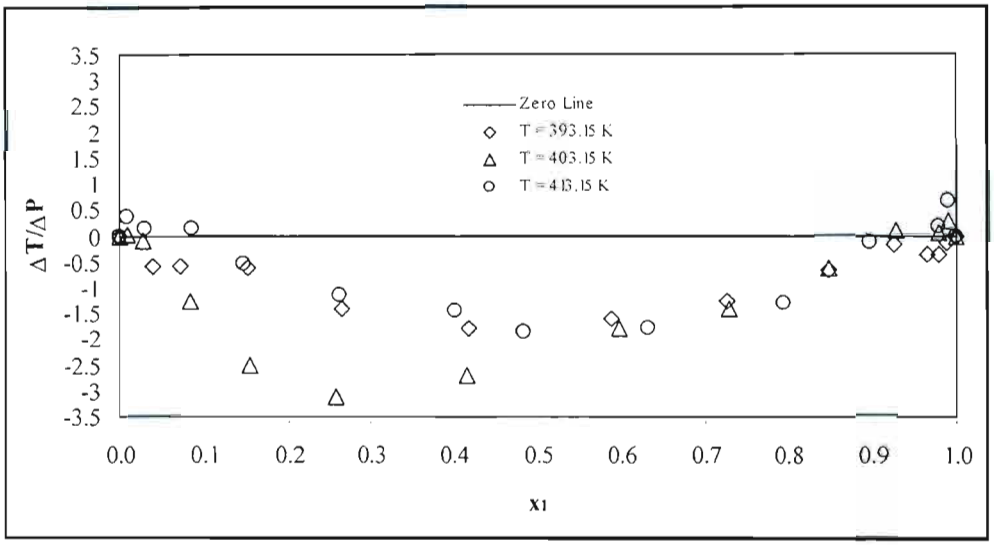

Figure B-20: Graph showing the deviation of the UNIQUAC model (with chemical theory) pressures and temperatures from the experimental values for the propionic acid (1) – valeric acid (2) system.

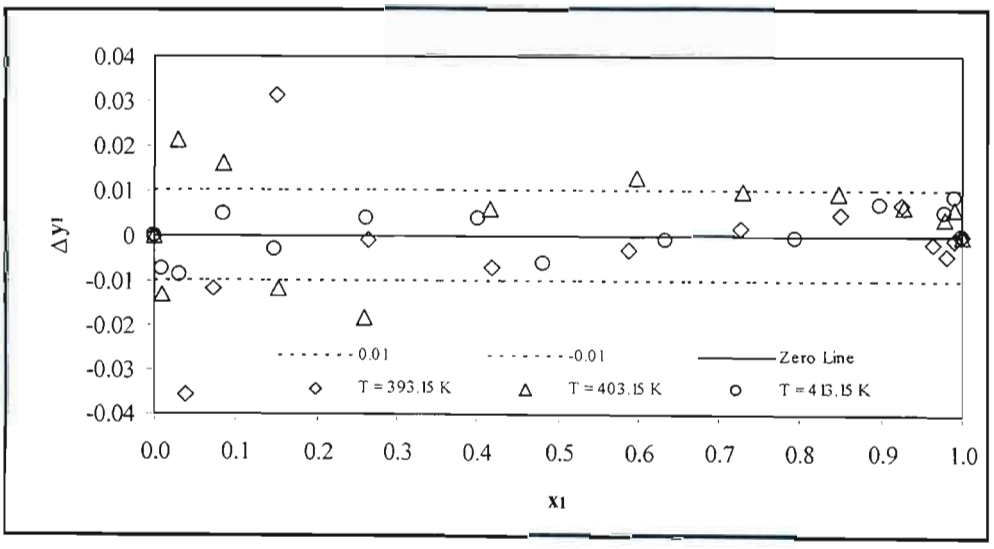

Figure B-21: Graph showing the deviation of the UNIQUAC model (with chemical theory) vapour compositions from the experimental values for the propionic acid (1) – valeric acid (2) system.

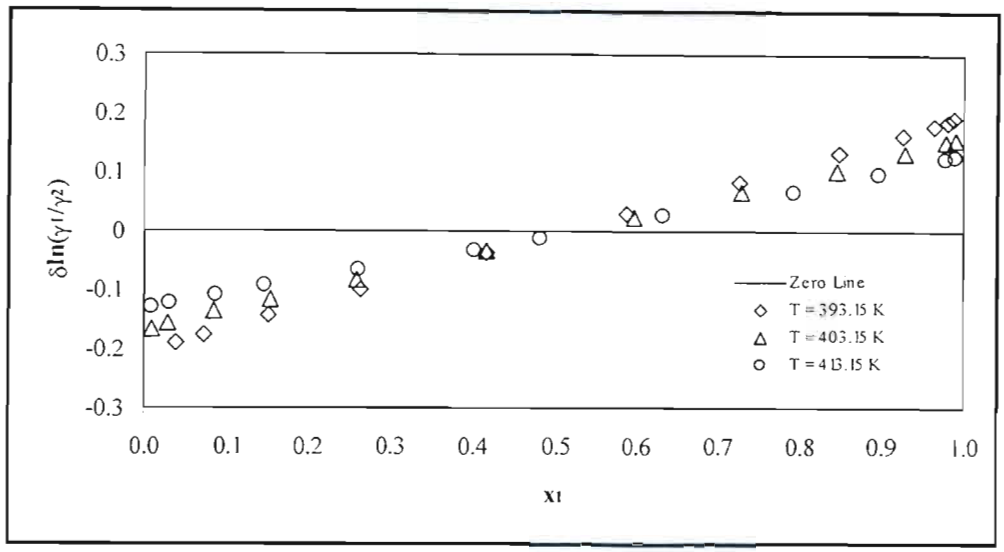

Figure B-22: Graph showing the deviation of the UNIQUAC model (with chemical theory) activity coefficients from the experimental values for the propionic acid (1) – valeric acid (2) system.

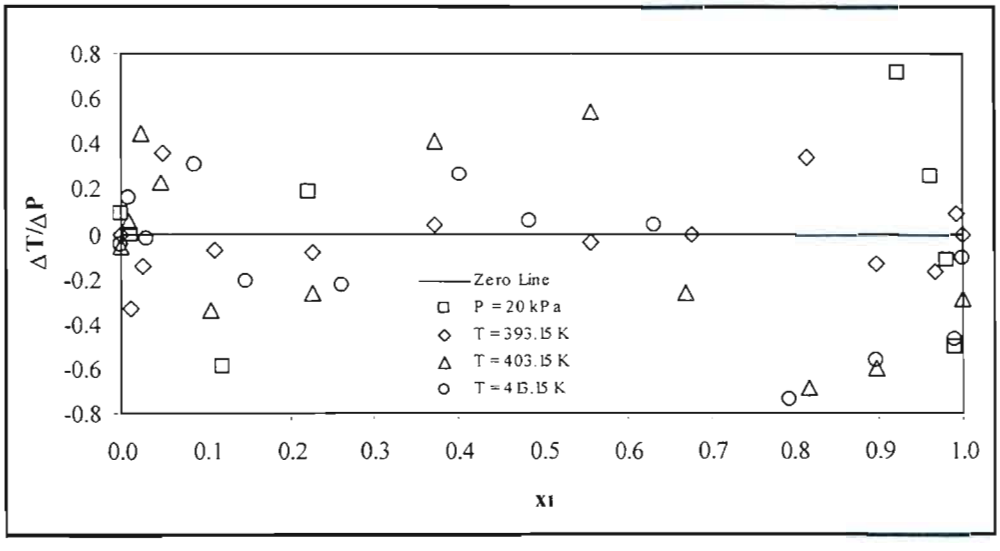

Figure B-23: Graph showing the deviation of the Peng-Robinson EOS (with Wong-Sandler mixing rule) pressures and temperatures from the experimental values for the propionic acid (1) – valeric acid (2) system.

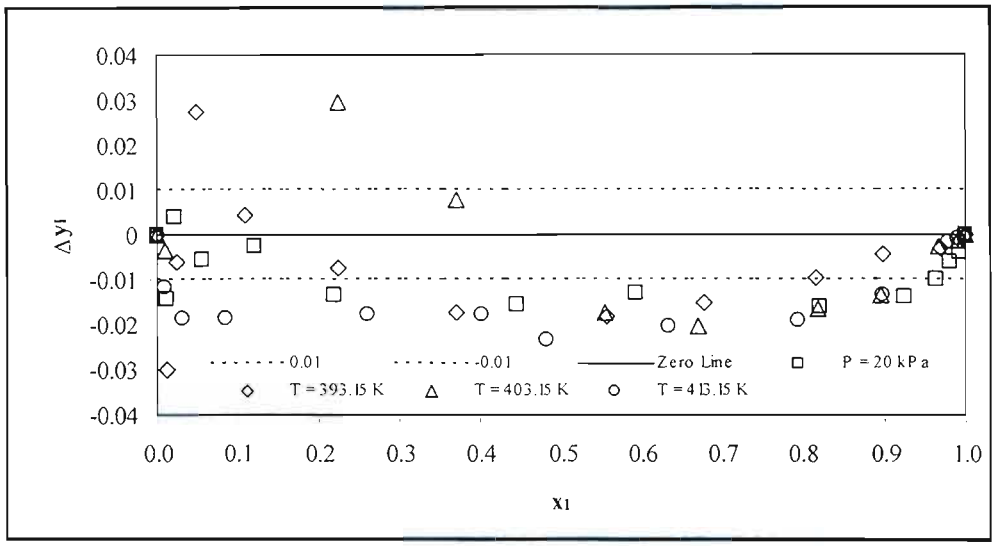

Figure B-24: Graph showing the deviation of the Peng-Robinson EOS (with Wong-Sandler mixing rule) vapour compositions from the experimental values for the propionic acid (1) – valeric acid (2) system.

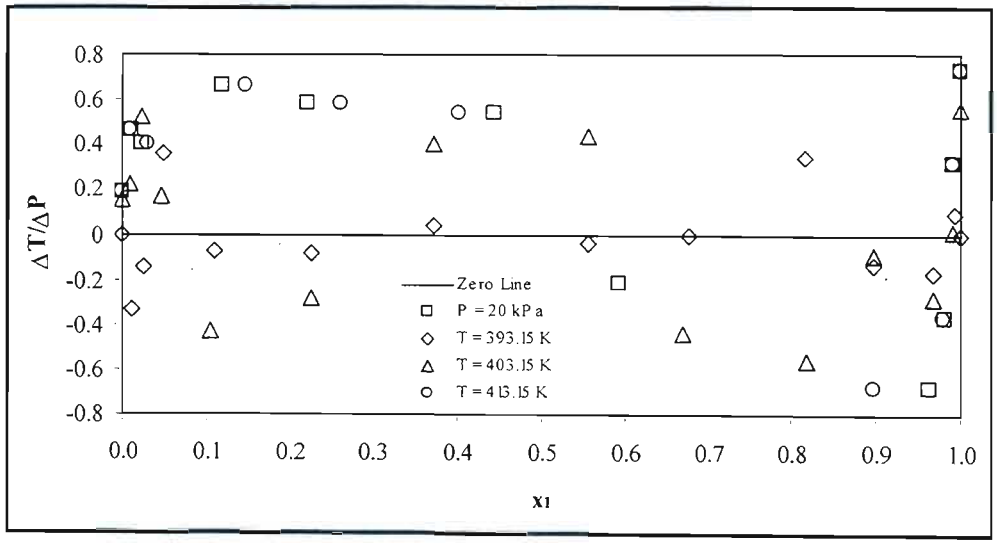

Figure B-25: Graph showing the deviation of the Peng-Robinson EOS (with Twu-Coon mixing rule) pressures and temperatures from the experimental values for the propionic acid (1) – valeric acid (2) system.

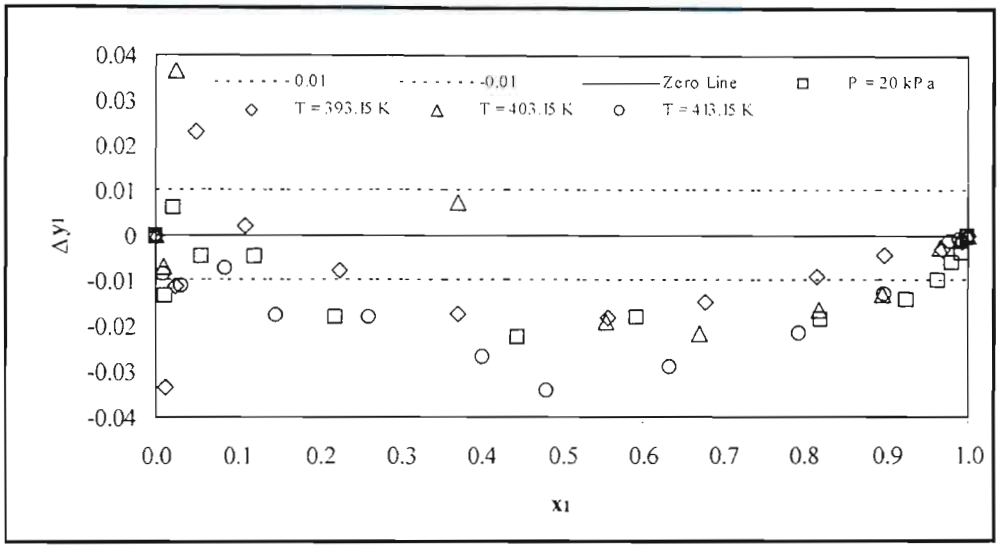

Figure B-26: Graph showing the deviation of the Peng-Robinson EOS (with Twu-Coon mixing rule) vapour compositions from the experimental values for the propionic acid (1) – valeric acid (2) system.

B.3 Isobutyric Acid (1) – Valeric (2) System

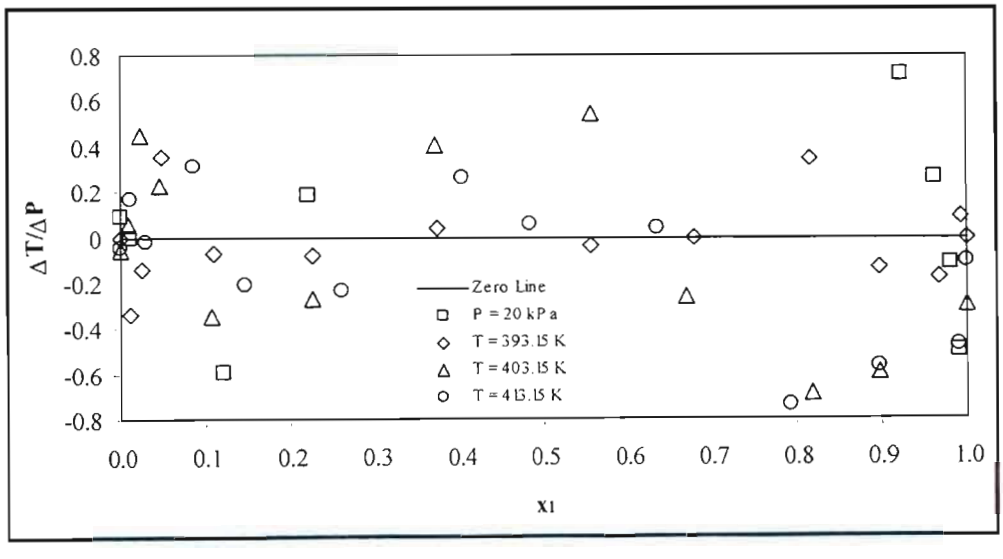

Figure B-27: Graph showing the deviation of the Wilson model (with Pitzer-Curl correlation) pressures and temperatures from the experimental values for the isobutyric acid (1) – valeric acid (2) system.

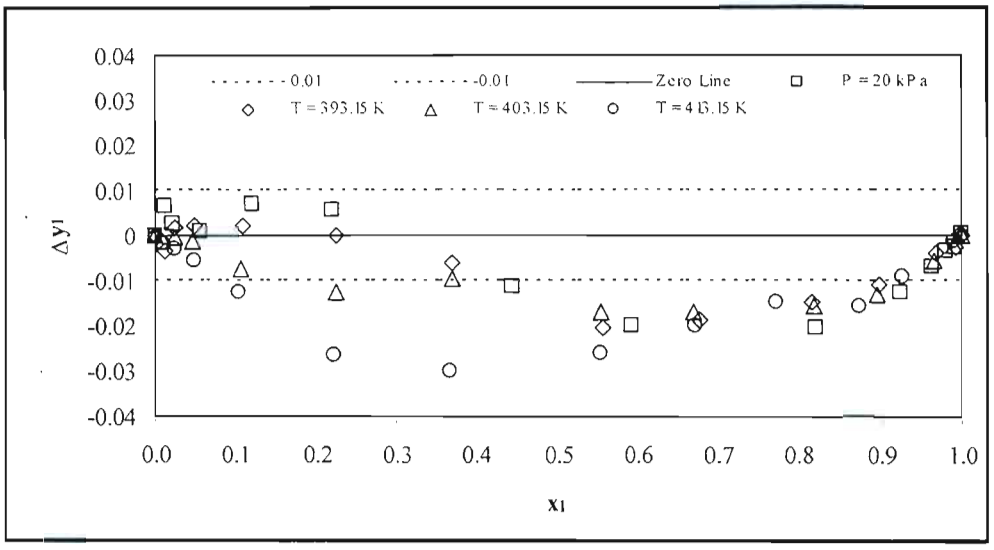

Figure B-28: Graph showing the deviation of the Wilson model (with Pitzer-Curl correlation) vapour compositions from the experimental values for the isobutyric acid (1) – valeric acid (2) system.

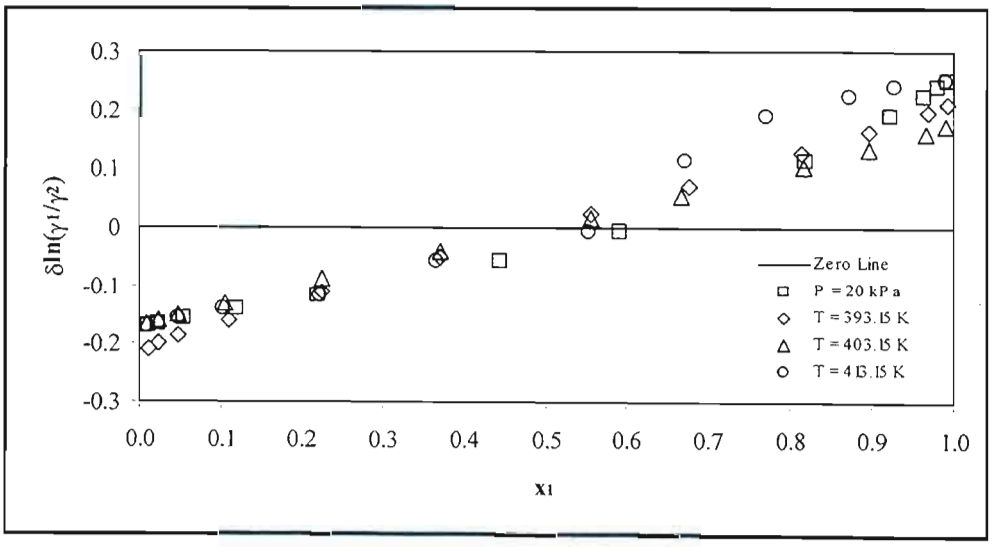

Figure B-29: Graph showing the deviation of the Wilson model (with Pitzer-Curl correlation) activity coefficients from the experimental values for the isobutyric acid (1) – valeric acid (2) system.

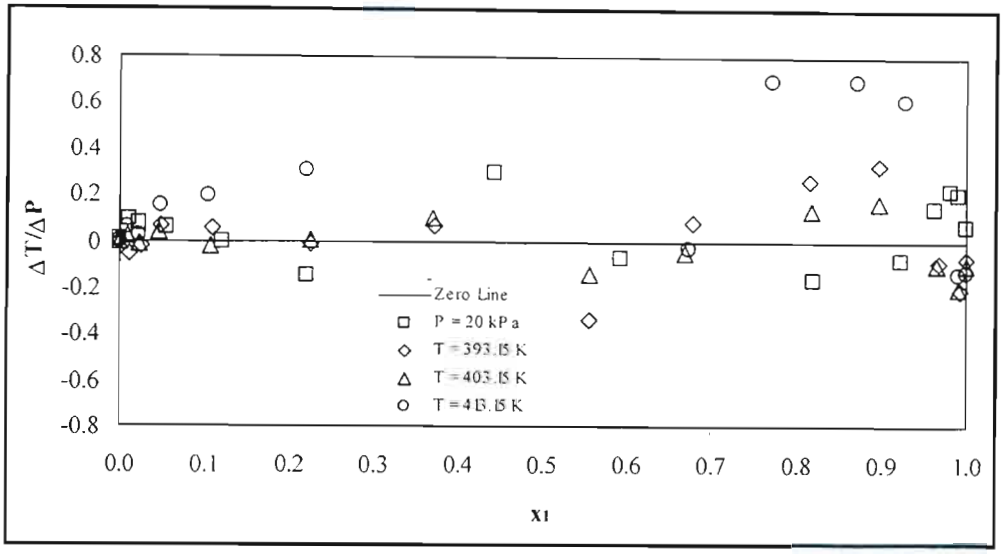

Figure B-30: Graph showing the deviation of the NRTL model (with Pitzer-Curl correlation) pressures and temperatures from the experimental values for the isobutyric acid (1) – valeric acid (2) system.

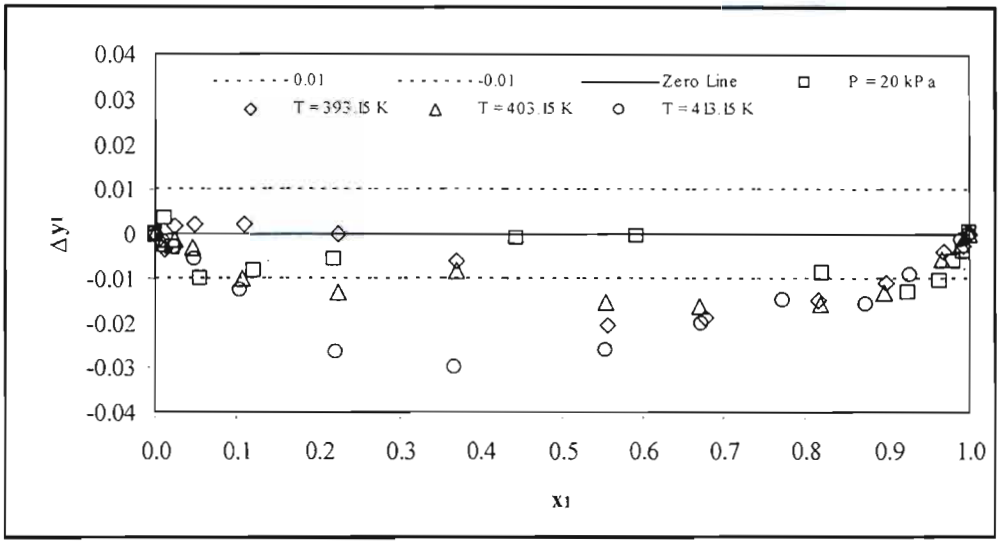

Figure B-31: Graph showing the deviation of the NRTL model (with Pitzer-Curl correlation) vapour compositions from the experimental values for the isobutyric acid (1) – valeric acid (2) system.

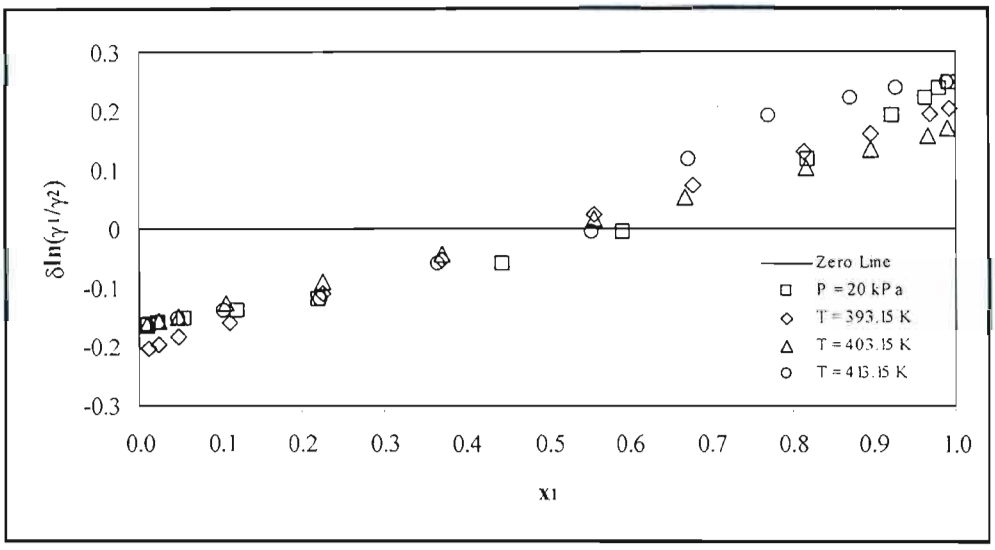

Figure B-32: Graph showing the deviation of the NRTL model (with Pitzer-Curl correlation) activity coefficients from the experimental values for the isobutyric acid (1) – valeric acid (2) system.

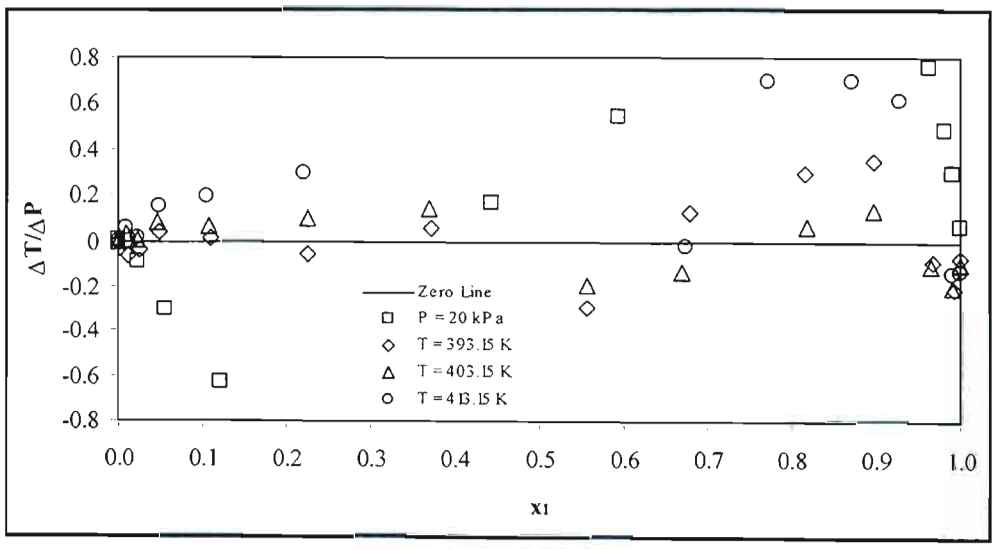

Figure B-33: Graph showing the deviation of the UNIQUAC model (with Pitzer-Curl correlation) pressures and temperatures from the experimental values for the isobutyric acid (1) – valeric acid (2) system.

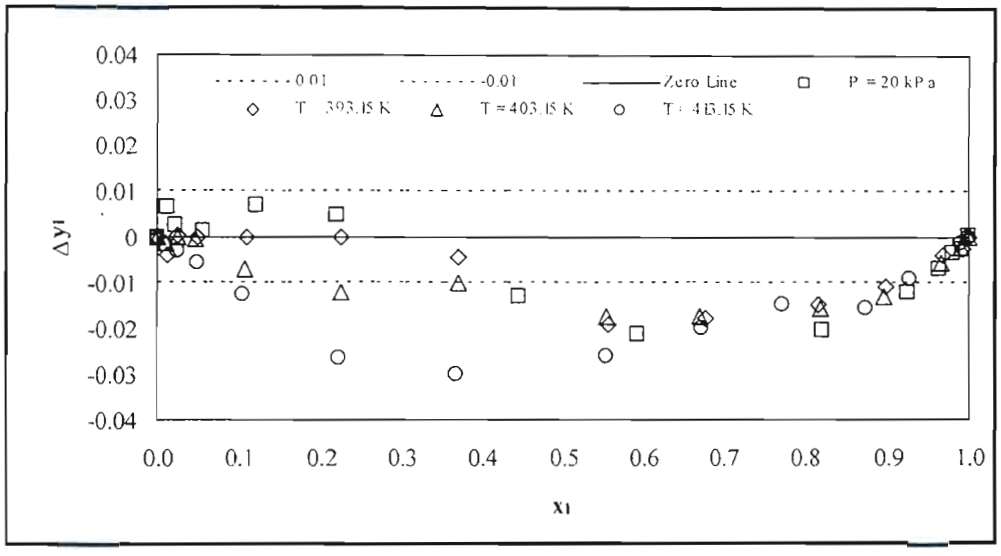

Figure B-34: Graph showing the deviation of the UNIQUAC model (with Pitzer-Curl correlation) vapour compositions from the experimental values for the isobutyric acid (1) – valeric acid (2) system.

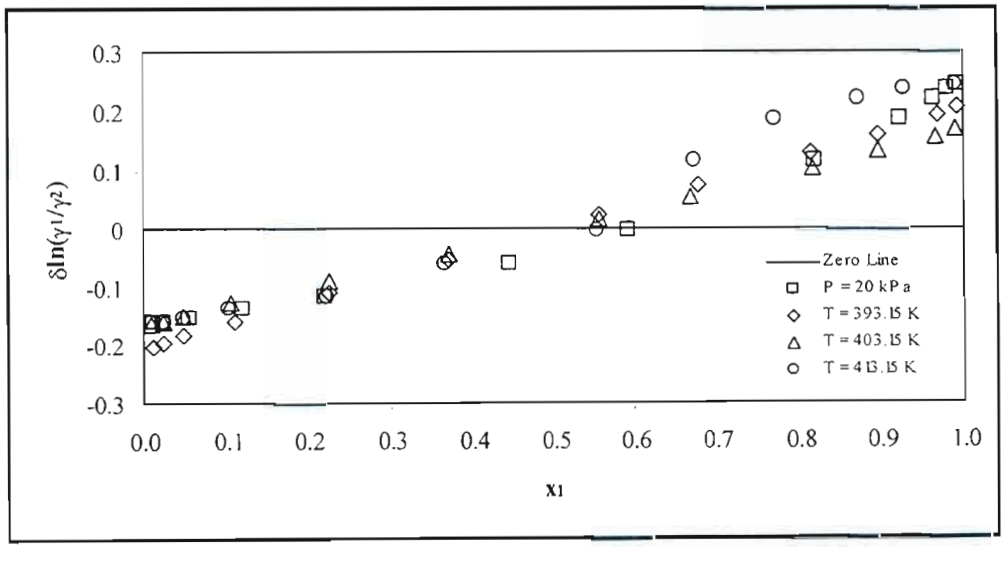

Figure B-35: Graph showing the deviation of the UNIQUAC model (with Pitzer-Curl correlation) activity coefficients from the experimental values for the isobutyric acid (1) – valeric acid (2) system.

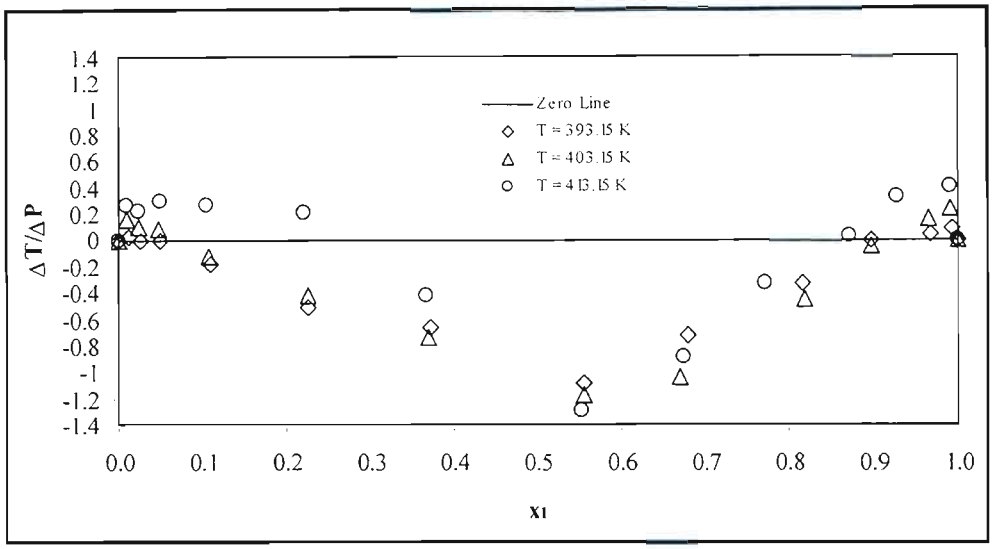

Figure B-36: Graph showing the deviation of the Wilson model (with chemical theory) pressures and temperatures from the experimental values for the isobutyric acid (1) – valeric acid (2) system.

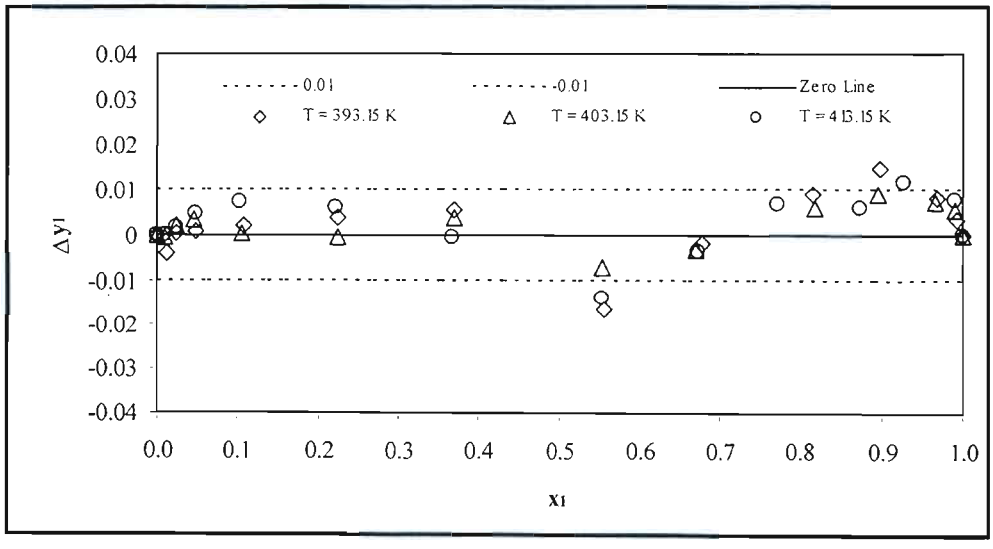

Figure B-37: Graph showing the deviation of the Wilson model (with chemical theory) vapour compositions from the experimental values for the isobutyric acid (1) – valeric acid (2) system.

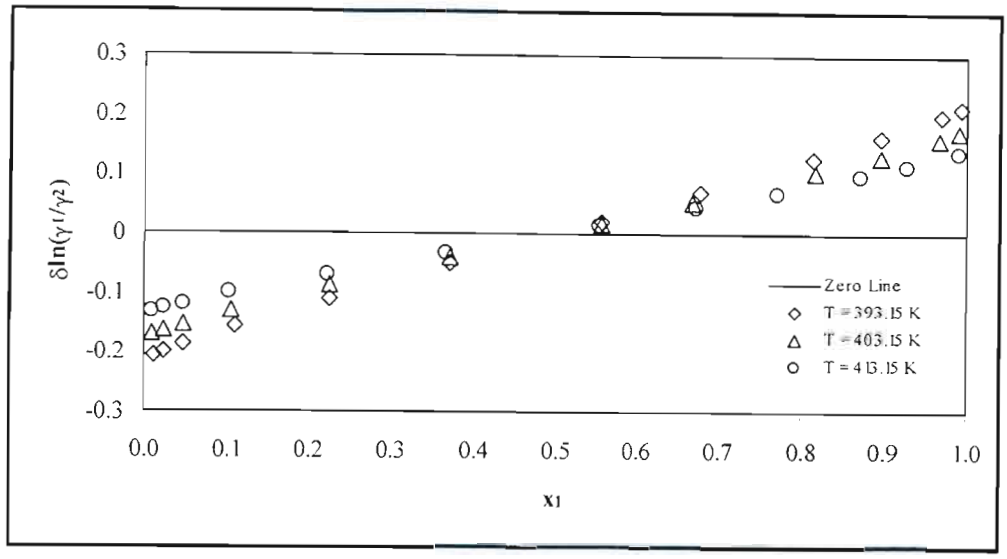

Figure B-38: Graph showing the deviation of the Wilson model (with chemical theory) activity coefficients from the experimental values for the isobutyric acid (1) – valeric acid (2) system.

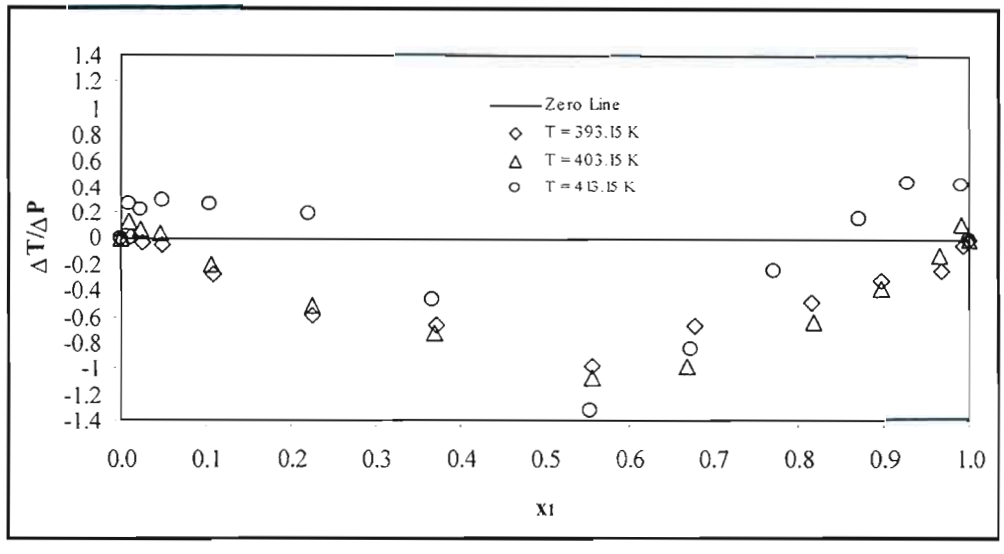

Figure B-39: Graph showing the deviation of the NRTL model (with chemical theory) pressures and temperatures from the experimental values for the isobutyric acid (1) – valeric acid (2) system.

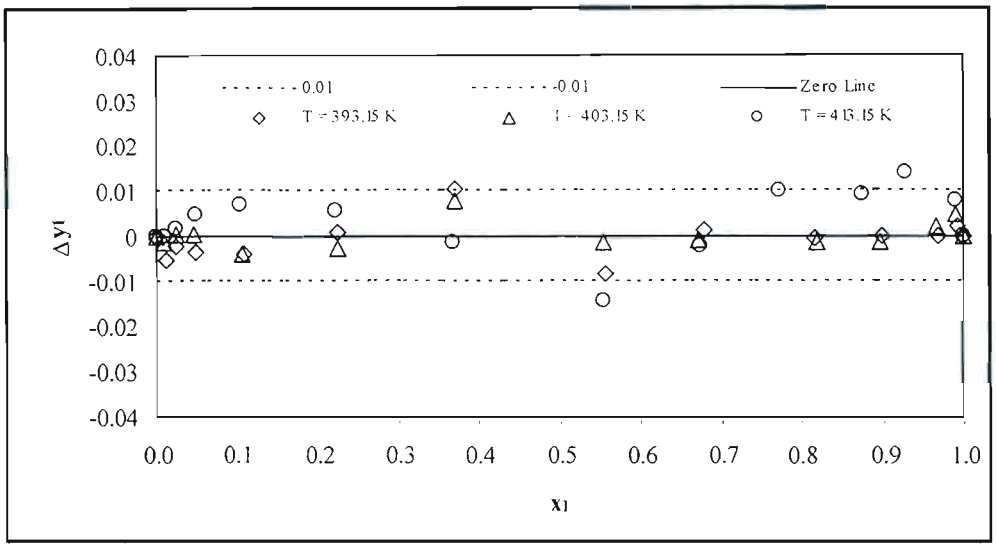

Figure B-40: Graph showing the deviation of the NRTL model (with chemical theory) vapour compositions from the experimental values for the isobutyric acid (1) – valeric acid (2) system.

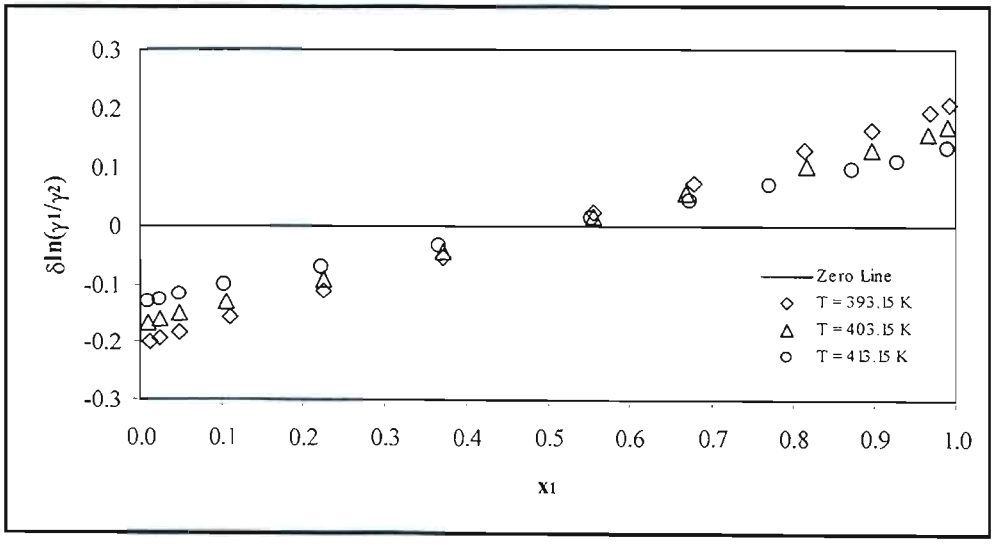

Figure B-41: Graph showing the deviation of the NRTL model (with chemical theory) activity coefficients from the experimental values for the isobutyric acid (1) – valeric acid (2) system.

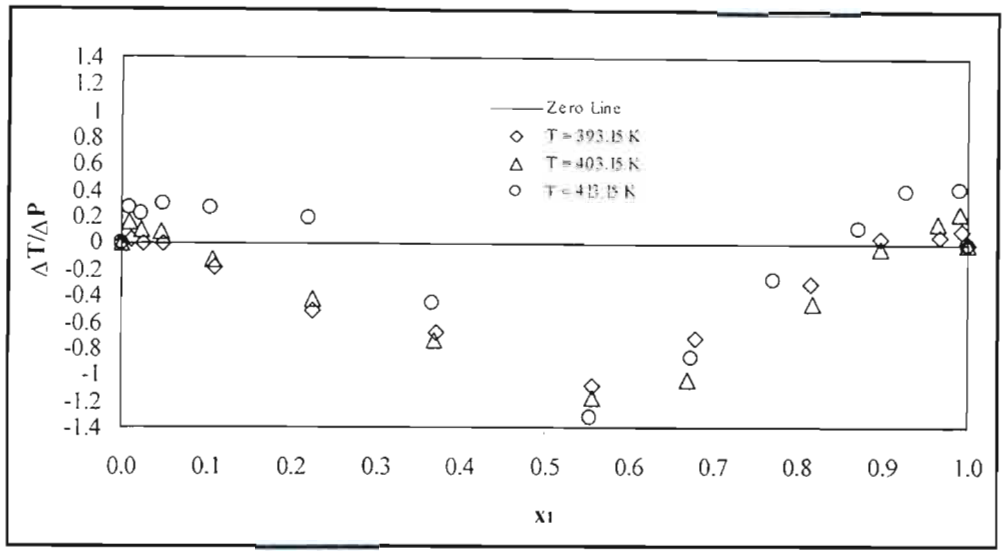

Figure B-42: Graph showing the deviation of the UNIQUAC model (with chemical theory) pressures and temperatures from the experimental values for the isobutyric acid (1) – valeric acid (2) system.

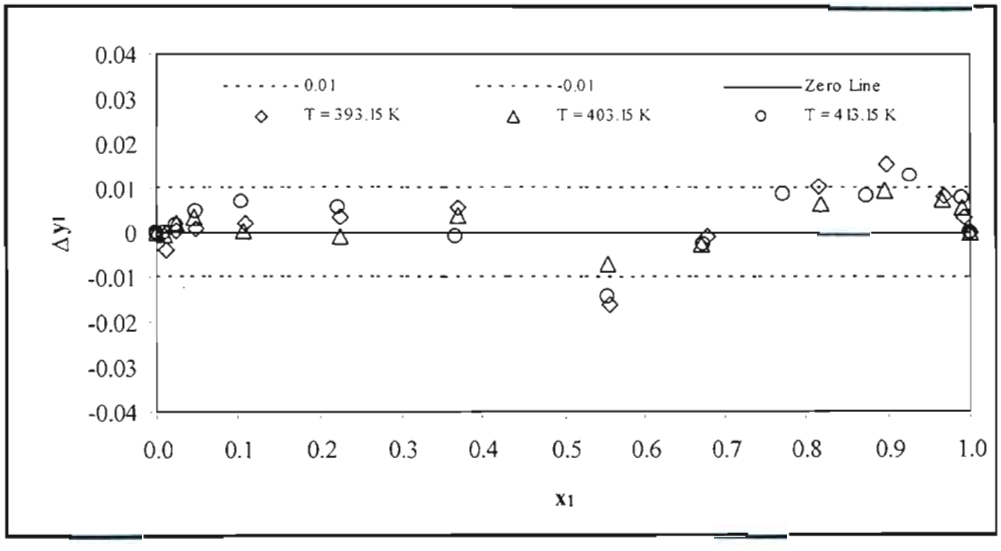

Figure B-43: Graph showing the deviation of the UNIQUAC model (with chemical theory) vapour compositions from the experimental values for the isobutyric acid (1) – valeric acid (2) system.

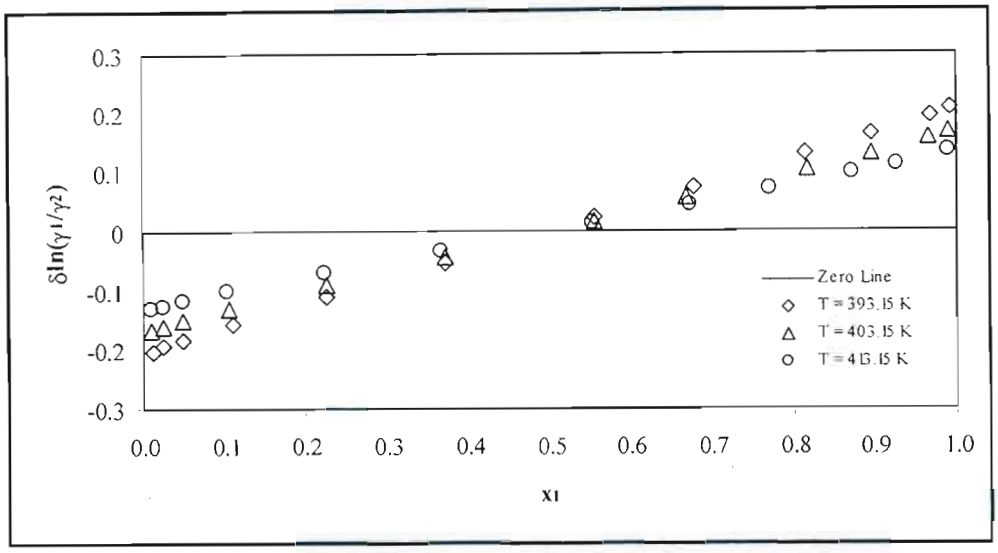

Figure B-44: Graph showing the deviation of the UNIQUAC model (with chemical theory) activity coefficients from the experimental values for the isobutyric acid (1) – valeric acid (2) system.

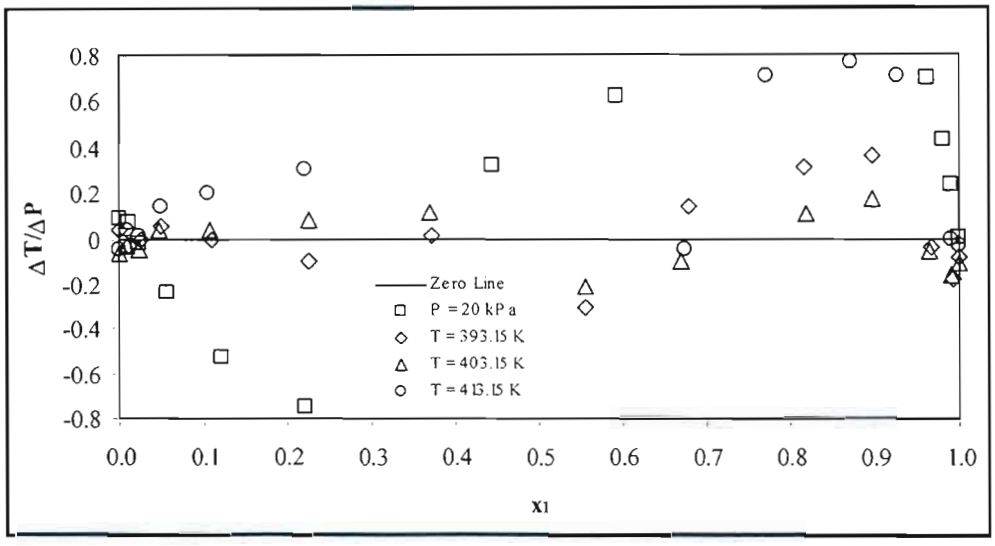

Figure B-45: Graph showing the deviation of the Peng-Robinson EOS (with Wong-Sandler mixing rule) pressures and temperatures from the experimental values for the isobutyric acid (1) – valeric acid (2) system.

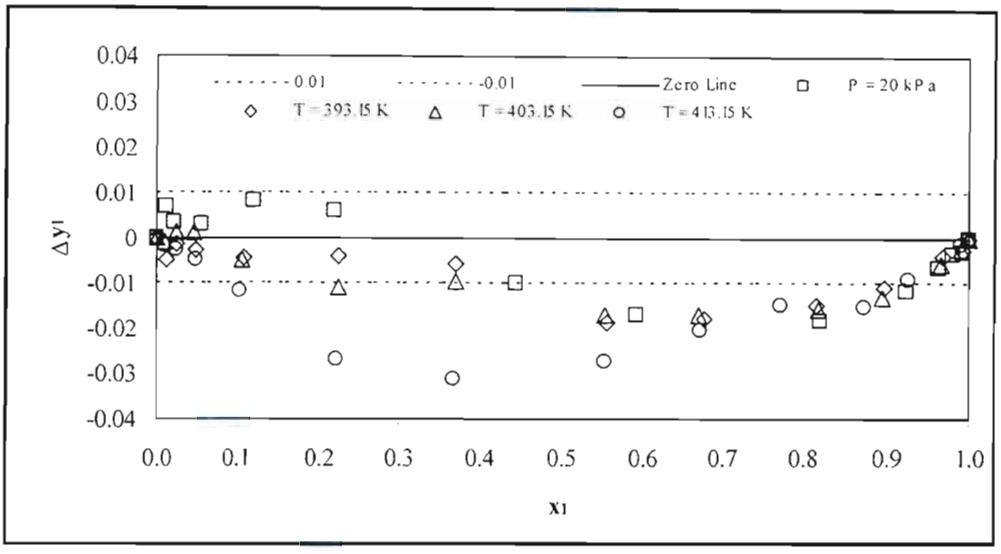

Figure B-46: Graph showing the deviation of the Peng-Robinson EOS (with Wong-Sandler mixing rule) vapour compositions from the experimental values for the isobutyric acid (1) – valeric acid (2) system.

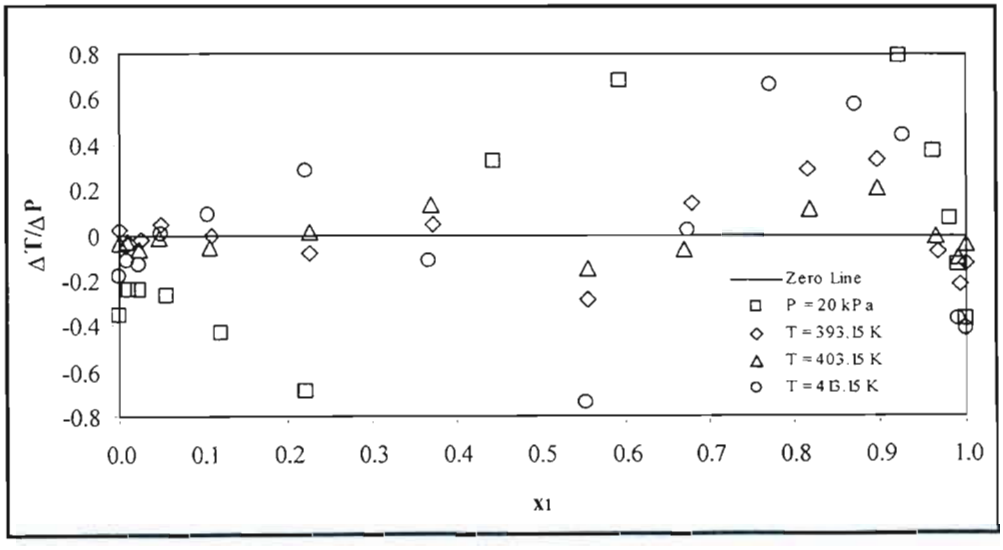

Figure B-47: Graph showing the deviation of the Peng-Robinson EOS (with Twu-Coon mixing rule) pressures and temperatures from the experimental values for the isobutyric acid (1) – valeric acid (2) system.

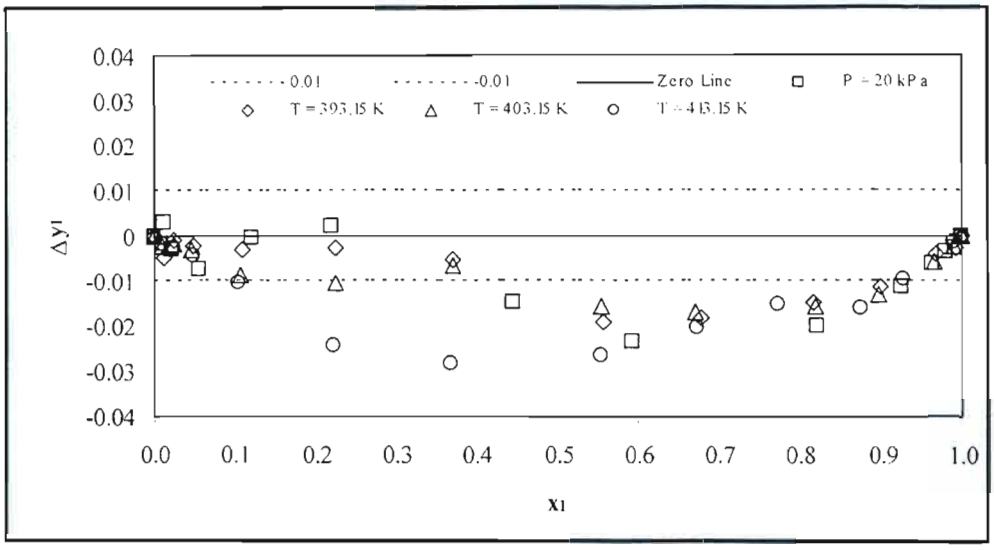

Figure B-48: Graph showing the deviation of the Peng-Robinson EOS (with Twu-Coon mixing rule) vapour compositions from the experimental values for the isobutyric acid (1) – valeric acid (2) system.

APPENDIX
C

EQUIPMENT PHOTOS

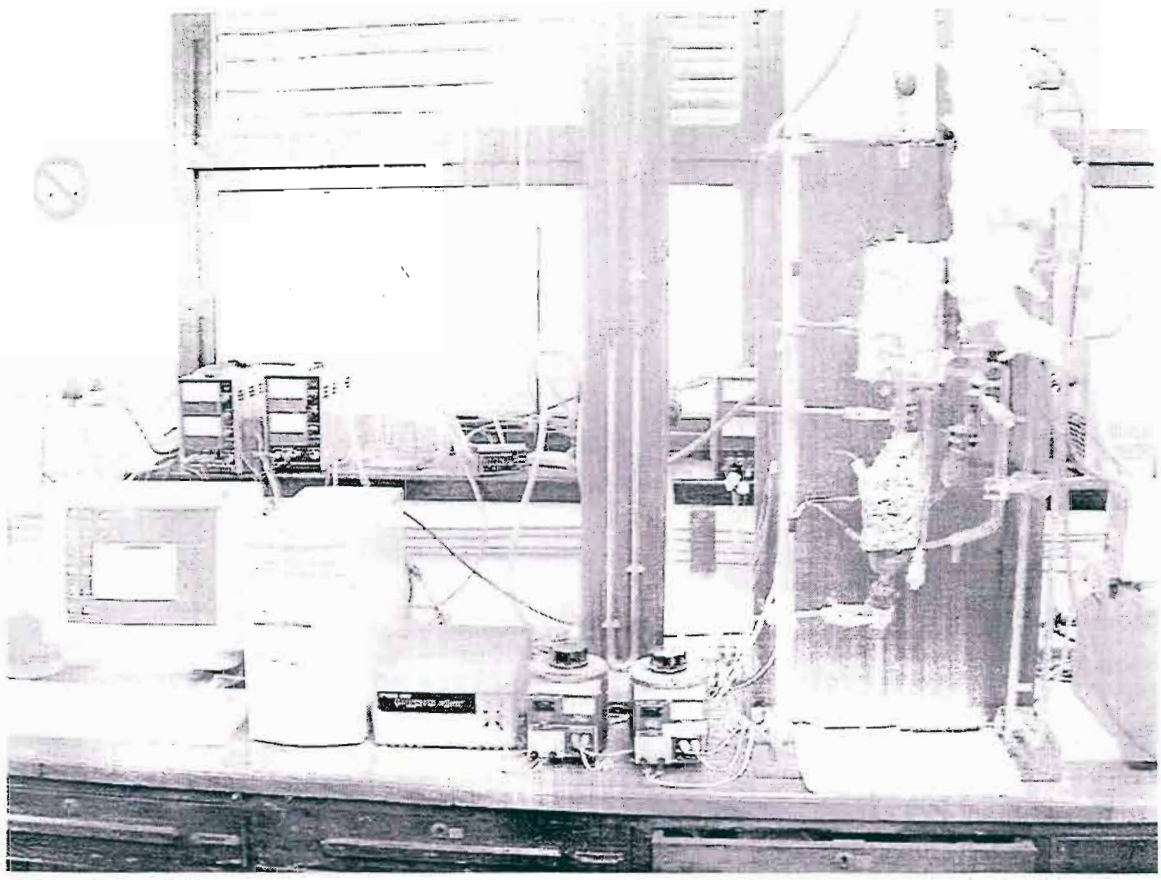

Figure C-1: Photo of the equipment that was used in measuring the carboxylic acid systems.

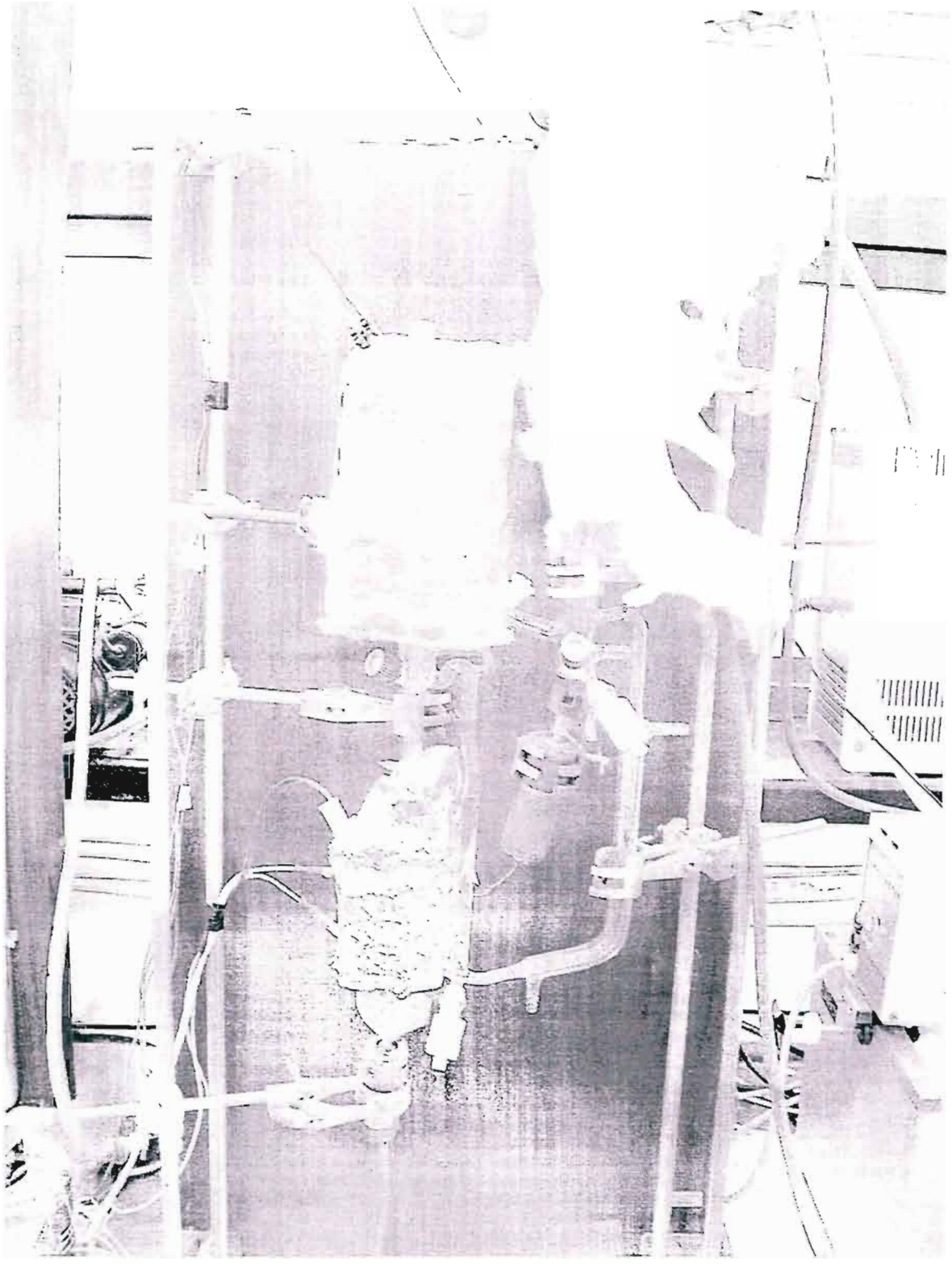

Figure C-2: Photo of the VLE still that was used in measuring the carboxylic acid systems (showing the insulation required due to the high acid boiling points).